Doctoral Thesis

Temporal and Spatial Variation Patterns of Seismicity in Relation to the Crustal Structure and Earthquake Physics, from the Analysis of several Seismic Sequences in Japan and Romania

Bogdan Dumitru ENESCU

Field of Geophysics,

Department of Earth and Planetary Sciences,

Graduate School of Science,

Kyoto University

December, 2003

Contents

Abstract

Large earthquakes are among the most damaging natural disasters, often being the cause of big destruction to humans and infrastructure alike. Earthquake prediction however, despite of an intense and continuous scientific effort for more than one hundred years, is still beyond our grasp.

One of the important issues that should be addressed in this context is the relation between the complex seismicity patterns, on one hand, and the physics of the Earth and earthquakes, on the other hand. There is also a recognized need to introduce or develop new algorithms to address more effectively the classification and recognition of different seismicity patterns.

The first chapter of the thesis is a short review on the subject. We start by briefly showing what has been achieved so far concerning the analysis of spatio-temporal and energetic earthquake patterns and the main approaches to deal with this complex subject. We are going to discuss as well about the physical interpretation of the spatio-temporal seismicity variations and the triggering effect of the static and dynamic stress changes caused by moderate to large earthquakes. The analysis of seismicity for the study of tectonic processes and earthquake recurrence requires knowledge of the precise spatial offset between the earthquake hypocenters. The double-difference relocation method, recently developed (Waldhauser and Ellsworth, 2000), can substantially improve the accuracy of hypocenters' location.

In the second chapter we are going to discuss different kinds of precursory phenomena occurred before the 1995 Hyogo-ken Nanbu earthquake (Kobe earthquake). Our study is mainly focussed on seismicity changes, but the correlation with physical processes and other geophysical anomalies are discussed in some detail. We report, in particular, that the seismicity rate, *b*-value and fractal dimension show clear precursory changes starting about 2-3 years before the large event.

In the third chapter we analyze in detail the seismic activity occurred before and after the 2000 Western Tottori earthquake. We focus especially on the spatio-temporal changes of *b*-value of the frequency-magnitude distribution and *p*-value of the Modified Omori Law. We found important variations of the parameters in both time and space. Notably, both *b* and *p* values are significantly lower for some previous earthquake swarms occurred in 1989, 1990 and 1997 than for the aftershocks of the 2000 Western Tottori earthquake. For the aftershocks themselves there is a significant spatial variation

of *b* and *p*, with relatively high values around the epicenter of the large event and relatively low values in the north part of the aftershock distribution. Our study discusses in detail the correlation between the parameters' variation and the crustal structure and stress changes caused by the occurrence of the larger events. Most of the computations performed with the occasion of this study were done by using an "*Aftershock Analysis Toolbox*" written in *Matlab* and conveniently integrated with the *Zmap* seismicity analysis software (author: S. Wiemer). The toolbox is available by request from the author (*benescu@rcep.dpri.kyoto.u.ac.jp*) and part of it is included already in *Zmap (version 6)*.

The fourth chapter reports on the seismic activity occurred during the 1998 Hida Mountain (Central Honshu) earthquake swarm. In order to have a more accurate view on the detailed seismicity structure, we relocate the earthquakes by using a double-difference approach. The clustering of seismicity is evident after relocation, especially in the south region, where there is a better coverage with seismic stations. The migration of seismicity, as well as the *b*-value spatial and temporal distributions are compared with the static stress changes caused by the largest 18 earthquakes in the swarm. This study reveals significant correlation between the seismicity pattern and *b*-value, on one hand, and the stress changes on the other hand. A toolbox for "*Coulomb Stress Analysis*" will be available for downloading from my web page (http://www.rcep.dpri.kyoto-u.ac.jp/~benescu/). It is written mainly in *Matlab* and can be used together with *Zmap* software.

The next chapter of the thesis is concerned with the temporal multifractal and chaotic analysis of the intermediate-depth seismicity in the Vrancea region, Romania. The main findings are: a clear separation between aftershocks and background seismicity in the multifractal spectrum (which displays a piece-wise structure), weak long-range correlations, as measured by *Hurst exponent* (*H*), and no detectable deterministic chaos. In other words, the series of inter-event times are very close to a non-*Gaussian* random white-noise process.

In Chapter 6 we introduce the wavelet-based analysis method of time series of earthquakes. The analysis of real data (Vrancea region and Hyoko-ken region) is complemented by the study of two simulated sequences obtained by using the *ETAS model* (Ogata, 1985, 1988, 1999) and a *cellular fault zone* in a three-dimensional elastic solid containing asperity and non-asperity regions (Ben-Zion and Rice, 1993). The wavelet-based method proves to be a versatile approach to discriminate between

different multifractal characteristics of the time-series under study: long-range correlation, power-law distribution of inter-event times or the presence of various trends. To my knowledge this is the first study which tries to explain the origins of (multi)fractality in the self-affine time series of earthquakes. The study highlights the ability of wavelets to reveal both time and frequency information. Further developments will extend the approach to 2D and 3D characterization of earthquake distributions. Part of the multifractal and non-linear analysis of the earthquake data were done by using the "*Non-linear Analysis toolbox*", made available on my web page together with a brief *User manual*.

The final chapter of the thesis discusses the main conclusions of the paper in an integrated and comparative manner.

Acknoledgements and a list of main publications on which this thesis is based conclude the present dissertation. References and the figures of each chapter are attached at the end of the thesis.

Chapter 1

INTRODUCTION

-SEISMICITY PATTERNS, A REVIEW-

1.1 Earthquakes as (marked) point processes

Statistical methods play a very important role in the analysis of seismicity patterns and, therefore, we consider appropriate to briefly introduce some basic statistical concepts related to earthquake occurrence. From a statistical point of view, earthquakes can be considered as stochastic (i.e. random) *point processes*. As Fig. 1.1 shows, a point-process is defined as a sequence of points t_i ($1 \le i \le n$, n – total number of points) in time, with the property $t_{i+1} > t_i$. Since earthquakes are characterized by their size (energy or magnitude), we refer to them as *marked point processes*. Moreover, as they have also a spatial location, they are *marked, spatio-temporal point-processes*.

As shown in Fig. 1.1, one possibility to describe a (simple) point-process is by considering the inter-event times between successive events. Depending on the distribution of the inter-event times, the earthquake temporal distribution may be considered a random (Poisson), a quasi-periodic or a clustered process. A review on seismicity analysis through point-process modeling is done by Ogata (1999).

1.2 Introduction into the subject. Recent studies concerning seismicity changes in time and space

It is rather difficult to review briefly a subject that has been tackled by many researchers, in many different ways. We hope however that together with the extensive references, our attempt might be worthy.

In Fig. 1.2 we show in a schematic way some possible approaches to analyze seismic activity, which even incomplete, may still provide useful information.

Catalog Completeness

The completeness of the catalog is one of the most important problems to be checked in order to obtain reliable results in any seismicity-related study. Besides, as shown by Habermann (1987, 1991), network configuration modifications and analyzing procedures can change as a function of time and introduce artifacts in the reported

magnitudes. These changes in the reporting history can introduce artificial variations of the *b*-value (Zuniga and Wyss, 1995).

Declustering

The declustering of the catalog (i.e., eliminating "dependent seismicity" – most obvious example are the aftershocks) is also an important issue, since the application of various statistical tests depends on the probability distribution of the events. For example, z-value statistical test (Habermann, 1983) compares the seismicity rates for two samples with a random (Poisson) distribution of events and, therefore, it is necessary to remove the aftershocks before applying the test. There are several declustering algorithms available, most commonly used being probably the one presented by Reasenberg (1985).

Seismic quiescence

While it is sometimes relatively easy to recognize a period of seismic quiescence only by eye, the application of a statistical test is necessary to quantify the significance of an anomalous change. As shown by Reasenberg and Matthews (1988), rather few quiescence anomalies, which were detected by eye, qualified as significant when they were tested statistically. In fact, Reasenberg and Matthews (1988) reported that the hypothesis of quiescence before larger earthquakes does not hold, when investigating several earthquake catalogs from United States and Japan. The authors concluded that many of the quiescence cases previously reported were not significant, being the result of a "biased" analysis.

The papers reporting quiescence before large events are, however, numerous and many of them use a rigorous statistical testing in order to assess the hypothesis. Thus, the anomalous decrease of seismicity rate before the 1978 Oaxaca major earthquake (M = 7.8), reported before the occurrence of the large event by Ohtake et al. (1977) is well documented and analyzed thoroughly and rigorously by Ohtake et al. (1981) and Habermann (1981, 1988). The quiescence anomaly was confirmed as a precursor of some large earthquakes in the wide area off the coast of the Tohoku district, Japan, by Ogata (1985, 1988), who used a reliable homogeneous data set. Wyss, Wiemer and their research group reported several cases of seismic quiescence around the world and proposed useful statistical tests to check the anomalous rate changes (see, for example, Wiemer and Wyss, 1994; Wyss and Wiemer, 1997). Still, the validation of quiescence as a reliable earthquake precursor is a debated subject.

Foreshocks

One of the most documented and generally accepted anomalous seismicity patterns is the relative increase in the events' rate preceding large earthquakes. Foreshocks were reported by Mogi (1985) for earthquakes in the Izu Peninsula, Japan, and their occurrence led to successful predictions in a few cases, such as the Haicheng, China, earthquake of 1975 (M = 7.5; Raleigh et al., 1977). Reasenberg (1999) discusses thoroughly the characteristics of foreshocks in world-wide catalogs over a 20 years interval. Foreshock activity typically becomes evident 5-10 days before the mainshock and rapidly accelerates up to its occurrence (Scholz, 1997). However, unfortunately, not all earthquakes are preceded by foreshocks. Besides, it is rather difficult to recognize the foreshock activity before the occurrence of the mainshock.

There are as well other seismicity patterns reported to have a precursory character. In a series of papers, Evison and Rhoades showed that swarms are often long-term precursors of large earthquakes, especially in the subduction regions (Evison and Rhoades, 1998).

Physical processes related to foreshocks ans quiescence

The seismic quiescence pattern and the foreshock activity briefly outlined above are probably among the most debated subjects in *Seismology*. Therefore, it is important to understand the physical mechanisms responsible for such anomalous changes of the seismicity rate. It is also important to know when such patterns occur and if there is any relationship between the temporal extent of the observed anomaly and the occurrence of a large earthquake. A thorough discussion on the subject, in the framework of the "seismic cycle concept", is made by Scholz (1997). We are going briefly to refer to this issue in the next section, "*1.3. Relating seismicity changes with crustal and/or earthquake processes".*

Aftershocks

Our presentation so far has been focused mainly on seismicity patterns that may have precursory character (the discussion on quiescence and foreshocks). However, there are other seismicity patterns that have been the subject of intensive study: the aftershock and swarm sequences. Both of them are the most obvious manifestation of earthquake clustering, both temporal and spatial. The aftershock activity following a large earthquake is well described by the so-called "Modified Omori Law", which describes the decrease with time of aftershock's rate (number of earthquakes / unit time). Chapter 3 of the thesis will introduce the most important characteristics of aftershock activity.

Other temporal seismicity patterns

There are as well other temporal seismicity patterns that have been investigated so far, as for example the presence of trends and cyclic behavior of seismic activity (review study: Ogata, 1999). The cyclic behavior might be related with the seasonal variations of precipitation, earth tides or other phenomena, which could act as triggering factors of earthquakes. The correlation between the Earth tides and earthquakes, in particular, has been the subject of many investigations. The present opinion, shared by most Earth scientists, is that the correlation between Earth tides and earthquakes is small or very small, probably not statistically significant (for a detailed study, see Vidale et al., 1998). The influence of external processes on seismicity, as well as the influence of seismic activity in a certain area on the seismicity in another region, are discussed in detail by Ogata (1999), together with some available code to check such correlations statistically. For the case of Vrancea (Romania) region, Enescu and Enescu (1999) investigate possible correlations between seismicity and some other geophysical phenomena: earth tides, geomagnetic jerks and the Chandler wobble.

ETAS model

As previously mentioned, many standard statistical tests to check for anomalous seismicity changes require the declustering of the earthquake catalog in advance. However, by eliminating the clustered seismicity some useful information is lost from the resulting data, not to mention the imperfections of the declustering algorithms themselves. To circumvent such problems, Ogata (1985, 1988) developed the *Epidemic Type Aftershock-Sequences* (*ETAS*) model for seismicity analysis. The basic idea behind the model is to consider that each earthquake has its own aftershocks and to model the process by using the Modified Omori law and a relation between aftershock productivity and the magnitude of the mainshock (see also Ogata 1999). One can then "measure" the deviations of real data from the model and reveal possible precursory seismicity changes.

Time-space-energy patterns and sophysticated modeling tools

The seismicity patterns discussed above are mainly temporal ones; however, their energetic and spatial characteristics are equally important. For example, the quiescence anomaly observed before large earthquakes occurs usually as a decrease in the number of events of moderate-size (it is also an energetic quiescence). Moreover, a characteristic "doughnuts" spatio-temporal pattern is sometimes observed (for more details and review, see Scholz, 1997).

In recent years, complex algorithms that can evaluate the characteristics of seismic activity in time, space and energy domain in an integrated way have been developed and applied to worldwide earthquake catalogs. The algorithm *CN*, for example, (Keilis-Borok and Rotwain, 1990) is structured according to a pattern recognition scheme to allow a diagnosis of the *Times of Increased Probability* (*TIPs*) for the occurrence of strong earthquakes. It indicates the probable occurrence, inside a given region and time window, of events with magnitude greater than a fixed threshold M_0, on the basis of a quantitative analysis of the seismic flow. The quantification of the seismicity patterns is obtained through a set of empirical functions of time, evaluated on the sequence of the events occurred in the analyzed region, and describing the level of seismic activity, seismic quiescence and space-time clustering of events. By performing an adapted *Principal Component Analysis* (*PCA*) of seismic activity in Southern California, Tiampo et al. (2002) showed that seismicity is a highly correlated process, across many time and space scales. The RTL algorithm is another example of a spatio-temporal approach to quantify seismicity changes (see, for example, Huang et al., 2002). *ETAS* model has been also extended to space-time patterns by Ogata (1998, 2003) and applied to describe the seismic activity in and around Japan (Ogata, 2003). Other recent approaches were concerned with the modeling of earthquake activity by considering the static stress changes produced by large events or other phenomena (for example, magma intrusion) (Toda et al., 1998, 2002). Spatial statistical features of seismicity using data sets that include focal mechanisms have been also investigated (for example, Kagan and Jackson, 1998).

Fractal, multifractal

The fractal and multifractal properties of earthquakes are closely related with the spatial and temporal clustering of the events. We will discuss in detail about this topic in Chapter 5 of the thesis. Closely related are the studies of Kagan and Knopoff, in early ’80, who discuss the spatial correlation of earthquakes (for example, the two-point correlation function: Kagan and Knopoff, 1980). Long-range correlation and temporal clustering is sometimes still evident even when aftershocks are removed from the catalog, but it is not clear why this clustering is occurring (Ebel and Kafka, 2002).

b-value

Probably one of the most studied seismicity parameters is *b*-value, the slope of the frequency-magnitude relation. We will discuss in Chapters 2, 3 and 4 about the *b*-value

temporal and spatial distribution and its correlation with the stress changes and crustal structure.

Simulations

We can not conclude this sub-chapter without mentioning about various simulation techniques that were used for better understanding seismicity patterns. The spring-block model of Burridge and Knopoff (1965) is the first computer model of a fault. Even it is very simple, produces seismic sequences remarkably similar with the real ones. A review and very good explanations on the subject can be found in Hergarten (2002). More realistic simulations of earthquake activity include the model of a "*Cellular Fault Zone embedded in a 3D Elastic Solid Containing Asperity and Non-Asperity Regions*" (Ben-Zion and Rice, 1993). The model consists of an upper crust overlying a lower crust and a mantle region, together defining an elastic half-space with a vertical half-plane fault. Such a model will be analyzed in Chapter 5 of the thesis.

1.3 Relating seismicity changes with crustal and/or earthquake processes

As we mentioned before, the relation between various seismicity patterns and physical processes is better understood if we consider the model of the seismic cycle. The release of stress after a large event, followed by the accumulation of stress due to tectonic processes and the occurrence of a new large event when the rocks' breaking strength is reached is a simplified explanation of the earthquake cycle model. Scholz (1997) reviews different precursory phenomena in the framework of the seismic cycle concept. Different types of seismic quiescence and earthquake activation are described, together with their possible physical interpretation. The author presents two broad families of physical models: those based on fault constitutive relations, which predict fault slip behavior but no change in properties in the material surrounding the fault, and those based on bulk rock constitutive relations, which predict physical property changes in a volume surrounding the fault. In the next chapter we will attempt an interpretation of the premonitory phenomena before Kobe earthquake by using the seismic cycle model.

We also discuss possible physical explanations for changes of various parameters characterizing earthquake activity: *b*-value, *p*-value of the Modified Omori law and the fractal dimension.

The Self-Organized Criticality (SOC) theory, developed by Bak and his coworkers (Bak et al., 1987), has been used to explain various natural phenomena. The theory states that large interactive systems will self-organize into a critical state (one governed by a power law). Once in this state small perturbations will result in chain reactions, which can affect any number of elements within the system. This concept is often used as an argument for the difficulty (or even impossibility) to predict earthquakes, as the earth crust itself might be in such a critical state. Details into the subject can be found in Scholz (1997) and Hergarten (2002).

The structure of the crust and upper mantle is an important factor to control the characteristics of earthquake activity. For example, the heterogeneity and the thermal gradient of the crust have a significant influence on the frequency-magnitude distribution of earthquakes, as we know from laboratory experiments and the analyses of real data (see next chapter). As has been pointed out (Sibson, 1984; Ito, 1990), the cutoff depth of seismicity is mainly dominated by the thermal structure of the crust. In addition, large earthquakes are likely to nucleate at the deep cutoff areas or in regions where the seismogenic depth has a steep change (Ito, 1992).

The study of static and dynamic stress changes produced by large events greatly helps to interpret the triggering and interaction of earthquakes. G.C.P. King, R. Stein, S. Toda and their collaborators have researched the relation between Coulomb stress changes and seismicity patterns for many earthquake sequences (for example, King et al., 1994, Toda et al., 1998, 2002). By combining the ΔCFF (Coulomb Failure Function) changes with a laboratory-based rate-and-state constitutive law (Dieterich, 1994), they modeled remarkably well the temporal and spatial evolution of seismicity. Such an analysis proves to be useful for seismic hazard assessment and earthquake forecasting (Toda and Stein, 2002). The stress induced by the passage of large amplitude seismic waves can also trigger earthquakes, sometimes at very large distances (see, for example, Anderson et al., 1994; Gomberg and Davis, 1996). The “dynamic triggering” phenomenon is a subject of active current research.

Chapter 2

-THE EVOLUTION OF SEISMICITY IN TIME AND SPACE, BEFORE AND AFTER THE 1995 HYOGO-KEN NANBU EARTHQUAKE (KOBE EARTHQUAKE)-

2.1. Introduction

A major earthquake (M_J = 7.2, M_W = 6.9) struck the south-western part of Japan on January 17, 1995. The Hyogo-ken Nanbu earthquake (Kobe earthquake) had a big impact not only in Japan, but also world-wide (Irikura and Ando, 1996). Some reports indicated that after the major event there was a clear increase in seismicity, in addition to aftershocks, surrounding the source area of the main shock (Katao and Ando, 1996). Hashimoto (1996) showed that the stress changes produced by the main shock might have caused the seismicity increase, observed over a broad area. Results of the GPS surveys show post-seismic ground deformations over a wide region (Hirahara et. al., 1996). In addition, precursory changes in ground deformation, decrease in earthquake frequency (Yoshida, 1995; Watanabe, 1998) and changes in ground water chemistry (Tsunogai and Wakita, 1996) were reported in and around the source area, within 34-36^0 N and 134-136^0 E.

In this chapter we analyse the evolution of seismic activity from 1976-1998, with special focus on possible premonitory changes, associated with the major Kobe earthquake, over a wide area of the seismic rupture zone. These precursory changes are studied by several different approaches, such as the distribution in time and space of seismicity, seismicity rate changes (z-values), b-values, and fractal dimension (correlation dimension, D_2) values. There are very few constraints imposed to the input data. Therefore, we believe that the results accurately reflect the seismicity evolution in time and space, during the studied period.

2.2 Outline of analysis methods

In order to analyse possible anomalies in the spatial and temporal evolution of the seismic activity, we first decluster the original catalogue described in Section 2.3, using a method developed by Reasenberg (1985). We also analyse its completeness using a

method proposed by Rydelek and Sacks (1989), as shown in Section 2.3. Section 2.4 presents the seismicity changes in time and space using the declustered catalogue. Using histogram representations of the number of earthquakes per month, diagrams of the cumulative number of earthquakes in time, and time-depth representations of the earthquakes for the declustered catalogue, we describe qualitatively the seismicity evolution during the studied period. In order to assess the significance of the observed changes in seismicity, we use a *z*-value parametric statistical test (see, for example, Wiemer and Wyss, 1994) and another test based on the Poissonian distribution of earthquakes (Ohtake et al., 1981). In Section 2.5 we study the seismicity change using the original catalogue. The evolution of seismic activity is compared with the variation in the fractal dimension (correlation dimension, D_2) of the epicentral distribution of earthquakes and *b*-value in time. Other geophysical precursors are compared with the seismological ones found in this study in Section 2.6. For the computations performed in this chapter we have used the *Zmap* program (Wiemer and Zuniga, 1994; Wiemer, 2001) and several routines written in *Qbasic*, available for downloading from my web page.

2.3. Data

The earthquake catalogue used consists of 19,604 shallow depth (h < 30 km) events with $M_J^* \geq 1.5$, occurring in the area delimited by 34-36^0 N and 134-136^0 E, between the years 1976-1998, recorded at the Abuyama Observatory, Kyoto University. The data were recorded by a telemetered network of 11 stations. The observation system has been changed twice, improving from analogue to digital recorders in 1980, and the dynamic range has been improved greatly by changes to the system in 1995. However, the 15km station spacing and accurate time keeping within 10 ms were enough to obtain accurate hypocenters through the observation periods. The phase picking was done by a person on the basis of the same criteria throughout the period. There was no essential lack of stations. Therefore, the same quality of hypocenter determination has been maintained for more than 20 years.

The original catalogue of the Abuyama Observatory, however, is not complete for moderate to large events with magnitudes greater than 3.5, because of the high-gain and

* M_j type magnitude is used throughout this chapter

small-dynamic range of the observation system. Therefore, the original catalogue is supplemented by bulletins of JMA (Japan Meteorological Agency) for large earthquakes. The study area was chosen to be large enough to determine the spatial extent of the seismic precursory phenomena related to the 1995 Kobe earthquake (M_J = 7.2) as shown in Fig. 2.1.

Catalogue declustering

The aftershock populations are identified by modelling an interaction zone around each earthquake in the catalogue. Any earthquake that occurs within the interaction zone of a prior earthquake is an aftershock and should therefore be considered statistically dependent on it. Events thus associated are referred to as belonging to a cluster. The interaction zones are modelled with one spatial and one temporal parameter. The spatial extent of the interaction zone is based on an estimate of the stress redistribution in the vicinity of each earthquake. Omori's law is used to determine the temporal extent of the interaction zone. The algorithm replaces each of the clusters with an equivalent event whose origin time is that of the cluster's largest event, whose epicentre is the mean position of the cluster, and whose magnitude corresponds to the cumulative moment of the cluster. Several parameters have to be chosen for the declustering procedure. Among them, errors of epicentre location and depth are of critical importance. These values were taken, after looking for the most appropriate result, as 1 km and 1.5 km, respectively. Other parameters were chosen as τ_{min} = 1 day, τ_{max} = 10 days, $P1$ = 0.95%, and R_{fact} = 20km, where τ_{min} is the look-ahead time for the unclustered events, τ_{max} is the maximum look-ahead time for clustered events, $P1$ is the probability of observing one or more events during the interval $(t, t + \tau)$, and R_{fact} is the factor for the interaction radius of dependent events. A detailed description of the parameters can be found in Reasenberg (1985) and ZMAP program documentation (Wiemer and Zuniga, 1994).

Figures 2.1a and 2.1b show the epicentral maps of the undeclustered and declustered catalogues, respectively. Figures. 2.2a and 2.2b show the cumulative number curves for the undeclustered and declustered catalogues. Obviously, the declustered catalogue has fewer events. When inspecting these cumulative-number plots after the occurrence of the Kobe earthquake, it is noticed that the curve in Fig. 2.2b is nearly linear, unlike the

non-linear one in Fig. 2.2a. This result verifies the validity of the declustering procedure.

Analysis for completeness of catalogue

Day-to-night noise modulation is used to develop a completeness test for earthquake catalogues, based on the assumption that the catalogues are Poissonian (Rydelek and Sacks, 1989). We assume that catalogues are complete when they indicate no significant modulation. Figure 2.3 concisely explains the method. The algorithm uses the simple idea that if a catalogue is incomplete in a certain magnitude band, it is expected that more of the events within this magnitude band are logged by night than during the day, because the cultural noise sources are diminished at night.

Figure 2.4 (a, b, c, d and e) shows the phasor sum plots for the declustered catalogue, for different magnitude bands. The plots are time oriented and scaled such that a confidence level of 95% is drawn with constant radius. If the walkout does not span the 95% confidence level for a certain magnitude band, the catalogue is considered complete at this level of confidence. In all tested magnitude bands the catalogue is proved to be complete. Of course, we are especially interested to test the completeness of the catalogue for smaller magnitudes. The following section explains how we used this test for events during the quiescence period of seismicity.

The results obtained in this section confirmed the good quality of the catalogue data used in this study. Furthermore, we carefully checked the catalogue for possible man-made changes in seismicity, for example missing stations or a change of analyst compiling the earthquake bulletin, before providing evidence for possible genuine anomalies in seismicity. The comparison between Abuyama Observatory data and JMA catalogue strengthened the quality of the catalogue used.

2.4. Seismicity change by use of the declustered catalogue

Section 2.2 briefly outlines the procedures that we used to examine the declustered catalogue. This section explains the statistical tests that we applied to catalogue analysis.

Method

In order to assess the significance of the observed changes in seismicity, we used a z-value parametric statistical test. This test compares the means of two independent samples. Because we want to compare seismicity rate changes, the means are in this case the average rates during two time periods (Habermann, 1983). The z value is defined as:

$$z = \frac{(m_1 - m_2)}{\sqrt{\frac{\sigma_1^2}{n_1} + \frac{\sigma_2^2}{n_2}}} \qquad (2.1)$$

where m_1 and m_2 are the mean rates during two periods that we want to compare, σ_1 and σ_2 are the standard deviations of these rates, and n_1 and n_2 are the number of samples in each period, respectively. The resulting z-value has the same interpretation in terms of significance as the number of standard deviations from the mean of a normal distribution. As pointed out by Matthews and Reasenberg (1987), the absolute values of z may not be so reliable. One technique is to determine the significance of a given value of the statistical test through a series of simulations, using data with a known distribution (Habermann and Wyss, 1987).

This study compares the calculated z-value with all other z-values (Wyss and Habermann, 1988; Wyss and Fu, 1989). In order to apply the method, we need to choose a windowing scheme. We choose a Rubberband function, in which a fixed duration window (w_2) is slid through the data, one sample at a time, and the rate in that window is compared with the rate in a background window (w_1), which expands behind the first window. This scheme is used because it is possible at any given time to take the longest possible period for a background estimate. Thus, we obtain a $z(t)$ curve showing the time evolution of z-value. Positive z-values mean a decrease in seismicity rate in w_2 compared with w_1. Negative z-values suggest an increase in w_2 compared with w_1.

In order to give more confidence to our findings, we used another statistical test. Based on the assumption of a Poissonian process for the seismicity, the probability (p) of observing x events in the time interval t, is given by:

$$p(x) = [(kt)^x e^{-kt}] / x!, \qquad (2.2)$$

where k is the mean rate of occurrence. In this way we can get the significance level of a detected seismic quiescence (Ohtake et al., 1981).

In order to determine the spatial characteristics of the observed seismicity rate anomalies, we made *z*-value maps using the same Rubberband function. The procedure employed to calculate such maps (Wiemer and Wyss, 1994) consists of superposing a dense grid of points and calculating at each grid point the cumulative number curve. At each grid point, the *N* closest earthquakes are sampled. The value *N* is chosen to achieve the optimum trade off between significance of calculated *z* values and resolution. In this way, we can compute a *z(t)* curve for each grid point. A *z*-value map gives the value of *z* for a "reference year", and compares the seismicity rate in the moving window w_2 (which starts at the "reference year") with the seismicity in the background window w_1. To visualise the changes in seismicity, we assign each *z*-value a colour, and plot them at time *t* on a map.

Results and discussion

From Fig. 2.2b, it is noticed that even for the declustered data, the seismicity rate is about 6 times bigger after the 1995 Kobe earthquake than before. This observation agrees with regional background seismicity triggered by the 1995 Kobe earthquake (Liu and Fu, 1999; Nakamura, 1999). Similar observations of seismic activation after a big earthquake were seen in the 1992 Landers and 1989 Loma Prieta earthquakes (Hill et al., 1993; Reasenberg and Simpson, 1992). A possible explanation for this phenomenon is the static stress change after a big earthquake (Reasenberg and Simpson, 1992; Hashimoto, 1996; Toda et al., 1998; Nakamura, 1999).

Figure 2.5a shows the time-depth distribution of events with $M \geq 1.5$ from 1976 to 1998. The histogram in Fig. 2.5b shows the number of earthquakes per month, from 1976 to the 1995 Kobe earthquake. A distinct seismic quiescence pattern is seen in these figures, from 1993 to October 1994 approximately (about three months before the 1995 Kobe earthquake). Figure 2.5c shows the cumulative number graph together with the curve *z(t)* for the declustered data. The moving-window, w_2, has a time-length of 1.5 years. A very big positive value of 10.4 in February 1993 indicates the existence and the significance of the observed anomaly. The slope of the cumulative number curve also illustrates the existence of seismic quiescence. We obtained similar results for the location and significance of the anomaly for varying w_2, 1.6, 1.7 and 1.8. Figure 2.5c shows that there is a relative increase in the seismic activity rate before the premonitory quiescence.

The seismicity rate from 1976 to 1993 is about 28 events/month. Considering different time periods from 1993-October 1994 and using formula (2.2), we found that the probability of finding by chance the number of events that occurred in these time periods is less than 1.5. We therefore conclude that the seismic quiescence could scarcely have occurred by chance. In order to check the day-to-night noise modulation of the catalogue in the quiescence period, we applied the method described in Section 2.3 to the data from 1993 - 1995. Figure 2.6 shows the phasor sum plot of the events occurred between 1993 and 1995. The test band of magnitude is greater than or equal to 1.5 and the total number of events is 470. The circle shows the 95% confidence level. Figure 2.6 shows that the catalogue is complete at a significant level of 95%.

Figures 2.7a and 2.7b present z-value maps for the reference years 1982 and 1993, respectively. We chose $N = 200$ and a rectangular grid with a spacing of about 2 km. The length of the moving window, w_2, is 1.5 years. Figure 2.7a shows that, for the reference year 1982, there is no significant seismicity rate decrease, as is also confirmed from previous figures. The map for the reference year 1993 (Fig. 2.7b) shows a clear seismicity rate decrease (relatively big positive values of z) in the focal area of the Kobe earthquake, when the detected anomaly reaches its maximum (see Fig. 2.5c). There are also other regions (see Fig. 2.7b) in the studied epicentral area where the z-values are relatively large (see the yellow and red coloured zones in the figure). Figures 2.8a and 2.8b, which show the histograms of z-values corresponding to the reference years 1982 and 1993, confirm the difference between a "normal period" of seismic activity and an anomalous one. It is worth noting in Fig. 2.8b the preponderance of positive z-values and the existence of some very big z-values for the reference year 1993.

2.5. Seismicity change by use of original catalogue. b-value and fractal dimension changes in time for the undeclustered (original) catalogue

In order to apply different statistical techniques that require a Poissonian distribution of earthquakes, it was necessary to decluster the initial catalogue as described above. However, the removal of dependent seismicity could eliminate useful information. For example, the declustering procedure may eliminate the foreshock activity, which sometimes precedes a big event. Therefore, it was decided to use all the data in the catalogue when applying the analysis of fractal dimension and b-value change with time. Histogram representations of the number of earthquakes per month

and time-magnitude plots have also been used for a meaningful interpretation of the results.

Method

(1) Correlation dimension D_2:

Fractal analysis based on the correlation integral (Grassberger and Procaccia, 1983) has been used in this investigation, to study the evolution in time of the earthquake epicentral distribution. The variation of correlation dimension with time illustrates the temporal variation of seismicity clustering in space. The correlation dimension D_2 is obtained from:

$$D_2 = lim(r \rightarrow 0)\ log\ C(r)/log\ r, \tag{2.3}$$

where r is the distance between two epicentres (hypocentres), and $C(r)$ is the correlation function:

$$C(r) = 2N_{R<r}/N(N-1), \tag{2.4}$$

where $N_{R<r}$ is the number of event pairs separated by a distance R less than r.

The correlation dimension is estimated by fitting a straight line to a plot of *log C(r)* against *log r*. The minimum and maximum values of r are chosen taking into account the error in the epicentre location and the finite size of the study zone, respectively. In fact, it is not necessary to choose these values, and the only condition that must be accomplished is a good linearity of the data. In order to certify the fractal structure, a range varying over an order is considered sufficient. Besides, the determined values of D_2 are given with 95% confidence level. The maximum value of D_2 for the epicentral distribution of earthquakes is two, corresponding to a random distribution of epicenters (in the 2-dimensional space). Smaller values of D_2 suggest a tendency toward clustering. Clustering appears when there is a significant increase in the number of earthquakes in a certain localized area, for example in the case of earthquake swarms and aftershocks, or does not necessarily concern such an increase but only changes in the distances between events. Thus, prior to large seismic events, earthquakes make small clusters or patches of 7-20 km (Ouchi and Uekawa, 1986). The increase in clustering can be associated with the increase in background stress level (Huang and Turcotte, 1988). According to Trifu (1990), these precursory phenomena can be

interpreted as clusterings of shear-stress-free surfaces bringing the major asperity into relief.

(2) b-value:

The *b*-value in the Gutenberg and Richter's relation:

$$log\ N = a - bM \tag{2.5}$$

has been determined using the maximum likelihood method (Aki, 1965, Utsu, 1965), suggested as preferable because it yields a more robust estimate than the least-squares regression method.

With large samples and slow temporal changes in b, the standard error of *b* (see Shi and Bolt, 1982) is:

$$\sigma(b) = 2.30\ b^2\ \sigma\left(\bar{M}\right), \tag{2.6}$$

where

$$\sigma^2\left(\bar{M}\right) = \sum_{i=1}^{n}\left(M_i - \bar{M}\right)^2 / n(n-1). \tag{2.7}$$

In order to determine the evolution in time of D_2 and *b*-value, we used a moving-window technique, taking n = 500 and n = 200 events in a window, respectively. The threshold magnitude is chosen as 1.5 for the computation of D_2 and 2.0 in the case of *b*-value. A brief explanation concerning these selected values is given in Fig. 2.10 (see next section, *Results and discussion*).

Results and discussion

Figures 2.9a and 2.9b show histograms of earthquake number per month, with M ≥ 1.5 and M ≥ 2, respectively, from 1976 to January 17, 1995, which is the date of the Kobe earthquake. A clear seismic quiescence pattern can be seen between 1993 and June 1994 approximately, followed by a short increase in the seismic activity several months before the Kobe earthquake.

Figure 2.10a shows the change of D_2 value with time for the events of M ≥ 1.5, occurred before the 1995 Kobe earthquake, from 1976 to 1995. The errors associated with D_2 determination are smaller than the former ones. The clear decrease of D_2 in 1994 corresponds with the increased seismic activity observed just before Kobe

earthquake, and is apparently caused by the many clustered events before the main-shock, over a rather broad area. Another important decrease of the fractal dimension is seen in the year 1987 and, as can be seen in Fig. 2.9, this anomalous change corresponds well with another important increase of earthquake frequency. The results obtained by Enescu and Ito (2001a) on the fractal properties of the earthquake data slightly differ from those presented here. The difference is due to a better computational approach and an improved estimation of the scaling region in the present study, and consists mainly in a decrease of the average fractal dimension with about 0.4. The smaller value of D_2 reported here is in better agreement with other similar studies. Moreover, the overall evolution of D_2 correlates better with seismicity changes. The main result, however, (i.e. the large, significant decrease of the fractal dimension just before the 1995 Kobe earthquake) is the same in both studies.

In Fig. 2.10b, the evolution of *b*-value in time is indicated for the events with $M \geq 2.0$. The mean *b*-value in this area is about 0.8. Therefore, there are two significant changes in *b*-value: a decrease from 1984-1986 and an increase followed by a decrease, from 1991-1994. The former change is probably associated with the occurrence of several moderate-size earthquakes, including events with $M \geq 5$ (see Fig. 5a). While the level of incompleteness of the original catalog might have been higher after some of these larger earthquakes occurred outside regions A and B, our tests indicate that a smaller b-value during this time period is still statistically reliable. From 1991-1994, there is an increase of *b*-value, followed by a decrease just before the Kobe earthquake ($M = 7.2$). Smith (1981) reports similar anomalies before large earthquakes in New Zealand, California and Venezuela. The observed anomaly of *b*-value corresponds closely with the seismic quiescence pattern. Thus, the large decrease in *b*-value that occurred during 1994 has a precursory character, and correlates well with the increased seismic activity detected just before the Kobe earthquake (see the histograms in Fig. 2.9).

Figure 2.11 presents the evolution of *b*-value, from 1976 to 1998, in Tanba region, situated NE from the main-rupture area of the 1995 Kobe earthquake. A clear increase in *b*-value started about 2.5 years before the major event. This increase in *b*-value suggests that the quiescence anomaly already discussed is also an “energetic anomaly” (a relative increase in the number of smaller-size events, and relative decrease in the

number of larger ones). As one can notice, *b*-value "recovers" after the 1995 Kobe earthquake.

2.6. Correlation between the precursory phenomena found in this study and other geophysical precursors

Figure 2.12 shows the time evolution of the seismicity rate, *b*-value and fractal dimension, five years before the main shock. The discussed precursors can be easily recognized. The variation of strain and precipitation with time (DPRI, Kyoto University) are also presented in Figure 2.12. It is clear that the precursory variation of seismicity parameters corresponds well to the change in stress at the crustal deformation observation stations Yamazaki, Abuyama and Amagase. In a recent study, Hirose et al. (2003) found that the so-called O1 tidal constituent showed significant precursory changes for about 3 years before the occurrence of the 1995 Kobe earthquake. Their findings correlate well with our results on *b*-value temporal changes.

Tsunogai and Wakita (1996) discuss several non-seismic precursory phenomena, including strain changes and ground water anomalies. Ito and Enescu (2001a) discuss other reports of long-, intermediate- and short-term geophysical precursors occurred before the 1995 Kobe earthquake.

An important class of physical models that are used to explain anomalous changes before large earthquakes is based on the dilatancy phenomenon, which is an inelastic increase of the volume of rocks under high deviatoric stresses. Scholz (1997) reviews various precursors that can be well explained if such models are assumed (Scholz et al., 1973). The volume dilatancy-hardening model, in particular, predicts the decrease of earthquake frequency in a rather broad region (volume) surrounding the hypocenter of the following large event, as a result of pore pressure increase and rock strengthening. The intermediate-term seismic quiescence found in the case of Kobe earthquake, which was not confined to the fault zone alone, might be well explained by using such a model. Together with the changes of seismicity, the model also predicts water-flow anomalies and crustal premonitory deformations. These precursors were observed as well in the case of the Kobe earthquake.

We believe, however, that only one physical model can not explain all the precursors observed before the large event. For example, the occurrence of several foreshocks just on the day before the occurrence of the mainshock, in its immediate vicinity (Katao and

Iio, 1995), is most likely a manifestation of the nucleation process of the 1995 Hyogo-ken Nanbu earthquake.

2.7. Conclusions

1. There is a clear seismic quiescence pattern between 1993 and October 1994 approximately, followed by an increase in seismic activity, several months before the Kobe earthquake (M = 7.2). The significance of the anomalous quiescence was confirmed by *z*-value statistical tests.

2. The spatial extent of the quiescence anomaly covers not only the source area of the Kobe earthquake, but also some other areas in "neighbouring" regions. This indicates that the precursory phenomenon is not confined to the source area, but occupies a much larger region corresponding to the preparation zone of the future event.

3. The seismicity rate following the 1995 Kobe earthquake in the studied area is about 6 times bigger than before the major seismic event.

4. The decrease of the fractal dimension in 1994 corresponds clearly with the premonitory increased seismicity rate before the Kobe earthquake.

5. The *b*-value also shows an anomalous decrease in 1984-1986 and an anomalous increase and decrease in 1993-1994. The latter shows premonitory change before the Kobe earthquake. The cause of the former change is not clear, but it seems to be correlated with the occurrence of several moderate-sized earthquakes.

6. There is good agreement between the observed anomalies in seismicity rate, *b*-value and fractal dimension changes with time in the 2-3 years before the Kobe earthquake. This result gives us more confidence in our findings regarding the premonitory phenomena of the 1995 Hyogo-ken Nanbu earthquake.

Chapter 3

-SPATIAL ANALYSIS OF THE FREQUENCY-MAGNITUDE DISTRIBUTION AND DECAY RATE OF AFTERSHOCK ACTIVITY OF THE 2000 WESTERN TOTTORI EARTHQUAKE-

3.1. Introduction

Aftershock sequences offer a rich source of information on the Earth's crust and source properties of large earthquakes, because a very large number of events occur over a short period of time in a small area. Aftershocks also pose a significant seismic hazard, which under certain circumstances can even exceed the main shock hazard. Two basic relations describe the aftershock activity, the Gutenberg-Richter law (see Chapter 2), which describes the power-law size distribution of earthquakes, and the modified Omori law, which describes the decay of the aftershock activity. The *b*-value of the frequency-magnitude distribution has been observed to vary spatially as well as temporally. Recently, several studies revealed spatial variations in the frequency-magnitude distribution in various tectonic regimes (Wiemer and Benoit, 1996; Wyss et al., 1997; Wiemer and Wyss, 1997), by using high-quality earthquake catalogs and a technique of high-resolution spatial mapping of the frequency-magnitude distribution.

Many factors can cause perturbations in *b* from its standard value of about one. Increased material heterogeneity results in high *b*-values (Mogi, 1962a), while an increase in the shear stress or decrease in the confining pressure (Scholz, 1968, Wyss, 1973) decrease the *b*-value. In addition, an increase in the thermal gradient may cause an increase in *b*-value (Warren and Latham, 1970).

The occurrence rate of aftershock sequences in time is empirically well described by the modified Omori formula (Utsu, 1957, 1961):

$$n(t) = K/(t+c)^p \qquad (3.1)$$

where $n(t)$ is the frequency of aftershocks per unit time, at time t after the main shock. K, c and p are constants. The characteristic parameter p usually changes in value from 0.9 to 1.5, regardless of the cutoff magnitude. The variability in p-value may be related to the structural heterogeneity, stress, and temperature in the crust (Mogi, 1962b;

Kisslinger and Jones; 1991, Utsu et al., 1995). However, it is not yet clear which of these factors is most significant in controlling the *p*-value. The *K* value is dependent on the total number of events in the sequence and *c* on the rate of activity in the earliest part of the sequence. The constant *c* is a controversial quantity (Utsu et al., 1995). It is strongly influenced by the incompleteness of the catalog in the early part of a sequence. Careful analyses showed that the *c*-value is non-zero at least for some aftershock sequences. The parameters in the modified Omori formula can be estimated accurately by the maximum likelihood method, assuming that the seismicity follows a non-stationary Poisson process (Ogata, 1983).

Here, we present a detailed analysis of the *b*-value of the frequency-magnitude distribution and the *p*-value of the modified Omori law, for more than 4000 earthquakes, identified in the first four months after the M7.3 (on JMA scale) Western Tottori earthquake that occurred on October 6, 2000 in southwest Japan. In the first part of this study, we analyze the variation of parameters in broad areas, while in the second part a detailed spatial analysis is performed. The third part analyzes the seismic activity before the Tottori earthquake, in order to understand better the physical mechanisms of the variations of *b* and *p* values. The results we present are important not only for the source process of the Western Tottori aftershock sequence itself, but also for the basic understanding of the aftershock phenomenon. Previous studies found considerable spatial variability of *b* and *p* for different aftershock sequences (Kisslinger and Jones, 1991; Guo and Ogata, 1997). Wiemer and Katsumata (1999) found significant spatial variation within one aftershock sequence for Landers, Northridge, Morgan Hill and Kobe aftershocks. More work has to be done, however, in order to understand the variation patterns and their underlying physical mechanism.

3.2. Data used and method of analysis

We used the JMA (Japanese Meteorological Agency) catalog for the study of the aftershocks of the Tottori earthquake. We selected all events with $M \geq 2$ that occurred from the time of the main shock (October 6, 2000) until January 24, 2001. The epicenters are included in a rectangle defined by $133^0$05'E to $133^0$45'E and $35^0$06'N to $35^0$27'N (Fig. 3.1a). The symbol A in Fig. 3.1a indicates the main aftershock area. The main aftershock area is presented alone, in Fig. 3.1b. B and C in Fig. 3.1a correspond to areas where the earthquake activity started about 2.5 days after the main shock. The

earthquakes in these regions are not aftershocks in a strict sense; however, we considered it appropriate to include them in this analysis, since they are probably triggered by the main shock. It has been shown, by using the Coulomb failure criterion (Earthquake Prediction Information Division, JMA, 2001), that these events occurred in regions where the static stress (stress associated with co-seismic fault displacements) increased due to the main shock. As we will see in the next section, the seismic activity in region B is well described by the modified Omori law. For these reasons, we will refer to the seismic activity in these areas as aftershocks. The examination of travel time data for earthquakes used in this study gave us confidence in the earthquake epicenters, since the events of magnitude greater than 2 have a sufficient number of P and S wave arrival times. We used the DPRI, Kyoto University, catalog extensively in order to test whether the results are similar with those obtained from the JMA catalog. We find similar results using the two catalogs. However, we use the results from the JMA catalog, since its magnitude of completeness is smaller for the earliest part of the aftershock sequence.

For the estimate of both the *b* and *p* values, it is important to use a data set that is complete for all magnitude bands included in the analysis. The estimate of the magnitude of completeness (*Mc*) is based on the assumption of a power-law Gutenberg-Richter relationship and taken as the magnitude where the first derivative of the frequency-magnitude curve has its maximum. For region A, we used an overlapping moving window technique to compute *Mc* as a function of time. We choose 150 events/window, the window being moved by 15 events. Figure 3.2 shows the variation of *Mc* with time. *Mc* is highest at the very beginning of the sequence (around two hours), and then decreases very quickly to about 2.3. Four days after the main shock *Mc* reaches a stable value around 2. This is because just after the main shock, when many aftershocks occurred, the data processing was restricted to larger events. Region B has only around 300 events; therefore the completeness magnitude is determined for all the shocks and not as a function of time. In region C the number of events with $M \geq 2.0$ is very small (less than 50) and consequently we exclude these shocks from further analysis.

In Subsection 3.3.1 we present the results obtained by analyzing regions A and B (Fig. 3.1a) separately. Also, based on the difference in the characteristics of the earthquake sequences, we select two sub-regions, A1 and A2 (Fig. 3.1b), inside the

main aftershock area (A) to study the individual *b* and *p* values in relation with the rupture process and the structure of the crust.

In order to ensure completeness in our analysis, two parameters need to be adjusted: (a) a minimum magnitude threshold *Mmin* and (b) a minimum time threshold T_{start}, i.e. excluding the first several hours to days from the analysis. We checked some values and chose *Mmin* = 3.2 and T_{start} = 0 to determine the frequency-magnitude distribution and the parameters of the Omori law for regions A, A1 and A2. In this way, even though the number of earthquakes is drastically reduced, we can include in the analysis the earliest part of the sequence and assure completeness. For region B, *Mmin* = *Mc* = 2.0 and T_{start} = 0 were chosen.

Due to the large number of events in region A, a more detailed spatial analysis is possible. The method employed is based on a gridding technique, which is described in detail at the end of this section. The obtained results are presented and discussed in Subsection 3.3.2. All the shocks with M ≥ 2.0 are included except for the events in the first 17 hours (0.72 days) after the main shock. The overall magnitude of completeness has a value around 2.2. By doing this, we do not include data with severe incompleteness, but have enough remaining events for a meaningful spatial analysis. In addition, the completeness magnitude is checked spatially, as outlined below.

The *b*-value in the frequency-magnitude relation has been determined using the maximum likelihood method (Aki, 1965; Utsu, 1965), because it yields a more robust estimate than the least-squares regression method. The standard error of *b*-value has been determined in the same way as in Chapter 2, by using the formula of Shi and Bolt (1982). The *b*-value and its standard error are computed also using a least-square method. The results obtained using the two approaches (maximum likelihood and least square) are similar in general, indicating that the determined *b* values do not depend on the method used.

We estimate the probability that two samples may come from the same population by Utsu's (1992) test.

$$Prob \approx exp(-dA/2-2), \tag{3.2}$$

where

$$dA = -2N\, ln(N) + 2N_1\, ln(N_1 + N_2 b_1/b_2) + 2N_2\, ln(N_1 b_2/b_1 + N_2) - 2,$$

and

$$N = N_1 + N_2,$$

where, N_1 and b_1 are the number of earthquakes and the b-value for the first sample, respectively; N_2 and b_2 are the number of earthquakes and the b-value for the second sample, respectively.

The parameters in the modified Omori formula can be estimated accurately by the maximum likelihood method, assuming that seismicity follows a non-stationary Poisson process (Ogata, 1983). The method allows one to obtain the asymptotic standard error of the maximum likelihood estimates, based on the variance-covariance matrix of the model. To establish the significance of differences between p values, we use the 95% confidence limit (1.96 standard deviations) of the difference in the standard deviations of the two p values.

For all our computations, we used the computer programs ASPAR (Reasenberg, 1994) and ZMAP (Wiemer and Zuniga, 1994; Wiemer, 2001). The new release of ZMAP (version 6 – freely available on Stefan Wiemer's home page, http://seismo.ethz.ch/staff/stefan/) includes most of the routines we wrote or adapted for Matlab and used for aftershock analyses. The routines are provided with instructions and explanations on their use.

In order to visualize the frequency-magnitude distribution and the decay rate of aftershocks in region A, we used a dense spatial grid of points and consider the nearest epicenters (*Ne*) for each node of the grid. For each node we estimate the goodness of fit for the observed frequency-magnitude distribution. The algorithm (Wiemer and Wyss, 1999) then determines the minimum threshold magnitude for which the goodness of fit is greater than or equal to 95%. If there is no such magnitude for the given confidence level, a 90% goodness of fit is assigned instead. If, however, the goodness of fit is less than 90% for any threshold magnitude, the magnitude where the frequency-magnitude distribution has its maximum curvature is determined. One of these magnitudes becomes the *Mc* for that grid point. If the number of earthquakes with $M \geq Mc$ is larger than or equal to Ne_{min}, b and p values are computed for that node by using only the earthquakes with $M \geq Mc$. Otherwise, the b and p values are not computed. Various values for the spacing of the grid and for *Ne* and Ne_{min} were chosen, in order to check the consistency of the results. The b and p values estimated in each node are translated into a color code. For a more detailed discussion of the spatial mapping of the b-value, refer to Wyss et al. (1997). The spatial mapping of the parameters was done by using the software ZMAP.

In the last part of our study (Subsection 3.3.3) we analyze the seismic activity that occurred before the Tottori earthquake, in order to get a better understanding of the variations of the pattern of *b* and *p* values. We have used the catalog of DPRI, Kyoto University, and selected all the events with magnitudes larger then or equal to 1.5 that occurred between 1978 and the main shock, in an area corresponding roughly with the region A1 in Fig. 3.1b. The overall magnitude of completeness is 1.5. The DPRI catalog was chosen for its better quality compared with the JMA catalog in the same period of time, but both catalogs were used for checking the compatibility of the results. Since the seismic activity before the Tottori earthquake is analyzed mainly as a function of time, the location of events is not an important issue in this case. Therefore, by choosing a lower threshold magnitude (1.5), the accuracy of the results is not affected by possible location errors.

3.3. Results and Discussion

3.3.1 Characterization of the aftershock activity in broad areas

Figures 3.3a and b present the cumulative number of earthquakes versus time for regions A and B, respectively. One can easily see the decreasing characteristics of the aftershock sequence. The largest aftershocks in both regions are indicated by stars in Fig. 3.3.

Figure 3.4 represents the space-time distribution of the earthquakes in Region A. The projection is taken along a profile D_1D_2, indicated in Fig. 3.1b. There are three M4.5 aftershocks very close temporally and spatially to the main shock. The other two M4.5 shocks and the largest aftershock (M = 5.0) are located NW from the main shock epicenter. Another qualitative observation can be made in Fig. 3.4: the earthquake frequency in the NW part (closer to D_1 in Fig. 3.1b) seems to decay slower with time than in the SE region. Later (Subsection 3.3.2) we show that a large region in the northwest is characterized by smaller *p*-values (≈ 0.8), while the region in the southwest has larger values of *p* (= 1- 1.35).

Figures 3.5a) and b) show the frequency-magnitude relation for the regions A and B, respectively. The magnitude of completeness was determined with the procedure outlined before, based on the goodness of fit of the data. We found that the completeness magnitude is 3.2 and 2.0 for the regions A and B, respectively. The magnitude of completeness in region A is the same as the largest value found for *Mc* as

a function of time (Fig. 3.2). Using these magnitudes of completeness we determined the *b*-value and its standard deviation, as well as the *a*-value of the Gutenberg-Richter relation. The rather large value of *b* (= 1.28) in region A shows a relative abundance in small earthquakes. The *b*-value in region B is close to 1.0.

Figure 3.6a shows the occurrence rate of aftershocks in region A considering two cases: for all the events with M ≥ 2.0 and only for the events with M ≥ Mc (= 3.2). T_{start} is assumed to be 0 in both cases. The *p*, *c* and *K* parameters were obtained using the maximum likelihood procedure and the occurrence rate was modeled by the modified Omori formula (equation 3.1). The obtained parameters (Fig. 3.6) have small standard deviations and the quality of fit is very good in both cases, according to the chi-square test. There is no significant difference in the *p*-value between the two cases. However, the *c*-value shows a significant difference. This result agrees well with that of Utsu et al. (1995). They pointed out that the *p*-value is independent of Mmin, but the *c*-value depends heavily on the magnitude completeness of the data. We can conclude that for the whole aftershock region the value of *p* is close to 1 and the *c*-value is around 0.01 days. We have tested our parameters for other values of $Mmin \geq Mc$. The result does not change significantly: *p*-value remains around 1 and *c*-value is about 0.01 days or slightly less. The values obtained for *Mc*, *b* and *p* in region A are very close with those determined by the Earthquake Prediction Information Division, JMA (2001).

Figure 3.6b shows the occurrence rate of aftershocks in region B, for events with $M \geq Mc$ (= 2.0). The origin time corresponds to the M5.5 earthquake occurrence. The standard deviations of parameters are small and the chi-square test indicates a good fit, as shown in Fig. 3.6b. The *p*-value is 0.83 +/- 0.03 and *c* = 0.008 +/- 0.007 days.

The *p*-value obtained for region A is close to one. Mogi (1962c) estimated *p* values for 31 aftershock sequences in Japan, and discussed their geographical distribution. In general, *p*-values are high for sequences on the Japan Sea side and low on the Pacific Ocean side. Mogi (1967) thought that the aftershock activity decays faster ($p \geq 1.3$) in regions of higher crustal temperature where the stress relaxes faster, based on the distribution of surface heat-flow values which are higher on Japan Sea side and lower on the Pacific Ocean side. The *p*-value for region A seems to be an exception, from this point of view. The *p*-value in region B has a relatively small value, indicating a slow decrease of earthquake rate in time. We attempt to explain this rather low value of *p* in

Subsection 3.3.2, when more information about the *p*-value variation in space will be available.

There are two opinions regarding the value of *c*: one is that essentially *c* equals to 0, and all the reported positive *c* values result from incompleteness in the early stage of an aftershock sequence and another is that positive *c*-values do exist. In the first case, if *c=0*, n(t) in equation (2) diverges at *t=0*. According to Kagan and Knopoff (1981) this difficulty can be explained by considering that the main shock is a multiple shock composed of numerous sub-events occurring in a very short time interval. In some cases, positive *c*-values have been obtained for well-observed and selected data (see Utsu et al., 1995). Yamakawa (1968) considers that the larger *c*-value ($c > 0.01$days) reflects more complex features of the rupture process of the main shock. In our case, the fit of the decay rate of earthquakes in region A indicates that *c*-value is small (about 0.01 days or less), but has probably a non-zero value. In the case of region B, the *c*-value is certainly very small, probably 0 or very close to 0. Based on the results obtained for both regions A and B, the *c*-value may reflect features of the rupture process, which is more complex for larger magnitude earthquakes.

So far, we presented a comparative analysis of aftershock activity in the regions A and B. The rather large area and the number of earthquakes available justifies a more in depth analysis for region A. Therefore, we have chosen two sub-regions A1 and A2 (Fig. 3.1b) in Region A and analyze the parameters for these two areas. The areas were selected based on some characteristics of the seismic activity. The sub-region A1 corresponds to the areas ruptured by previous moderate events (M is about 5) in the swarm-like activities in 1989, 1990 and 1997 (Shibutani et al., 2001, 2002). Also, this area corresponds roughly with the largest slip on the fault during the main shock (Yagi and Kikuchi, 2000; Sekiguchi and Iwata, 2000). Sub-region A2, situated in the NW portion of region A, had not ruptured for more than 20 years before the 2000 main shock. In addition, as pointed out by Ohmi et al. (2001) and Fukuyama et al. (2001), the aftershock activity extended towards the northwest (and also in the SE extremity) about one hour after the main shock. As shown in Fig. 3.1b, the seismicity in sub-region A2 is more diffuse than other parts of the aftershock area. These observations suggest that the A1 and A2 regions have different characteristics and are good candidates for comparing the aftershock activity.

Figure 3.7 shows the frequency-magnitude distribution for the regions A1 and A2, for events larger than or equal to 3.2 (the magnitude of completeness for region A).

Region A1 is characterized by a large *b*-value of 1.42 +/- 0.1, while region A2 has a *b*-value close to 1.0. This result suggests a correlation between the rupture process and the *b*-value spatial distribution. Region A1, which experienced rupture during the previous earthquake swarms and also during the 2000 Tottori main shock is characterized by a large *b*-value, while region A2 (as well as region B studied before) has a lower value of *b*. Utsu's test confirms that the two frequency-magnitude distributions are significantly different. When checking the *p*-values for the A1 and A2 areas we could not find a significant difference between the two regions.

We tried to fit other models to the data, like the exponential model, suggested in several studies (Utsu, 1957; Mogi, 1962c; Watanabe and Kuroiso, 1970) as being more appropriate for describing the decay of aftershock activity in later periods of the sequence. For our sequence, the Omori law seems to better describe the occurrence rate decay for all the period considered. Both Utsu (1957) and Mogi (1962c) show that for about 100 days after the main shock, the decay rate is better modeled by Omori's formula for many cases. In our case the total period under consideration is about 110 days.

3.3.2 Detailed spatial distribution of b and p values in Region A

Figs. 3.8a and b) show the spatial variation of *b* and *p* values in more detail, using the procedure described in Section 3.2. The grid used has a nodal separation of 0.002^0 (about 0.2 km). The closest $Ne = 150$ events for each node were considered and Ne_{min} is taken as 100. Thus, *b* and *p* values for each node are computed by using between 100 and 150 earthquakes. The parameter values for nodes where the sampled earthquakes (150) are within $r = 2$ km distance from the node are represented by using a color code, on the map. *Ne* and *r* can be thought as resolution parameters. An important assumption is that we chose a fixed $c = 0$ days, in the modified Omori formula for the estimation of *p*-value, since T_{start} (= 0.72 days) is much larger than the value of *c* (≈ 0.01 days) for region A. The magnitude of completeness was carefully checked for each node of the grid, as explained in Section 3.2. The magnitude of completeness varies spatially between 2.0 and 2.3, but, for most of the nodes, it has a value of 2.0. As a consequence, *b* and *p* values were determined using 150 events for most of the nodes. The range of values for *Mc* agrees with the decreased values of about 2, observed after several hours when studying *Mc* as a function of time (Fig. 3.2).

The *b* and *p* values, obtained as described above, are shown in Figs. 3.8a, and b, respectively. The *b*-values in Fig. 3.8a vary between about 0.8 and 1.4. The goodness of fit for the frequency-magnitude distribution at each node is between 86% and 98%. However, the goodness of fit is larger than or equal to 95% for most nodes. The standard deviation of *b* values varies spatially between 0.06 and 0.13, with most of the standard deviations less than 0.1. The *p*-values in Fig. 3.8b vary between 0.51 and 1.35 with standard deviations less than 0.1.

In order to demonstrate the difference of *b* values clearly, we have chosen two regions R1 and R2 (Fig. 3.8a), having 150 earthquakes each, and compute their frequency-magnitude distribution. The graphs, together with some relevant parameters, are presented in Fig. 3.9. As can be seen, the *b*-value for region R1 is 0.79 +/- 0.06, while 1.27 +/- 0.10 for region R2. The probability that the two distributions come from the same mother population, as computed by Utsu's test, is very small (= 0.00016).

The differences in *p*-value for the regions R3, R4 and R5 (Fig. 3.8b) were also tested and the results are presented in Figs. 3.10a and b. The sample in region R3 includes 633 earthquakes and its *Mc* equals 2.0. The *p*-value obtained for this sample is 0.86 +/- 0.03. For region R4, we sampled 123 earthquakes, with $Mmin = Mc = 2.0$, and obtained $p =$ 1.31 +/- 0.07. The graphs in Fig. 3.10a show clearly that the distributions from regions R3 and R4 are different. Also, applying the test suggested in Section 3.2, the difference is found significant at 95% confidence limit. In Fig. 3.10b we compare the decay of aftershock activity in the regions R3 and R5. The *p*-value for region R5 is 1.31 +/- 0.07. Again there is a significant difference between the two distributions. Checking the decay of the occurrence rate for small samples in the NW part of the aftershock area, we found a decreased goodness of fit for the Omori formula. For this reason, we believe that some very small values of *p* (0.5-0.8) are not determined well. Figure 3.10a shows that when using larger samples the *p*-value is well resolved, so there is a significant difference in *p* values between the regions R3 and R4 and also between R3 and R5.

In the previous subsection we showed that the area of large slip during the mainshock (region A1) is characterized by a large *b*-value, while the regions A2 and B have smaller values of b. Figure 3.8a shows *b* values between 1.0 to 1.4 in an area extending roughly 10km on both sides of the main shock, with the exception of a small patch P1 (Fig. 3.8a). The slip distribution on the fault of the main shock for the Tottori earthquake (Yagi and Kikuchi, 2000 and Sekiguchi and Iwata, 2000) shows that slip occurred approximately 10km on both sides of the epicenter of the main shock, along a

NW-SE oriented striking fault. Thus, the larger values of *b* in Fig. 3.8a correlate with the region where large slip occurred during the main shock. However, largest slip occurred in the southeast region of the earthquake fault where *b*-value is not largest in value. We believe that the history of previous ruptures together with the slip during the main shock are both responsible for the distribution of *b*-value (see fig. 3.8c).

The patch P1, an "island" of small *b*-values surrounded by larger ones, seems to correspond to a slight change in the strike of the fault of the main shock, as can be seen from the aftershock distribution. It is plausible to assume that this change may have affected the distribution of *b*-value. Probably a very detailed knowledge of the evolution of rupture process and the fault characteristics can explain such exceptions like the patch P1.

Wiemer and Katsumata (1999), by mapping the distribution of *b*-value within the M7.2 Landers, M6.7 Northridge, M6.2 Morgan Hill and M7.2 Kobe aftershock sequences, found for all four cases that the *b*-value tends to be high near the area of largest slip of the main shock. In the case of the Tottori earthquake both the history of previous ruptures and the slip during the main shock seem to be responsible for the observed spatial patterns of *b*-value. Wiemer and Katsumata (1999), when studying the *b*-value spatial distribution for the aftershocks of Landers earthquake, found an increased *b*-value not only in the region where the slip was largest during the main shock, but also in the area that ruptured about 2 months before in the M6 Joshua Tree event, which occurred relatively close to the epicenter of Landers earthquake. Regarding the higher values of *b* found in this study, several physical explanations are possible. One can assume that in the areas that experienced larger slip during the main shock and during previous seismic activity, the stress was reduced significantly, favoring higher *b*-values for the aftershocks. Areas with relatively low *b*-value, on the other hand, are probably regions under higher applied shear stress after the main shock. According to the Coulomb failure criterion analysis (Earthquake Prediction Information Division, JMA, 2001) both ends of the aftershock area, as well as the regions B and C have an increased stress due to the main shock. Alternatively, one can hypothesize that the areas that experienced slip are more fractured, favoring higher *b*-values (Mogi, 1962a; Main, 1996). For a more detailed discussion of various mechanisms that can affect the *b*-value (and *p*-value) spatial distribution, we refer to Wiemer and Katsumata (1999).

Mori and Abercrombie (1997) demonstrated that there is a clear depth-dependence of earthquake frequency-magnitude distributions in California, *b*-value decreasing with depth. The authors suggest that the *b*-value variation is due to decreasing heterogeneity with depth and greater stress. Shibutani et al. (2001) showed that the aftershocks of Tottori earthquake are shallower in the northwest part and also in the SE extremity of the aftershock area. If the spatial variation in *b*-value were a consequence of the depth distribution of the events, one would expect the value of *b* to be larger in these regions, which is not the case. Therefore, the lateral variations in *b*-value are probably related to the slip distribution during the main shock and previous ruptures. However, the crustal structure may explain some details of the *b*-value spatial distribution.

There are two main regions that are characterized by higher values of *p* (=1.2 – 1.35); one is the area marked as P2 in Fig. 3.8b and another one is R5 region, in the vicinity of the largest aftershock in region A (Fig. 3.8b). The former region corresponds quite clearly with the distribution of largest slip during the main shock (Yagi and Kikuchi, 2000; Sekiguchi and Iwata, 2000; Fig. 3.8c). Similar observations were made in the case of the Morgan Hill aftershock sequence (Wiemer and Katsumata, 1999): the volumes that experienced a high slip during the main shock have faster decay rates (i.e. larger *p*-values). They hypothesized that in some instances the frictional heating created during the main shock influences the *p*-value. Frictional heating is concentrated in high slip areas and causes a faster decay of aftershocks in these regions. This model, according to Wiemer and Katsumata (1999), is consistent with the findings of Kisslinger and Jones (1991), that describe that areas of high heat flow in the crust tend to have a higher *p* value. In our case, the regions where the slip was large during the main shock probably also experienced such an increased frictional heating. Besides the slip during the main shock, the recent seismic activity in the region A1 may have produced also an increase in the frictional heating, which in turn favored a larger *p*-value observed in the region surrounding the main shock epicenter. However, because of the moderate size of these previous events, the associated frictional heating was probably relatively small. The relatively large value of *p* in R5 area can not be readily explained. It may be possible that the occurrence of several aftershocks with $M \geq 4.3$ (the largest $M = 5.0$) reduced the local stress, accelerating the decay of seismic activity. The local crustal properties may offer an alternative explanation for this significantly larger *p*. Thus, the heterogeneity of the crust may be related with the spatial variability of *p*-value (Mikumo and Miyatake,

1979; Utsu et al., 1995). The large value of *p* in R5 area explains why we couldn't find, in the previous section, a significant difference between the regions A1 and A2, when analyzing their *p* values.

As we mentioned previously, the *p*-value in region B is significantly small. Also, as can be seen in Figs. 3.8b and 3.10, a large area in the NW extremity of region A is characterized by relatively small *p* values. The activity in these regions continues with a small occurrence rate even after seven month from the main shock. We consider that this rather low decrease rate occurs in regions that did not experience significant recent ruptures.

We can not conclude without a brief discussion on the correlation between *b* and *p* values. The results obtained in the previous section show that both *b* and *p* values are less in region B than in region A. As Figs. 3.8a and 3.8b indicate, the largest *b* and *p* values within region A are found in the vicinity of the main shock, while the smallest values are found in the NW region. However, in a part of the NW region, around the large aftershock of M5.0, *p*-value is high despite of a small *b*-value. While it can be noticed that the region A1 (previously ruptured area) is generally characterized by relatively large *b* and *p* values, the highest values of both parameters are found in slightly different places, R2 (Fig. 3.8a) for *b* values and R4 (Fig. 3.8b) for *p*-values, respectively. We do not have yet a clear explanation for such features, but we can speculate that they are an effect of both stress and crustal structure at a local scale (Ito and Enescu, 2001b).

The significant spatial variation in both *b* and *p* values found in this study confirms the idea by Wiemer and Katsumata (1999) and Wiemer (2000) that the aftershock hazard after a main shock can be substantially improved if accurate information regarding the parameters spatial distribution is provided immediately following the main shock. This idea is based on the fact that the aftershock hazard depends strongly on both *b* and *p* values (Wiemer and Katsumata, 1999).

Finally, we would like to point out that we rigorously checked the completeness of magnitude as a function of time and space. However, we do not exclude that the *Mc* values are underestimated in some limited cases, especially around the epicenter of the main shock. Therefore, the values of *b* and *p* might be also underestimated. The correction would be an increase in these values around the main shock. However, such an increase would favor the hypothesis that large *b* and *p* values occur in regions that experienced larger slip during the main shock.

We believe that the spatial patterns observed for both *b* and *p* values are reliable and are not due to some systematic artifacts in the catalog. Our opinion is based on the stability of the results and also the fact that both JMA and Kyoto University catalogs show similar spatial distributions of the parameters.

3.3.3 The seismic activity before the 2000 Western Tottori earthquake

As can be seen in Fig. 3.1c, the region characterized by increased seismic activity due to the occurrence of several moderate earthquakes and their aftershocks in 1989, 1990 and 1997 corresponds well with the A1 area (Fig. 3.1b). Figure 11 shows the cumulative number curve for the earthquakes in Fig. 3.1c, from 1978 to the M7.3 Tottori earthquake. The threshold magnitude is 1.5, the overall magnitude of completeness. The seismic activity is low until 1989, but starts increasing after 1989, in association with several moderate sized earthquakes. The aftershocks following the M5.5 earthquake in 1997 are characterized by a relatively faster decay than the aftershocks following the moderate events in 1989 and 1990. The *p*-value given after each sequence, corresponding to the time periods TP1 and TP2 (Fig 3.11), supports this observation.

Figure 3.12 compares the frequency-magnitude distribution for the earthquakes that occurred before and after the 1997 M5.5 earthquake, taking into account the magnitude of completeness for the two periods of time. There is an increase in *b* for the later time period and a clear difference between the two distributions. Utsu's test shows that the distributions are significantly different.

The above results suggest that the seismic activity has different characteristics before and after the M5.5 earthquake. The M5.5 earthquake probably ruptured the whole A1 area, while the moderate earthquakes that occurred before ruptured only parts of the same region (Shibutani et al., 2001; Matsumura, 2001). This suggests that the M5.5 event and its aftershocks "prepared" the fault for the occurrence of M7.3 Tottori earthquake. In this respect, our previous assumption (Subsections 3.3.1 and 3.3.2) that the ruptures before the Tottori earthquake have influenced the characteristics of the seismic activity, in particular the spatial distribution of *b* and *p* values of the aftershocks of the 2000 Tottori event, proved to be true. The results argue that, besides the rupture during the 2000 Tottori earthquake, the rupture during the 1997 M5.5 event is responsible for the large *b* and *p* values found in the region A1 (Subsections 3.1 and

3.2). The large incompleteness of data immediately after the Tottori earthquake does not permit an analysis of *b*-value variation in time. However, qualitatively, based on the value of *b* before the Tottori earthquake and our work with the aftershocks of the 2000 Western Tottori earthquake, we guess that the *b*-value in region A1 continues to increase after the Tottori earthquake, reaching a stable, higher value several days after the main shock. As we have shown already, *b* has values between 1.0 to 1.4 for aftershocks in the region A1.

3.4. Conclusions

1. The *b*-value for the main aftershock region (A), computed by using events with M ≥ 3.2 (*Mc* = 3.2), equals to 1.28 +/- 0.06. When analyzing in more detail the spatial distribution of *b* values within region A, the *b*-value (1.42 +/- 0.11) is larger in an area that experienced large slip during the main shock and/or recent previous ruptures. In contrast, regions where there was no recent seismic activity and relatively small slip during the main shock have rather small values of *b*. Region B of triggered seismic activity is characterized by a relatively low *b*-value of 1.05 +/- 0.062.
2. The modified Omori formula models well the decay of the occurrence rate in both regions A and B. Fitting the data for earthquakes with M ≥ 3.2, we obtained $p = 1.05$ +/- 0.03 and a c-value about 0.01 for region A. The value of *c* is small, but seems to have a non-zero value. For region B, the *p*-value is relatively small: 0.83 +/- 0.03 and the *c* value is probably zero or very close to zero. Within region A the *p*-value shows a significant spatial variability.
3. Both *b* and *p* parameters show a significant change as a function of space. The *b*-value is found to vary between 0.8 and 1.4, while *p*-value varies between 0.8 and 1.35. These results argue that it is an oversimplification to assign one single *b* and *p* value to an aftershock sequence.
4. The spatial variations in the parameters *b* and *p* are important, and may reflect the rupture process of the main shock and/or the crustal heterogeneity in the aftershock region. Our results suggest that the rupture process of the Tottori earthquake and previous earthquake activity are the most important factors in controlling the spatial distribution of both *b* and *p* value. The rather large *b* values found for areas that have ruptured recently may be explained by the relatively low stress in these regions.

Areas with relatively low *b*-value, on the other hand, are probably regions under higher applied shear stress after the main shock. Alternatively, one can hypothesize that the areas that experienced slip are more fractured, favoring higher *b* values. The larger *p* values correlate with the regions that experienced large slip during main shock, while small *p* values are found generally in regions which did not experience significant rupture. The *p*-value might be controlled by the frictional heating produced during rupture and/or the heterogeneity in the crust. Future studies are needed in order to understand better the underlying physical mechanism of the *b* and *p* value variation patterns.

5. The analysis of seismicity before the 2000 Western Tottori earthquake suggests that the seismic activity associated with some moderate events in 1989, 1990 and 1997 had an influence on the future seismicity in the area, in particular on the spatial distribution of *b* and *p* values observed for the aftershocks of Tottori earthquake. The aftershocks of the 1997 M5.5 earthquake have a larger *p* value than previous aftershock sequences, while *b*-value has a significant increase following the M5.5 event.
6. The obtained results indicate some significant correlation between *b*-value and *p*-value, which can be summarized as follows. Both parameters are larger in region A than in region B (conclusion no. 1 and 2). Inside region A one can find larger *b* and *p* values for the aftershocks of the Western Tottori earthquake around the epicenter of the main shock and smaller values for both parameters in NW of the region. As pointed out (conclusion no. 5) the *b* and *p* values are smaller before the 1997 event than after it. The explanation of such correlated changes relates mainly with stress changes due to experience of previous ruptures (conclusion no. 4).

Chapter 4

-THE 1998 HIDA MOUNTAIN, CENTRAL HONSHU, JAPAN, EARTHQUAKE SWARM: DOUBLE-DIFFERENCE EVENT RELOCATION, FREQUENCY-MAGNITUDE DISTRIBUTION AND COULOMB STRESS CHANGES-

4.1 Introduction

The discrimination between different physical mechanisms responsible for the occurrence of earthquakes in a certain region is generally a difficult task. Besides, a reliable interpretation of the results depends heavily on the quality and accuracy of the data to be analyzed. Therefore, we have considered a very good opportunity to attempt such an investigation in the case of the 1998 Hida Mountain swarm, for which the amount and quality of data is high.

The 1998 Hida Mountain earthquake swarm started on August 7 and its most active period lasted for about two months. In this period, 18 shocks with $M \geq 4.0$ occurred, the largest one ($M = 5.0$) being recorded on August 16. The swarm started in the south and migrated toward the north, reaching the northern most point in about one month. Most of the largest events in the sequence (fifteen) occurred during this South-to-North migration period. For the following month, an opposite, North-to-South migration of seismicity was observed. The average speed of migration was of about 1-2 km/day (Wada et al., 2000). We refer to the papers of Katsumata et al. (1995) and Aoyama et al. (2002) for details on the crustal structure and the geological setting of Hida Mountains.

The purpose of our study is to determine the fine structure of seismicity during the swarm and to search for a physical interpretation of the b-value changes and seismicity pattern found as a result of this investigation. Moreover, we compare the results of our ΔCFF analysis with those obtained by Aoyama et al. (2002), who use a different pore-pressure model for their computations.

4.2 Data and method of analysis

As a first step in analyzing our data we have relocated the events of the swarm recorded by DPRI (Kyoto University), by using the double-difference relocation algorithm (Waldhauser and Ellsworth, 2000). The method minimizes the residuals between observed and theoretical travel-time differences (or double-differences) for pairs of earthquakes at each station while linking together all observed event-station pairs. A least-squares solution is found by iteratively adjusting the vector difference between hypocentral pairs. We have used only absolute P-and S-wave travel-time differences. However, the location method can incorporate also cross-correlation differential travel-time measurements. We adopted in this study the velocity structure that is used to determine hypocenter locations at the Kamitakara observatory (Kyoto University), which is located at about 30km distance from the epicentral region.

The *b*-value of the frequency-magnitude distribution is determined by using a maximum likelihood procedure (Aki, 1965; Utsu, 1965). To check if two distributions come from the same mother population, we have used Utsu's (1992) test. For more information on the methods used to determine the b-value and the physical processes that control the frequency-magnitude distribution we refer to the previous chapters.

In order to correlate the static stress changes with the seismic activity and, finally, the *b*-value changes, the ΔCFF associated with the largest earthquakes during the 1998 Hida Mountain earthquake swarm was computed. According to the Coulomb criterion, failure occurs on a plane when the Coulomb stress σ_f exceeds a specific value:

$$\sigma_f = \tau_\beta - \mu'\sigma_\beta \qquad (4.1)$$

where τ_β is the shear stress on the failure plan, σ_β is the normal stress and μ' is the effective coefficient of friction, which incorporates as well the effects of pore fluid pressure (e.g. King et al., 1994). The change in the Coulomb stress is defined by the difference between the Coulomb failure stresses after and before an earthquake.

The expression of μ' depends on the choice of the pore model. One possibility, considered in most of the stress-triggering studies, is to assume that the apparent coefficient of friction is a material constant, i.e.,

$$\mu' = \mu(1-B), \qquad (4.2)$$

where *B* is Skempton's coefficient, which relates to the degree of saturation of pores in soils and rocks (Skempton, 1954). Another choice (Beeler et al., 2000) is to assume that μ' changes with location and with fault orientation. Beeler et al. (2000) recommended to

follow both approaches and to compare the results for a reliable interpretation. As Aoyama et al. (2002) have studied the static stress triggering for the 1998 Hida Mt. swarm by considering a constant μ', we decided to adopt the second choice.

The results of this study were obtained by using the computer programs: Zmap (Wiemer, 2001), the Coulomb failure stress modeling tools GNStress 1_5 (author: R. Robinson, Doser and Robinson, 2002), CFF (author M. Hashimoto, Kyoto University) and DLC (author B. Simpson, USGS). A new toolbox for stress analysis, written in Matlab and integrated with the Zmap software, will be available for downloading from my web page.

4.3 Results and discussion

4.3.1 Earthquake relocation by using the DD algorithm

Figure 4.1a presents the epicentral map of the original and relocated events of the sequence having M ≥ 1.7. The double-difference relocation was performed in a number of 10 iterations. During iterations 6-10 the catalog data was re-weighted according to misfit and event separation to remove or down-weight outliers. Re-weighting leads to the rejection of about 4% of the data. However, the number of events that get deleted during relocation because they loose connection to other events is insignificant. As can be noticed the relocated events show a sharper image of seismicity compared with the more diffuse catalog locations. The 2σ standard errors of the relocated events average about 90 m, in relative horizontal coordinates, and about 200 m in depth. The *rms* residual decreases from about 130msec (P-wave) and 250msec (S-wave) before relocation to about 50ms and 90ms after relocation, for P- and S-waves respectively. The events occurred in the south (*S* region in Fig. 4.1a), during a period of intense observation (August 25 – November 10), are most accurately determined, due to a better coverage with seismic stations (27 stations, in total). By examining Fig. 4.1a, especially the epicentral map of the relocated events, one can notice two main directions defined by the epicenters' distribution: one oriented N-S, corresponding to the main direction of earthquake migration, and another one oriented approximately E-W; both of them probably reflect the directions of the regional stress. Also, a careful analysis of the relocated epicenters' map shows that the seismic activity occurs mainly as small, concentrated clusters of events.

In Figure 4.1b we present the space-time diagram obtained by projecting on a N-S oriented profile the epicenters of all relocated earthquakes (M ≥1.0). One can see the clear south-north-south migration of events during the swarm. The arrows in the figure indicate the directions of the main, overall migration of earthquakes and a more localized one in the south and middle part of the swarm's spatial distribution. There is also a clear gap of seismicity between the northern group of earthquakes and the rest of the events. A smaller gap can be seen as well in the south. Figure 4.1c shows in more detail the local spatio-temporal evolution of seismicity, as revealed by the precise relocation of events.

The physical processes that determined the observed pattern of seismicity are complex and relate probably with the different triggering mechanisms that acted during the swarm. A detailed analysis of the physical processes that may have occurred during the swarm and determined its main spatial and temporal characteristics is made by Aoyama et al. (2002).

4.3.2 Spatial and temporal changes of b-value

Several studies (Enescu and Ito, 2001b, 2002b; Sakai et al., 2002) found a relatively large *b*-value in the south part of the Hida Mt. comparing with the northern part. Besides, in our previous studies, we found an increase of *b*-value with depth. The variations of *b*-value were related in these investigations with the proximity of the Yakedake volcano to the southern cluster of events, which may have caused a higher thermal gradient in the south. The depth variation of b-value was related with a low *Q*, low-velocity and low-density anomaly found at 5-15 km depth, under the Hida Mountains (Katsumata et al., 1995).

By using the relocated events, we have computed the *b*-values for the north and south clusters (indicated by N and S in Fig. 4.1) during the campaign of intense observation (August 25 – November 10), when both the location and the magnitude of completeness are good enough. The result of the analysis is presented in Fig. 4.2a. As one can notice, the two frequency-magnitude distributions are significantly different, with particularly small *b*-values for the northern cluster, where three earthquakes larger than or equal to 4.0 occurred. Similar significant differences between north and south were obtained when using JMA (Japanese Meteorological Agency)(see Fig. 4.2b), NIED (National Inst. for Earthquake Disaster) and JUNEC (a joint catalog of several research

institutions in Japan). Therefore, we believe that the difference in *b*-value between south and north is highly reliable. On the other hand the significant variation of *b*-value with depth, found in our previous study, could not be confirmed. The previous result, showing a large *b*-value (1.5-1.7) at depth (4-7 km), near Yakedake volcano, was probably due to the miss-location of small-size events. In fact, Enescu and Ito (2001b) recognized this possibility and suggested the relocation of events, for a reliable depth determination.

There are two main possibilities that could explain the difference in *b*-value between the northern and southern clusters. Thus, one can assume that the structure of the crust, i.e. its heterogeneity or thermal gradient, is the responsible factor for the spatial variation of the frequency-magnitude distribution. Alternatively, the change in *b*-value could be attributed to changes of stress during the swarm. In this case, the variation of *b*-value is mainly a temporal one.

In order to understand better the differences in the frequency-magnitude distribution, we analyzed also the *b*-value change with time in the south part of Hida Mt., from the beginning of the swarm until the end of 1999. Because this time we are not interested in a precise location, we have used the catalog data by Kyoto University, DPRI. Figure 4.3 presents the time variation of *b*-value for the southern seismicity cluster. One can notice that *b*-value is varying significantly with time: small values ($\cong$ 0.75) at the very beginning, followed by a relative increase toward a stable *b*-value of about 1.0-1.1. Figure 4.4 shows the frequency-magnitude distribution for the first 620 events occurred in the south cluster. The well-defined frequency-magnitude graph suggests that the relatively small *b*-value observed at the beginning of the swarm is reliable and not a consequence of magnitude incompleteness. Due to the relatively small number of events occurred in the north (N) cluster, a similar temporal analysis could not be performed.

It is worth stressing at the end of this paragraph that, in order to avoid possible erroneous results due to the incompleteness of the data, we have investigated carefully the catalogs and applied simple statistical tests to evaluate our assumptions. We believe that the changes of *b*-value are genuine and that possible "local" incompleteness did not influence significantly our conclusions.

4.3.3 Static stress changes and a possible physical interpretation

The static stress changes associated with the 18 largest ($M \geq 4.0$, magnitudes determined by the Earthquake Research Institute, University of Tokyo) earthquakes in

the swarm may offer important clues for understanding the rather complex *b*-value spatio-temporal "puzzle". Aoyama et al. (2002) performed an in-depth analysis of the static and dynamic stress changes for the 1998 Hida Mt. earthquake swarm. Therefore, we do not intend to repeat their detailed analysis here.

We have considered the focal mechanism of the largest 18 events of the swarm and infer their source extent and average slip by using the relationship between focal dimension and seismic moment (Kanamori and Anderson, 1975), in a similar manner to Aoyama et al. (2002). We have considered a range of values for both B ($0 \le B < 1$) and the coefficient of friction μ ($0.2 \le \mu \le 0.8$). A selection was made based on the best correlation between seismicity and ΔCFF, as it is explained below.

Figure 4.5 presents the Coulomb stress changes, calculated on optimum failure planes, as a result of the 18 largest earthquakes in the sequence. We considered a general case, without any "a-priori" assumption made about the optimum failure planes or type of faulting. The orientation of the regional principal stresses was an important element to control the pattern of the stress changes. We have chosen a maximum compressional stress oriented $N35^0$ W, which is in good agreement with observation data (Wada et al., 2000). The ΔCFF pattern presented in the figure is similar with the one obtained by Aoyama et al. (2002) (see fig. 4 of their paper), by using a different pore fluid-pressure model. The relocated events with $M \ge 2.5$ were superposed on the Coulomb stress map. Due to the main south-to-north migration of seismicity and to the moderate size of the earthquakes for which we computed the ΔCFF, the superposition suggests correctly the correlation between seismicity and stress changes.

The ΔCFF agrees better with the seismicity pattern if one assumes $\mu \le 0.4$, while the choice of Skempton's coefficient B does not influence significantly the results. A small μ value could be interpreted as an argument for a weak fault-zone, but only a detailed analysis (e.g. Iio, 1997) may offer a reliable explanation. By choosing $\mu = 0.4$ and $B = 0.5$, about 80% of the relocated earthquakes occurred in regions with a positive stress change. The probability to obtain this by chance is less than 0.1. By assuming a pore-pressure model with a constant μ' and the same values for μ (0.4) and B (0.5), one obtains by using relation (4.2) $\mu' = 0.2$, which is the same as in the study of Aoyama et al. (2002).

As the swarm progressed from south to north, the stress changes advanced as well in the same direction (see fig. 4a-f of Aoyama et al., 2002 and the seismicity and stress

changes obtained in this study). The small values of *b* could be well explained by an increased stress at the beginning of the earthquake activity in the south or north part of the swarm area. The release of stress was associated with a gradual increase of *b*-value for the southern cluster. The inset of Fig. 4.5 shows clearly that the seismic activity of the northern group occurred in an area of increased ΔCFF, due to previous moderate-size events. Thus, it seems reasonable to assume that the changes in stress may explain, at least in part, the *b*-value changes. The insufficient number of events did not allow us, unfortunately, to map the spatio-temporal changes of *b*-value not only for the southern and northern clusters, but also for the other areas where the swarm occurred.

Enescu et al. (2003a) found a similar *b*-value variation in the case of the 2002 Middle Western Tottori sequence. The static stress changes associated with the largest earthquake of the sequence (a moderate size event, M = 5.3) could explain well the occurrence of an off-fault cluster of subsequent seismicity. The *b*-value was found to change as a function of time, with *b*-values around 0.9 at the beginning of the sequence and relatively large *b*-values, around 1.4, for the rest of the sequence. The difficulty to estimate ΔCFF on the fault (or very close to it) made difficult the interpretation of *b*-value pattern in terms of stress changes.

4.4 Conclusions

The precise double-difference relocation of the events that occurred during the 1998 Hida Mt. sequence revealed the fine structure of seismicity in the studied area and the local and general migration of seismic activity during the swarm.

The epicentral distribution of earthquakes defines two main directions, N-S and E-W, which probably reflect the regional stress pattern. The earthquake activity occurs mainly as small clusters of events.

It was found that the variation of stress caused by moderate-size events has an important influence on the distribution and migration of seismicity and, possibly, on the spatio-temporal *b*-value pattern of the 1998 Hida Mountain earthquake swarm. Thus, the small *b*-value in the north could be well explained by an increased level of stress during the investigated time period, while the larger *b*-value in the south corresponds probably with a relatively lower level of stress for the same period of time.

Chapter 5

MULTIFRACTAL AND CHAOTIC ANALYSIS OF VRANCEA (ROMANIA) INTERMEDIATE-DEPTH EARTHQUAKES -INVESTIGATION OF THE TEMPORAL DISTRIBUTION OF EVENTS-

5.1 Introduction

Since the pioneering work of Mandelbrot (1983), a large number of studies were devoted to characterize the self-similar (or scale-invariant) properties of a wide variety of natural phenomena, by using the concepts of fractal geometry and fractal dimension. These concepts have also been applied to describe the spatial and temporal distribution of earthquakes (e.g., Smalley et al., 1987, Turcotte, 1989 and Kagan and Jackson, 1991). At present, however, the notion of monofractals appears to be insufficient to address the various aspects of non-linear behaviour. The natural framework to describe such non-linear dynamic systems seems to be better described by multifractals. In the case of earthquake phenomena, several studies found that the temporal, epicentral and hypocentral, and also the energy distribution of earthquakes, have multifractal characteristics. In other words, the earthquake process is multifractal or heterogeneous in the fractal dimension (e.g. Geilikman et al., 1990, Hirabayashi et al., 1992, Goltz, 1997, Godano et al., 1997).

Another important question concerning the earthquake occurrence process is: do earthquake sequences have a long "memory"? Kagan and Jackson (1991), by analyzing statistically several instrumental earthquake catalogs, concluded that besides the short-term clustering, characteristic for aftershock sequences, there is a long-term earthquake clustering in the residual (declustered) catalogues. Xu and Burton (2002) did *a Rescaled Range Analysis* (*RSA*) (Hurst, 1965), for a catalog of Mediterranean earthquakes and found that both the natural and aftershocks-removed distributions of moderate to strong events in this area are persistent time series, with long memory. Wyss and Toya (2000), by studying some intermediate and deep earthquake sequences world-wide, argued that

both the short and long term clustering are embedded in a background seismicity produced at a stationary Poissonian rate.

Relatively recent studies raised the question if the earthquake occurrence process is a "truly" random one, or, under a "noisy appearance", does it have an underlying determinism. Using classical linear methods one can not usually address such problems. Advances in non-linear science, however, have occurred in the early 1980's and have been broadly applied in various fields such as the physical sciences, biology, economics and medicine. These methods can evaluate if a system dynamics is chaotic (in a deterministic sense) or random. The theory suggests that if we can measure any single suitable variable with sufficient accuracy and for sufficiently long periods, it is possible to make quantitatively meaningful inferences about the dynamics of an entire system from the behaviour of a single variable. Goltz (1997) and Matcharashvili et al. (2000) analyzed seismicity using such non-linear methods and found evidence of low-dimensionality for some earthquake systems, by using the inter-event times between successive earthquakes.

Studies of seismicity evolution of the Vrancea (Romania) region in time and space have a quite long history. Some papers were devoted to analyse, from a statistical point of view, the major earthquake occurrences, in order to find periodicities for earthquake forecasting (e.g. Enescu et al., 1974, Purcaru, 1979, Enescu and Enescu, 1999). Other papers dealt with the recognition of different patterns of seismicity as premonitory phenomena for large Vrancea earthquakes (e.g. Marza, 1979, Radulian and Trifu, 1991, Trifu and Radulian, 1994). Radulian and Trifu (1991) found a decrease of both the fractal dimension of the depth distribution of earthquakes and the background seismicity *b*-value prior to the major 1986 Vrancea event ($M_W = 7.3$).

The next sub-chapter gives some brief information regarding the Vrancea (Romania) seismic region and the data to be analyzed. Sub-chapter 5.3 describes qualitatively and quantitatively the scaling and multifractal features of the time distribution of Vrancea intermediate-depth earthquakes, while sub-chapter 5.4 is concerned with the correlation properties of this temporal distribution. In sub-chapter 5.5 we attempt to determine whether our earthquake system is chaotic or not, by using the distribution of inter-event times. We end our study with some general conclusions and a brief discussion on the implications of our results for the prediction and hazard assessment of Vrancea earthquakes.

Most of the computations performed in this study were done using a user-friendly

software toolbox that we designed for the non-linear analysis of earthquake sequences. The toolbox is written under Matlab and Zmap (Wiemer and Zuniga, 1994; Wiemer, 2001) and is an extension of the "Fractal toolbox" of Zmap software package for seismicity analysis. The routines can compute the multifractal spectrum (D_q or $f(\alpha)$) for the hypocentral, epicentral and temporal distribution of earthquakes, using the two methods outlined before. The package also includes routines to estimate the correlation properties of a time series, by using the DFA and the Rescaled Range Analysis methods, and can be downloaded from the web page: http://www.rcep.dpri.kyoto-u.ac.jp/~benescu/. We plan to add in the near future some tools for the chaotic analysis of earthquakes.

We acknowledge the use of the free software packages for non-linear analysis of Kaplan (1998) and tstool (Merkwirth et al., 2002) to obtain some of the results of sub-chapter 5.4 and perform the chaotic analysis of sub-chapter 5.5.

5.2 General features of Vrancea (Romania) region seismicity

The Vrancea seismic region is situated beneath the Eastern Carpathians in Romania and is characterized by well-confined and persistent intermediate depth activity (60 km < h < 220 km) (Fig. 5.1). The crustal seismic activity is rather low, with maximum magnitudes in the range 5.0-5.5 (Radu, 1979). Most of the seismotectonic models proposed for the Vrancea region (e.g. Fuchs et al., 1978, Constantinescu and Enescu, 1985) agree that the Vrancea subcrustal earthquakes occur in an old subducted lithospheric slab which is sinking gravitationally.

The catalog used in this study consists of 5630 intermediate-depth events with Mw ≥ 1.5, occurring between 1974 and 2002. The initial catalog was produced by Trifu et al. (1990) and has been continuously updated. Trifu and Radulian (1991, 1994), Radulian and Trifu (1991), Bazacliu and Radulian (1999) and Popescu et al. (2001) present in detail the catalog together with the main characteristics of the intermediate-depth seismicity. The magnitude of completeness of the catalog, evaluated using a procedure by Rydelek and Sacks (1989), is a function of depth (h): the 95% completeness magnitude thresholds are 2.2, 2.6 and 2.8 for h = 60-115 km, 116-145 km and 146-220 km, respectively. One of the remarkable characteristics of the Vrancea intermediate-depth seismicity is the non-linearity of its frequency-magnitude distribution. Thus, Trifu and Radulian (1991) showed that around M = 3.5 there is a

significant change in the slope of the frequency-magnitude distribution, which probably marks the transition between two different earthquake-generating mechanism regimes. Previous studies also suggested that the Vrancea intermediate-depth seismogenic region consists of two seismic zones of distinct activity, centered around 70-110 km and 120-160 km. In the following analysis, the number of events is one of the important factors to be considered for obtaining reliable results; therefore we will not separate the events depending on their depth range and consider the magnitude dependence only in appropriate cases.

Figure 5.2 presents the inter-event time distribution of the catalog for $M \geq 2.6$. An exponential distribution fits the data well, with a coefficient of determination close to one. We have also used other threshold magnitudes (from 2.8 to 3.6) and the results do not change significantly. Thus, on a large scale, the seismic series behaves as a Poissonian (random) process. However, clustering may occur locally, associated, for example, with the aftershock activity following some large events.

In this study we analyse the original catalog (containing aftershocks), as well as the declustered catalog obtained by eliminating the aftershock sequences following the three major earthquakes that occurred in 1977, 1986 and 1990 (Fig. 5.3). The abnormal aftershock activity occurs in time windows of several months, but is especially concentrated in the first hours and days following the occurrence of a major event. It should be noted that the number of aftershocks associated with other smaller events is generally extremely small, as it is the case for the intermediate and deep earthquakes.

5.3 Multifractal characteristics of the Vrancea intermediate-depth seismicity

5.3.1 Method of analysis and tools. The multifractal spectrum

A useful way to quantify the clustering of a process is provided by the fractal concept. Considering the distribution of the inter-event times between events, a Poissonian process will have a fractal dimension equal to unity, while it will be less than one for a clustered sequence (Smalley et al., 1987, Godano et al., 1997). Distributions that are characterized by a single power-law and, therefore, by a single fractal dimension and by a unique scaling behavior, are called mono-fractals. Many natural fractals are, however, not homogenous. In such cases, a single fractal dimension is not enough to characterize the fractal properties of such phenomena. There is a spectrum D_q

of dimensions (with real q ranging from -∞ to +∞) needed to describe the distributions. Suppose we cover our distribution with m balls (i.e. spheres for a 3D distribution) of size r, centered on m randomly chosen reference points.

Then,

$$D_q = \frac{1}{q-1} \lim_{r \to 0} \frac{\log \left(\sum_i \{ P_i(r) \}^q \right)}{\log r} \qquad (5.1)$$

where $P_i(r)$ is the probability or density (or, more generally, any measure or "mass") in the ith ($i = 1, 2, \ldots, m$) ball of radius r. In practice, one can determine $P_i(r)$ for a range of r values and estimate D_q from the slope of a linear region (the scaling region) in a plot of $\log(\Sigma_i \{P_i(r)\}^q)$ versus $\log r$. $\Sigma_i \{P_i(r)\}^q$ is called the partition function and the procedure described is known as the fixed-radius method. Another technique is to cover the distribution with balls of different radii, but all containing the same mass P. By determining an average radius for different P, it is possible to determine D_q. For more details, see Badii and Broggi (1988) and Hirabayashi et al. (1992). According to Badii and Broggi (1988), the fixed-radius method works better for $q > 1$, while the fixed-mass method gives better results for $q \leq 1$.

As can be expected from formula (5.1), D_q for larger positive q accentuates the fractal property of dense regions, where $P_i(r)$ is large, while D_q for negative q accentuates the fractal property of sparse regions, where $P_i(r)$ is small. For $q = 0, 1$ and 2 we obtain the well-known capacity, information and correlation dimension, respectively. D_0 is a geometric measure, and it shows how well the fractal distribution is filling the space (in our case the temporal axis). The information dimension, D_1, describes the non-uniformity of the data, while D_2 is related to the global clustering degree. Two other interesting quantities are D_∞ and $D_{-\infty}$, which indicate the most and the least intense clustering of the distribution.

Another equivalent way to describe such phenomena is the singularity spectrum $f(\alpha)$. The Holder exponent (or singularity strength) α is defined by,

$$P_i(r) \approx r^{-\alpha_i} \qquad (5.2)$$

α_i corresponds to the fractal dimension at i and can vary from place to place. The spectrum $f(\alpha)$ captures how "frequently" a value α is found. The number of balls of

radius r with the same singularity strength α behaves as $r^{-f(\alpha)}$. Thus, $f(\alpha)$ is the fractal dimension of the subset in which α_i equals α.

The generalized dimension, D_q, and the singularity spectrum, $f(\alpha)$, are connected via a Legendre transformation:

$$f(\alpha_q) = q\,\alpha_q - \tau_q$$
$$\alpha_q = \frac{d\,\tau_q}{dq} \tag{5.3}$$

where, $\tau_q = (q-1)D_q$ is the τ_q spectrum.

5.3.2. Multifractal spectrum of the inter-event occurrence times of Vrancea intermediate-depth seismicity

This sub-chapter presents investigations of the earthquake clustering in time for the Vrancea intermediate-depth seismicity, by applying the multifractal procedure to the series of inter-event times. The catalog used consists of 5630 intermediate-depth events ($M \geq 1.5$) recorded from January 1974 to September 2002. The magnitude of completeness of the catalog slightly increases with depth, from 2.2 to 2.8 (Trifu and Radulian, 1991). Therefore, we have selected for analysis the earthquakes with M ≥ 2.8, and the resulting catalog has 3905 events.

The partition functions (Fig. 5.4) of the inter-event times for the entire catalog (including aftershocks) show two domains characterized by a distinct scaling behavior. Region B characterizes the small-range interactions (11 – 194 min.), while Region D characterizes long-range interactions (250 – 2957 days). The variation of the spectrum of the generalized dimensions is significant in particular for the first domain (Region B) (Fig. 5.5), indicating a strong clustering at small scales (small inter-event times), undoubtedly associated with the aftershock generation processes. D_2, the dimension that is usually computed in fractal studies, has a value of about 0.85, indicating that even for the aftershock populations there is a relatively weak general clustering. As q increases, however, D_q is decreasing significantly, indicating that locally the clustering degree might be high. As can be seen in Fig. 5.6, the scaling Region D has a close to monofractal spectrum. By examining visually the seismicity, we observed that several larger aftershocks occurred soon after the three major Vrancea events. Each of these aftershocks has its own aftershock activity, clustered in a very small time interval

(minutes to few hours). This better explains the clear multifractality found at these interaction ranges. The D_q (q = 2,…,7) values vary between about 0.9 and 0.95, a range comparable with the error of the dimension estimation. They are close to one, which suggests a weak clustering or a quasi-Poissonian behavior at large time scales. Region C marks the transition between the two domains. The aftershocks are still present and interacting at this time scales, but the numbers are rather small for good statistics. Their contribution to the partition functions is superposing with the long-range nearly monofractal behavior seen in Region D (Fig. 5.6). Region A and E (Fig. 5.4) are characterized by severe "edge effects" due to insufficient statistics.

For the declustered catalog, the partition functions (Fig. 5.7) show only one well-defined scaling region (Region B). The clear result of the aftershock removal (including the aftershocks of larger aftershocks) is the absence of the small-scale scaling, which, for the original, undeclustered catalog showed a clear multifractal spectrum (Fig. 5.4). Region B in Fig. 5.7 corresponds to Region D in Fig. 5.4. The lower limit of region B (Fig. 5.7) is of about 11 days, less than the lower bound of about 250 days for Region D (Fig. 5.4). The lower limit decrease can be explained by the removal of aftershocks, which no longer interfere with the longer-range monofractal behavior. Region A and C are characterized by insufficient statistics. Figure 5.8 plots the D_q spectrum for Region B in the previous figure. The spectrum is monofractal and close-to-Poissonian. The absence of small scale scaling does not mean that there is no more clustering present at very small scales (days). There are small clusters of events, but they are very "weak" and have a poor statistics.

In the analysis performed so far we have limited our computations to multifractal dimensions having $q \geq 2.0$, since the fixed-radius method gives the best results in such a case. However, we can learn more about our distributions if the spectrum is computed for a larger q range, including negative values. In Fig. 5.9 we show the multifractal spectrum computed using a fixed-mass approach, for the case of the declustered catalog, using q between –4 and 5. The scaling region used for obtaining the spectrum ranges from days to several years. The D_q values for positive and negative q's are very close to one, suggesting that at this resolution (defined by the range of q values) there is no significant clustering or quiescence in the catalog.

We performed similar multifractal analysis on data sets with threshold magnitudes between 2.9 and 3.5. We observed a slight increase of the range of values for the D_q

spectrum, as the threshold magnitude increases. Thus, for a threshold magnitude of 3.5, D_7 is about 0.9, comparing with 0.94 in the case of a 2.8 threshold magnitude. The result may suggest a slight increase of the clustering degree with magnitude, but we can not draw definitive conclusions as the tendency is rather weak and the data are relatively few.

The computations performed so far consider a q value range between –4 and 7. By examining Figures 5.8 and 5.9, we notice that the spectrum does not saturate, but has a decreasing trend towards positive q and an increasing trend for negative q. Therefore, one wonders how this observation relates with our conclusion of randomness in the catalog. In our computations we also considered q values as high as 20, but there were no values for D_q less than 0.9, even in such cases. We have not displayed these results, since the estimation errors are much larger. We have also analyzed subsets of the data, but the results do not change: the catalog still shows a very weak temporal clustering and multifractality. This result may reflect a particularity of deep seismic activity, since for crustal earthquakes in a variety of tectonic environments (including volcanic regions where there are generally no clear aftershocks, see Godano et al., 1997), a clustered, multifractal pattern is usually found. On the other hand, Eneva (1996) showed that monofractal distributions could be easily misinterpreted as multifractal ones, if an insufficient number of data is used for the analysis.

5.4 Fluctuation analysis of Vrancea (Romania) intermediate-depth seismicity

5.4.1. Method of analysis

The results in the previous sub-chapter pointed out that the long-term characteristics of Vrancea seismicity are monofractal and random, while for the short-term aftershock activity the seismicity is clustered (non-Poissonian) and multifractal. In this sub-chapter we perform a complementary investigation, using the *Detrended Fluctuation Analysis* (DFA) method, introduced by Peng et al. (1994), to possibly reveal hidden local or long-term non-random patterns of our inter-event time series.

In recent years the DFA method has become a widely used technique for the determination of (mono-)fractal scaling properties and the detection of long-range correlations in noisy, non-stationary time series. It has successfully been applied to

diverse fields such as cardiac dynamics, bioinformatics, economics, and meteorology (for a brief review, see Hu et al., 2001).

Consider a time series *X(i) (i = 1, 2,…,Nmax)*. The series is divided into blocks of size *s*, and then within each block, the partial sums of the series are calculated:

$$Y(t) = \sum_{i=1}^{t} X(i) \tag{5.4}$$

A least-square line (or higher order polynomial) is fitted to the partial sums within each block, and the sample root mean square fluctuation is computed:

$$F(s) = \sqrt{\frac{1}{s} \sum_{t=1}^{s} (Y(t) - Y_{fit}(t))^2} \tag{5.5}$$

The root mean square fluctuation, *F(s)*, is proportional to s^C. The parameter *C*, called the scaling exponent or correlation exponent, represents the correlation properties of the signal. If $C = 0.5$, there is no correlation; if $C < 0.5$, the signal is anticorrelated; if $C > 0.5$ there are positive correlations in the signal. It should be stressed that deviations from the scaling-law do occur for (very) small scales *s*, since the scaling behavior is only approached asymptotically.

The main advantage of the DFA method over other non-detrending techniques (power-spectrum and auto-correlation function estimations, *Rescaled Range Analysis* (Hurst, 1965)) is that it can estimate the intrinsic correlation properties of a signal in the presence of trends, without filtering the data. It is known that filtering can introduce spurious effects by destroying the scaling over a wide range of scales. In many cases, we even do not know the origin and shape of these trends. The DFA method can successfully address such problems, and it is a non-parametric method, which performs well when the data have a non-*Gaussian* probability distribution.

5.4.2. Results of the DFA analysis

The (multi)fractal analysis of earthquakes, like the one performed in the previous sub-chapter, has a quite clear "geometric" character. Earthquakes are treated as a set of points distributed in a one, two or three-dimensional space, depending on whether one performs a temporal, epicentral or hypocentral analysis, respectively. However, the multifractal analysis was introduced in the context of "measures" (see Peitgen et al., 1992, for a discussion on the subject). In the case of earthquakes, this means that one can give a "weight" to each event, depending on its magnitude, for example. At present,

such an approach has been followed only by Hirabayashi et al. (1992). A further generalization is from "measures" to functions. One can analyze in this way the (multi)fractal properties of almost any physical signal. The DFA method, among others, is such a function-oriented approach, with the parameter *C* previously defined as being closely related to the fractal dimension of the function. In our case, the signal (function) is given by the integration of the inter-event times between successive earthquakes, while on the x-axis we have the order number of the corresponding inter-event time. By integrating the inter-event times, one performs a smoothing of the original inter-event time series, but this is not a problem as we are more interested in longer-range correlations.

Figure 5.10 presents the results of the DFA analysis performed on the declustered catalog of Vrancea intermediate-depth seismicity ($M \geq 2.6$). The correlation exponent of the integrated inter-event times, obtained by fitting a straight line in the graph of *log(F(s))* versus *log(s)*, is 0.55. This value is very close to 0.5, which would indicate no-correlation, but we need to assess the significance of the result. This is done by computing the correlation exponent for the case of an integrated Brownian process (a continuous time random-walk), which we know has a theoretical $C = 0.5$. The computed *C*, obtained for a time series with the same length as the inter-event time series (4255 events), is 0.54. The small deviation from the theoretical value, 0.5, comes from the fact that the power-law scaling is approached asymptotically towards larger scales. Thus, we can conclude that our time series of inter-event times is similar to a white noise signal. We compared our result with other random time series, having non-*Gaussian* distributions, such as exponential or power-law, and the conclusion does not change. Our results hold from small (days) to large (years) scales, as can be seen from the scaling range of Fig. 5.10. Similar analysis performed for magnitude thresholds between 2.7 and 4.0 lead to similar conclusions.

The results obtained above do not depend on the order of the detrending polynomial, as we also tried several different choices, including no detrending, and the results do not change significantly. Also we have used other techniques, as for example *the Rescaled Range Analysis*, and the results are the same. Enescu et al. (2002, 2004) applied a wavelet analysis technique to data of inter-event times for different earthquake sequences in Japan and Romania (see also Chapter 6 of the thesis). This technique can reveal, in the case of a multifractal signal, a range of correlation coefficients. However,

the Vrancea declustered time series showed a monofractal pattern, with a correlation coefficient very close to the one obtained in this study using a monofractal technique. It is interesting to mention that the declustered seismicity before the 1995 Kobe earthquake (from 1976 to 1995) also displayed a monofractal pattern, but the correlation exponent was very high (0.8-0.9), suggesting possible increased temporal correlations before this major 1995 event. Enescu and Ito (2001a, 2003), among others, identified several seismicity precursors occurring in a rather large area around the epicenter of the 1995 Kobe earthquake (for more details see the Chapter 2 of the thesis). These observations may indicate that long temporal and spatial correlations of seismicity occurred in the region of the Kobe earthquake. An important problem we would like to address in a future study is if the observed high correlation exponent is a result of genuine long-range correlations or is caused by oscillatory and/or power-law trends present in the data (see Hu et al., 2001, for a discussion in the context of DFA analysis).

5.5 Vrancea intermediate depth earthquakes: deterministic chaos or stochasticity ?

5.5.1 Method of analysis

The general objective of the non-linear analysis is to evaluate qualitatively and, if possible, quantitatively the dynamical evolution of a complex system. To achieve this goal it is necessary to consider the evolution of the system in phase space, i.e. the space that is spanned by system's variables. Because of the complexity of natural systems, full information about their state is generally lacking. So, from the practical point of view, nonlinear time series analysis is based on concepts of an embedding theorem (Takens, 1981). It is suggested that if we can measure any single suitable variable with sufficient accuracy and for sufficiently long time periods, it is possible to make quantitatively meaningful inferences about the dynamics of an entire system from the behavior of the single variable (Theiler, 1990, Kantz and Shreiber, 1997). In this study we use such an approach, by considering as a variable the inter-event times between successive intermediate-depth earthquakes of the Vrancea region.

Suppose that we have a time series $x_1, x_2, ..., x_N$ (in our case the series of inter-event times). Using the method of delays (Takens, 1981) it is possible to reconstruct the phase-space from an observed scalar quantity. Thus, we can convert this scalar sequence

into state-vectors in a d-dimensional space:

$$y_i(d) = (x_i, x_{i+\tau}, \ldots, x_{i+(d-1)\tau}),\ i = 1, 2, \ldots, N - (d-1)\tau, \qquad (5.6)$$

where d is the embedding dimension and τ is the time-delay. If the sequence is random (in a stochastic sense) than one needs an infinite (or a very high) number of coordinates for the phase-space to properly describe the dynamics of the system under study. In the case of deterministically chaotic signals, however, the number of coordinates is limited and hence the embedding dimension has a finite value. Characteristic for such systems is that no matter what the initial conditions are, after some transient time, their dynamics is "attracted" to a complicated d-dimensional structure, known as a chaotic or strange attractor. In fact, many deterministic chaotic systems prove to be low-dimensional, or in other words, the number of coordinates needed to properly unfold their dynamics and reveal the attractor is low.

There are several methods usually used to choose the minimum embedding dimension (Cao, 1997), with probably the most common one being based on computing some invariant measure, for example the fractal dimension. This method was used also by Goltz (1997) and Matcharashvili et al. (2000) for seismicity-related studies. However, the typical problems of this approach are that it is often very data intensive, certainly subjective, and time-consuming for computation (Cao, 1997).

Therefore, we choose to apply the method of false neighbors (Kennel et al., 1992), in an improved form (Cao, 1997, Cao et al., 1998). The method (Cao, 1997) first defines:

$$a(i,d) = \frac{\left\| y_i(d+1) - y_{n(i,d)}(d+1) \right\|}{\left\| y_i(d) - y_{n(i,d)}(d) \right\|}, \qquad \mathrm{i} = 1, 2, \ldots, \mathrm{N} - \mathrm{d}\tau \qquad (5.7)$$

where $\| \cdot \|$ is some measurement of the Euclidean distance and is given in this paper by the maximum norm; $y_i(d+1)$ is the i-th reconstructed vector with embedding dimension $d + 1$; $n(i, d)$ $(1 \le n(i, d) \le N - d\tau)$ is an integer such that $y_{n(i,d)}(d)$ is the nearest neighbor of $y_i(d)$ in the d-dimensional reconstructed phase space, in the sense of the Euclidian distance defined above.

If d qualifies as an embedding dimension, than any two points that stay close in the d-dimensional reconstructed space will be still close in the $(d+1)$-dimensional reconstructed space. Such pairs of points are called true neighbors, otherwise, they are called false neighbors. Perfect embedding means that no false neighbors exist. The idea

of the false neighbor method is to diagnose a false neighbor by seeing whether the *a(i,d)* is larger than some given threshold value. In order to avoid the problem of choosing an appropriate threshold value, Cao (1997) defines the mean value of all *a(i,d)*'s, denoted as *E(d)*. To investigate its variation from *d* to *d + 1*, one defines,

$$E1(d) = E(d+1)/E(d). \quad (5.8)$$

It is found that *E1(d)* stops changing when *d* is greater than some value d_0, if the time series comes from an attractor. Then $d_0 + 1$ is the minimum embedding dimension which we look for. Since in practical computations it is difficult to resolve whether *E1(d)* is slowly increasing or has stopped changing for sufficiently large *d*, Cao (1997) introduces another quantity, $E^*(d)$, which is useful to distinguish deterministic signals from stochastic signals. The *E*(d)* statistic discards all past outputs and simply averages between the future outputs of each pair of nearest neighbors in the time series. Further, define:

$$E2(d) = E^*(d+1)/E^*(d). \quad (5.9)$$

For random data, since the future values are independent of the past values, *E2(d)* will be equal to 1 (or very close to 1) for any *d*. However, for deterministic data, *E2(d)* is certainly related to *d*, and as a result, it can not be a constant for all *d*. In other words, there must exist some values of *d* such that $E2(d) \neq 1$.

Although in principle the embedding dimension is not dependent on the delay parameter τ, in practice, the minimum embedding dimension is dependent on τ. We determined this parameter by using the method based on the correlation function. The τ parameter is chosen as the time lag where the correlation function becomes approximately equal to *1/e*.

5.5.2 Results of the non-linear time series analysis

As stated above, we are using the inter-event times between successive earthquakes as input in our non-linear analysis. Our choice was made by considering that the earthquake occurrence time is one of the most reliable and accurate parameters that define a seismic event. Also, our choice was based on the relevance of earthquake recurrence times for earthquake hazard and prediction. There is also theoretical support for our choice from Hegger and Kantz (1997), who showed theoretically and practically that the embedding of sequences of time intervals is a valid approach in non-linear

analysis. We used for our analysis the declustered earthquake catalog and choose the magnitude threshold as 2.8 (the magnitude of completeness).

As we demonstrated in the previous sub-chapter, for a large range of scales, there is no significant correlation between the earthquake inter-occurrence times in the case of the declustered catalog. The autocorrelation function (Fig. 5.11) confirms this result, as it becomes very small (less than *1/e*) for $\tau = 2$. Here, we determined τ by using the mutual information method (Fraser and Swinney, 1986), which proved superior in the non-linear context, but the result does not change significantly. The results of the autocorrelation analysis, together with a broad power spectrum and the absence of a clear structure (attractor) in phase-space plots and return maps (simple visual tools, not shown here), all exclude dynamical simplicity (Kantz and Schreiber, 1997) and indicate complexity of the process.

Before showing *E1* and *E2* for our series, it is worthwhile to see how these statistical estimators change in the case of a well-known low-dimensional system, the Lorentz system. The Lorentz attractor is described in almost any book on chaos and is a simplified model of a dissipative chaotic flow, consisting of three differential equations, which was used by Lorentz (1963) to model atmospheric dynamics. Even though the Lorentz system is purely deterministic, it behaves in a complex, chaotic way. Linear methods can not distinguish its dynamics from a random, stochastic process. Figure 5.12 presents *E1(d)* and *E2(d)*, for dimensions *d* between 1 and 10. One can see that *E1*, after an abrupt increase, reaches a relatively stable plateau for dimensions $d \geq 2.0$. Further conclusive evidence about the low-dimensionality of the system comes from the graph of *E2*, which steeply increases for $d = 1$ to $d = 2$, so it is certainly far from being a constant. Based on the saturation value of *E1*, we can infer that the minimum embedding dimension of the Lorentz system is three, in agreement with the theoretical results.

Figure 5.13 shows the *E1* and *E2* parameters versus dimension, for the case of the earthquake data. *E1* gradually increases with *d* and does not reach a stable nearly constant value, as in the case of the Lorentz system. *E2*, on the other hand, varies in a very narrow band, and essentially does not change with dimension. Both results indicate clearly that our time series belongs to a stochastic process rather than a deterministic one. Since the applied method works well even when the dimensionality of the system is high, in the cases of moderately noisy data and does not depend strongly on the

number of data available (Cao, 1997), we consider that the reliability of the results is high. During our tests, we encountered situations when *E1* stopped changing at large *d*, because the data sets were limited. However, in all situations *E2* remained very close to one, with no significant variations.

We tested the Vrancea intermediate-depth catalog for other threshold magnitudes, up to 4.0, and in all situations the result remains the same, showing there is no evidence of even high-dimensional deterministic chaos.

The method employed in this analysis is strongly related to the predictability of the system under study, especially through the parameter *E2*. In some situations, when the predictability of the system is very low, but the system is still deterministic (with a high Lyapunov exponent), the method may find it difficult to distinguish such a system from a stochastic one (Cao et al., 1998). However, for our purposes, the very low predictability is already an important result. Therefore, we have tested the predictability of our time series (1-step ahead prediction) by using the existing prediction techniques. In all situations we found that the predictability is extremely low, even for high embedding dimensions. This result implies that, at least for practical purposes, the studied earthquake process is stochastic, for the range of the tested threshold magnitudes.

Goltz (1997) and Matcharashvili et al. (2000) found evidence of chaotic dynamics in earthquake systems by applying a fractal dimension method on series of inter-event times, for earthquakes in Japan and the Caucasian region, respectively. The authors of both papers used undeclustered catalogs in their analysis. Moreover, Matcharashvili et al. (2000) found that by eliminating the aftershock sequences, the low-dimensionality found for the original, undeclustered catalog disappears. The authors argue that by filtering out the aftershocks, the attractor dynamics might have been altered and, thus, the low-dimensionality could not be detected anymore. It is worth arguing that the presence of aftershocks in the analyzed time series does introduce temporal correlations, which are not desirable in the context of non-linear time series analysis. Surrogate data tests, however, showed that the low-dimensionality found for the original catalogs is a reliable result. In our study, the aftershocks are very few, relatively easy to identify, easy to eliminate and clearly posses a distinct scaling behavior. Therefore, we believe that by filtering them out our results are not influenced. In order to confirm this, however, we checked by using similar procedures on the undeclustered catalog, and the results do not change.

A very elaborate non-linear analysis was performed by Anghel et al. (2002) on the deformation field produced along a cellular fault zone embedded in a 3D elastic solid. The authors found low-dimensional chaos for major events, while the smaller shocks were found to be random noise. The results obtained so far for the Vrancea region seem to be in agreement with such findings.

5.6 Conclusions and remarks

The main purpose of this study was to characterize the temporal occurrence of the Vrancea intermediate-depth earthquakes, by using advanced linear and non-linear techniques. At the same time, we offer an easy-to-use software package, which can be readily applied to seismicity studies. Our results were explained in detail already, but here we point out the important, general conclusions and suggest possible further studies.

1. The multifractal analysis performed on the original (undeclustered) catalog revealed the existence of two distinct scaling regions, with different fractal properties. The clear separation of these two domains is probably a peculiarity of intermediate or deep earthquakes, characterized by a small number of aftershocks, which are clustered in a very short time interval after the mainshock. This may imply that different physics underlie small and large time scales. We are not aware of other similar results, probably because previous studies focused on the multifractal characteristics of crustal seismicity. In such cases, there is no crossover and a unique multifractal spectrum characterizes the earthquake sequences.

2. The study of the correlation properties of the integrated inter-event times, performed using the DFA method, revealed a non-correlated Brownian process, the correlation exponent being close to 0.5. This result contrasts with the temporal evolution of crustal seismicity, where both short and long range correlations were observed (Kagan and Jackson, 1991, Xu and Burton, 2002, Enescu et al., 2002).

3. The results of auto-correlation, power-spectrum and mutual information analyses, as well as some visually-oriented investigations (phase-space plots and return maps), exclude dynamical simplicity for the Vrancea earthquake system. A modified false neighborhood method, applied to the series of inter-event times, showed evidence of stochasticity and lack of deterministic chaos for the earthquake generation process in the Vrancea region. We also carried out our analysis for threshold magnitudes between

2.6 and 4.0, but the results do not change significantly. It seems that the predictability of events in a large magnitude range is low or very low. However, the major Vrancea earthquakes ($M_W \geq 6.5$) may posses some complex periodicities, as indicated by several previous studies (Enescu et al., 1974, Purcaru, 1979, Enescu and Enescu, 1999). In a future investigation we will try to understand the occurrence of these large events in a non-linear framework. Although the number of major earthquakes seems prohibitively small, some analysis tools, like the recurrence quantification analysis (Zbilut and Webber, 1992), are especially designed for such cases.

4. All of the performed analyses, complementary in their nature, bring new evidence on the complexity and randomness of the earthquake occurrence process, and thus on the difficulty of predicting earthquakes. However, as other studies suggest, the evolution in time of the spatial pattern of seismicity may reveal precursory information. This will be the subject of a next study we are going to tackle.

Chapter 6

-WAVELET-BASED MULTIFRACTAL ANALYSIS OF REAL AND SIMULATED TIME SERIES OF EARTHQUAKES-

6.1 Introduction

The notion of scaling is defined loosely as the absence of characteristic scales of a time series. Its main consequence is that the whole and its parts cannot be statistically distinguished from each other. The absence of such scales requires new signal processing tools for analysis and modeling. The *exact self-similar*, scale-invariant processes, like for example the fractional Brownian motion, are mathematically well defined and well documented. In actual real-world data, however, the scaling holds only within a finite range and will typically be approximate. Therefore, other "scaling models" are more appropriate to describe their complexity. *Long-range dependence* (*LRD*) or long-memory is a model for scaling observed within the limit of the largest scales. Research on LRD (or *long-range dependence (correlation)*) characteristics of "real" time series is the subject of active research in fields ranging from genetics to network traffic modeling. Another broad class of signals corresponds to "*fractal processes*", which are usually related to scaling in the limit of small scales. Such time series are described by a (local) scaling exponent, which is related to the degree of regularity of a signal. If the scaling exponent varies with position (time), we refer the corresponding process as multi-fractal. The fractal concept, however, is usually used in a broader sense and refers to any process that shows some sort of self-similarity.

(Multi)fractal structures have been found in various contexts, as for example in the study of turbulence or of stock market exchange rates. The concepts of "fractal analysis" have also been applied to describe the spatial and temporal distribution of earthquakes (e.g. Smalley et al., 1987, Turcotte, 1989 and Kagan and Jackson, 1991). Geilikman et al. (1990), Hirabayashi et al. (1992) and Goltz (1997) have all employed a multifractal approach to characterize the earthquake spatial, temporal or energy distribution. Their results suggest that seismicity is an inhomogeneous fractal process. Kagan and Jackson (1991), by analysing statistically several instrumental earthquake

catalogs, concluded that besides the short-term clustering, characteristic for aftershock sequences, there is a long-term earthquake clustering in the residual (declustered) catalogues.

Wavelet analysis is a powerful technique, well suited to understanding deeply the complex features of real world processes: different "kinds" of (multi)fractality, LRD, non-stationarity, oscillatory behavior and trends. The purpose of this study is to apply wavelet analysis to reveal the multifractal and LRD characteristics of the occurrence times of earthquakes. More precisely, we apply the wavelet transform modulus maxima (*WTMM*) method that has been proposed as a generalization of the multifractal formalism from singular measures to fractal distributions, including functions (Arneodo et al., 1991, Muzy et al., 1994 and Arneodo et al., 1995). By using wavelet analysis, we reveal the clear fractal characteristics of the analyzed time series and successfully describe the main features of our earthquake sequences. The study focuses on the interpretation and explanation of the various temporal fractal patterns found in earthquake time series and thus, we hope, will be useful for future related studies. To the best of our knowledge, this is the first systematic study of the multifractal and correlation properties of earthquake time series by using a wavelet approach. Ouillon and Sornette (1996) have developed a wavelet-based approach to perform multifractal analysis, and applied it in a related field: the study of earthquake' fault patterns.

In the next sub-chapter we introduce the *WTMM* method and explain the relation between multifractality and wavelets. The data to be analysed are introduced in Section 6.3 and consist of four earthquake time series. Two of them are real earthquake sequences, while the other two are simulations. Firstly, we generate a sequence of events by using the *ETAS* model (Ogata, 1985, 1988). The second "artificial" time series is obtained by using a realistic earthquake model: an inhomogeneous cellular fault embedded in a three-dimensional elastic solid (Ben-Zion and Rice, 1993, Ben-Zion, 1996).

6.2 The Continuous Wavelet Transform (CWT) and the wavelet-based multifractal analysis

The wavelet transform is a convolution product of the data sequence (a function $f(x)$, where x, referred to in this study as "position", is usually a time or space variable) with the scaled and translated version of the mother wavelet, $\psi(x)$. The scaling and

translation are performed by two parameters; the scale parameter *s* stretches (or compresses) the mother wavelet to the required resolution, while the translation parameter *b* shifts the analysing wavelet to the desired location:

$$(Wf)(s,b) = \frac{1}{s}\int_{-\infty}^{+\infty} f(x)\psi^*\left(\frac{x-b}{s}\right)dx, \qquad (6.1)$$

where *s*, *b* are real, $s > 0$ for the continuous version (CWT) and ψ^* is the complex conjugate of ψ. The wavelet transform acts as a microscope: it reveals more and more details while going towards smaller scales, i.e. towards smaller *s* values.

The mother wavelet ($\psi(x)$) is generally chosen to be well-localized in space (or time) and frequency. Usually, $\psi(x)$ is only required to be of zero mean, but for the particular purpose of multifractal analysis $\psi(x)$ is also required to be orthogonal to some low-order polynomials, up to the degree *n*:

$$\int_{-\infty}^{\infty} x^m \psi(x)\,dx = 0, \qquad \forall m, \quad 0 \le m < n \qquad (6.2)$$

Thus, while filtering out the trends, the wavelet transform can reveal the local characteristics of a signal, and more precisely its singularities. (The Holder exponent can be understood as a global indicator of the local differentiability of a function.) By preserving both scale and location (time, space) information, the *CWT* is an excellent tool for mapping the changing properties of non-stationary signals. A class of commonly used real-valued analyzing wavelets, which satisfies the above condition (6.2) is given by the successive derivatives of the *Gaussian* function:

$$\psi^{(N)}(x) = \frac{d^N}{dx^N} e^{-x^2/2} \quad , \qquad (6.3)$$

for which $n = N$. In this study, the analyzing wavelet is the second derivative of the *Gaussian*. The computation of the *CWT* was carried out in the frequency domain, by using the *Fast Fourier Transform*. The time series were padded with zeros up to the next power of two to reduce the edge distortions introduced by the Fourier transform, which assumes the data is infinite and cyclic (Torrence and Compo, 1998).

It can be shown that the wavelet transform can reveal the local characteristics of *f* at a point x_o. More precisely, we have the following power-law relation:

$$W^{(n)} f(s, x_0) \sim |s|^{h(x_0)} \qquad (6.4)$$

where h is the Hölder exponent (or singularity strength). The symbol "*(n)*", which appears in the above formula, shows that the wavelet used ($\psi(x)$) is orthogonal to polynomials up to degree n (including n). The scaling exponent C, estimated by using the DFA method in the previous chapter, known also as the Hurst exponent, is a global measure of self-similarity in a time series, while the singularity strength h can be considered a local version (i.e. it describes "local similarities") of the Hurst exponent. In the case of monofractal signals, which are characterized by the same singularity strength everywhere ($h(x) = ct$), the Hurst exponent equals h. Depending on the value of h, the input series could be long-range correlated (h > 0.5), uncorrelated (h = 0.5) or anti-correlated (h < 0.5).

The continuous wavelet transform described in Eq. 6.1 is an extremely redundant representation, too costly for most practical applications. To characterize the singular behavior of functions, it is sufficient to consider the values and position of *the **W**avelet **T**ransform **M**odulus **M**axima* (*WTMM*) (Mallat and Hwang, 1992). The wavelet modulus maxima is a point (s_0, x_0) on the scale-position plane, (s,x), where $|Wf(s_0, x)|$ is locally maximum for x in the neighborhood of x_0. These maxima are located along curves in the plane (s,x). The WTMM representation has been used for defining the partition function-based multifractal formalism (Muzy et al., 1994, Arneodo et al., 1995).

Let $\{u_n(s)\}$, where n is an integer, be the position of all local maxima at a fixed scale s. By summing up the q's power of all these WTMM we obtain the partition function Z:

$$Z(q,s) = \sum_n |Wf(u_n, s)|^q \qquad (6.5)$$

By varying q in Eq. 6.5, it is possible to characterise selectively the fluctuations of a time series: pozitive q's accentuate the "strong" inhomogeneities of the signal, while negative q's accentuate the "smoothest" ones. In this work, we have employed a slightly different formula to compute the partition function Z by using the "supremum method", which prevents divergences from appearing in the calculation of $Z(q,a)$, for $q < 0$ (e.g. Arneodo et al., 1995).

Often scaling behavior is observed for $Z(q,s)$ and the spectrum $\tau(q)$, which describes how Z scales with s can be defined:

$$Z(q,s) \sim s^{\tau(q)} \qquad (6.6)$$

If the $\tau(q)$ exponents define a straight line, the analysed signal is a monofractal; otherwise the fractal properties of the signal are inhomogeneous, i.e. they change with location, and the time series is a multifractal. By using the Legendre transformation we can obtain the multifractal spectrum $D(h)$ from $\tau(q)$. $D(h)$ is a generalization of the $f(\alpha)$ singularity spectrum (defined in the previous chapter) from measures to functions and captures how "frequently" a value h is found.

For the computations made in this work, we acknowledge the use of the *Matlab* software package (http://www.mathworks.com), Matlab's *Wavelet Toolbox* and the free software programs: *Wavelab* (Stanford University – http://www-stat.stanford.edu/~wavelab) (Buckheit and Donoho, 1995), *Fraclab, A Fractal Analysis Software* (INRIA - http://fractales.inria.fr/) and other *Matlab* routines (http://paos.colorado.edu/research/wavelets/; Torrence and Compo, 1998). We also developed some routines, in *Matlab*, which are going to be made available on the web (http://www.rcep.dpri.kyoto-u.ac.jp/~benescu/). Software and data for earthquake simulations were kindly provided by Y. Ogata, for the *ETAS* model, and Y. Ben-Zion and M. Anghel, for the 2D heterogeneous fault model, embedded in a 3D elastic half-space.

6.3 Data

We have applied the wavelet-based approach to the analysis of four sets of earthquake data; two of them are real and the other two are simulations. The data consists of inter-event times between successive earthquakes above a threshold magnitude. The results of the multifractal analysis ($\tau(q)$, $D(h)$) correspond, however, to the integrated inter-event times. In this way, we made our results directly comparable with those obtained by Enescu et al. (2003b) (see also Chapter 5 of the thesis), who uses the *Detrended Fluctuation Method* (*DFA*) to analyze the seismicity of the Vrancea (Romania) region. The method (*DFA*) requires integrating the data in advance. Nonetheless, the integration just adds a constant value (one) to the obtained h, the results being otherwise identical (Arneodo et al., 1995). The four sets of data are explained briefly below.

The Vrancea (Romania) region seismic activity

As a first application, we considered the intermediate-depth seismicity (60-200km depth) of the Vrancea region, Romania, between 1974-2002 (Fig. 6.1a). We have used an up-dated version of the Trifu and Radulian (1991) catalog. The magnitude of completeness of the catalog slightly increases with depth, being on average around 2.6 (Trifu and Radulian, 1991). Therefore, we have selected for analysis the earthquakes with $M \geq 2.6$, and the resulting catalog has 4254 events. A detailed description of the catalog and its main statistical features can be found in Trifu et al. (1990), Trifu and Radulian (1991) and Enescu et al. (2003b).

The seismic activity before the 1995 Kobe earthquake

The second case studied is represented by the crustal seismic activity which occurred in the Northern Hyogo area, Japan, from 1976 to January 17, 1995 Kobe earthquake (Mw = 6.9), in a broad area surrounding the epicenter of the big event (Fig. 6.1b). We have used the high quality earthquake catalog of the Disaster Prevention Research Institute, Kyoto University, which for the area and period under investigation, is complete in earthquakes of magnitude $M \geq M_C = 1.5$. The data set (6583 events) was thoroughly tested statistically by Enescu and Ito (2001a) and also in this thesis (Chapter 2). Therefore we refer to these studies for further details.

ETAS model simulation

The *ETAS* (*Epidemic-Type Aftershock sequence*) model (Ogata, 1985, 1988) is a point process model representing the activity of earthquakes of magnitude *Mc* and larger occurring in a certain region, during a certain interval of time. We have simulated such a process by using the following parameters: $Mc = 1.5$, $b = 1.0$, $\mu = 0.1$, $K = 0.04$. $c = 0.01$, $\alpha = 0.4$ and $p = 1.2$ (Fig. 6.1c). The first parameter represents the magnitude of completeness for the simulated data. The *b*-value is the slope of the frequency-magnitude distribution of earthquakes. The following five parameters represent the characteristics of earthquakes in the simulated time series. Among them, the last two parameters, α and *p*, are the most important in describing the temporal pattern of seismicity. Thus, the *p* value describes the decay rate of aftershock activity, and the α value measures the efficiency of an earthquake of a certain magnitude to generate its offspring, or aftershocks, in a wide sense. For the physical interpretation of the other parameters and more details we refer to Ogata (1992). In this study we have chosen a

small α value to simulate a sequence of 7000 events with "low-productivity" of aftershocks.

Simulation of seismicity by using a 2D heterogeneous fault embedded in a 3D elastic half space.

The model we use (Ben-Zion, 1996) generate seismicity along a fault segment that is 70km long and 17.5 km deep. The fault is divided into square cells with dimensions of 550 m. The boundary conditions and model parameters are compatible with the observations along the central San Andreas Fault. Eneva and Ben-Zion (1997) applied several pattern recognition techniques to examine four realizations of the model, with the same creep properties, but different brittle properties. The simulated catalog of this study is identical to the case (A), described by Eneva and Ben-Zion (1997), and is the result of a fault model containing a Parkfield-type asperity of size 25 km X 5 km. From now on we will refer to this simulation as EBZ_A (25880 events in total; Fig. 6.1d).

We decided to decluster both "real" earthquake catalogs before analysis (i.e. to eliminate the aftershock sequences from the catalogs), by using Reasenberg's (1985) algorithm, for two main reasons:

a) We are more interested in searching for *LRD* in the catalog and therefore the elimination of shorter-range dependent seismicity (i.e., aftershocks) is considered appropriate, since it may influence the results on *LRD*.

b) The magnitude of completeness might be sub-evaluated immediately after the occurrence of some larger events, during the periods and in the regions under study. However, in the case of the intermediate-depth Vrancea earthquakes, the number of aftershocks is small even after major earthquakes, like those that occurred in 1977 (Mw = 7.4), 1986 (Mw = 7.1) and 1990 (Mw = 6.9). For the crustal, shallow events in the Hyogo area, there are no major earthquakes during the period of investigation.

6.4 Results and discussion

Figure 6.1 shows the series of inter-event times between consecutive earthquakes for all the four cases studied. The graphs look rather similar, with no clear distinctive characteristics. Only for the EBZ_A simulation (Fig. 6.1d), some kind of regular and quasi-periodic behavior can be observed.

Figure 6.2 displays the "*tau spectrum, (τ(q)*", obtained by using the WTMM method, in the case of a "classic" example of a recursive fractal function: *the Generalized Devil's Staircase*, associated with the *Multinomial Cantor Measure*. The measure is constructed by dividing recursively the unit interval *[0, 1]* in four sub-intervals of the same lengths and distributing the "measure" or "mass" μ among them, with the weights *p1*, *p2*, *p3* and *p4* (*p1+p2+p3+p4 = 1*) (Peitgen et al., 1992, Appendix B). One can notice the very good agreement between the theoretical and the computed spectrum, for *q* values between –7 and 10. The spectrum is curved, which indicates the multifractal nature of the time series. By using the Legendre transform, we obtain the spectrum *D(h)*, represented in Fig. 6.3, which clearly confirms the non-uniqueness of the Hölder exponent *h*, and thus the multifractality of the process.

Figure 6.4a shows the *CWT* representation in the case of the Vrancea region earthquake intervals. A zoomed view is displayed in order to observe better the clear self-similar (*fractal*) pattern. From an intuitive point of view, the wavelet transform consists of calculating a "resemblance index" between the signal and the wavelet, in this case the second derivative of the *Gaussian*. If a signal is similar to itself at different scales, then the "resemblance index" or wavelet coefficients also will be similar at different scales. In the coefficients plot (Fig. 6.4a), which shows scale on the vertical axes, this self-similarity generates a characteristic pattern. We believe that this is a very good demonstration of how well the wavelet transform can reveal the fractal pattern of the seismic activity at different times and scales. Fig. 6.4b displays the maxima lines of the *CWT* (i.e. the *WTMM* tree) in the case of the Vrancea time series. One can notice the branching structure of the *WTMM* skeleton, in the *(position, scale)* coordinates, which enlightens the hierarchical structure of time series singularities.

Figure 6.5 represents in a logarithmic plot the partition functions *Z (q,s)* versus scale *(s)*, obtained from the *WTMM* skeleton representation (Fig. 6.4b). One can notice the existence of a well-defined, relatively broad scaling region, as it is indicated in the figure. This scaling domain corresponds approximately to time periods from days to several years.

Figure 6.6 shows the *D(h)* plot in the case of the Vrancea (Romania) integrated inter-event times. The spectrum is narrow (i.e. the Hurst exponent (*h*) takes values in a very limited range). The *tau* spectrum, represented in the inset of the figure, can be well fitted by a straight line. These observations suggest that our time series is the result of a

monofractal (or almost monofractal) process. One can also notice that the "central" *h* value of the spectrum is close to 0.5, which is an indication of the quasi-random behavior of the time series. Enescu et al. (2003b) (see also Chapter 5 of the thesis) obtained a similar result, by using a "monofractal" approach, the *Detrended Fluctuation Analysis* (*DFA*) technique. We conclude that the defining temporal characteristics of the analyzed data set ($M \geq 2.8$) are mono-fractality and randomness. We can not exclude, however, the existence of a non-random (quasi-periodic?) pattern for the major Vrancea earthquakes, as discussed by Enescu et al. (2003b).

Figure 6.7 shows the partition functions *Z(q,s)* computed from the WTMM skeleton of the second time series considered here for analysis: the inter-event times of the Northern Kinki area sequence. One can easily notice that there are two distinct, well-defined, scaling domains, at smaller scales and larger ones, respectively, as indicated in the figure. Further evidence for the existence of these two scaling regions is presented in Fig. 6.8, which displays the amplitude of the *Wavelet Transform* along *Ridges* (i.e. maxima lines). As Eq. 6.4 also suggests, the slopes of these maxima lines correspond to the local Hölder exponents (or local singularities) of a time series. However, for most "real" signals, these "local" slopes are intrinsically unstable (mainly because the singularities are not isolated), thus making very difficult the estimation of these local exponents. In contrast, the partition function approach provides global estimates of scaling, which are statistically more robust. However, by closely examining Fig. 6.8, one can notice that again there is a rather clear crossover between large and small scales.

By computing the corresponding *D(h)* spectrum for each of the two scaling domains, at small scales ($2^1 \sim 2^4$) we observed a multifractal behavior, while at larger scales ($2^4 \sim 2^9$) the series is monofractal, with an exponent of about 0.8. The first scaling domain extends roughly from hours to days, while the second one corresponds to periods of times up to 2-3 years. As is known, $h > 0.5$ could indicate the presence of correlations (or long-range correlations), but there is also another important factor that can produce $h > 0.5$. It relates to the probability distribution of the time series (in our case the probability distribution of the inter-event times). Thus, for series with a power-law like probability distribution (or other distributions characterized by heavy-tails), one observes $h > 0.5$. A method to discriminate between *LRD* and the results of the probability distribution effects is to analyze the shuffled version of the signal. By

shuffling the series, the correlation is lost but the power-law like distribution, if present, remains unchanged. In other words, the shuffled series would have $h = 0.5$ in the first case (only *LRD*) and $h > 0.5$ in the second one (only power-law like distribution). We shuffled our series and obtain $h = 0.5$, which excludes the possibility of an h larger than 0.5 caused by the probability distribution.

There is still one more factor that could "induce" *LRD*-like characteristics: the presence of trends within the data. As already mentioned, the wavelet-approach eliminates the effect of polynomial trends, if an appropriate mother-wavelet is used to compute the *CWT*. However, there are situations when other types of trends are present in the time series, like for example power-law or oscillatory trends. As shown by Kantelhardt et al. (2001) and Hu et al. (2001), both kinds of non-stationarities, superposed on LRD data, could produce crossovers of the scaling region. By carefully analyzing our sequence, we identified some oscillatory behavior and also periods of "accelerating seismicity" or quiescence. As shown by Enescu and Ito (2001a) and in Chapter 2 of this thesis, anomalous earthquake-frequency changes occurred several years before the 1995 Kobe earthquake. The increase and decrease of earthquake frequency could have been associated with power-law (or higher order polynomial?) trends of the earthquake intervals. Therefore, it is possible that such rather complex non-stationary patterns are responsible for the large value of h obtained in this study. We would like to note, however, that while a clear distinction should be made between simple, trivial trends and genuine long-range dependence, such a separation is probably less definite in the case of trends having complex, low-frequency characteristics. On the other hand, probably more important to emphasize in our case is the existence of two distinct scaling domains, both of them associated with fluctuations that are *intrinsic* to the data. More research has to be done, however, to identify "the nature" of these fluctuations and their physical background.

The computation of the *D(h)* spectrum at small scales (2^1 to 2^4 ; see Fig. 6.7) showed multifractality, which probably corresponds to a inhomogeneous local scaling behavior of the time series. The result may also reflect the incomplete detection and removal of aftershocks. However, these findings are less reliable due to the limited length of the data set and a rather short scaling domain.

Our third case is concerned with the analysis of a simulated earthquake sequence, obtained by using the *ETAS* model. Figure 6.9 shows the *D(h)* spectrum computed by using a scaling region of the partition functions Z between 2^3 and 2^{10}. The plot shows a

monofractal spectrum, with a Hurst exponent (h) close to 0.5. It is an expected finding for a sequence that has low offspring-productivity and thus behaves almost randomly in the range of scales mentioned above. The result demonstrates that the small number of aftershocks, which occurred for very short periods of time, could not influence significantly the spectrum's characteristics at larger scales.

Our final analysis is concerned with another earthquake simulation, EBZ_A (see sub-chapter 6.3). We are primarily interested here to see if oscillatory behavior of the time series could induce a crossover in scaling and apparent long-range correlation. Figure 6.10 shows the result of a basic statistical testing of data. We represent the cumulative probability distribution of the inter-event times in a half-logarithmic plot. A random occurrence of earthquakes corresponds to an exponential distribution of the inter-event times and, thus, in such a case, one would expect a straight line of the plot. The evident departure from linearity is a clear proof that the simulated earthquakes do not occur randomly. The step-like shape of the plot suggests that some recurrence intervals are strongly preferred, or in other words that our data has several quasi-periodicities.

Figure 6.11a presents the frequency of earthquakes versus time (the total time span of the earthquake sequence is 150 years). The graph confirms the periodic behavior found before. We have also analyzed the variation of CWT coefficients with time and found the same oscillatory behavior. Figure 6.11b displays the partition functions in the case of the EBZ_A simulation, only for $q = 2, 3$ *and* 4. As in the case of the *"Northern Kinki seismicity time series*", one can see a segmented plot, which indicates different characteristics across scales. It is beyond the purpose of this study to analyze in detail the influence of oscillatory trends on the multifractal characteristics of the analyzed signal, as they are revealed by wavelet analysis. Some preliminary results indicate, however, that such a relation could be "quantified" and employed as a useful tool to analyze the behavior of complex signals.

6.5 Conclusions

The present study presents an in-depth analysis of the multifractal and correlation properties of real and simulated time series of earthquakes, using a wavelet-based approach. Our study reveals the clear fractal pattern of the analyzed series of inter-event times and their different scaling characteristics.

In the case of the intermediate-depth seismic activity in Vrancea, Romania, we found random and monofractal behavior that occurs for a rather broad range of scales. The crustal seismic activity in the Hyogo area, Japan, has different characteristics, the most notable ones being the crossover in scaling and the long-range correlation signature observed at larger scales. It is not certain, however, what is the "nature" of this LRD-like behavior. We are inclined to believe that the complex non-stationarities of the data (trends) are responsible for the result. There is some evidence in support of our assumption, coming from theoretical studies of LRD with superposed oscillatory or power-law trends.

The investigation of two simulated earthquake sequences helped to understand the fractal and correlation properties of the real data. Thus, the analysis of the ETAS model sequence, with a "low-productivity" of aftershocks, showed that the clustering which occurs "locally" does not have any influence on the results at larger scales. The investigation of the time series of earthquakes, simulated by using a cellular fault embedded in a 3D elastic medium, revealed the quasi-cyclic behavior of the earthquake occurrence. We have shown that there are several crossovers of scaling, which are probably associated with the oscillatory trends of the simulated sequence of earthquakes.

The fractal characteristics of our time series were mainly addressed in this study by computing "global estimates of scaling". However, by using a recently developed technique (Struzik, 1999) one can evaluate the Holder exponent at an arbitrary location and scale. Such an approach has led to interesting findings in different fields, such as medicine (Ivanov et al., 1999) or economy (Struzik, 2001). In our next studies we are planning to follow such a "local" approach to study the complexity of earthquake time series. Moreover, by using a 2D wavelet-transform, we would like to extend our research from time series to spatial patterns of seismicity.

Chapter 7
-GENERAL DISCUSSION AND PLANS FOR FUTURE WORK-

As shown in the last five chapters of the thesis, there are a variety of temporal and spatial patterns of seismicity, which require a careful analysis and interpretation. Besides, when analyzing real earthquake data, it is critically important to carefully check the catalogs before stepping into further investigation. Many times artificial, man-made changes of the catalog could be easily considered as being genuine if proper action is not taken in advance.

In Chapters 2 to 4, the tools for analyzing the data are somehow "classical" and have been used extensively by many other researchers. In the case of the statistical investigations, I believe strongly that only by doing several complementary tests, one can draw reliable conclusions. Thus, in Chapter 2, to investigate the precursory phenomena **before** the 1995 Kobe earthquake, I analyzed both the original and declustered catalogs by using a set of statistical approaches, among them *z*-value tests, *b*-value and fractal dimension computations. As concerns Chapter 3, both *b* and *p* values were analyzed for their spatial and temporal variations before and especially **after** the 2000 Western Tottori earthquake. The completeness of the catalog was also checked. In all cases the significance of the results was carefully addressed. In the case of Hida Mountain **earthquake swarm**, in particular, the precise double-difference relocation of events and the computation of the static stress changes caused by the largest shocks of the sequence, were important for explaining the pattern of seismic activity, including its migration, and the *b*-value spatial and temporal changes.

In all these studies I tried to correlate the patterns of seismic activity with other physically meaningful parameters and, when possible, to build a simple but realistic model to explain the results. In this concluding chapter I would like to bring together several conclusions, which I believe synthesize the common points and the differences between the analyzed earthquake sequences. Thus, one of the possible "keywords" for the seismicity, *b*-value and *p*-value temporal changes for all the studied sequences, is "*Stress*" (absolute or relative). The increase of stress in the Northern Kinki region caused probably the dilatancy of rocks in a rather broad area and, as a result, determined

the onset of seismic quiescence, as it is described in the thesis. The significant increase of *b*-value prior to the major event shows that the quiescence is seen especially for larger shocks, in agreement with many other similar observations (Smith, 1981). The sudden increase of seismic activity before Kobe earthquake could be attributed to the "final" accelerated stress increase, just before the main rupture. The pattern of *b*- and *p*-value observed before and after the 2000 Western Tottori earthquake is probably caused by stress changes, as it is described in Chapter 3. The distribution of *b*- and *p*-value for the aftershocks of the 1995 Kobe earthquake (Wiemer and Katsumata, 1999) shows a similar pattern as the one we found in the case of the Western Tottori earthquake. Large values of the parameters were found in areas of intense rupture and relatively small values were obtained in areas of high stress after the mainshock. Finally, the migration of seismic activity during the 1998 Hida Mountain earthquake swarm and the significant difference of b-value in the northern and southern part of its epicentral area is also attributed to stress changes (see Chapter 4). When interpreting the b-value for the aftershocks of the 2000 Western Tottori earthquake and in the case of the Hida Mountains region, we point out that the crustal structure (i.e., its heterogeneity and thermal structure) might offer an alternative explanation in certain situations. Another keyword of the thesis would be "*Predictability*". The seismic activity before and after the 1995 Kobe earthquake and the 2000 Western Tottori earthquake showed clear non-random patterns, as suggested by the anomalous behavior of several statistical parameters, most of them having a precursory nature. The predictability of earthquake sequences was further and deeper addressed in Chapters 5 and 6, for intermediate-depth, shallow and simulated earthquake sequences. As one can notice, we have studied earthquakes occurred in regions with different tectonic backgrounds and compare the results of the analysis.

In the *Introduction* of the book "*GeoComplexity and the Physics of Earthquakes*", J.B. Rundle, D.L. Turcotte and W. Klein comment on "an exciting new kind of science", which is being born and that focuses on the temporal and spatial evolution of complex systems. This new and growing area of research explores how fractals and chaos theory can clarify complex Earth systems such as earthquakes, leading eventually to proven methods of prediction.

Chapters 5 and 6 are a modest attempt to apply several techniques from similar areas of statistical physics and chaotic systems to earthquakes, in particular to seismic

activity. I also address the problem of predictability of the studied earthquake systems, by using the non-linear analysis approach. The results obtained in these chapters emphasize the difference between shallow and deep seismic activity. For the first case we found increased inhomogeneity at small scales and significant correlation of seismic activity at large scales (2-3 years). In the second case the seismic activity at both small and large scales is random, with no significant temporal correlation. We note, however, that the statistical estimates used in these last two chapters are global, so in future studies we are planning to compute also local estimates, which may offer more detailed information.

Chapter 6 introduces a new method for analyzing the temporal pattern of seismic activity, by using wavelet analysis. In collaboration with Z. R. Struzik (*Centre for Mathematics and Computer Science, The Netherlands*) and A. Khalil (*Laval University, Canada*), I am testing a new methodology that would extend the temporal analysis to spatial (*2D*) patterns of earthquake distributions. We believe this would be useful to characterize the local and global behavior of seismic activity. Together with M. Anghel (*Los Alamos National Laboratory, USA*), I try to combine wavelets and chaotic analyses to understand the occurrence pattern of large earthquakes. I am particularly interested to test these new methods on both simulated and real earthquake sequences and to compare the results. Moreover, as the wavelet approach is ideal to investigate the evolution of non-stationary time series, I would like to apply it to other kinds of data, like for example GPS, stress, strain or groundwater data.

Seismicity analysis for the study of tectonic processes, earthquake recurrence and earthquake interaction requires good knowledge of the location of earthquake hypocenters. Therefore, in collaboration with J. Mori (*Kyoto University*), I apply the newly developed DD-tomography technique (Haijiang and Thurber, 2003) to invert for both earthquake location and crustal structure for several seismogenic regions in Japan.

Last, but not least, I am looking very forward to participate together with my Ph.D. supervisor K. Ito (*Kyoto University*) in a new project of refraction profiling, which I hope will help me understand better and deeper the relation between the crustal structure and earthquake occurrence.

Acknowledgements

I express my deepest gratitude to my supervisor, Kiyoshi Ito, for his patience, valuable comments and encouragement during the elaboration of this thesis. Without his continuos support for more than four years, the work that I carried out here would not have been possible.

When I arrived for the first time in Japan, about five years ago, I was like a newborn in a different land and culture. Without the patient guidance and understanding of Kiyoshi Ito and Torao Tanaka, I could not say today that I feel here like home.

I express my sincere gratitude to Y. Umeda and M. Shimada for their valuable support. I thank J. Mori for very useful discussions and ideas during the elaboration of this thesis. I acknowledge the useful comments of S. Ohmi, H. Katao, K. Matsumura, M. Hashimoto, F. Takeuchi, I. Kawasaki and T. Shibutani. My appreciation goes to all the staff members of DPRI, Kyoto University for their support and for providing me earthquake data.

I thank Z.R. Struzik for his insights into wavelet analysis and friendship and to S. Wiemer for collaboration and useful discussions.

I benefited from the inspired comments and help of Y. Ogata, M. Wyss, H. Gupta, M. Ando, S. Toda, Y. Ben-Zion, A. Yoshida, D.D. Jackson, H. Kanamori, K. Aki, K. Katsumata, S. Matsumura, M.B. Geilikman, J. Zhuang, M. Anghel, M. Holschneider, B. Simpson, R. Robinson and D. Kaplan.

I thank my collaborators from the National Institute for Earth Physics, Romania, for useful discussions and for providing earthquake data.

I am indebted to my colleagues Y. Kano, T. Mizuno, T. Ueno, A. Okubo and all the others for their friendly help with Japanese language and computers.

I thank the Japanese Ministry of Education, Culture, Sports, Science and Technology (Monbu-Kagakusho) for providing me with a scholarship to study in Kyoto University.

My wife Makiko and my son Alexandru-Akihiro made it all worthwhile. I am grateful for their understanding of the many hours I was away from them, while working for the thesis. Without their love and strong support this dissertation would not have been possible.

I deeply thank to my parents for their infinite understanding, love and support. To them I dedicate this thesis.

List of main papers on which this thesis is based:

1. Enescu, B. and Ito K.,
   Some premonitory phenomena of the 1995 Hyogo-ken Nanbu earthquake: seismicity, b-value and fractal dimension,
   Tectonophysics, Elsevier Science, **338**, 3-4, 297-314, 2001.

2. Enescu, B. and Ito K.,
   Spatial analysis of the frequency-magnitude distribution and decay rate of aftershock activity of the 2000 Western Tottori earthquake,
   Earth, Planets and Space, Terrapub, Tokyo, **54**, 847-859, 2002.

3. Enescu, B., Ito K., Radulian, M., Popescu, E. and Bazacliu, O.
   Multifractal and chaotic analyses of Vrancea (Romania) intermediate-depth earthquakes -Investigation of the temporal distribution of events-,
   Pure and Applied Geophysics, Birkhäuser Verlag AG, accepted for publication, 2003.

4. Enescu, B. and Ito K.,
   The 1998 Hida Mountain earthquake swarm: double-difference event relocation, frequency-magnitude distribution and stress changes,
   Tectonophysics, Elsevier Science, submitted, 2004.

5. Enescu, B., Ito K. and Struzik, Z.R.,
   Wavelet-based multifractal analysis of real and simulated time series of earthquakes,
   Geophysical Journal International, Blackwell Publishing, submitted, 2004.

References

1. Anghel, M., Ben-Zion, Y., and Rico-Martinez, R., Dynamical system analysis and forecasting of deformation produced by an earthquake fault, *Pure and Appl. Geophys.*, 2003 (in press).
2. Aki, K., Maximum Likelihood Estimate of b in the Formula log N = a-bM and its Confidence Limits, *Bull. Earthquake Res. Inst.*, Tokyo Univ., **43**, 237-239, 1965.
3. Anderson, J.G., Brune, J.N., Louie, J.N., Zeng, Y., Savage, M., Yu, G., Chen, Q. and dePolo, D., Seismicity in the western Great Basin apparently triggered by the Landers, California, earthquake, 28 June 1992, *Bull. Seism. Soc. Am.*, **84**, 863-891, 1994.
4. Aoyama, H., Takeo, M and Ide, S., Evolution mechanisms of an earthquake swarm under the Hida Mountains, central Japan, in 1998, *J. Geophys. Res.*, **107**, B8, 10.1029/2001JB000540, 2002.
5. Arneodo, A., Bacry, E., and Muzy, J.F., Wavelets and multifractal formalism for singular signals: application to turbulence data, *Phys. Rev. Lett.*, **67**, 3515-3518, 1991.
6. Arneodo, A., Bacry, E. and Muzy, J.F., The Thermodynamics of Fractals Revisited with Wavelets, *Physica A*, **213**, 232-275, 1995.
7. Badii, R., and Broggi, G., Measurement of the dimension spectrum f(α): fixed-mass approach, *Physics Letters A*, **131**(6), 339-343, 1998.
8. Bak, P., Tang, C. and Wiesenfeld, K., Self-organized criticality. An explanation of 1/f noise. *Phys. Rev. Lett.*, **59**, 381-384, 1987.
9. Bazacliu, O., and Radulian, M, Seismicity patterns in Vrancea (Romania) region, *Natural Hazards*, **19**, 2-3, 165-177, 1999.
10. Beeler, N.M., Simpson, R.W., Hickman, S.H. and Lockner, D.A., Pore fluid pressure, apparent friction, and Coulomb failure, *J.Geophys.Res.*, **105**, 25533-25542, 2000.
11. Ben-Zion, Y., Stress, slip and earthquakes in models of complex single-fault systems incorporating brittle and creep deformations, *J. Geophys. Res.*, **101**, 5677-5706, 1996.

12. Ben-Zion, Y. and Rice, J.R., Earthquake failure sequences along a cellular fault zone in a three-dimensional elastic solid containing asperity and non-asperity regions, *J. Geophys. Res.*, **98**, B8, 14109-14131, 1993.
13. Buckheit, J.B., and Donoho, D.L., Wavelab and Reproducible Research, in A. Antoniadis and G. Oppenheim (Eds.), *Wavelets and Statistics* (pp. 55-81), New York, Springer-Verlag, 1995.
14. Burridge, R. and Knopoff, L., Model and theoretical seismicity*, Bull. Seismol. Soc. Am*., **57**, 341-371, 1967.
15. Cao, L., Practical method for determining embedding dimension of a scalar time series, *Physica D*, **110**, 43-50, 1997.
16. Cao, L., Mees, A., Judd, K., and Froyland, G., Determining the minimum embedding dimensions of input-output time series data*, Int. J. of Bifurcation and Chaos*, **8**, 1491-1504, 1998.
17. Constantinescu, L., and Enescu, D., The Vrancea earthquakes in a scientific and technological framework (Romanian Academy Publishing House), pp. 82-93, 1985.
18. Doser, D.I. and Robinson, R., Modeling stress changes induced by earthquakes in the southern Marlborough region, South Island, New Zealand*, Bull. Seismol. Soc. Am.*, **92**, 8, 3229-3238, 2002.
19. Earthquake Prediction Information Division, JMA, Outline of the western Tottori Prefecture earthquake in 2000, *Rep. Coord. Comm. Eq. Pred.*, **65**, 525-535, 2001 (in Japanese, with English explanation of figures).
20. Ebel, J.E. and Kafka, A.L., A non-Poissonian element in the seismicity of the northeastern United States, *Bull. Seismol. Soc. Am.*, **92**, 5, 2040-2045, 2002.
21. **Enescu, B.** and Ito, K., Some possible precursory phenomena of the 1995 Hyogo-ken Nambu earthquake, Fall Meeting of the Seismological Society of Japan, *Book of abstracts*, P29, 1998.
22. **Enescu, B.** and Ito, K., Some premonitory phenomena of the 1995 Hyogo-ken Nanbu earthquake: seismicity, b-value and fractal dimension, *Tectonophysics*, **338**, 3-4, 297-314, 2001a.
23. **Enescu, B.** and Ito, K., Temporal and spatial variations in b-values during the 1998-1999 Hida Monutain earthquake swarm, Central Honshu, Japan, 2001 IAGA-IASPEI Joint Scientific Assembly, Vietnam, Hanoi, *Book of abstracts*, S1/P(1279), 2001b.

24. **Enescu, B.** and Ito, K., Spatial analysis of the frequency-magnitude distribution and decay rate of aftershock activity of the 2000 Western Tottori earthquake, *Earth, Planets and Space*, **54**, 847-859, 2002a.
25. **Enescu, B.** and Ito, K., Temporal and spatial variations of seismicity during the 1998 Hida Mountain Earthquake swarms, central Honshu, Japan -Preliminary results-, *Annuals of Disas. Prev. Res. Inst.*, **45**, B-1, 591-594, 2002b.
26. **Enescu, B.**, and Ito, K., b and p values: variation and relation to physical processes for earthquakes in Japan, *Annuals of Disast. Prev. Res. Inst.*, **46**, 709-719, 2003.
27. **Enescu, B.**, Ito, K., Katao, H., Mori, J. and M. Hashimoto, Spatial and temporal frequency-magnitude changes and their physical significance for several earthquake sequences occurred in Japan, Earth and Planetary Science Joint Meeting, poster presentation, 2003a.
28. **Enescu, B.**, Ito, K., Radulian, M., Popescu, E. and Bazacliu, O., Multifractal and chaotic analysis of Vrancea (Romania) intermediate-depth earthquakes-Investigation of the temporal distribution of events-, *Pure and Appl. Geophys.*, 2003b (Accepted for publication).
29. **Enescu, B.**, Ito, K., and Struzik, Z.R., (Multi)fractality of earthquakes by use of wavelet analysis, EOS Trans., AGU, Fall Meeting 2002, 83(47), NG62B-0947, 2002.
30. **Enescu, B.**, Ito, K., and Struzik, Z.R., Wavelet-based multifractal analysis of real and simulated time series of earthquakes, 2004 (submitted).
31. Enescu D. and **Enescu B.**, Possible cause-effect relationships between Vrancea (Romania) earthquakes and some global geophysical phenomena, *Natural Hazards*, Kluwer Academic Publishers, **19**, 233-245, 1999.
32. Enescu, D., Marza, V., and Zamarca, I. (1974), Contributions to the statistical prediction of Vrancea earthquakes, *Rev. Roum. de Geophysique*, **19**, 67-79, 1974.
33. Eneva, M., Effect of limited data sets in evaluating the scaling properties of spatially distributed data: an example form mining-induced seismic activity, *Geophys. J. Int.*, **124**, 773-786, 1996.
34. Eneva, M., and Ben-Zion, Y., Application of pattern recognition techniques to earthquake catalogs generated by model of segmented fault systems in three-dimensional elastic solids, *J. Geophys. Res.*, **102**, B11, 24513-24528, 1997.

35. Evison, F.F. and Rhoades, D.A., Long-term seismogenic process for major earthquakes in subduction zones, *Phys. Earth and Planetary Interiors*, **108**, 185-199, 1998.
36. Fraser, A.M., and Swinney, H.L., Independent coordinates for strange attractors from mutual information, *Phys. Rev. A.*, **33**, 1134-1140, 1986.
37. Fuchs, K., Bonjer, K. P., Bock, G., Cornea, I., Radu, C., Enescu, D., Jianu, D., Nourescu, A., Merkler G., Moldoveanu, T., and Tudorache, G., The Romanian Earthquake of March 4, 1977. II. Aftershocks and migration of seismic activity, *Tectonophysics*, **53**, 225-247, 1978.
38. Fukuyama, E., W.L. Ellsworth, F. Waldhauser, and A. Kubo, Very fine fault structure of the 2000 western Tottori, Japan, earthquake*, Proceedings of the 2001 Japan Earth and Planetary Science Joint Meeting*, Tokyo, S3-007, 2001.
39. Geilikman, M.B., Golubeva, T.V., and Pisarenko, V.F., Multifractal patterns of seismicity, *Earth and Planetary Science Letters*, **99**, 127-132, 1990.
40. Godano, C., Alonzo, M.L., and Vilardo, G., Multifractal approach to time clustering of earthquakes. Application to Mt. Vesuvio seismicity, *Pure and Appl. Geophys.*, **149**, 375-390, 1997.
41. Goltz, C., Fractal and Chaotic Properties of Earthquakes, Springer-Verlag, 1997.
42. Gomberg, J. and Davis, S., Stress/strain changes and triggered seismicity at The Geysers, California, *J. Geophys. Res.*, **101**, 733-749, 1996.
43. Grassberger, P. and Procaccia, I., Measuring the strangeness of strange attractors, *Physica D*, **9**, 189-208, 1983.
44. Guo, Z., and Y. Ogata, Statistical relations between the parameters of aftershocks in time, space, and magnitude, J. Geophys. Res., 102, B2, 2857-2873, 1997.
45. Gutenberg, R., and C.F. Richter, Frequency of earthquakes in California, *Bull. Seismol. Soc. Am.*, **34**, 185-188, 1944.
46. Habermann, R.E., Precursory seismicity patterns: Stalking the mature seismic gap. In *Earthquake Prediction, an International Review.* **M Ewing Ser. 4**, ed. D. Simpson and P. Richards. Washington, D.C.: American Geophysical Union, 29-42, 1981.
47. Habermann, R.E., Teleseismic detection in the Aleutian Island Arc, *J. Geophys.Res.*, **88**, B6, 5056-5064, 1983.
48. Habermann, R.E., Man-made changes of seismicity rates, *Bull. Seism. Soc. Am.*, **77**, 141-159, 1987.

49. Habermann, R.E., Precursory seismic quiescence: Past, present and future, *Pageoph.*, **126**, 277-318, 1988.
50. Habermann, R.E., Seismicity rate variations and systematic changes in magnitudes in teleseismic catalogs, *Tectonophysics*, **193**, 277-289, 1991.
51. Habermann, R.E. and Wyss, M., Reply, *J. Geophys. Res.*, **92**, B9, 9446-9450, 1987.
52. Hashimoto M., Static stress changes associated with the Kobe earthquake: Calculation of changes in Coulomb failure function and comparison with seismicity change, *Jour. Seism. Soc. Jpn.*, **48**, 521-530 (in Japanese with English abstract), 1996.
53. Hegger, R., and Kantz, H., Embedding of sequences of time intervals, *Europhys. Lett.*, **38**, 267-272, 1997.
54. Hergarten, S., Self-organized criticality in Earth systems, Springer, 2002.
55. Hill, D.P., Reasenberg, P.A. and Michael, A, Seismicity Remotely Triggered by the Magnitude 7.3 Landers, California, Earthquake., *Science*, **260**, 1617-1623, 1993.
56. Hirabayashi, T., Ito, K., and Yoshii, T., Multifractal analysis of earthquakes, *Pure and Appl. Geophys.*, **138**(4), 591-610, 1992.
57. Hirahara, K., Nakano, T. and 24 others, GPS observations of post-seismic crustal movements in the focal region of the 1995 Hyogo-ken Nanbu earthquake*, J. Phys. Earth*, **44**, 301-315, 1996.
58. Hirose, I., Kawasaki, I., Takemoto, S. and Tamura, Y., Temporal variations of tidal constituents in strainmeter records prior to the occurrence of two large earthquakes, J. Geod. Soc. Japan, 49, 4, 2003, in Japanese (in press).
59. Hu, K., Ivanov, P. Ch., Chen, Z., Carpena, P. and Stanley, H.E., Effect of trends on detrended fluctuation analysis, *Physical Review E*, **64**, 01114, 1-19, 2001.
60. Huang, J. and Turcotte, D.L., Fractal distributions of stress and strength and variations of b-value, *Earth and Planetary Science Letters*, **91**, 223-230, 1988.
61. Huang, Q., Oncel, A.O. and Sobolev, G.A., Precursory seismicity changes associated with the Mw = 7.4 1999 August 17 Izmit (Turkey) earthquake, *Geophys. J. Int.*, **151**, 235-242, 2002.
62. Hurst, H.E., Black, R.P., and Simaika, Y.M., Long-term storage: an experimental study, Constable, London, 1965.
63. Iio, Y., Frictional coefficient on faults in a seismogenic region inferred from earthquake mechanism solutions, *J. Geophys. Res.*, **102**, B3, 5403-5412, 1997.

64. Ito, K., Regional variations of the cutoff depth of seismicity in the crust and their relation to heat flow and large inland-earthquakes, *J. Phys. Earth*, **38**, 223-250, 1990.
65. Ito, K., Cutoff depth of seismicity and large earthquakes near active volcanoes in Japan, *Tectonophysics*, **217**, 11-21, 1992.
66. Ito, K. and **Enescu, B.**, Precursory Evidence for the 1995 Hyogoken-Nanbu Earthquake, from Seismic Observations, in The occurrence process of the 1995 Hyogo-Ken Nanbu (Kobe) earthquake from micro-earthquake observation*, Report for the Tokyo Memorial Foundation for the Promotion of Earthquake Prediction Research*, 3-26, 2001a (in Japanese).
67. Ito, K. and **Enescu, B.**, Heterogeneous structure and b and p values relating to the rupture of the 2000 Tottori-Ken Seibu earthquake, *Proceedings of the International Symposium on Slip and Flow Processes in and below the Seismogenic Region*, Sendai, Japan, 78-1:78-6, 2001b.
68. Ito, K. and **Enescu, B.**, The 2000 Tottori-Ken Seibu Earthquake and the heterogeneous structure, *Chikyu Monthly*, **38**, 167-174, 2002 (in Japanese).
69. Irikura, K. and Ando, M., Learning from 1995 Hyogo-ken Nanbu earthquake*, J. Phys. Earth*, **44**, I-V, 1996.
70. Ivanov, P. Ch., Amaral, L. A. N., Goldberger, A. L., Havlin, S., Rosenblum, M. G., Struzik, Z. R. and Stanley, H. E., Multifractality in human heartbeat dynamics, *Nature*, **399**, 461-465, 1999.
71. Kagan, Y.Y., and Jackson, D.D., Long-term earthquake clustering, *Geophys.J.Int.*, **104**, 117-133, 1991.
72. Kagan, Y. Y., and Knopoff, L., Spatial distribution of earthquakes: The two-point correlation function, *Geophys. J. Roy. Astr. Soc.*, **62**, 303-320, 1980.
73. Kagan, Y.Y., and L. Knopoff, Stochastic synthesis of earthquake catalogs, *J. Geophys. Res.,* **86**, 2853-2862, 1981.
74. Kagan, Y.Y. and Jackson, D.D., Spatial aftershock distribution: effect of normal stress, *J. Geophys. Res.*, **103**, 24453-24467, 1998.
75. Kanamori, H. and Anderson, D.L. (1975): Theoretical basis of some empirical relations in seismology, *Bull. Seismol. Soc. Am*., **65**, 1073-1095, 1975.
76. Kantelhardt, J.W., Koscienly-Bunde, E., Rego, H.H.A., Havlin, S. and Bunde, A., Detecting long-range correlations with detrended fluctuation analysis, *Physica A*, **295**, 441-454, 2001.

77. Kantz, H., and Schreiber, T., Non-linear time series analysis, Cambridge University Press, 1997.
78. Kaplan, D. Non-linear time series software, http://www.macalester.edu/~kaplan, 1998.
79. Katao, H. and Ando, M., Crustal movement before and after the Hyogo-ken Nanbu earthquake, *Kagaku*, **66**, 78-85, 1996 (in Japanese).
80. Katao, H and Iio, Y., Abnormal initial rise of the foreshocks of the 1995 Southern Hyogo Prefecture Earthquake, Rep. Coord. Committee for Earthquake Prediction, 54, 620-623, 1995.
81. Katsumata, K., Urabe, T. and Mizoue, M., Evidence for a seismic attenuation anomaly beneath the Hida Mountain Range, central Honshu, Japan, Geophys. J. Int., 120, 237-246, 1995.
82. Keilis-Borok, V.I., and Rotwain, I.M., Diagnosis of time of increased probability of strong earthquakes in different regions of the world: algorithm CN, *Phys. Earth Planet. Inter.*, **61**, 57-72, 1990.
83. Kennel, M.B., Brown, R., and Abarbanel, H.D.I., Determining embedding dimension for phase-space reconstruction using a geometrical construction, *Physical Review A,* **45**(6), 3403-3411, 1992.
84. King, G.C.P., Stein, R.S. and Lin, J., Static stress changes and the triggering of earthquakes, *Bull. Seismol. Soc. Am.*, **84**, 935-953, 1994.
85. Kisslinger, C., and L.M. Jones, Properties of aftershocks in southern California*, J. Geophys. Res.*, **96**, 11947—11958, 1991.
86. Liu, G.-P. and Fu, Z.-X., Regional Seismicity Triggered by the Hyogo-Ken Nanbu, Japan, M=7.2 earthquake on January 17, 1995, *Acta Seism. Sinica*, **12**, 3, 277-284, 1999.
87. Lorentz, E.N., Deterministic nonperiodic flow, *J. Atmos. Sci.*, **20**, 130-141, 1963.
88. Main, I.G., Statistical physics, seismogenesis, and seismic hazard, *Reviews of Geophysics*, **34** (4), 433-462, 1996.
89. Mallat, S. and Hwang, W.L., Singularity detection and processing with wavelets, *IEEE Trans. on Information Theory*, **38**, 2, 1992.
90. Mandelbrot, B. B., The fractal geometry of nature, W. H. Freeman, New York, 1983.

91. Matcharashvili, T., Chelidze, T., and Javakhishvili, Z., Nonlinear analysis of magnitude and interevent time interval sequences for earthquakes of the Caucasian region, *Nonlin. Processes in Geophys.*, **7**, 9-19, 2000.
92. Marza, V. I., The March 4, 1977 Vrancea earthquake seismic gap, *Bull. Seism. Soc. Am.*, **69**, 1, 289-291, 1979.
93. Matsumura, K., Seismic activity in the region around the Tottori-Shimanen border before the 2000 Tottoriken-Seibu earthquake, *Special publication of DPRI, Kyoto University*, dedicated to the 2000 Tottoriken-Seibu earthquake, 5-11, 2001 (in Japanese).
94. Matthews, M.V. and Reasenberg, P., Comment on Habermann's method for detecting seismicity rate changes, *J. Geophys. Res.*, **92**, B9, 9443-9450.
95. Merkwirth, C., Parlitz, U., Wedekind, I., and Lauterborn, W., Tstool Ver. 1.11, A non-linear time series analysis software, http://www.physik3.gwdg.de/ tstool/index.html, 2002.
96. Mikumo, T., and T. Miyatake, Earthquake sequences on a frictional fault model with non-uniform strengths and relaxation times, *Geophys. J.*, **59**, 497-522, 1979.
97. Mogi, K., Magnitude-frequency relation for elastic shocks accompanying fractures of various materials and some related problems in earthquakes, *Bull. Earthquake Res. Inst.*, Univ. Tokyo, **40**, 831-853, 1962a.
98. Mogi, K., Study of the elastic shocks caused by the fracture of heterogeneous materials and its relation to the earthquake phenomena*, Bull. Earthquake Res. Inst.*, Univ. Tokyo, **40**, 125-173, 1962b.
99. Mogi, K., On the time distribution of aftershocks accompanying the recent major earthquakes in and near Japan, *Bull. Earthq. Res. Inst.*, Univ. Tokyo, **40**, 107-124, 1962c.
100. Mogi, K., Earthquakes and fractures, *Tectonophysics*, **5**, 35-55, 1967.
101. Mogi, K., Earthquake prediction, Tokyo: Academic Press, 1985.
102. Mori, J., and R.E. Abercrombie, Depth dependence of earthquake frequency-magnitude distributions in California: Implications for rupture initiation*, J. Geophys. Res.*, **102**, B7, 15081-15090, 1997.
103. Muzy, J.F., Bacry, E., and Arneodo, A., The multifractal formalism revisited with wavelets, *Int. J. Bifurc. Chaos*, **4**, 245-302, 1994.

104. Nakamura, M., Decay of Micro-Earthquake Seismicity Activated by Static Stress Change, 22nd General Assembly of IUGG, Birmingham, England, *Book of Abstracts*, A. 166, 1999.

105. Nishenko, S.P. and Buland, R., A generic recurrence interval distribution for earthquake forecasting, *Bull. Seismol. Soc. Am.*, **77**, 1382-1399, 1987.

106. Ohtake, M., Matumoto, T., and Latham, G., Seismicity gap near Oaxaca, southern Mexico as a probable precursor to a large earthquake, *Pageoph*, **115**, 375-385, 1977.

107. Ohtake, M., Matumoto, T., and Latham, G., Evaluation of the forecast of the 1978 Oaxaca, southern Mexico earthquake based on a precursory seismic quiescence. In *Earthquake Prediction, an International Review*. **M Ewing Ser. 4**, ed. D. Simpson and P. Richards. Washington, D.C.: American Geophysical Union, 53-62, 1981.

108. Ogata, Y., Estimation of the parameters in the modified Omori formula for aftershock frequencies by the maximum likelihood procedure, *J. Phys. Earth*, **31**, 115-124, 1983.

109. Ogata, Y., Statistical models for earthquake occurrences and residual analysis for point processes, *Res. Memo.* (Technical Report) **288**, Inst. Statist. Math., Tokyo, 1985.

110. Ogata, Y., Statistical models for earthquake occurrences and residual analysis for point processes, *J. Amer. Statist. Asoc.*, **83**, 9-27, 1988.

111. Ogata, Y., Detection of precursory relative quiescence before great earthquakes through a statistical model, *J. Geophys. Res.*, **97**, B13, 19845-19871, 1992.

112. Ogata, Y., Space-time point-process models for earthquake occurrences, *Ann. Inst. Statist. Math.*, **50**, 379-402, 1998.

113. Ogata, Y., Seismicity analysis through point-process modeling: a review, *Pure and Appl. Geophys.*, **155**, 471-507, 1999.

114. Ogata, Y., Katsura, K. and M. Tanemura, Modeling heterogeneous space-time occurrences of earthquakes and its residual analysis, *J. Royal Stat. Soc., Series C*, **52**, 4, 499-509, 2003.

115. Ohmi, S., K. Watanabe, T. Shibutani, S. Nakao, N. Hirano, A. Nakao, H. Takeuchi, F. Takeuchi, S. Miwa, A. Shito, A. Kim, B. Enescu, The 2000 Tottori-ken Seibu earthquake – seismic activity derived from the compilation of DPRI, JMA and Hi-net data -, *Bull. Disas. Prev. Res. Inst.*, **44**, 2001.

116. Oncescu, M. C., Mârza, V., Rizescu, M., and Popa, M., The Romanian earthquake catalogue between 984 –1996, *In Vrancea Earthquakes: Tectonics, Hazard and Risk Mitigation* (Eds. Wenzel, F., Lungu, D., and Novak, O.), Kluwer Academic Publishers, pp. 43-49, 1999.

117. Ouchi, T. and Uekawa, T., Statistical analysis of the spatial distribution of earthquakes – variation of the spatial distribution of earthquakes before and after large earthquakes, *Physics of the Earth and Planetary Interiors*, **44**, 211-225, 1986.

118. Ouillon, G. and Sornette, D., Unbiased multifractal analysis; application to fault patterns, *Geophys. Res. Lett.*, **23**, 3409-3412, 1996.

119. Peitgen, H.-O., Jürgens, H., and Saupe, D., Chaos and Fractals, New Frontiers of Science, Springer-Verlag, New York, pp. 921-953 (Appendix B), 1992.

120. Peng, C.K., Buldyrev, S.V., Simons, M., Stanley, H.E., and Goldberger, A.L., Mosaic organization of DNA nucleotides. *Physical Review E*, **49**, 1685-1689, 1994.

121. Popescu, E., Bazacliu, M., and Radulian, M., Time clustering properties of the Vrancea (Romania) subcrustal earthquakes, Reports in Physics, 53(38), 507-518, 2001.

122. Purcaru, G., The Vrancea, Romania, earthquake of March 4, 1977*, Phys. Earth Planet. Int.*, **18**, 274-287, 1979.

123. Radu, C., The catalogue of strong earthquakes occurred on the territory of Romania. Part I- before 1901; Part II- 1901-1979, In Seismological studies on the March 4, 1977 earthquake (Eds. I. Cornea and C. Radu), Central Institute of Physics, Bucharest-Magurele, pp. 723-752, 1979 (in Romanian).

124. Radulian, M, and Trifu, C-I., Would it have been possible to predict the 30 August 1986 Vrancea earthquake?, *Bull. Seismol. Soc. Am.*, **81**, 2498-2503, 1991.

125. Raleigh, C.B., Bennet, G., Craig, H., Hanks, T., Molnar, P., Nur, A., Savage, J., Scholz, C., Turner, R., and Wu, F., Prediction of the Haicheng earthquake, *EOS*, **58**, 236-272, 1977.

126. Reasenberg, P., Second-Order Moment of Central California Seismicity, 1969-1982, *J. Geophys. Res.*, **90**, B7, 5479-5495, 1985.

127. Reasenberg, P., Foreshock occurrence before large earthquakes, *J. Geophys. Res.*, **104**, 4755-4768, 1999.

128. Reasenberg, P.A., Computer programs ASPAR, GSAS and ENAS and APROB for the statistical modeling of aftershock sequences and estimation of aftershock hazard, *USGS Open File Rep.*, 94-221, 1994.

129. Reasenberg, P.A., and M.V. Matthews, Precursory seismic quiescence: A preliminary assessment of the hypothesis, *Pure and Appl. Geophys.*, **126**, 373-406, 1988.

130. Reasenberg, P.A. and Simpson, R.W., Response of Regional Seismicity to the Static Stress Change Produced by the Loma Prieta Earthquake, *Science*, **255**, 1687-1690, 1992.

131. Rydelek, P.A. and Sacks, S., Testing the Completeness of Earthquake Catalogues and the Hypothesis of Self-Similarity, *Nature*, **337**, 251-253, 1989.

132. Sakai, T., Takagi, A., and Yoshida, A., On the b value in the frequency-magnitude distribution of earthquakes near and around volcanoes, Earth and Planetary Science Joint Meeting, *Book of abstracts*, S041-P019, 2002.

133. Scholz, C.H., Sykes, L.R. and Aggarwal, Y.P., Earthquake prediction: A physical basis, Science, 181, 803-810.

134. Scholz, C.H., The frequency-magnitude relation of microfracturing in rock and its relation to earthquakes, *Bull. Seismol. Soc. Am.*, **58**, 399-415, 1968.

135. Scholz, C.H., The mechanics of earthquakes and faulting, Cambridge University Press, edition 1997.

136. Sekiguchi, H., and T. Iwata, Rupture process of the 2000 Tottori-Ken Seibu earthquake using strong ground motion data, Web page: http://sms.dpri.kyoto-u.ac.jp/iwata/ttr_e.html, 2000.

137. Shi, Y. and Bolt, B.A., The Standard Error of the Magnitude-Frequency b Value, *Bull. Seism. Soc. Am.*, **72**, 5, 1677-1687, 1982.

138. Shibutani, T., Nakao, S., Nishida, R., Fumio, T., Watanabe, K., and Umeda, Y., Swarm-like seismic activities in 1989, 1990 and 1997 which preceded the western Tottori earthquake (6 October 2000, MJ = 7.3), *Rep. Coord. Comm. Eq. Pred.*, **65**, 576-578, 2001 (in Japanese, with English explanation of figures).

139. Shibutani, T., Nakao, S., Nishida, R., Takeuchi, F., Watanabe, K., and Umeda, Y., Swarm-like seismic activity in 1989, 1990 and 1997 preceding the 2000 Western Tottori earthquake, *Earth, Planets and Space*, 54, 831-845, 2002.

140. Sibson, R.H., Roughness at the base of the seismogenic zone: Contribution factors, *J. Geophys. Res*., **89**, 5791-5799, 1984.

141. Skempton, A.W., The pore pressure coefficients A and B, *Geotechnique*, **4**, 143-147, 1954.

142. Smalley, R.F., Jr, Chatelain, J.-L., Turcotte, D.L., and Prevot, R., A fractal approach to the clustering of earthquakes: applications to seismicity of the New Hebrides, *Bull. Seism. Soc. Am.*, **77**, 1368-1381, 1987.

143. Smith W.D., The b-value as an Earthquake Precursor, *Nature*, **289**, 136-139, 1981.

144. Struzik, Z.R., Local effective Holder exponent: estimation on the Wavelet Transform Maxima tree. In Michel Dekking, Jacques Levy Vehel, Evelyne Lutton and Claude Tricot, *Fractals: Theory and Applications in Engineering*, 93-112, Springer-Verlag, 1999.

145. Struzik, Z.R., Wavelet methods in (Financial) time-series processing, *Physica A*, **296**, 1-2, 307-319, 2001.

146. Takens, F., Dynamical systems and turbulence, *Lecture Notes in Mathematics*, vol. **898**, Springer, 1981.

147. Theiler, J., Estimating fractal dimension, *J. Opt. Soc. Am.*, **7**(6), 1055-1071, 1990.

148. Tiampo, K.F., Rundle, J.B., McGinnis, S. and Gross, S.J., Eigenpatterns in southern California seismicity, *J. Geophys. Res.*, **107**, B12, 2354, 10.1029/2001JB000562, 2002.

149. Toda, S., Stein, R.S., Reasenberg P.A., Dieterich J.H. and Yoshida, A., Stress transferred by the Mw=6.9 Kobe, Japan, shock: Effect on aftershocks and future earthquake probabilities, *J. Geophys. Res.*, **103**, 24,543-24,565, 1998.

150. Toda, S. and Stein, R.S., Response of the San Andreas fault to the 1983 Coalinga-Nunez earthquakes: An application of interaction-based probabilities for Parkfield, *J. Geophys. Res.*, **107**, B6, 10.1029/2001JB000172, 2002.

151. Toda, S., Stein, R.S., and Sagiya, T., Evidence from the AD 2000 Izu islands earthquake swarm that stressing rate governs seismicity, *Nature*, **419**, 58-61, 2002.

152. Torrence, C. and Compo, G.P., A Practical Guide to Wavelet Analysis, *Bull. Am. Meteorol. Soc.*, **79**, 1, 61-78, 1998.

153. Trifu, C-I., Detailed configuration of intermediate seismicity in Vrancea region, *Rev. Geofis.*, **46**, 33-40, 1990.

154. Trifu, C-I., and Radulian, M., Frequency-magnitude distribution of earthquakes in Vrancea: Relevance for a discrete model, *Journ.Geophys.Res.*, **96**, B3, 4301-4311, 1991.

155. Trifu, C-I., and Radulian, M., Dynamics of a seismic regime: Vrancea – A Case History, Nonlinear Dynamics and Predictability of Geophysical Phenomena, *Geophysical Monograph 83*, IUGG, **18**, 43-53, 1994.

156. Trifu, C-I., Radulian, M., and Popescu, E., Characteristics of intermediate depth microseismicity in Vrancea region, *Rev. Geofis.*, **46**, 75-82, 1990.

157. Tsunogai, U. and Wakita, H., Anomalous change in ground water chemistry - Possible precursors of the 1995 Hyogo-ken Nanbu earthquake, *J. Phys. Earth*, **44**, 381-390, 1996.

158. Turcotte, D.L., Fractals in geology and geophysics, *Pure and Appl. Geophys.*, **131**, 171-196, 1989.

159. Utsu, T., Magnitudes of earthquakes and occurrence of their aftershocks, Zisin, Ser. 2, 10, 35-45, 1957 (in Japanese).

160. Utsu, T., A statistical study on the occurrence of aftershocks, *Geophys. Mag.*, **30**, 521-605, 1961.

161. Utsu, T., A method for determining the value of b in formula log N = a - bM showing the magnitude-frequency relation for earthquakes, *Geophys. Bull.* Hokkaido Univ., **13**, 99-103, 1965 (in Japanese).

162. Utsu, T., On seismicity, Report of the Joint Research Institute for Statistical Mathematics, Inst. for Stat. Math., pp. 139-157, Tokyo, 1992.

163. Utsu, T., Y. Ogata, and R.S. Matsu'ura, The centenary of the Omori formula for a decay law of aftershock activity, *J. Phys. Earth*, **43**, 1-33, 1995.

164. Vidale, J.E., Carr Agnew, D., Johnston, M.J.S. and Oppenheimer, D.H., Absence of earthquake correlation with earth tides: an indication of high preseismic fault stress rate, *J. Geophys. Res.*, **103**, 24 567-24 572, 1998.

165. Wada, H., Ito, K. and Ohmi, S. 1998 Hida earthquake swarm, Tectonic stress and large in-land-earthquakes in the Hida Mountain Region, *DPRI, Kyoto University report*, principal investigator: I. Kawasaki, pp. 36-49, 2000.

166. Waldhauser, F. and Ellsworth, W.L., A double-difference earthquake location algorithm: method and application to the Northern Hayward fault, California, *Bull. Seism. Soc. Am.*, **90**, 6, 1353-1368, 2000.

167. Warren, N.W., and G.V. Latham, An experimental study of thermally induced microfracturing and its relation to volcanic seismicity, *J. Geophys. Res.*, **75**, 4455-4464, 1970.

168. Watanabe, H., The 1995 Hyogo-ken-Nanbu earthquake and the accompanying seismic activity, -Behaviour of the background seismicity-, *Annuals of Disas. Prev. Res. Inst., Kyoto Univ.*, **41A**, 25-42 (in Japanese with English abstract), 1998.

169. Watanabe, H., and A. Kuroiso, Aftershocks of the earthquake of the central part of Gifu Prefecture, September 9, 1969, *Bull. Earthq. Res. Inst.*, Univ. Tokyo, **48**, 1195-1208, 1970 (in Japanese).

170. Wiemer, S., Introducing probabilistic aftershock hazard mapping, Geophys. Res. Lett., 27, 20, 3405-3408, 2000.

171. Wiemer, S., A software package to analyze seismicity: ZMAP, Seis. Res. Lett., 72, 2, 374-383, 2001.

172. Wiemer, S., and Benoit, J., Mapping the b value anomaly at 100 km depth in the Alaska and New Zealand subduction zones, Geophys. Res. Lett., 23, 1557-1560, 1996.

173. Wiemer, S., and Katsumata, K., Spatial variability of seismicity parameters in aftershock zones, J. Geophys. Res., 104, B6, 13,135-13,151, 1999.

174. Wiemer, S. and Wyss, M., Seismic quiescence before the Landers (M = 7.5) and Big Bear (M = 6.5) 1992 earthquakes, *Bull. Seismol. Soc. Am.*, **84**, 3, 900-916, 1994.

175. Wiemer, S., and M. Wyss, Mapping the frequency-magnitude distribution in asperities: An improved technique to calculate recurrence times, J. *Geophys. Res*., **102**, 15115-15128, 1997.

176. Wiemer, S., and M. Wyss, Minimum magnitude of complete reporting in earthquake catalogs: examples from Alaska, the Western United States, and Japan, *Bull. Seismol. Soc. Am.*, **90**, 859-869, 2000.

177. Wiemer, S., and R.F. Zuniga, ZMAP - A software package to analyse seismicity (abstract), *EOS, Trans. AGU*, **75(43)**, Fall Meet. Suppl., 456, 1994.

178. Wyss, M., Towards a physical understanding of the earthquake frequency distribution, *Geophys. J. R. Astron. Soc.*, **31**, 341-359, 1973.

179. Wyss, M. and Fu, Z., Precursory Seismic Quiescence before the January 1982 Hilea, Hawaii, Earthquake, *Bull. Seism. Soc. Am.*, **79**, 3, 756-773, 1989.

180. Wyss, M. and Habermann, R.E., Precursory Seismic Quiescence, *Pure and Appl*. *Geophys*., **126**, 2-4, 319-332, 1988.

181. Wyss, M., Shimazaki, K. and Wiemer, S., Mapping active magma chambers by b values beneath the off-Ito volcano, Japan, *J. Geophys. Res*., **102**, B9, 20413-20433, 1997.

182. Wyss, M., and Toya, Y., Is background seismicity produced at a stationary poissonian rate?, *Bull. Seism. Soc. Am.*, **90**, 5, 1174-1187, 2000.

183. Wyss, M. and Wiemer, S., Two current seismic quiescences within 40km of Tokyo, *Geophys. J. Int.*, **128**, 459-473, 1997.

184. Xu, Y., and Burton, P.W., Rescaled range analysis of the frequency of occurrence of moderate-strong earthquakes in the Mediterranean area, *In Emergent Nature; Patterns, Growth and Scaling in the Sciences* (Ed. Miroslav M. Novak), World Scientific, 2002, pp. 305-314, 2002.

185. Yagi, Y., and M. Kikuchi, Source Rupture Process of the Tottori-ken Seibu earthquake of Oct. 6, 2000, Web page: http://wwweic.eri.u-tokyo.ac.jp/yuji/tottori/, 2000.

186. Yamakawa, N., Foreshocks, aftershocks, and earthquake swarms (IV) – Frequency decrease of after shocks in its initial and later stages, *Pap. Met. Geophys.*, **19**, 109-119, 1968.

187. Yoshida, A., Variations in seismic activity before and after the Hyogo-ken Nanbu earthquake in and around the source area and tectonics in the Kinki district, *Chishitsu News*, **490**, 26-32, 1995.

188. Zbilut, J.P., and Webber, Jr., C.L., Embeddings and delays as derived from quantification of recurrence plots, *Physics Letters A*, **171**, 199-203, 1992.

189. Zhang, H. and Thurber, C. H., Double-difference tomography: The method and its application to the Hayward fault, California, *Bull. Seismol. Soc. Am.*, **93**, 5, 1875-1889, 2003.

190. Zuniga, R., and Wyss, M., Inadvertent changes in magnitude reported in earthquake catalogs: Influence on b-value estimates, *Bull. Seism. Soc. Am.*, **85**, 1858-1866, 1995.

Earthquakes as (marked) point processes. What is a point process:

Simple (no magnitude associated with the events):

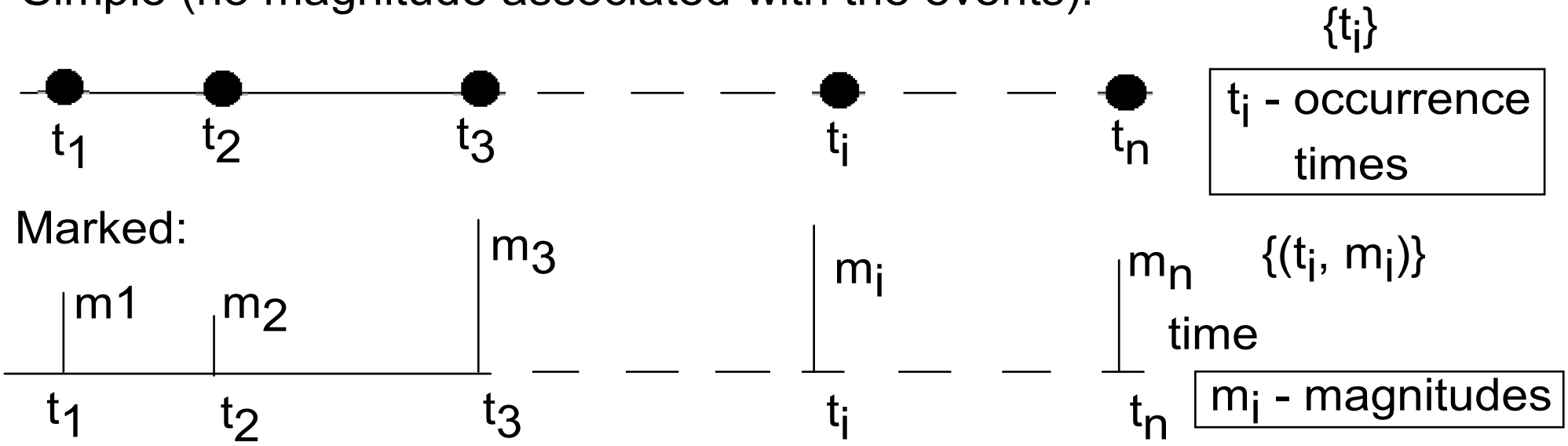

Characterization of a point process (one possibility): by the inter-event times between successive events, i.e., t_2-t_1, ...t_i-t_{i-1}, ... → distribution of inter-event times (d.i.t)

if d.i.t. is exponential → the events are randomly distrib. (Poisson) (e.g., background seismicity)

if d.i.t is log-normal, Gauss etc... → quasi-periodicity (Nishenko and Bullard, 1987) (main-shocks, large events)

if d.i.t is power-law → tendency to clustering, fractality: applies to aftershocks, foreshocks, also mainshocks.

Fig. 1.1 Temporal characteristics of earthquakes occurrence from a statistical point of view.

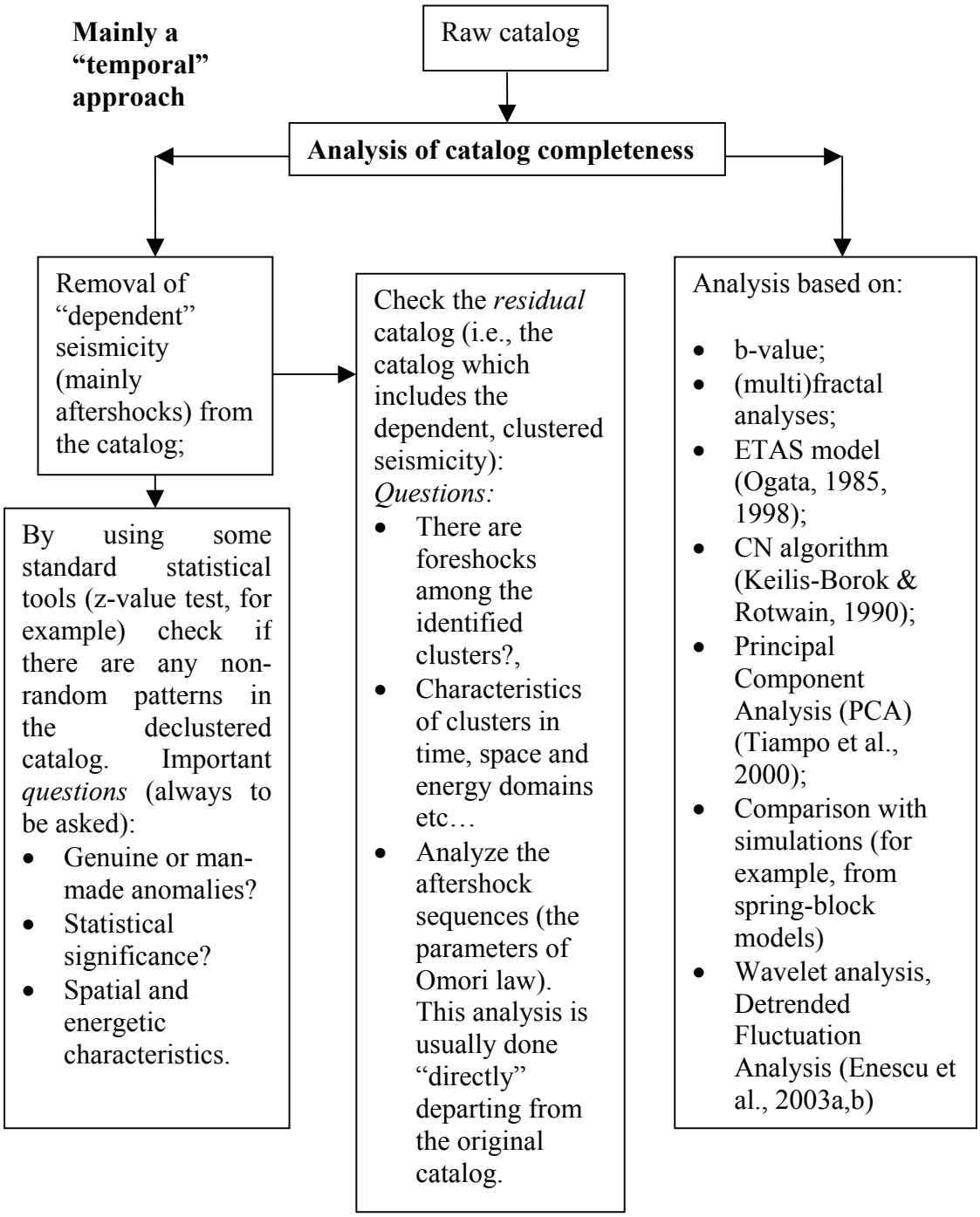

Fig. 1.2 A possible "recipe" to seismicity investigation. The analysis of catalog completeness (i.e., determination of the minimum magnitude above which the catalog includes all the events occurred in the area it covers) is a necessary step for most of the studies on seismicity and seismic hazard assessment by probabilistic means.

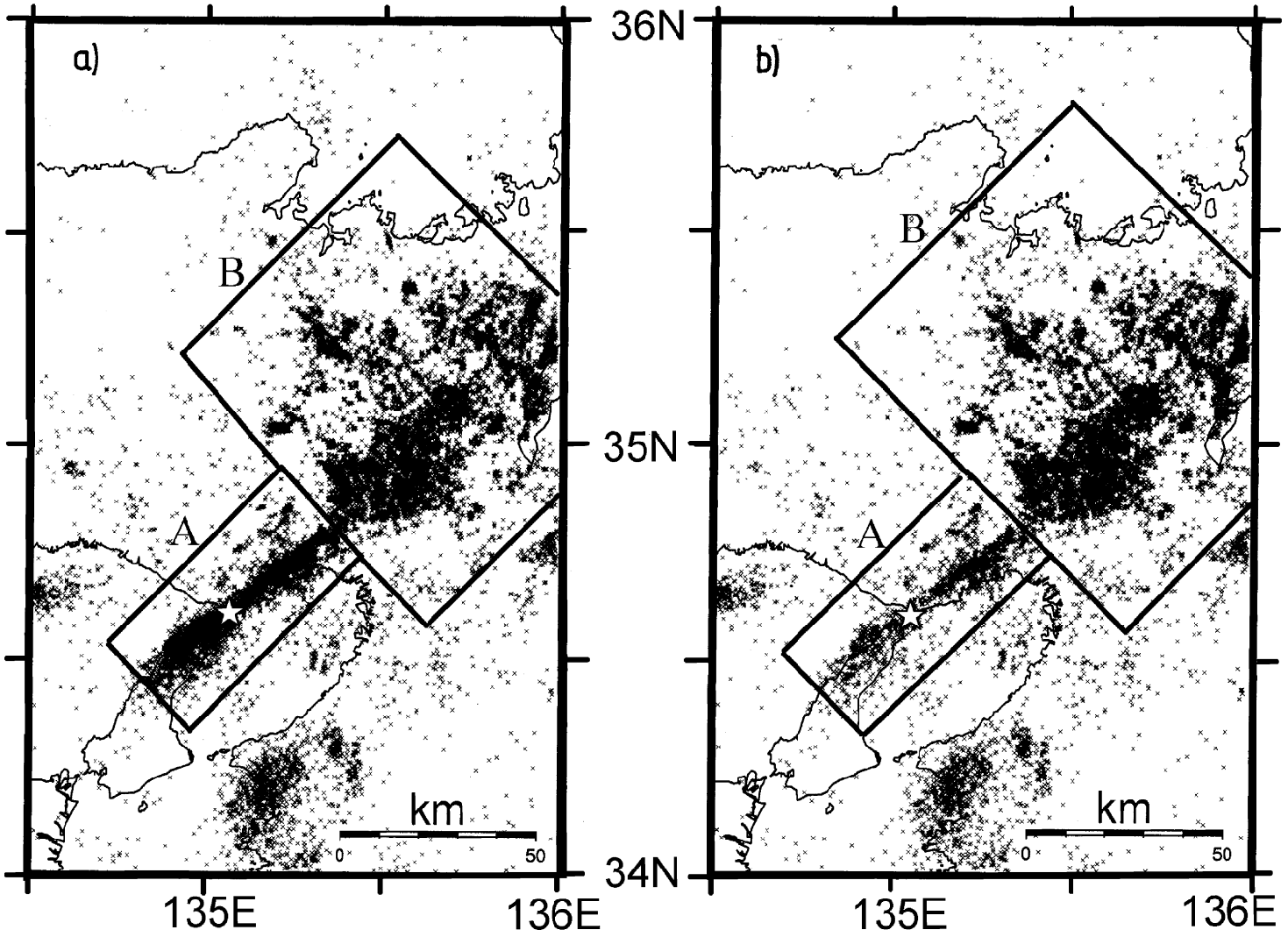

Fig. 2.1 Original (a) and declustered (b) seismicity (1976-1998, M >= 1.5) in a large region surrounding the epicenter of the 1995 Kobe earthquake. A - epicentral region, B - Tanba region. The epicenter of the 1995 Kobe earthquake is indicated by a star.

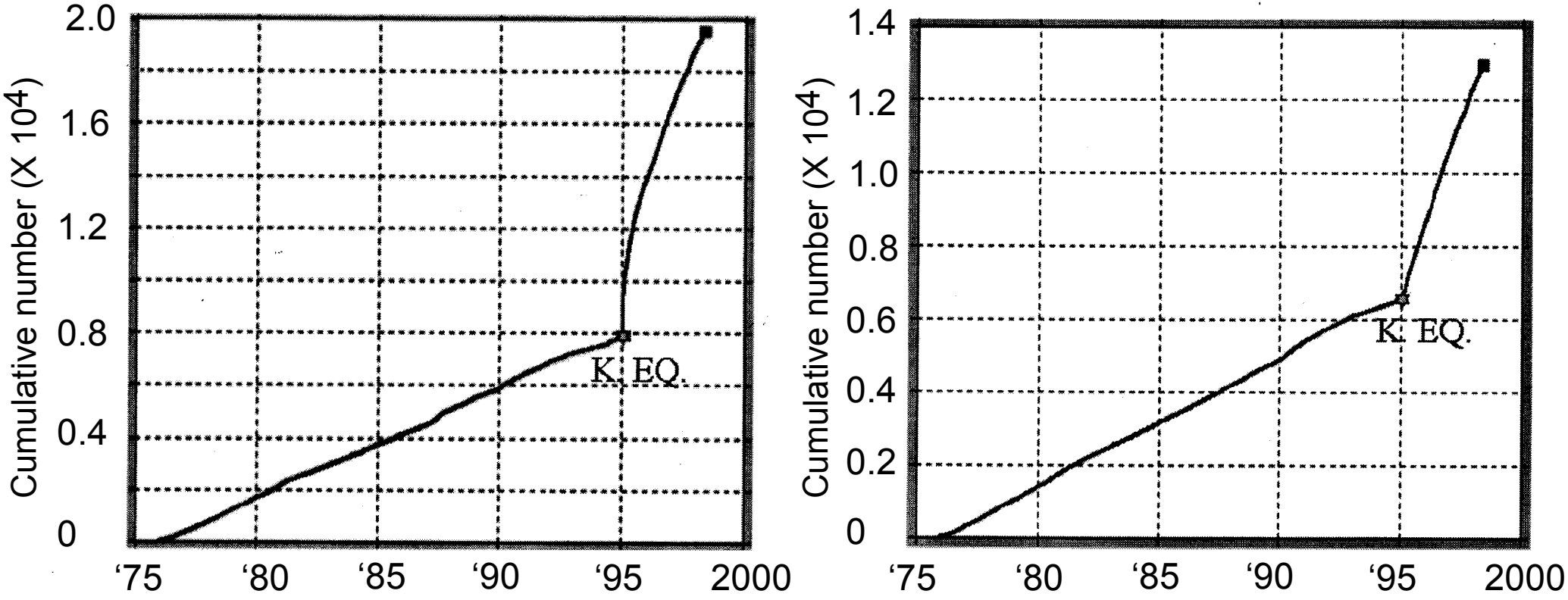

Fig. 2.2 Cumulative number curves for the undeclustered (a) and declustered (b) data. K. EQ. indicates the time of occurrence of the 1995 Kobe earthquake.

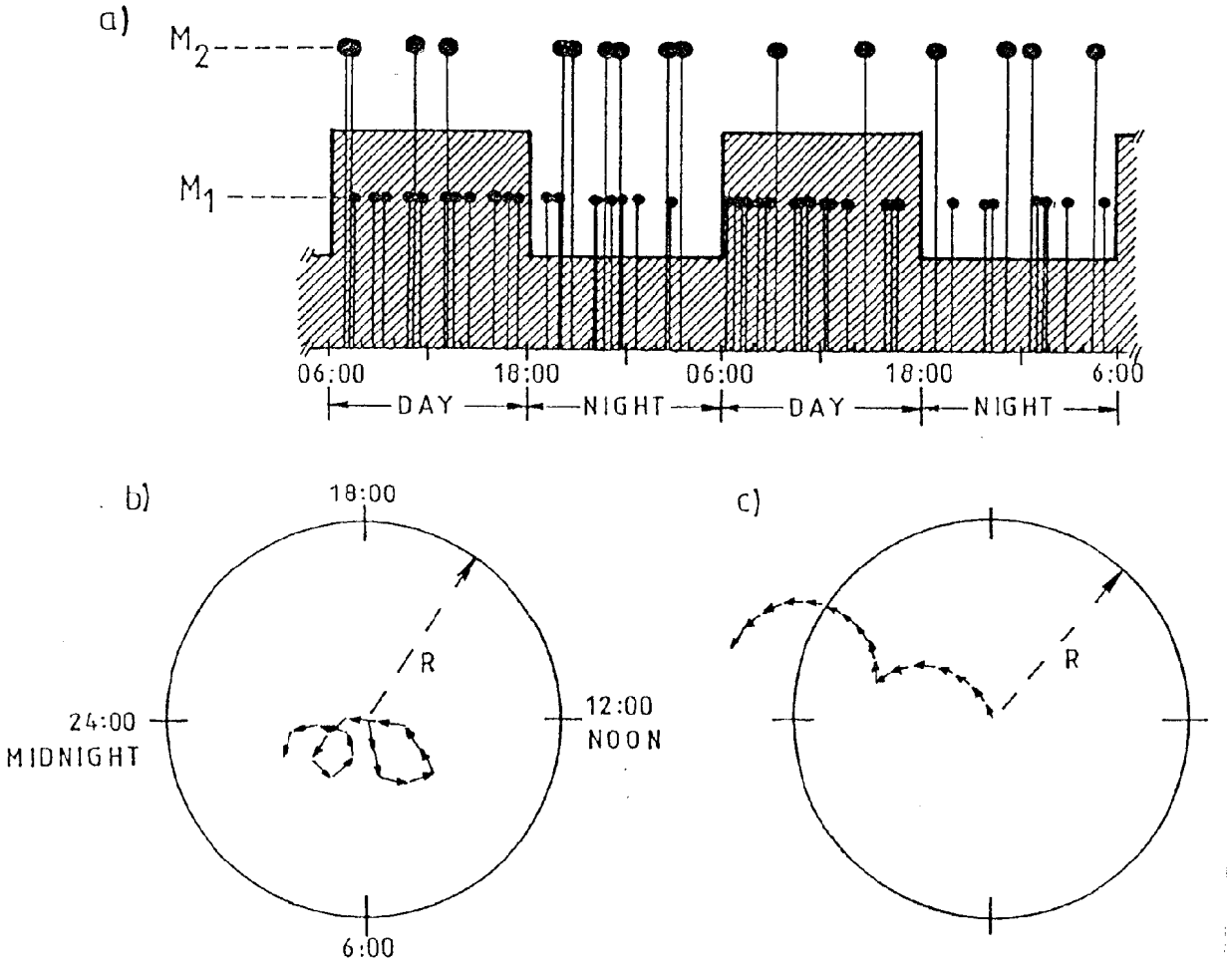

Fig. 2.3 An example of day-night noise modulation using a synthetic earthquake sequence of two different-magnitude events which follow the Poisson distribution a) The larger earthquakes (M2) exceed the background noise (stippled area), so the phasor plot of these events (N = 16, R = 6.9) shows no bias in the walkout. b) Since the smaller events (M1) are detected only at night, when the background noise is reduced, these events show a significant phasor walkout (N = 50, R = 12.2) c). The circles in b and c are drawn at the 95% confidence level for an equivalent random walk (Brownian motion). The Poisson rate for the smaller events is one event per hour and the b-value is 0.5. After Rydelek and Sacks, 1989, with permission from the authors and “Nature” Journal.

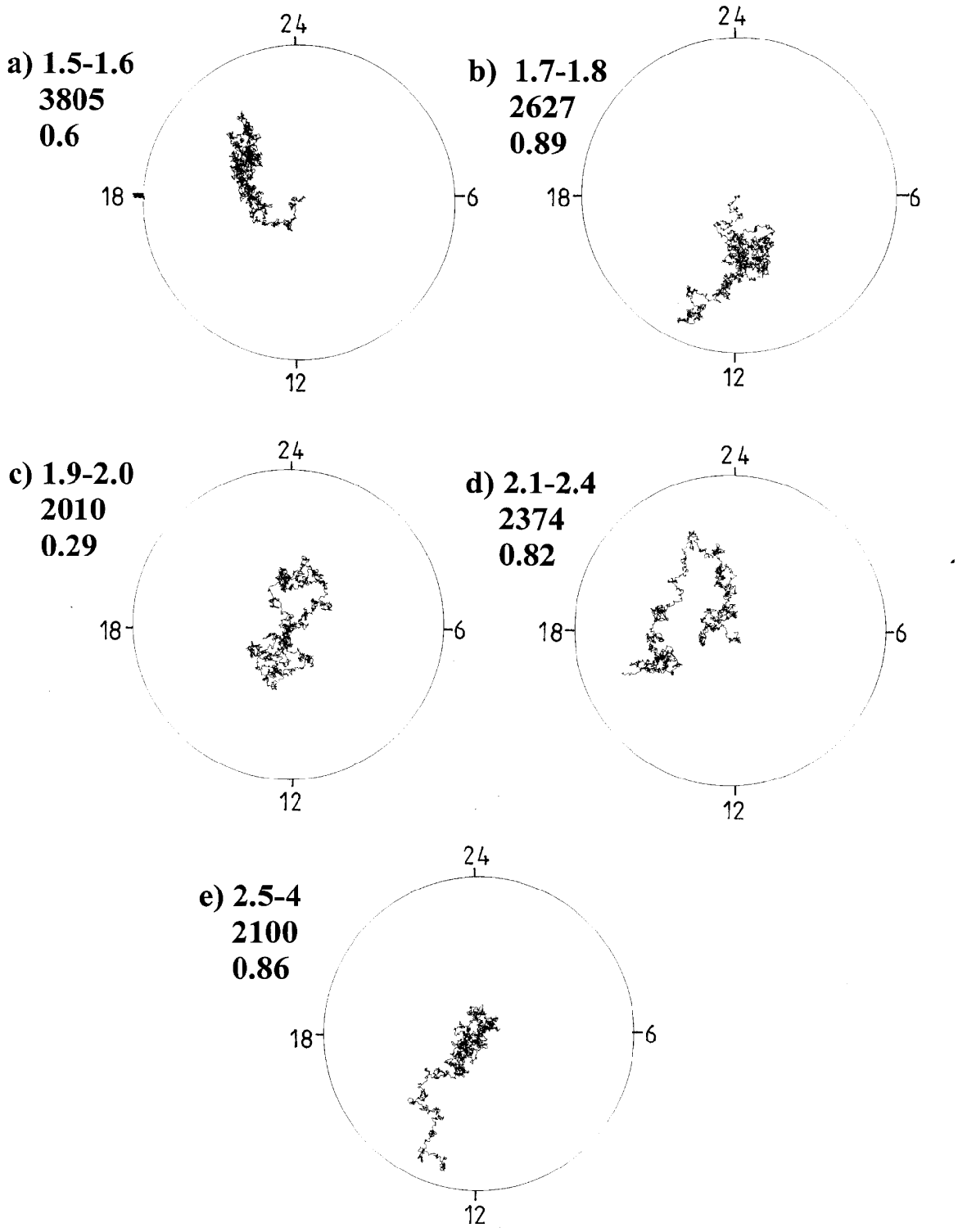

Fig. 2.4 Test of catalogue completeness in different magnitude bands (a, b, c, d and e), using a method by Rydelek and Sacks (1989). The numbers in the left of each figure refer to the tested magnitude band and the total events in that band. The circles correspond to 95% confidence level. All magnitude bands proved to be complete with 95% confidence level (there is no significant phasor walkout).

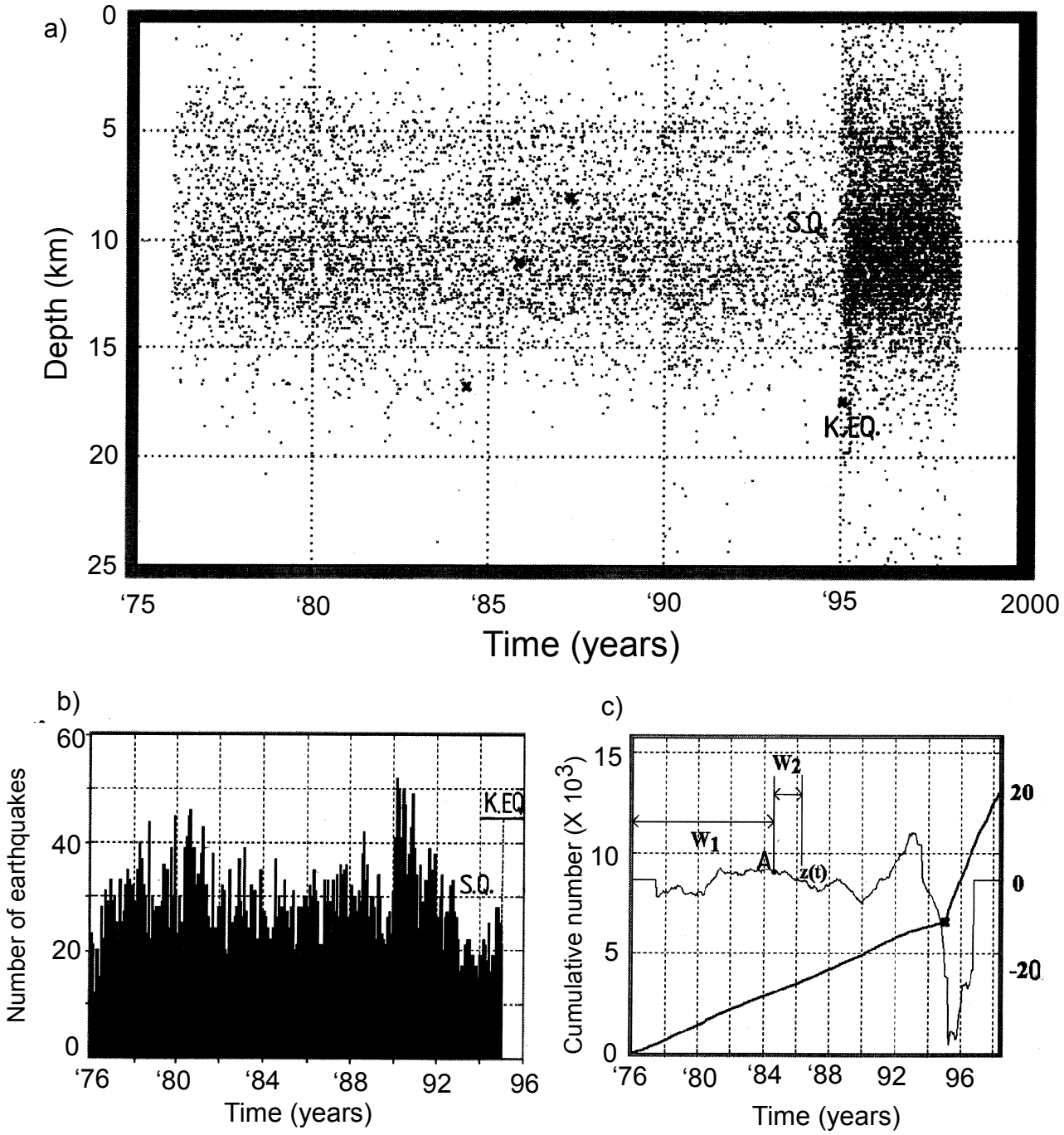

Fig. 2.5 a) Time-depth distribution of the earthquakes with M >= 1.5, between 1976-1998, for the declustered catalogue. Cross signs indicate moderate sized earthquakes with M >= 5. K. EQ. shows the hypocentre of Kobe earthquake and S.Q. indicates seismic quiescence.

b) Histogram of the monthly number of earthquakes (M >= 1.5) for the declustered catalogue from 1976 to the 1995 Kobe earthquake. S.Q. indicates seismic quiescence and K. EQ. indicates the Kobe earthquake.

c) Statistical analysis of the declustered catalogue. Cumulative number curve (scale in the left side of the graph) and the function z(t) (scale in the right side of the graph). The maximum value of z is 10.4 in January 1993. w2 is taken to be 1.5 years. The graph shows schematically the windows w1 and w2 at point A.

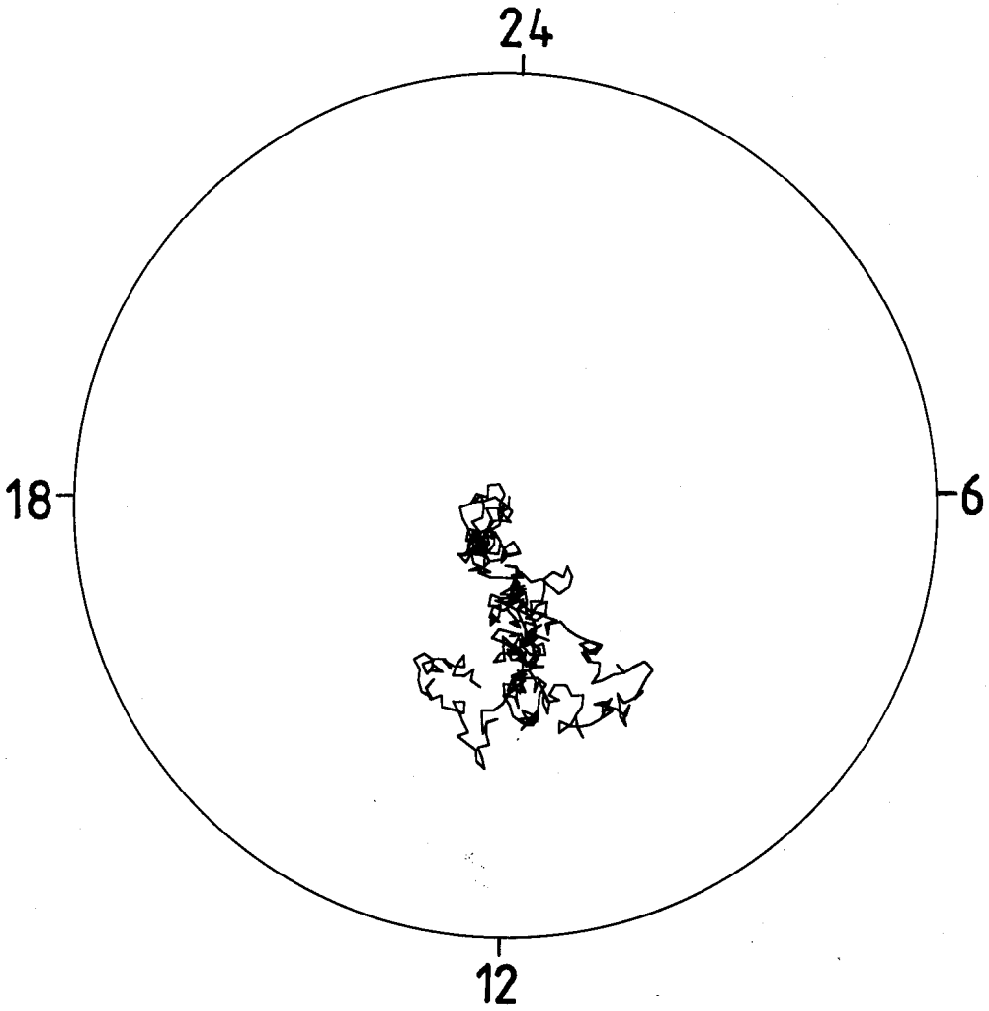

Fig. 2.6 Test of catalogue completeness for the events during the seismic quiescence in 1993-1995. The circle shows the 95% significance level. See Fig. 2.3 for other explanations. The catalogue is proved to be complete with 95% significance level.

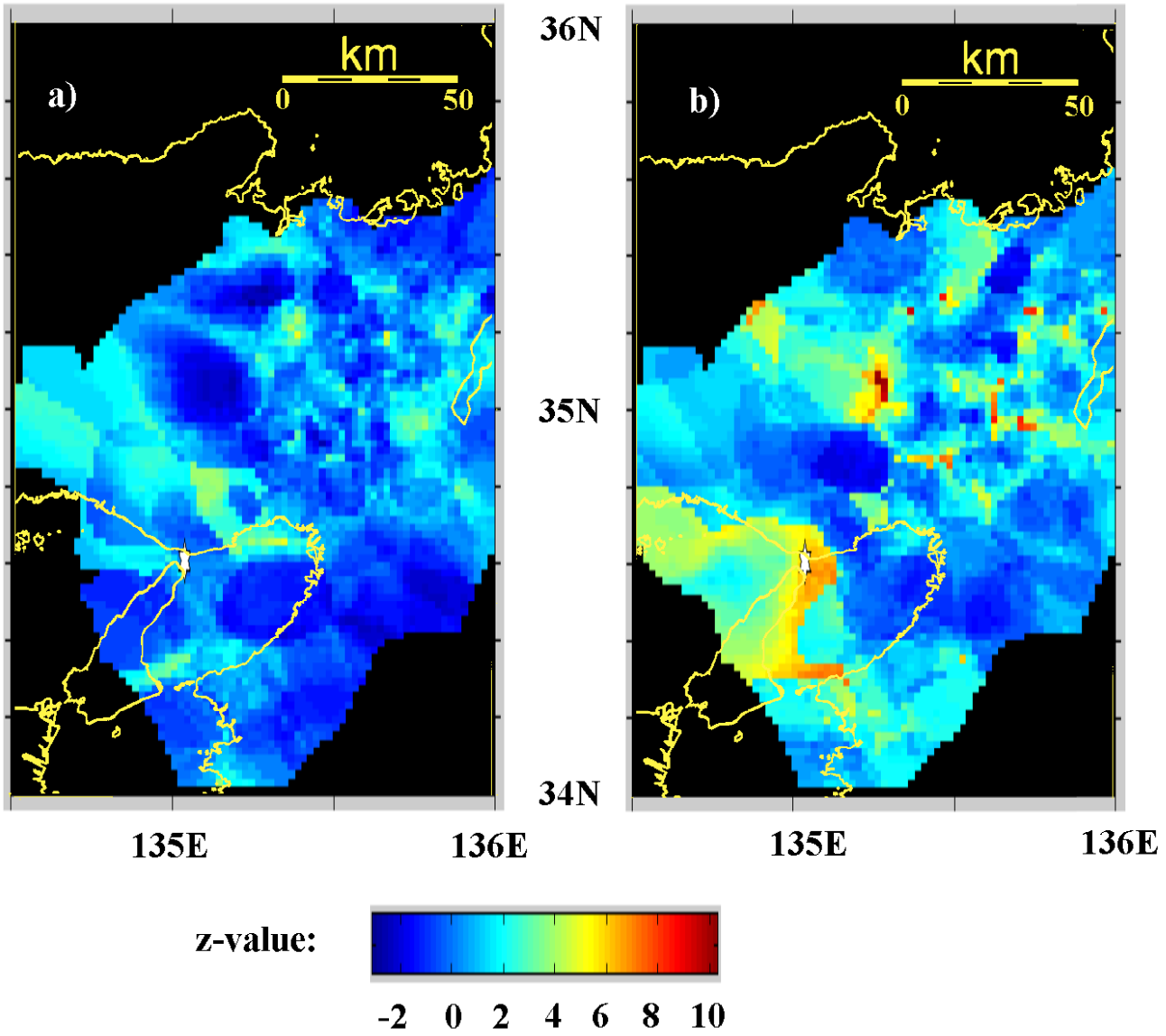

Fig. 2.7 Z-value map at the “reference year” 1982 (a) and at the “reference year” 1993 (b). Rubberband window length (w2) is 1.5 years. The star represents the epicentre of the Kobe earthquake. Lighter colours (yellow, orange, red) indicate regions of decreased seismicity rate.

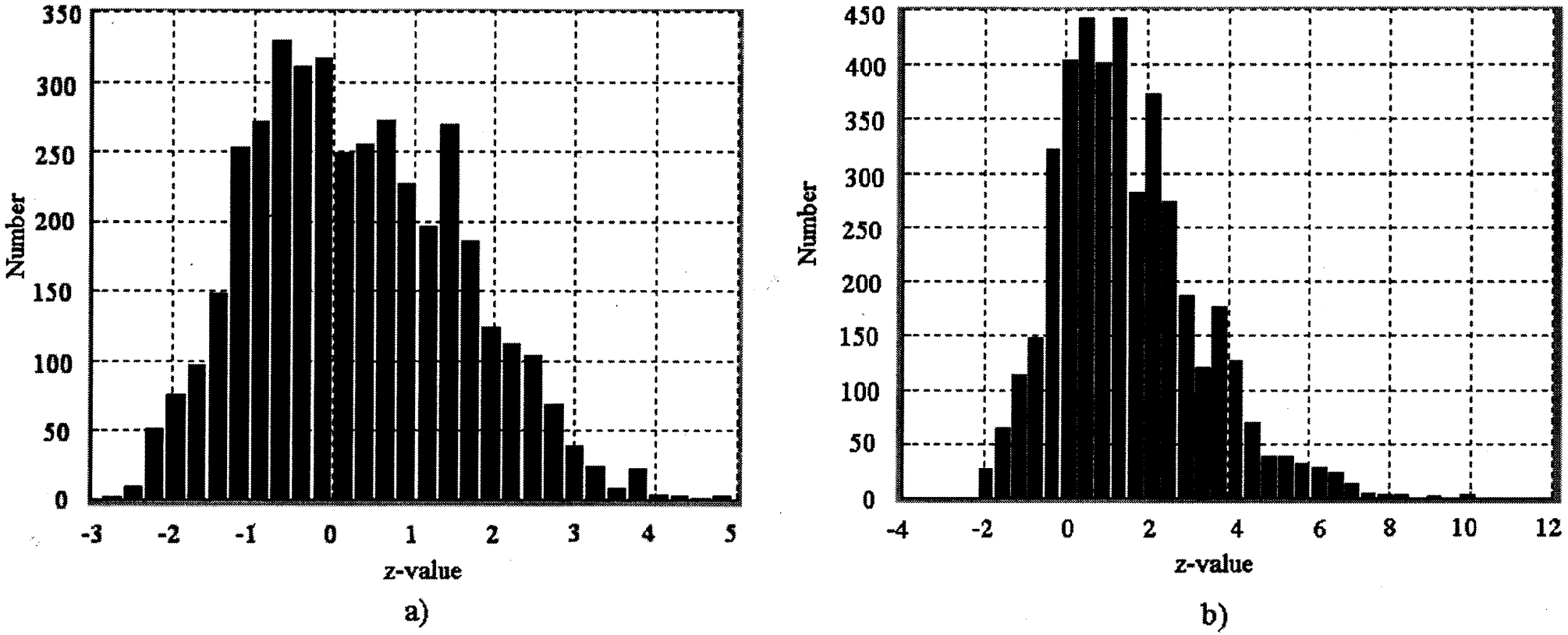

Fig. 2.8 Histograms of z-value corresponding to the z-value maps with the “reference year” 1982(a) and 1993(b).

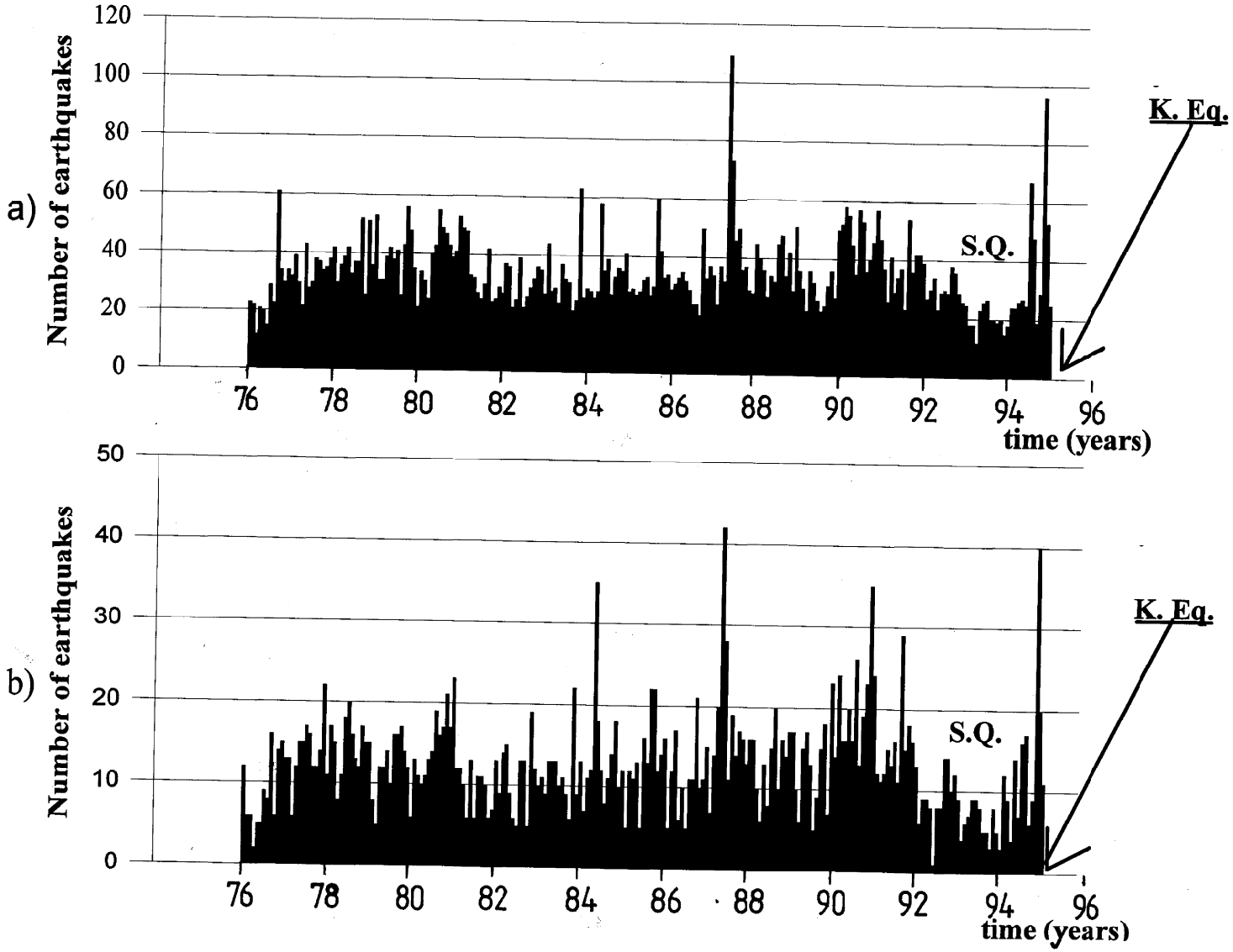

Fig. 2.9 Histograms of the monthly number of earthquakes for the undeclustered catalogue. a) M >= 1.5 ; b) M >= 2.0. S.Q. indicates the period of seismic quiescence and K. Eq. shows Kobe earthquake.

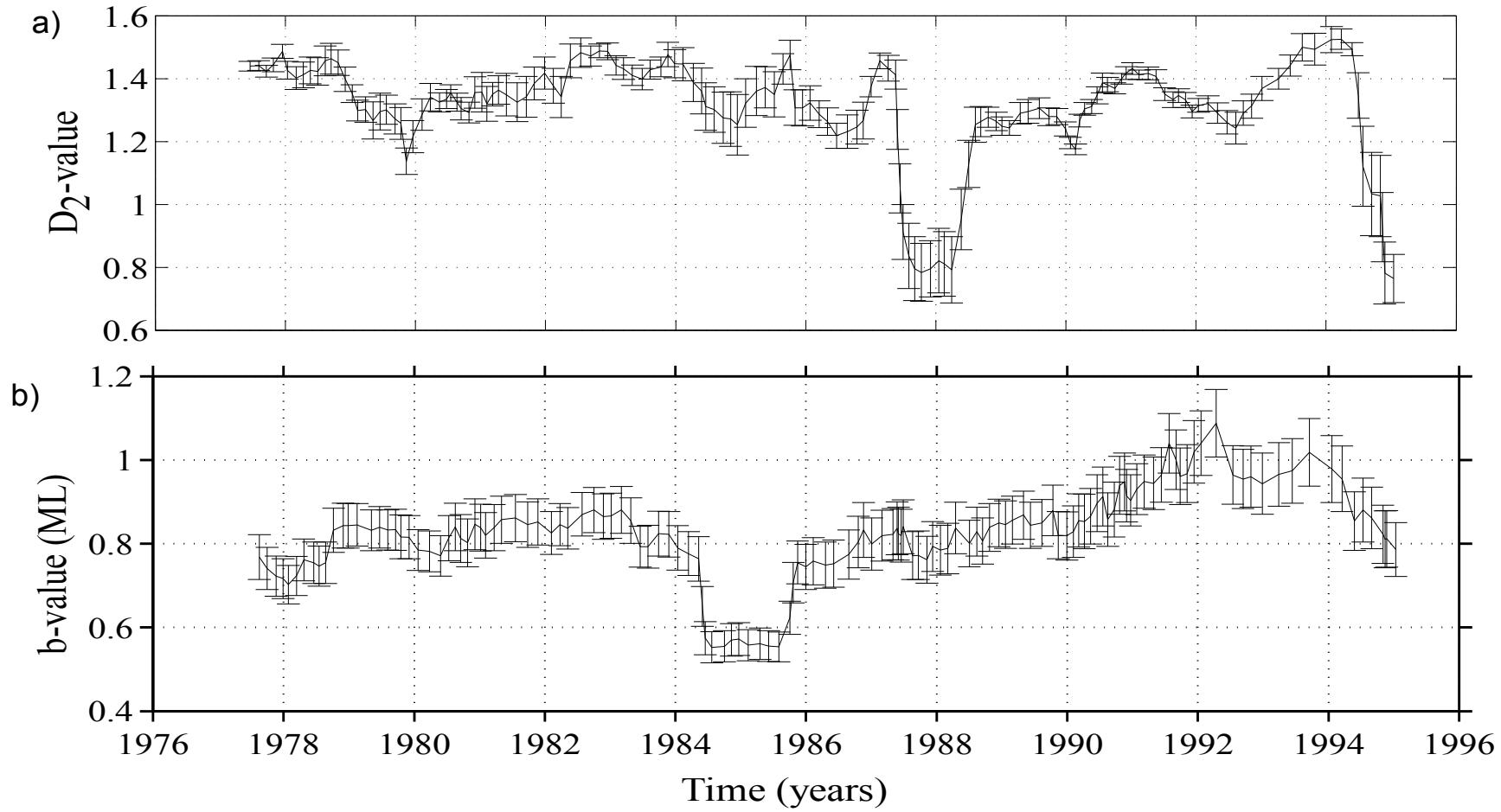

Fig. 2.10 Temporal variation of the fractal dimension of the epicentral distribution of earthquakes, D_2-value, (a) and the b-value (b). For the computation of D_2-value we selected the following parameters: M >= 1.5, moving window = 500 events; in the case of b-value: M >= 2.0, moving window = 200 events. In the case of D_2-value, a larger window is necessary to obtain statistically reliable results. For b-value computation, the threshold magnitude is critical, therefore we chose 200 events in a moving window.

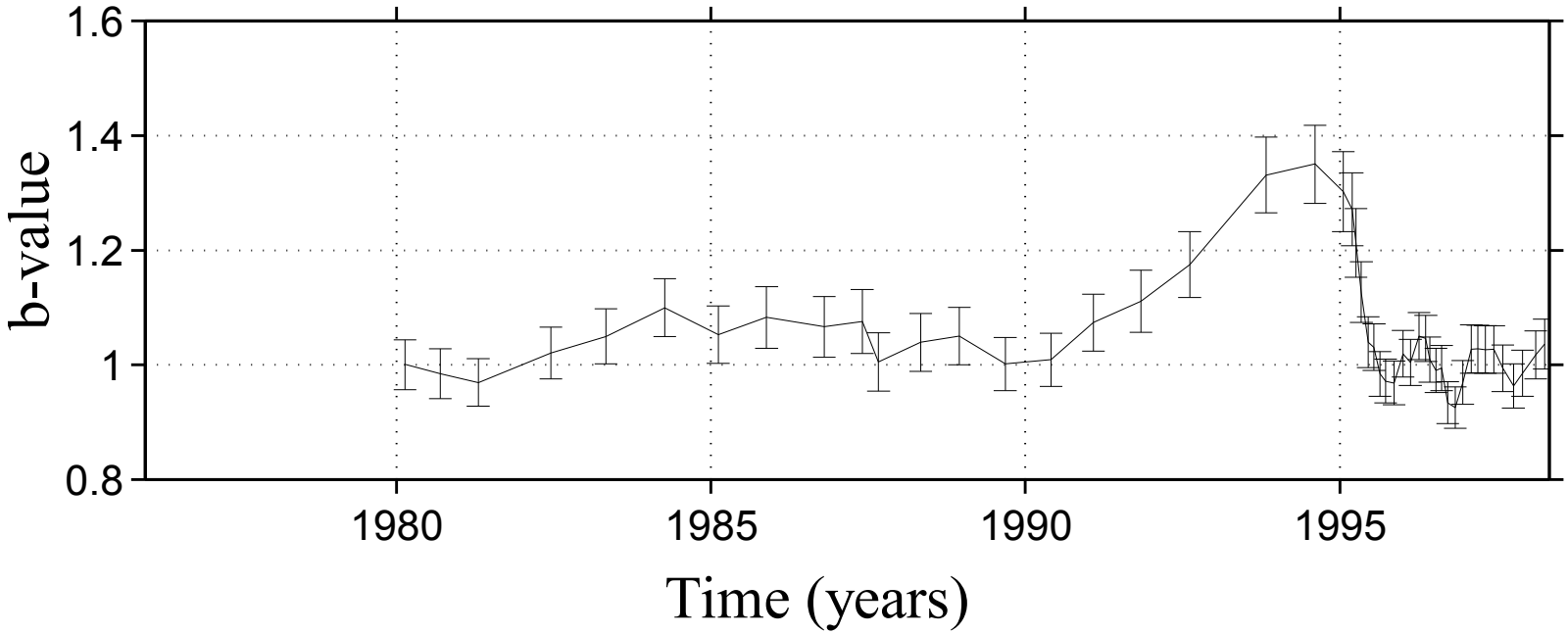

Fig. 2.11 b-value variation in the Tanba region, before and after the 1995 Kobe earthquake. One can notice the significant increase of b-value, before the occurrence of the large event, and the “recovery” that follows its occurrence.
There are 500 events in a moving-window.

Precursors before Kobe earthquake

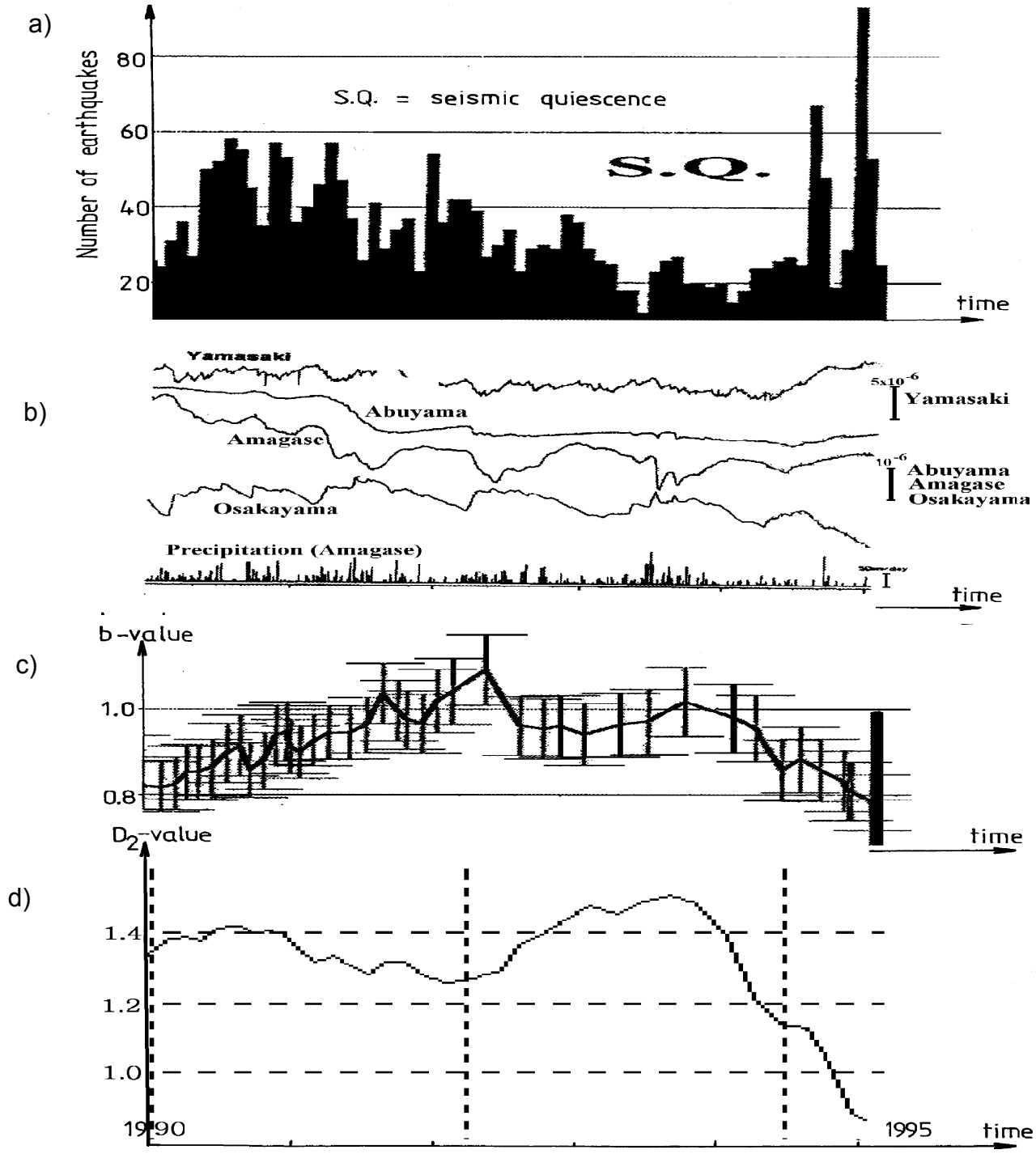

Fig. 2.12 From up do down: a) seismicity rate changes, with a clear seismic quiescence pattern (SQ) followed by an increase in seismic activity(ISA), several months before the Kobe earthquake; b) strain variation and precipitation (DPRI, 1); c) b-value changes: increase and decrease before Kobe earthquake; d) changes in the fractal dimension, D_2. of the epicentral distribution of earthquakes: large decrease associated probably with ISA, correlates well with the decrease in b-value. The same scale is used for all graphs (a-d).

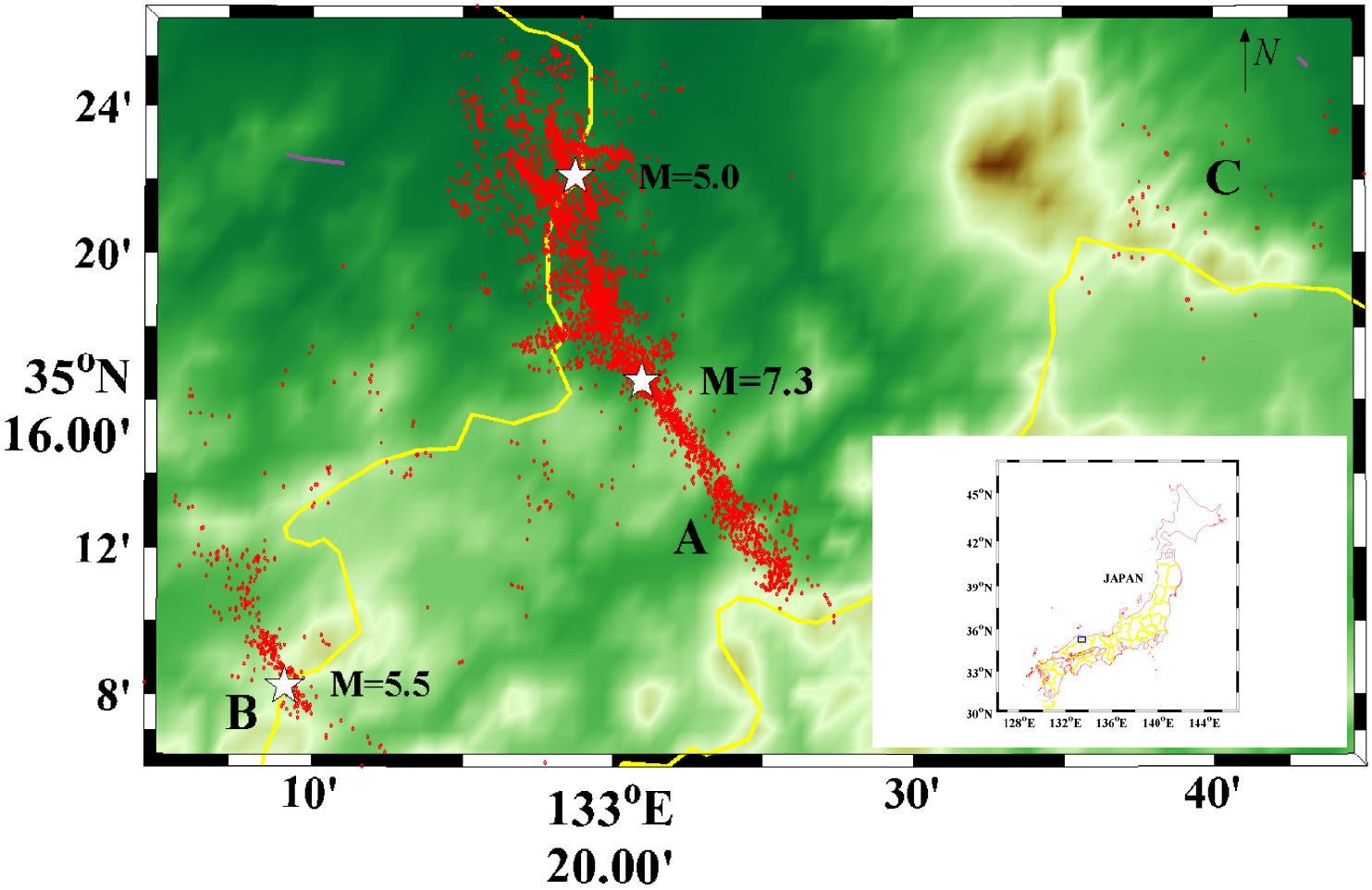

Fig. 3.1 (a) Epicenters of the aftershocks of the Western Tottori earthquake. A, B and C regions are referred in the text. The epicenters of the main shock and of the largest aftershocks are marked by stars. Inset shows studied area as a small blue rectangle.

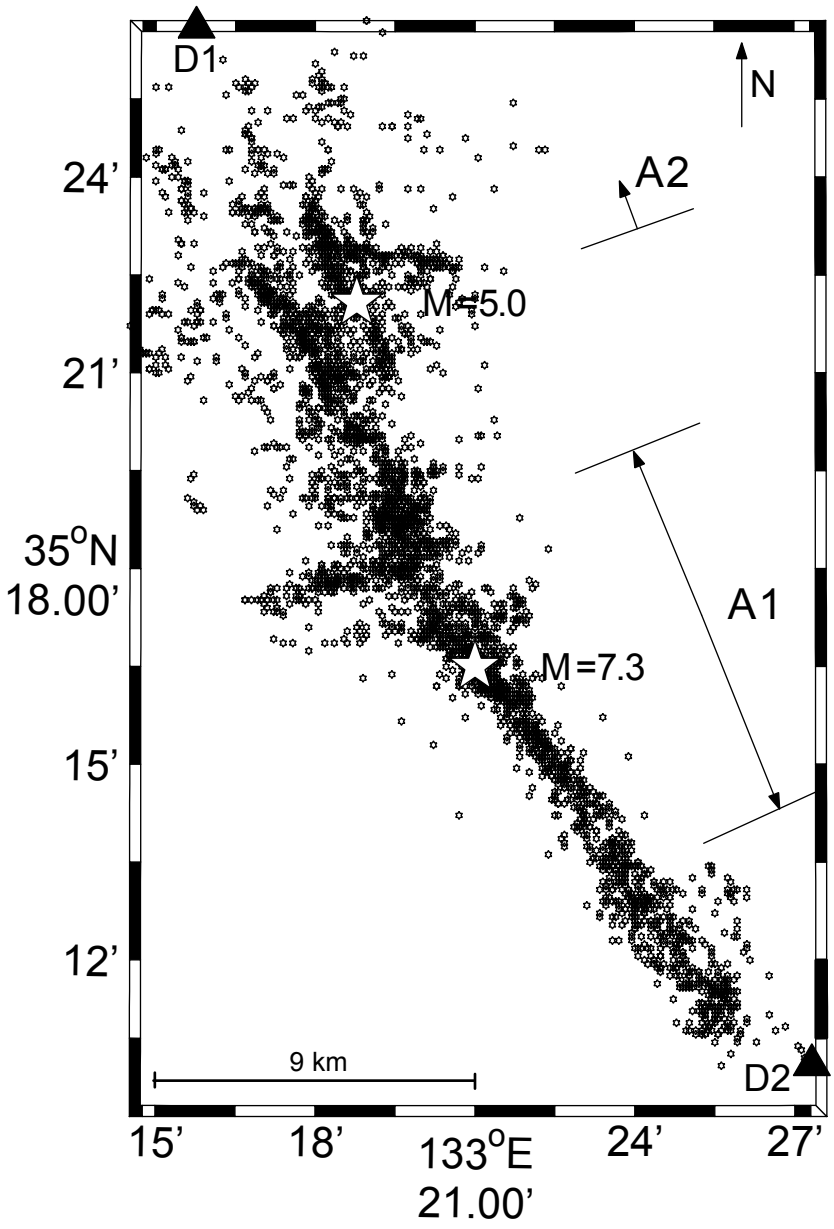

3.1 (b) An enlarged region A (Fig. 3.1a). A1 and A2 indicate two sub-regions for which the aftershock activity is compared (see text). D1 and D2 indicate the profile used for projection in Fig. 3.4. Stars mark the epicenters of the main shock and of the largest aftershock in the region.

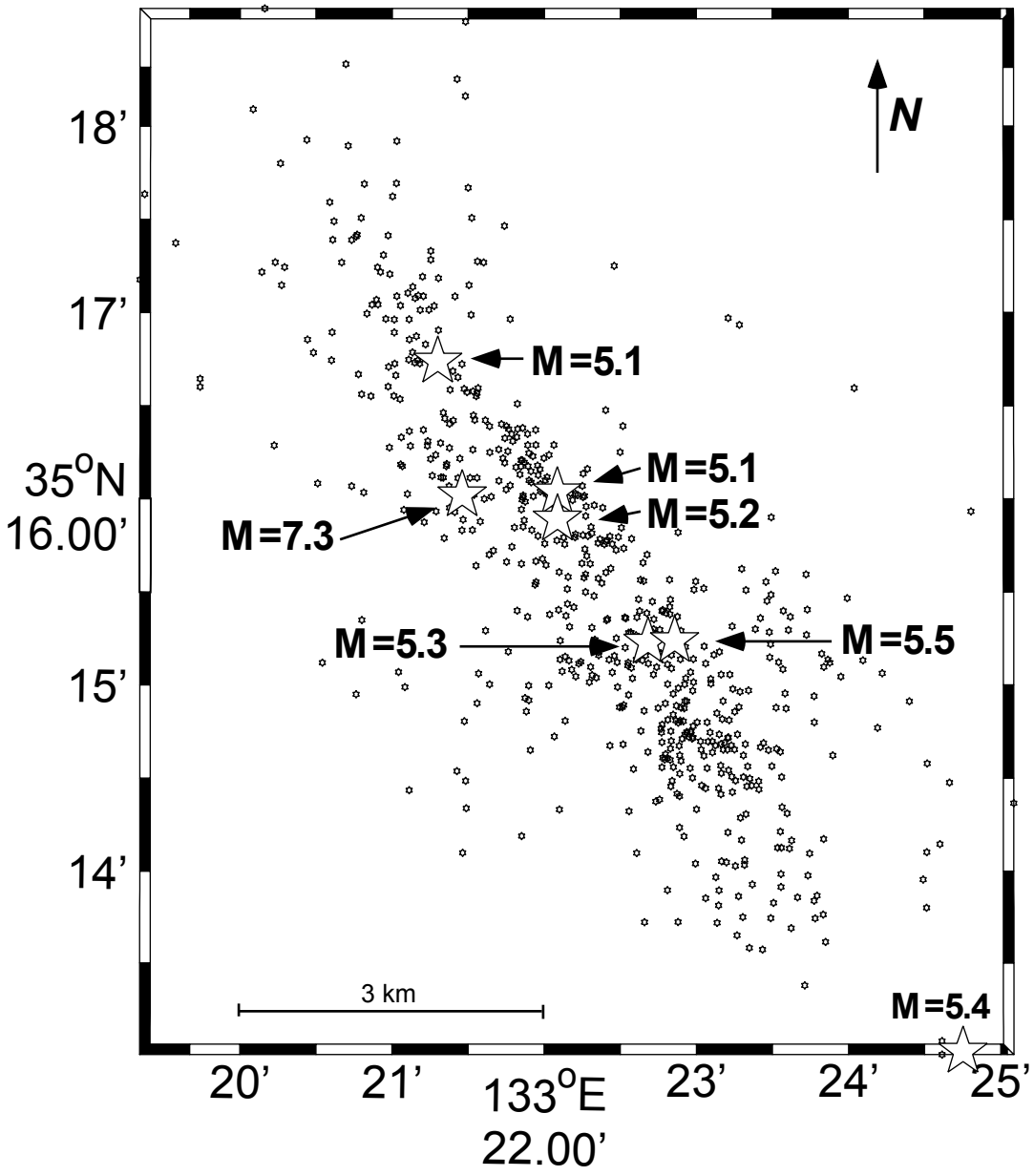

3.1 c) The seismic activity (M >= 1.5) before M7.3 Tottori earthquake, from 1978 to the main shock. The epicentral area corresponds to the occurrence of several seismic swarms in 1989, 1990 and 1997. The epicenters of the main shock and of the largest aftershocks are marked by stars. Stars mark the earthquakes with M >= 5.0.

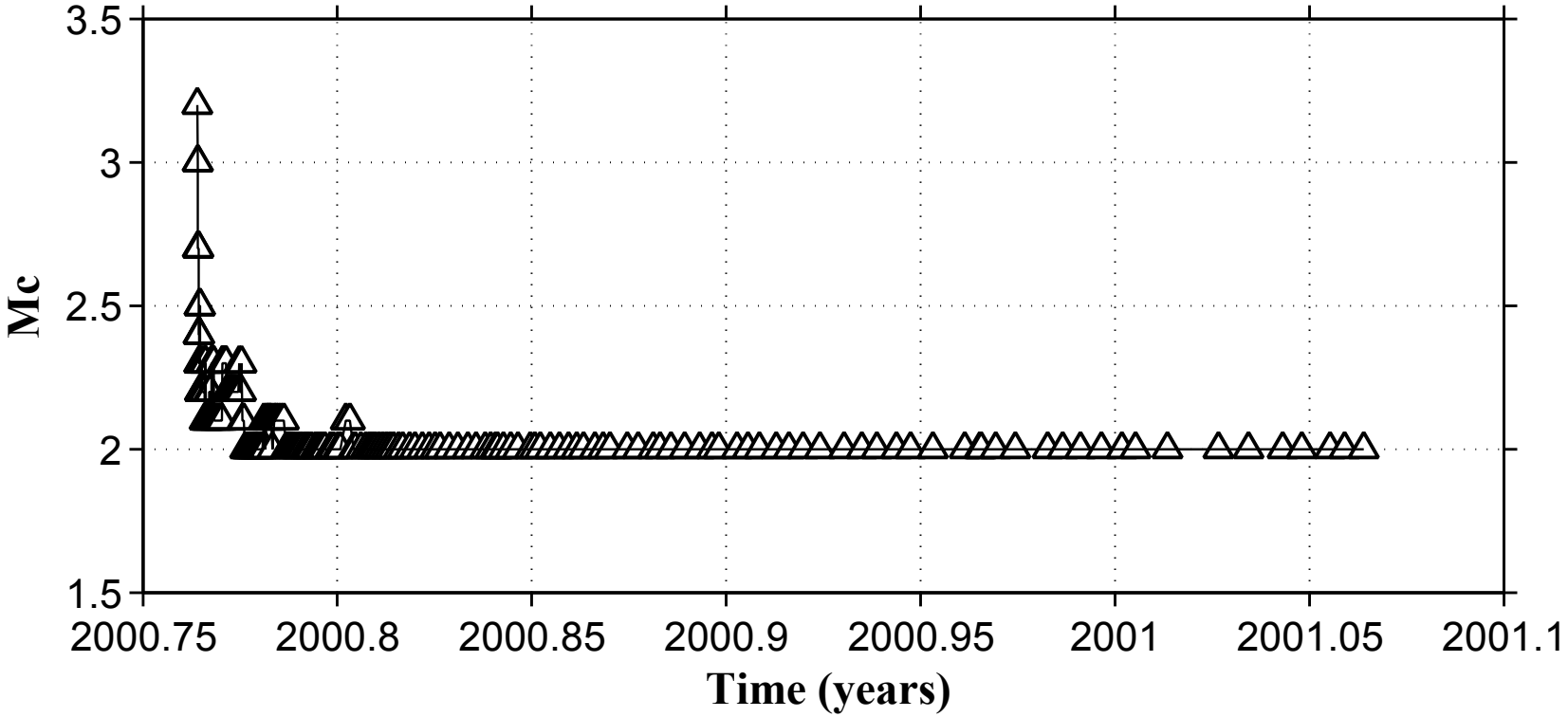

Fig. 3.2 *Mc* (magnitude of completeness) as a function of time for region A. There are 150 earthquakes in a moving-window, the window being moved by 15 events. The values of *Mc* are assigned at the end of the moving-window.

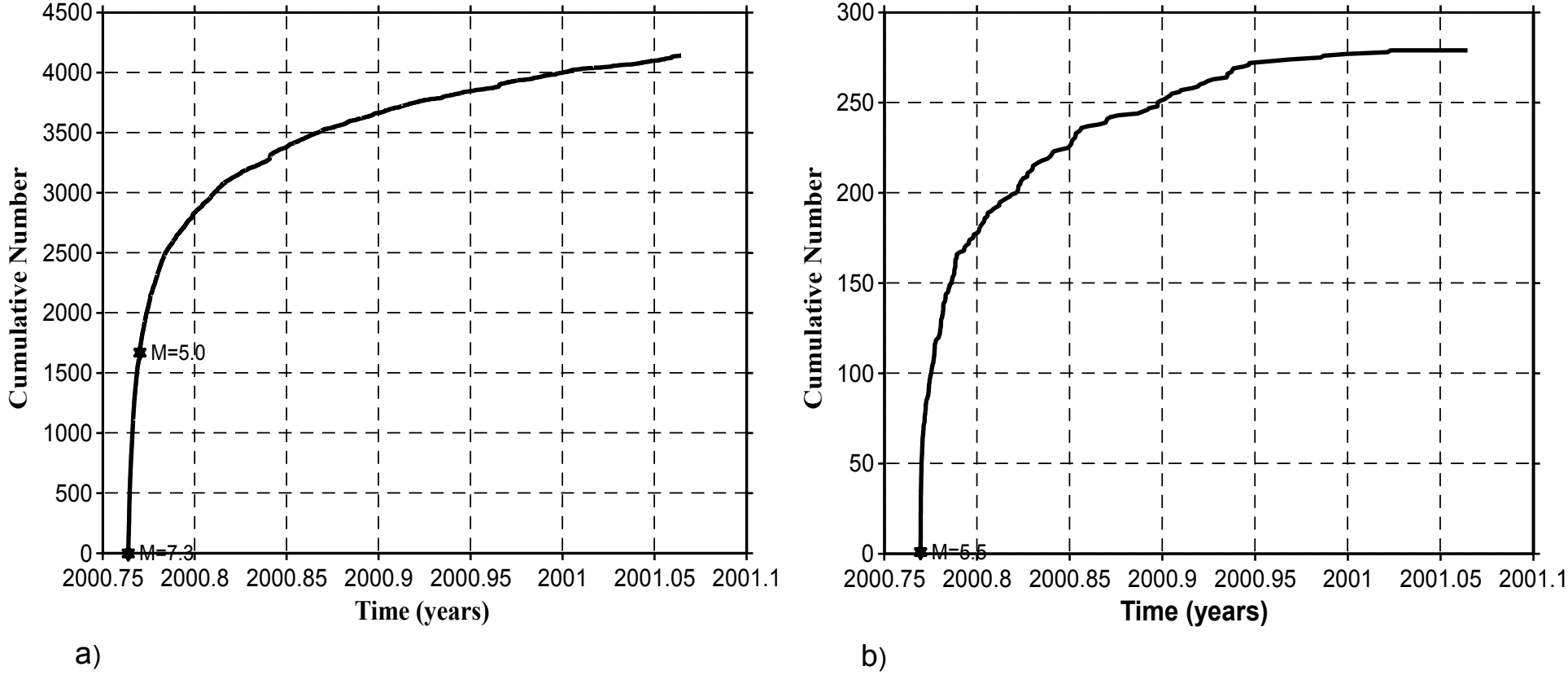

Fig. 3.3 Cumulative number of events versus time for all earthquakes (M >= 2) in region A (a) and B (b). The main shock and the largest aftershocks are marked by stars.

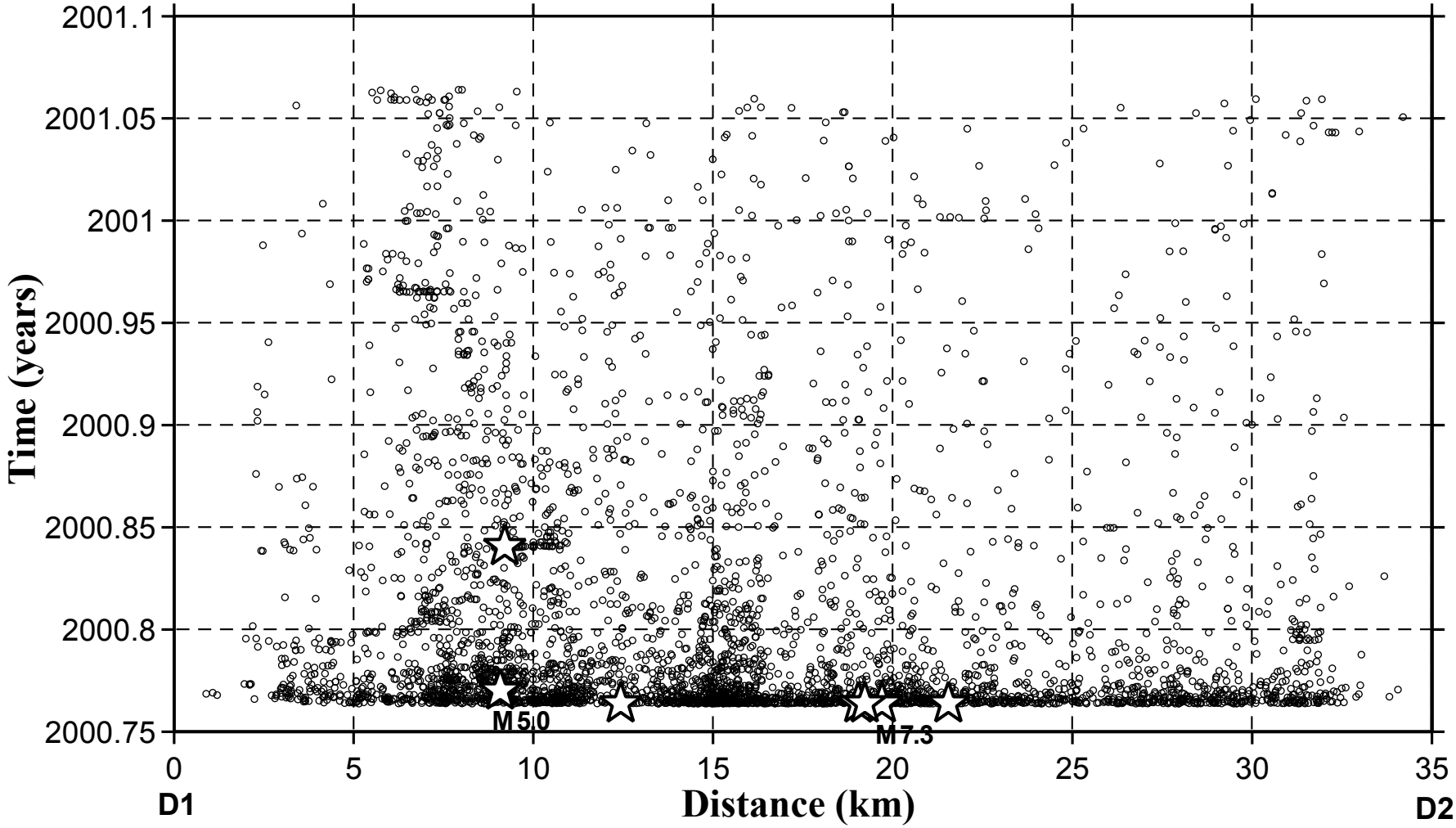

Fig. 3.4 Space-time diagram for the aftershocks in region A. Events are projected along the D1($133^0$15.94‘W, $35^0$25.93’N) to D2($133^0$27.24‘W, $35^0$10.41’N) direction shown in Fig. 3.1b. The earthquakes with M >= 4.5 are marked by stars. The main shock and the largest aftershock in region A are indicated also by “M7.3" and “M5.0", respectively.

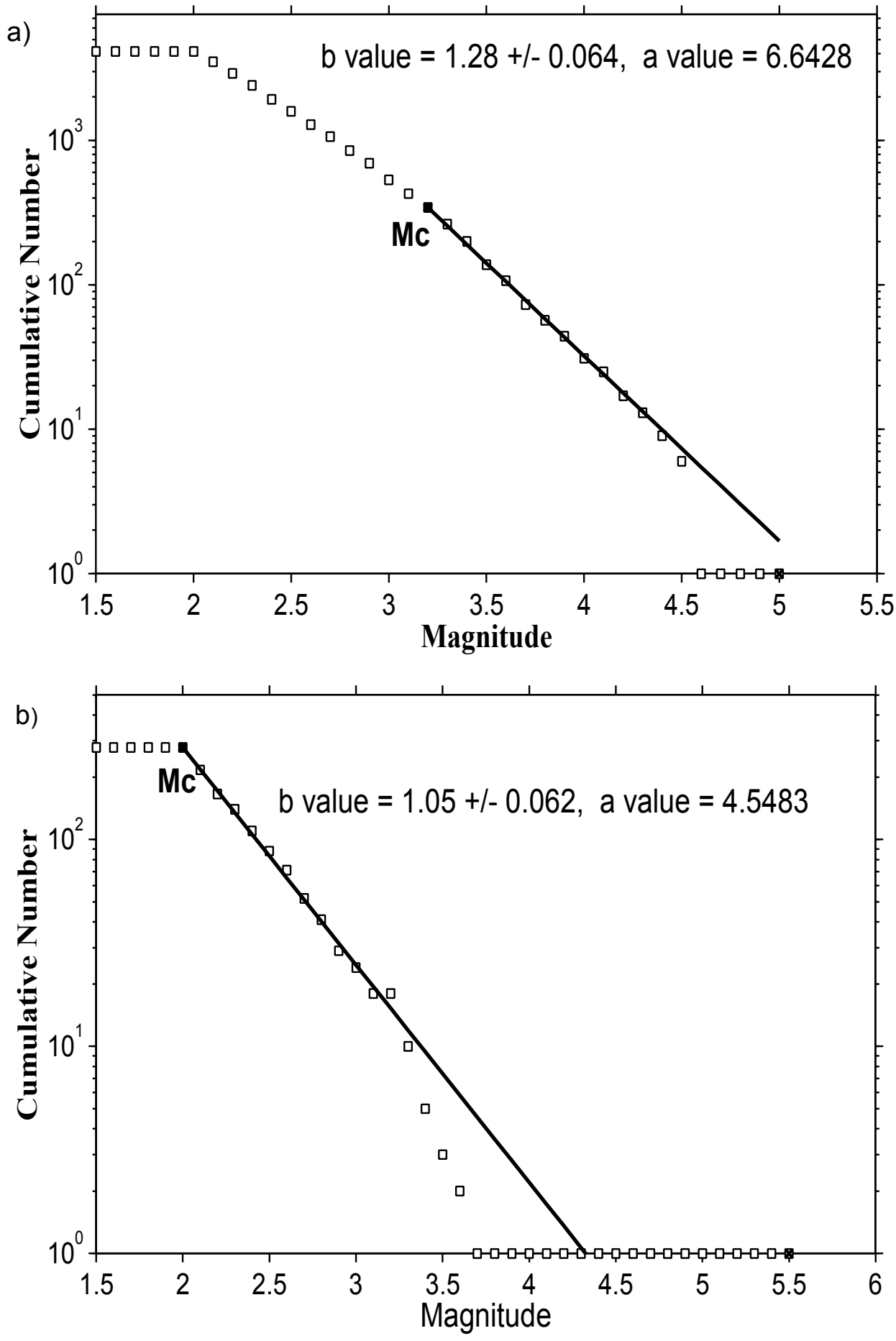

Fig. 3.5 Frequency-magnitude graphs for regions A (a) and B (b). b-value is determined for earthquakes with M >= Mc. Please refer to text for the method used for determining Mc. The b-value and its standard deviation, as well as the a-value in the Gutenberg-Richter relation for each region are given.

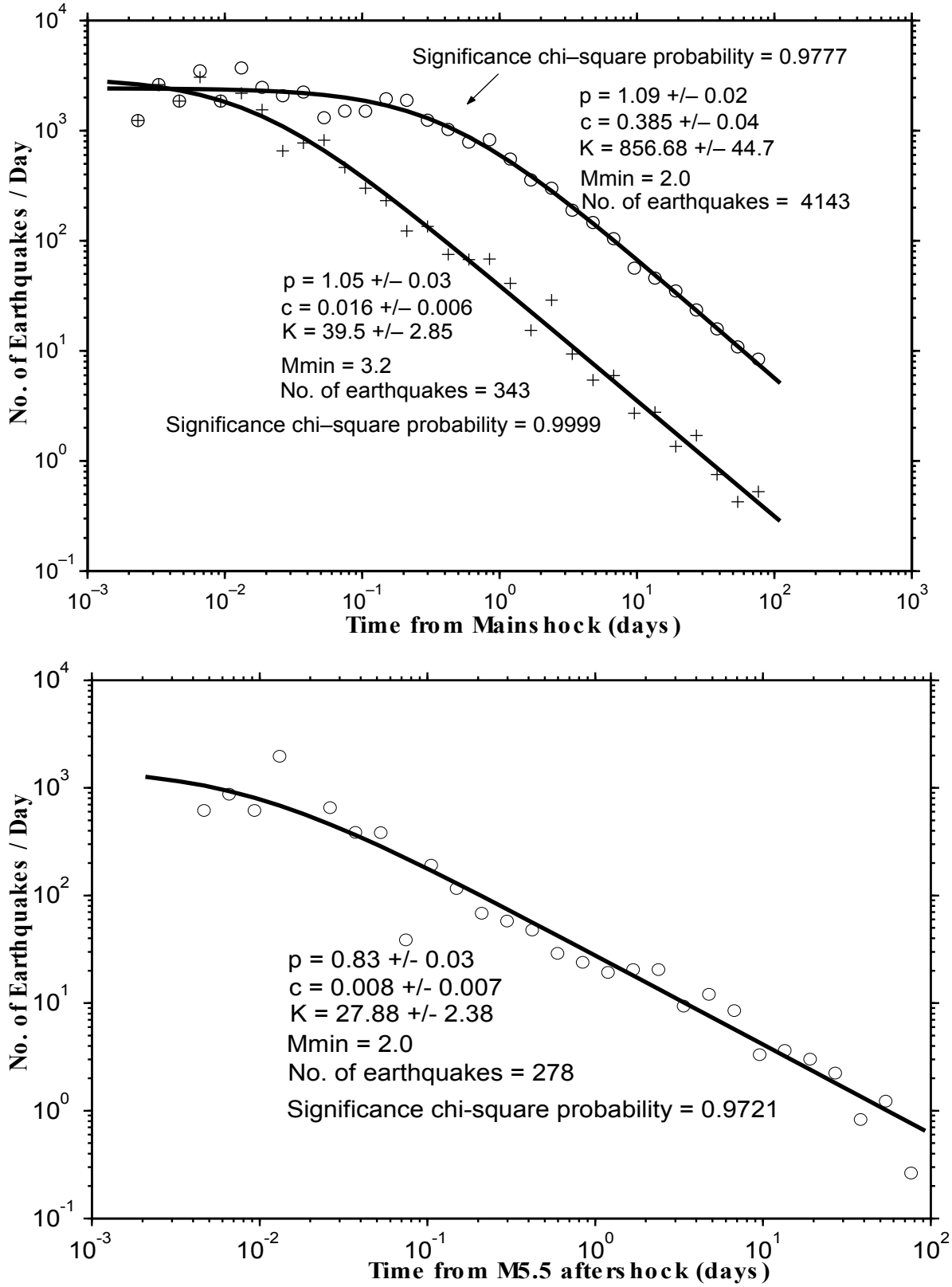

Fig. 3.6. a) Occurrence rate of earthquakes versus time in region A for two cases: M >= 2 and M >= 3.2, represented by circles and crosses, respectively. The curves represent the modified Omori formula fit to the data for the two cases. Near each distribution some relevant parameters of the fit are given: the values of p, c and K in the modified Omori formula, the minimum magnitude for the data, the number of earthquakes and the significance chi-square probability of the fit.

b) Occurrence rate of earthquakes for region B. The data are represented by circles. The same relevant parameters as for the Fig. 3.6a are given.

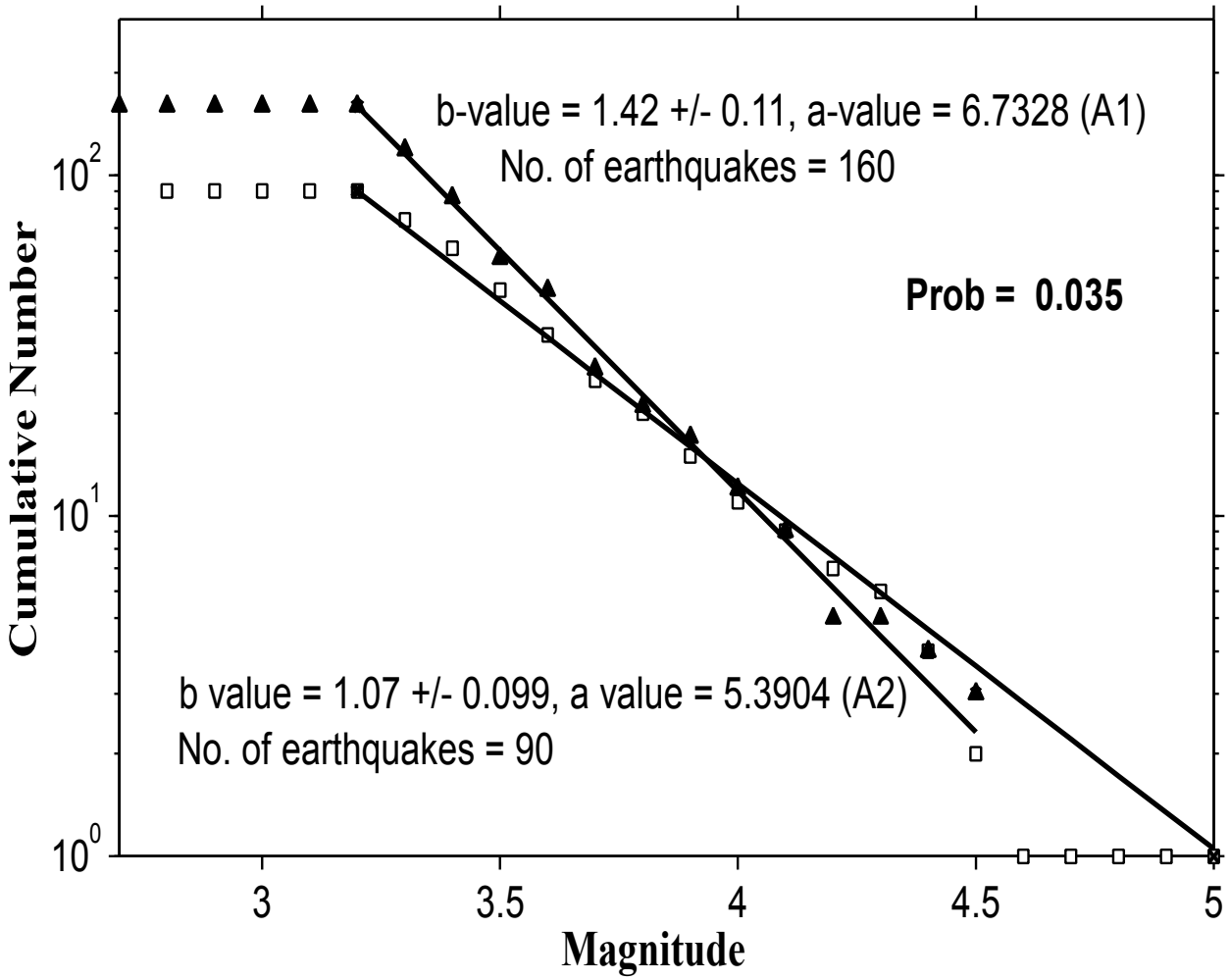

Fig. 3.7 Comparison between the frequency-magnitude distributions in the sub-regions, A1 and A2 in Fig. 3.1b. The triangles correspond to region A1 and the squares to region A2. The values of b and a for the two sub-regions and the number of earthquakes for each sub-region are given. 'Prob' represents the probability that the two distributions come from the same population.

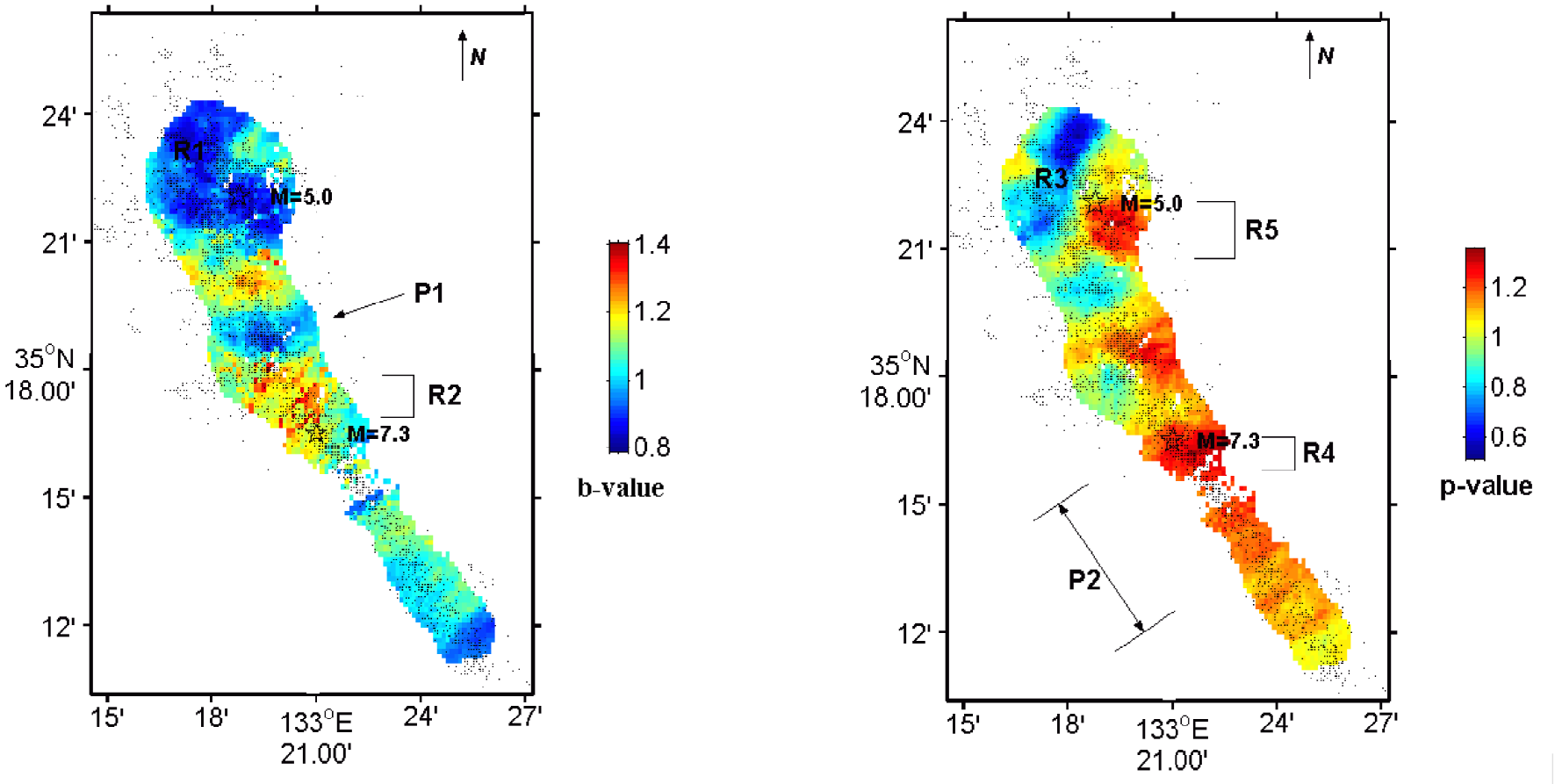

Fig. 3.8 a) b-value map using all earthquakes with M >= 2 and Tstart = 0.72 days. A b-value was determined by sampling the nearest 150 earthquakes for each node of a grid with nodal separation of 0.002^0 (about 0.2 km). The actual number of earthquakes used for determining the value of b at each grid point is between 100 and 150, depending on the completeness of magnitude (Mc) in each node. The b-value was computed using the maximum likelihood method. The values of b are color-coded and plotted at each node. Only the values for nodes where the sampled earthquakes are within 2km distance from the node are represented. The regions R1 and R2 are used for testing the significance of the spatial variation of b-value (see Fig. 3.9 and text). P1 indicates a region with small b-value, as mentioned in the text. b) A p-value map using the same grid and number of earthquakes in each grid-node as in the case of b-value map. The p-value was determined using a maximum likelihood method. Regions R3, R4 and R5 are used for testing the significance of the difference in p-value (see Fig. 3.9 and text). P2 indicates a region with high p values.

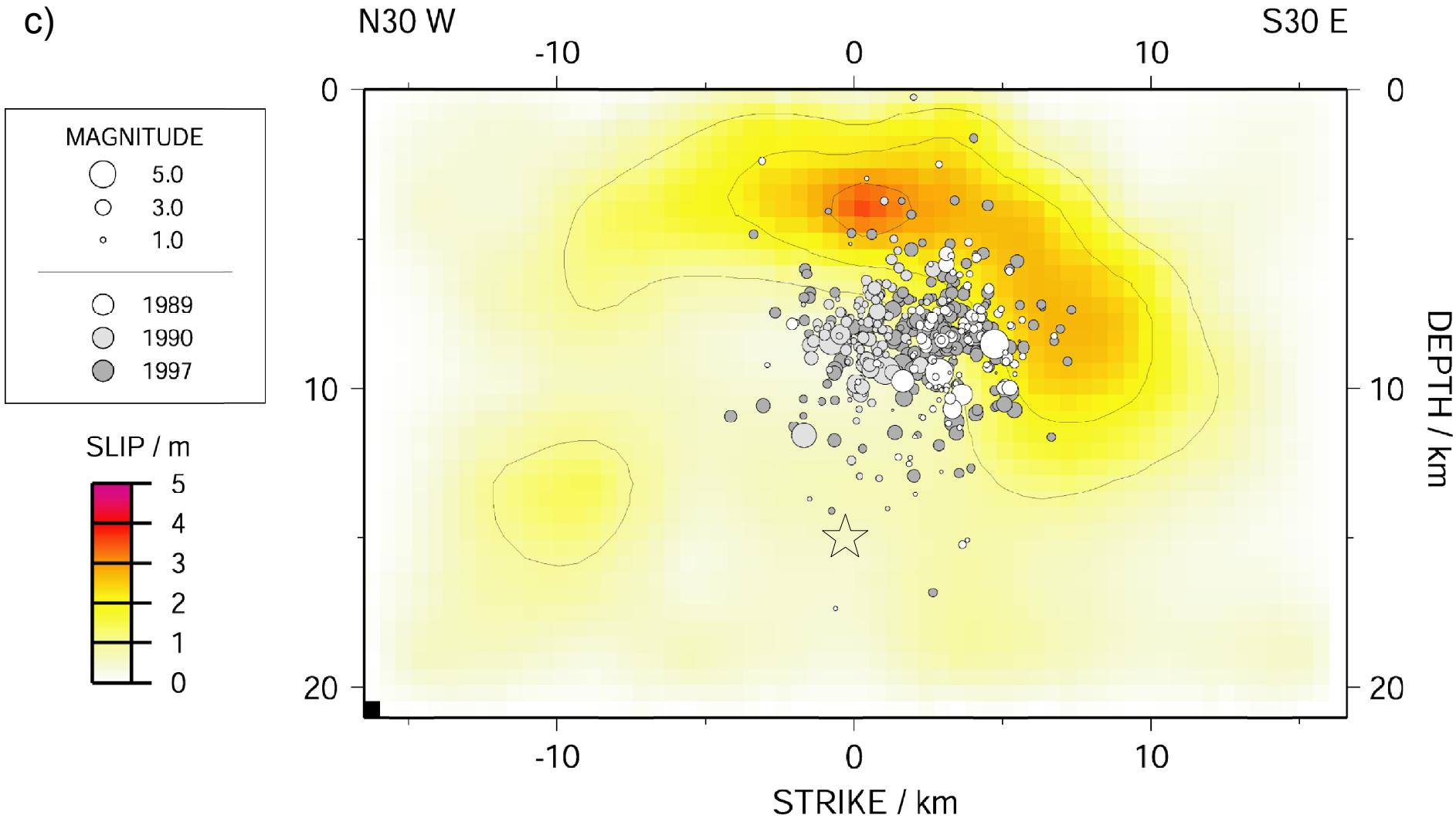

Fig. 3.8 c) Depth distribution of slip for the 2000 Western Tottori earthquake. The hypocenters of earthquakes occurred during the 1989, 1990 and 1997 earthquake sequences are also shown. The hypocenter of the 2000 Western Tottori earthquake, marked by an open star in the figure, corresponds to the origin (“0 km”) of the profile. After Shibutani et al., 2001, 2002.

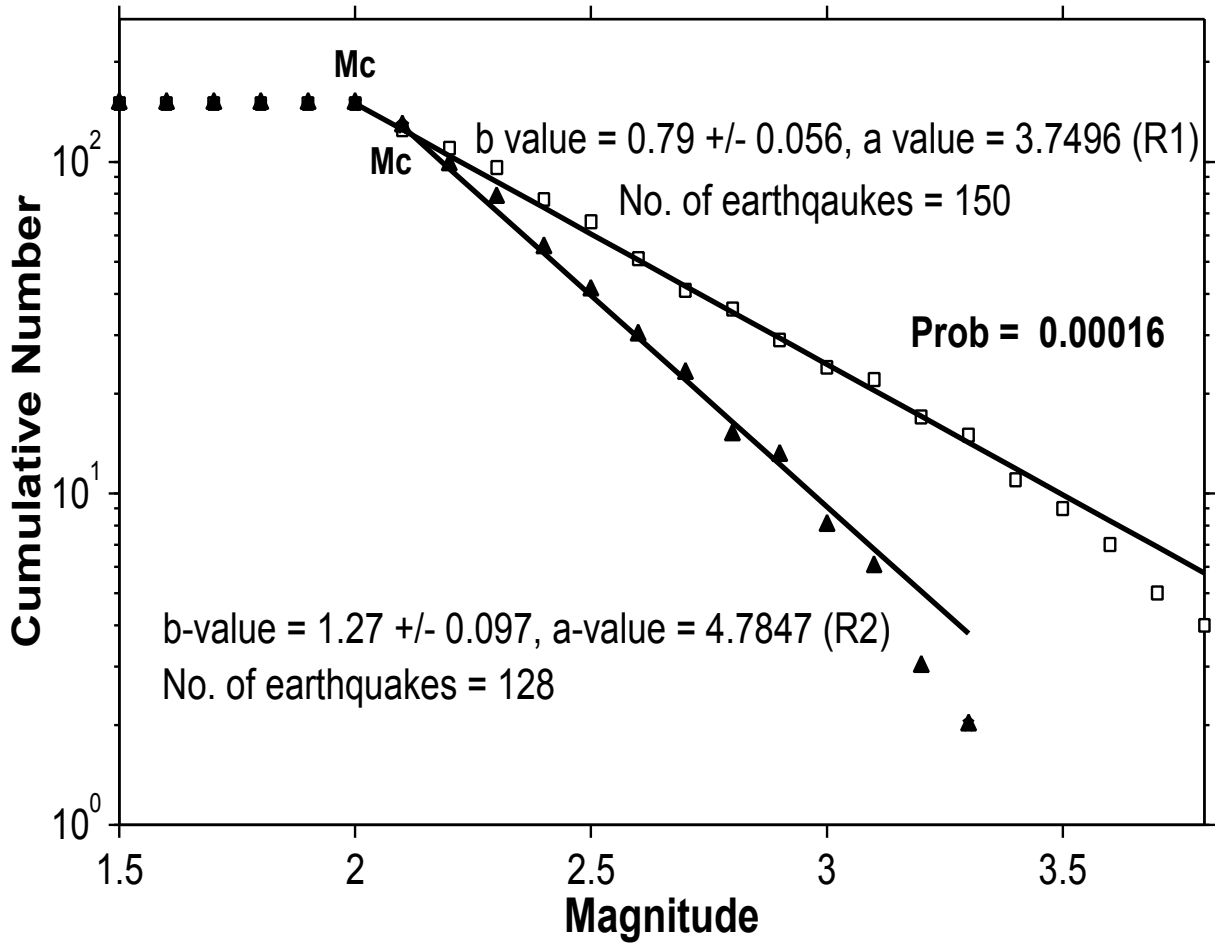

Fig. 3.9 Comparison between the frequency-magnitude distributions in two different regions, R1 and R2 in Fig. 3.8a. The squares correspond to region R1 and the triangles correspond to region R2. The magnitude of completeness is indicated near each sample. The b and a values for the two samples and the number of earthquakes for each sample are given. 'Prob' represents the probability that the two distributions come from the same population.

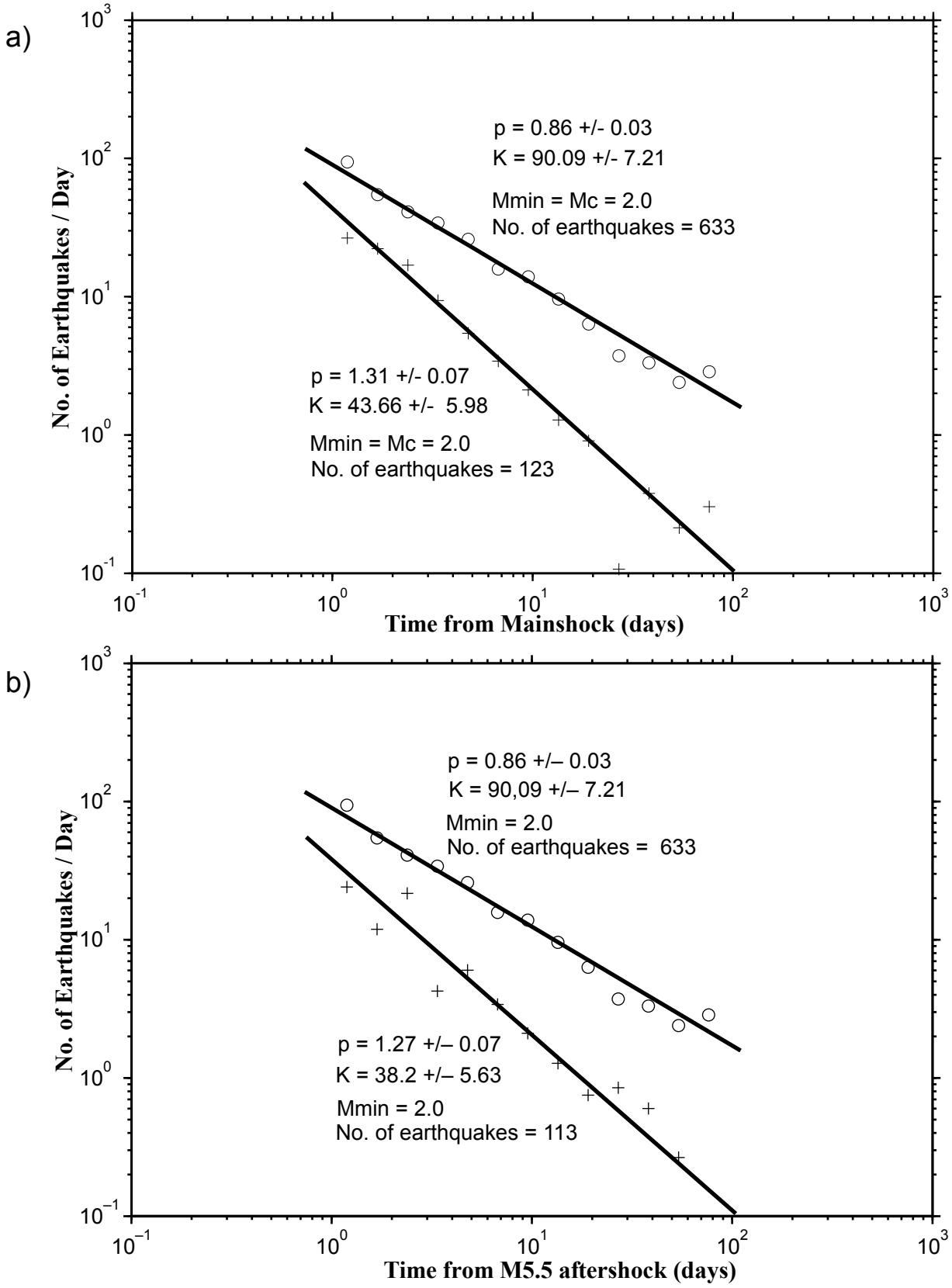

Fig. 3.10 Comparison between the p-value in the modified Omori formula for samples in the regions R3 and R4 (a) and R3 and R5 (b). The circles correspond to region R3 and the crosses to region R4 in Fig. 10a and R5 in Fig. 10b. The curves represent the modified Omori formula (c=0) fit to the data for the three cases. Near each distribution some relevant parameters of the fit are given: the values of p and K in the modified Omori formula, the minimum magnitude for the data and the number of earthquakes in the sample.

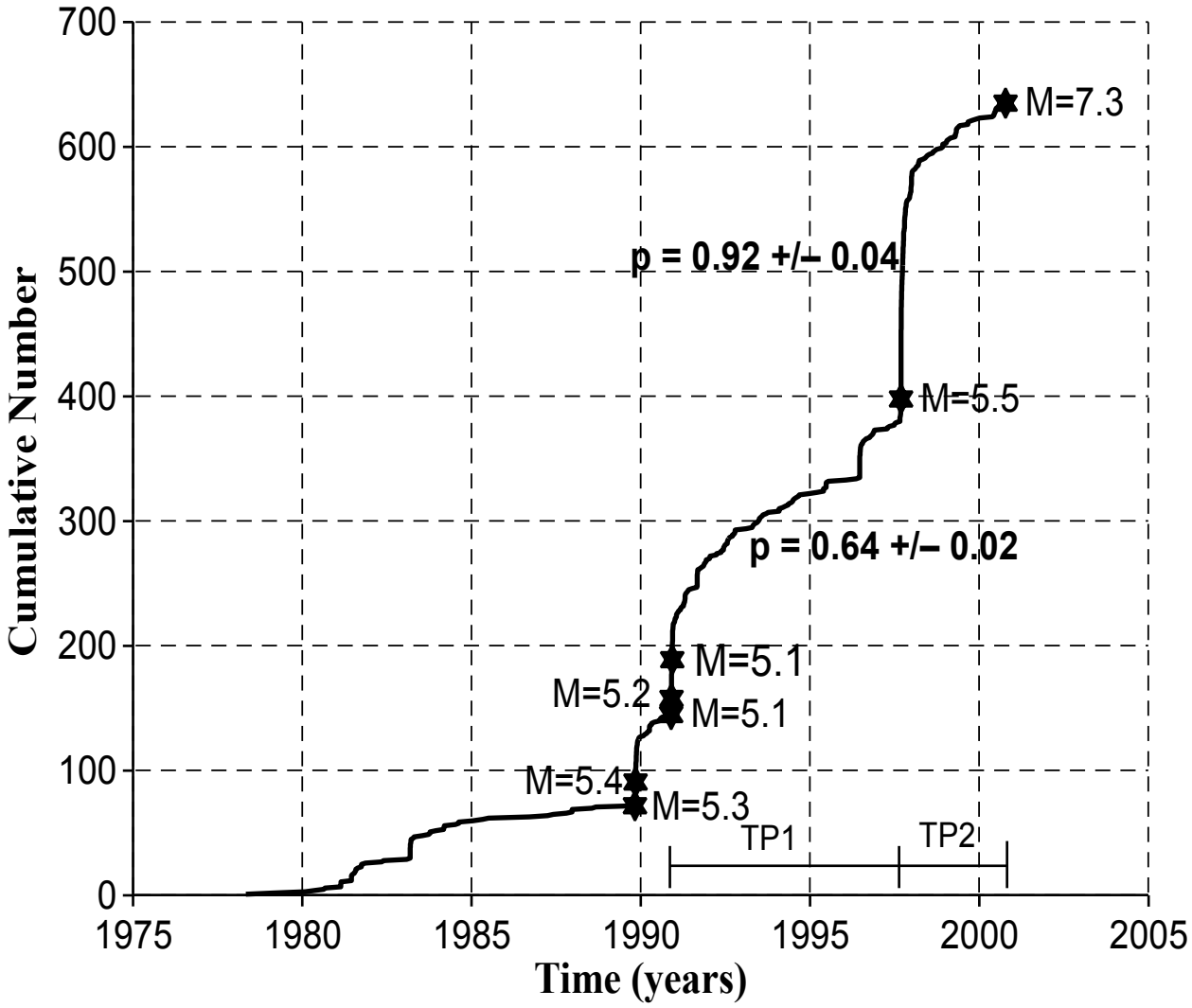

Fig. 3.11 Cumulative number curve of earthquakes with M >= 1.5 that occurred between 1978 and the 2000 Western Tottori earthquake. Stars mark the events with M >= 5.0. The values of p given in the figure characterize the decrease rate of seismic activity in the periods TP1 and TP2, respectively, and were computed using the modified Omori formula. The magnitude of completeness for the two time periods is 1.5 and 2.5, respectively.

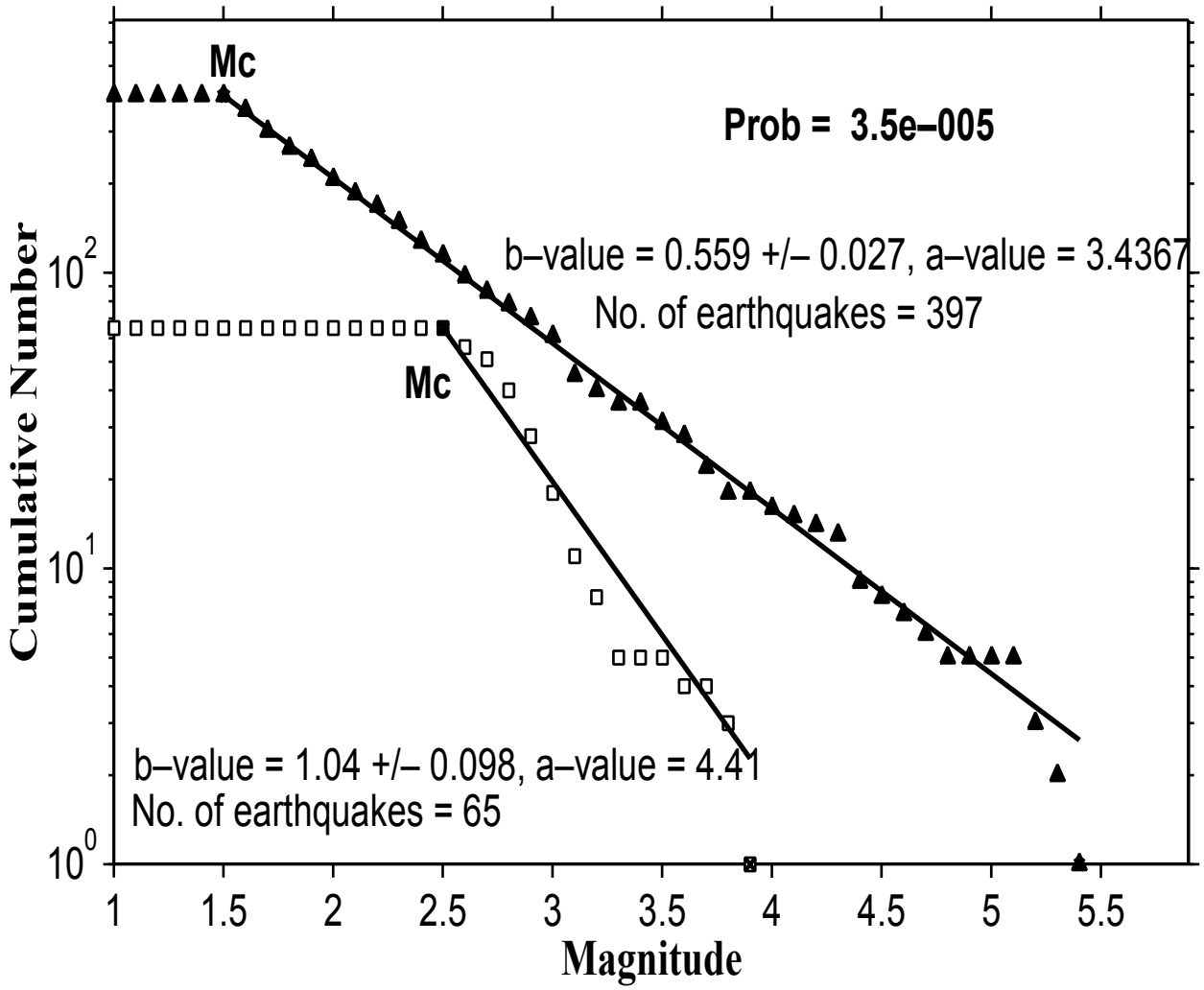

Fig. 3.12 Comparison of the frequency-magnitude distribution before (triangles) and after (squares) the 1997 M5.5 earthquake. Some relevant parameters for each distribution, as well as the probability that the two distributions come from the same mother population are given. “Mc” marks the magnitude of completeness in each case.

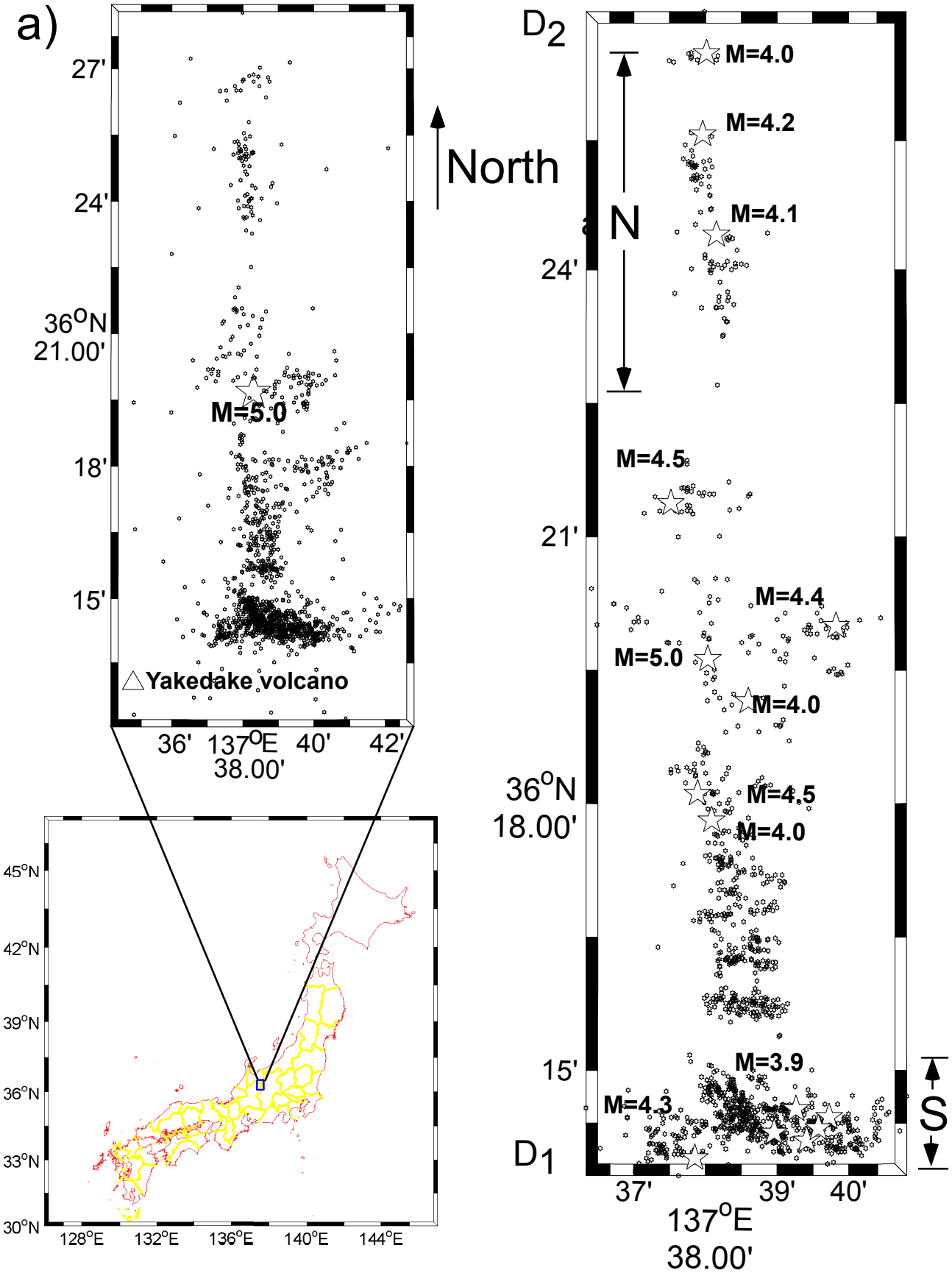

Fig. 4.1a **Right**: *Up*: Epicentral map of the 1998 Hida Mt. earthquake swarm (DPRI data, M >= 1.7). Star indicates the largest event of the swarm. *Down*: Map of Japan, which indicates by a small blue rectangle the Hida Mountain region.
Left: Relocated seismicity for Hida earthquake swarm. (M>=1.7). N and S refer to the north and south regions that are compared for their frequency-magnitude distribution in Fig. 4.2. Stars show events with M>=3.9.
D_1D_2 indicates the profile used for projection in fig. 4.1b)

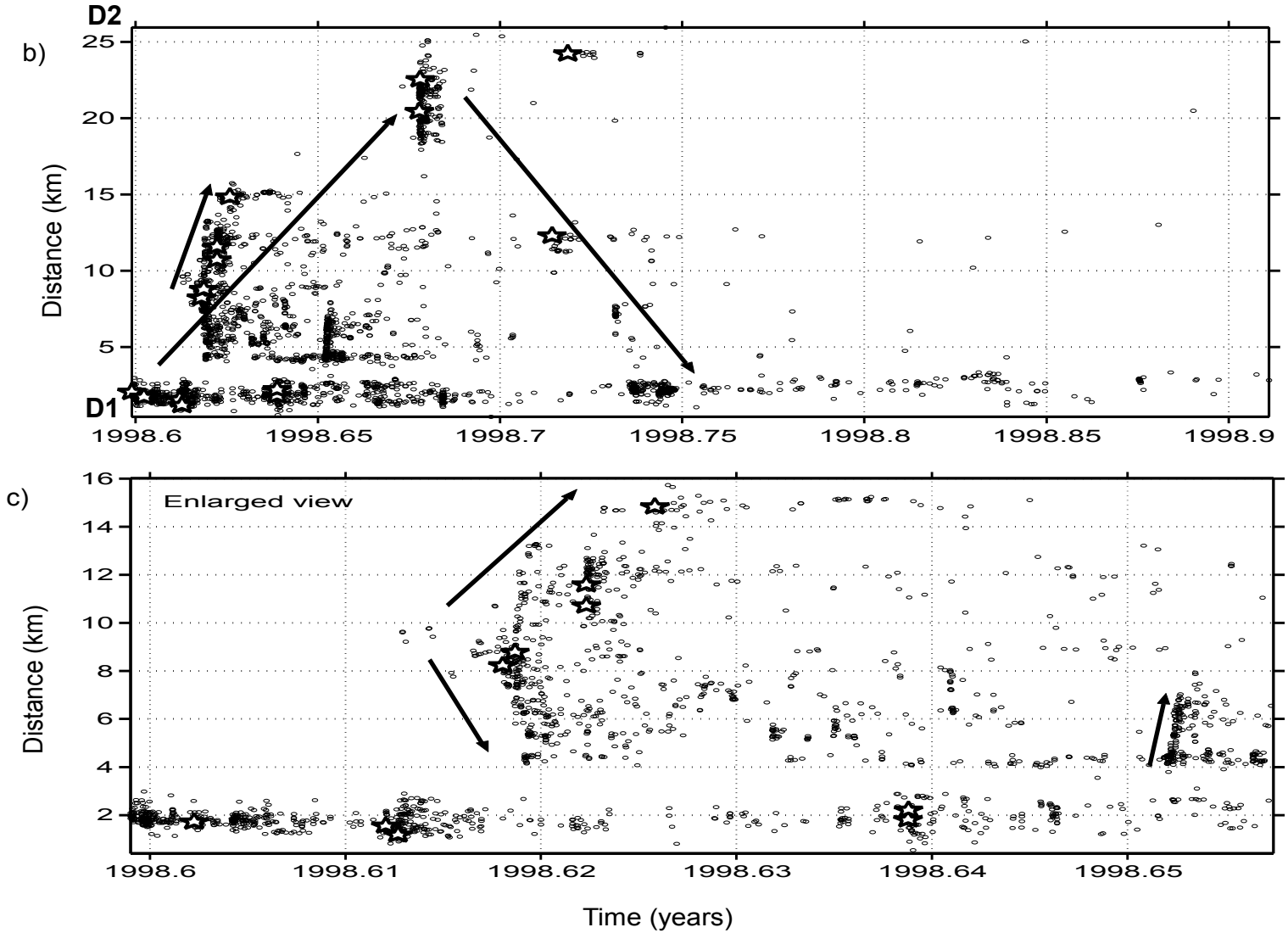

Fig. 4.1 b) Time-space diagram of all relocated earthquakes. Events are projected along the D_1D_2 direction shown in Fig. 4.1a).

c) Zoomed view of b) (the beginning of the swarm, south and central part).
The arrows indicate directions of migration. Stars mark events with M >= 3.9.

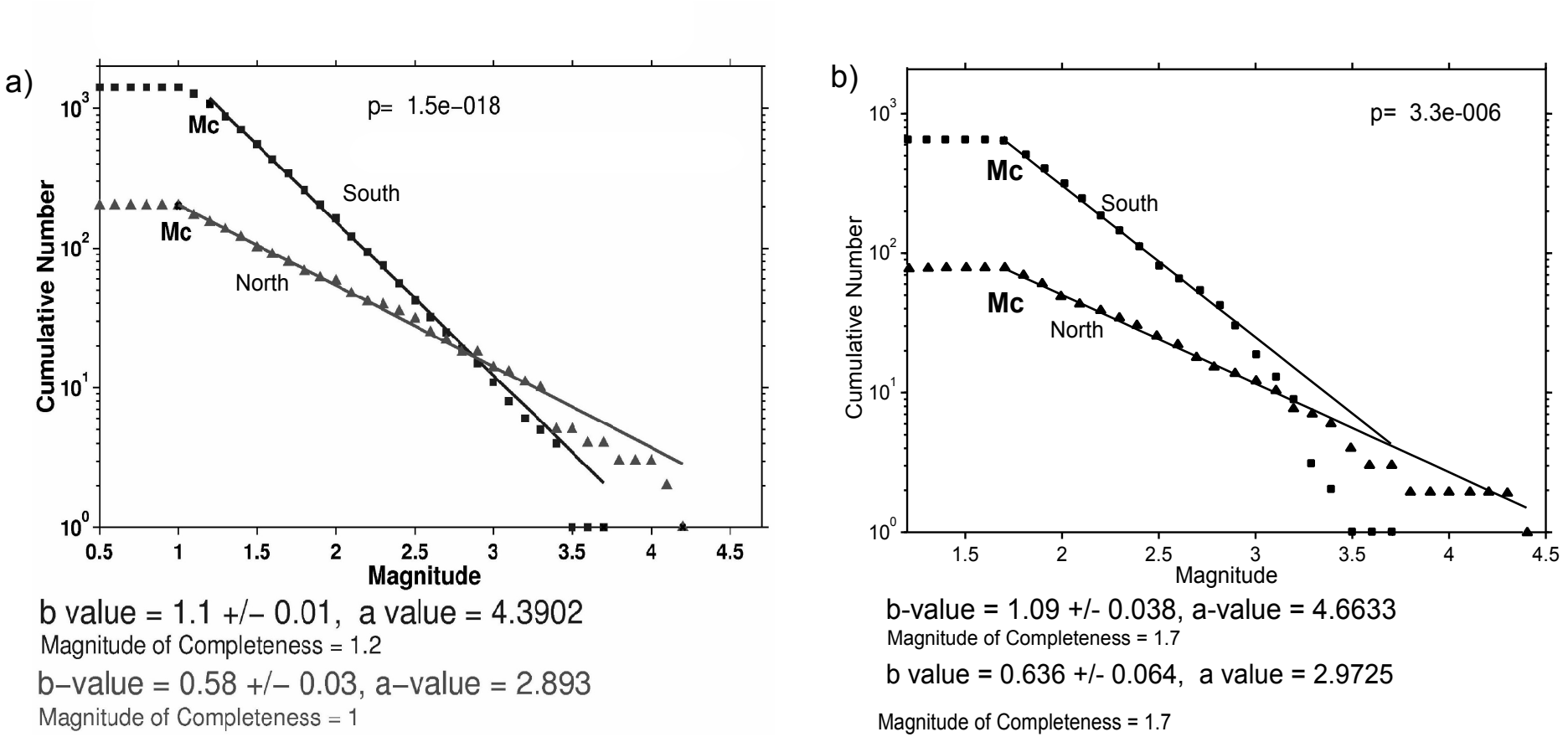

Fig. 4.2 Frequency-magnitude distribution in the north (N region in Fig. 4.1a) and south (S region in Fig. 4.1a) of Hida Mt., by using DPRI (a) and JMA (b) data, during the same time period. One can notice the good agreement between the corresponding frequency-magnitude distributions of the two data sets. (Of course, some differences are expected as there are two different catalogs). The p-value indicates here the probability that the two distributions (from the North and South region, respectively) come from the same mother population. The small value of p shows that the two distributions are very different. Squares and triangles correspond to the south and north region, respectively.

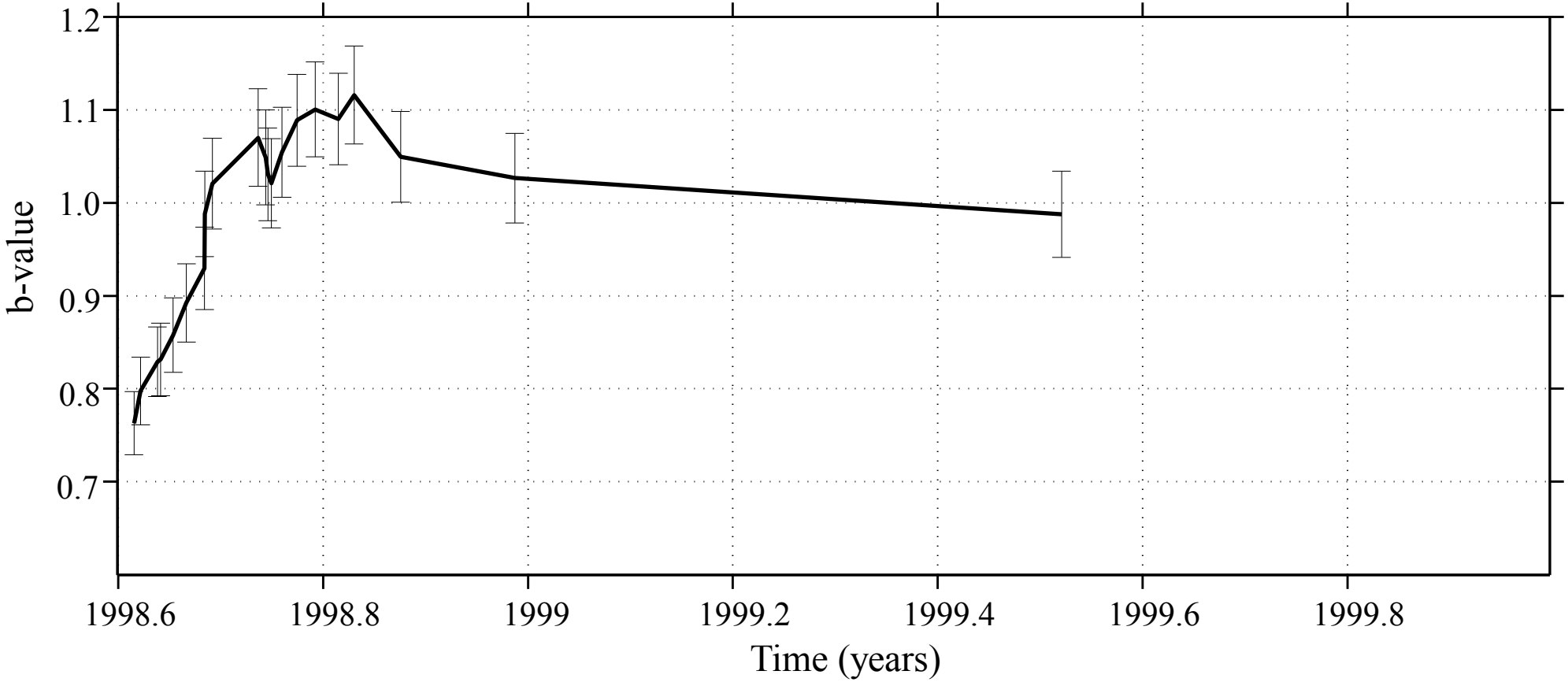

Fig. 4.3 Variation of b-value with time, for the south region (S in Fig. 4.1a) of Hida Mountain, when using all the events with M >= 1.5 located by DPRI, Kyoto University. There are 400 events in a moving window.

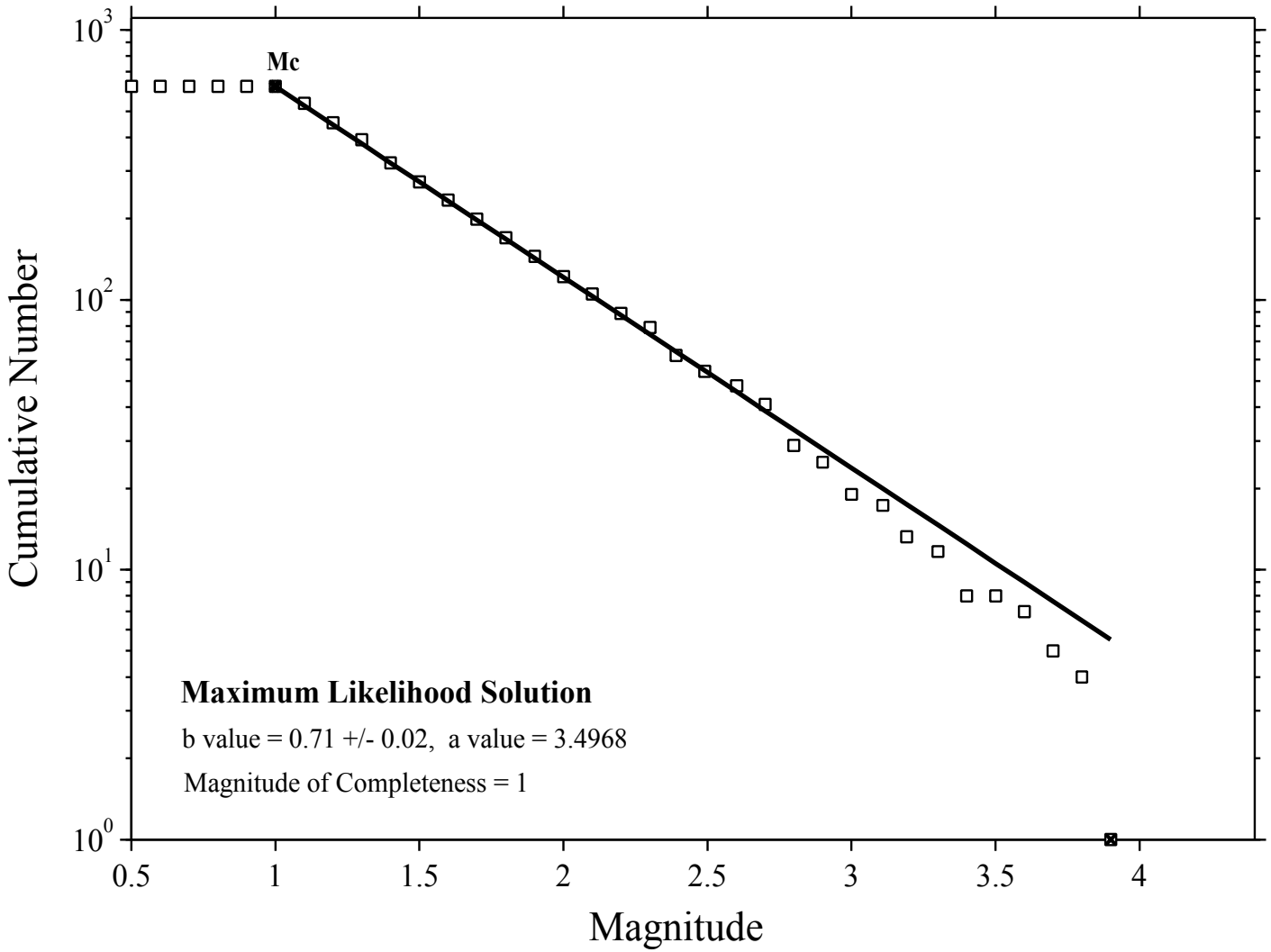

Fig. 4.4 Frequency-magnitude distribution for the beginning of the swarm sequence in the southern cluster (S in figure 4.1a)). Mc indicates the magnitude of completeness. b-value was obtained by using the maximum likelihood method.

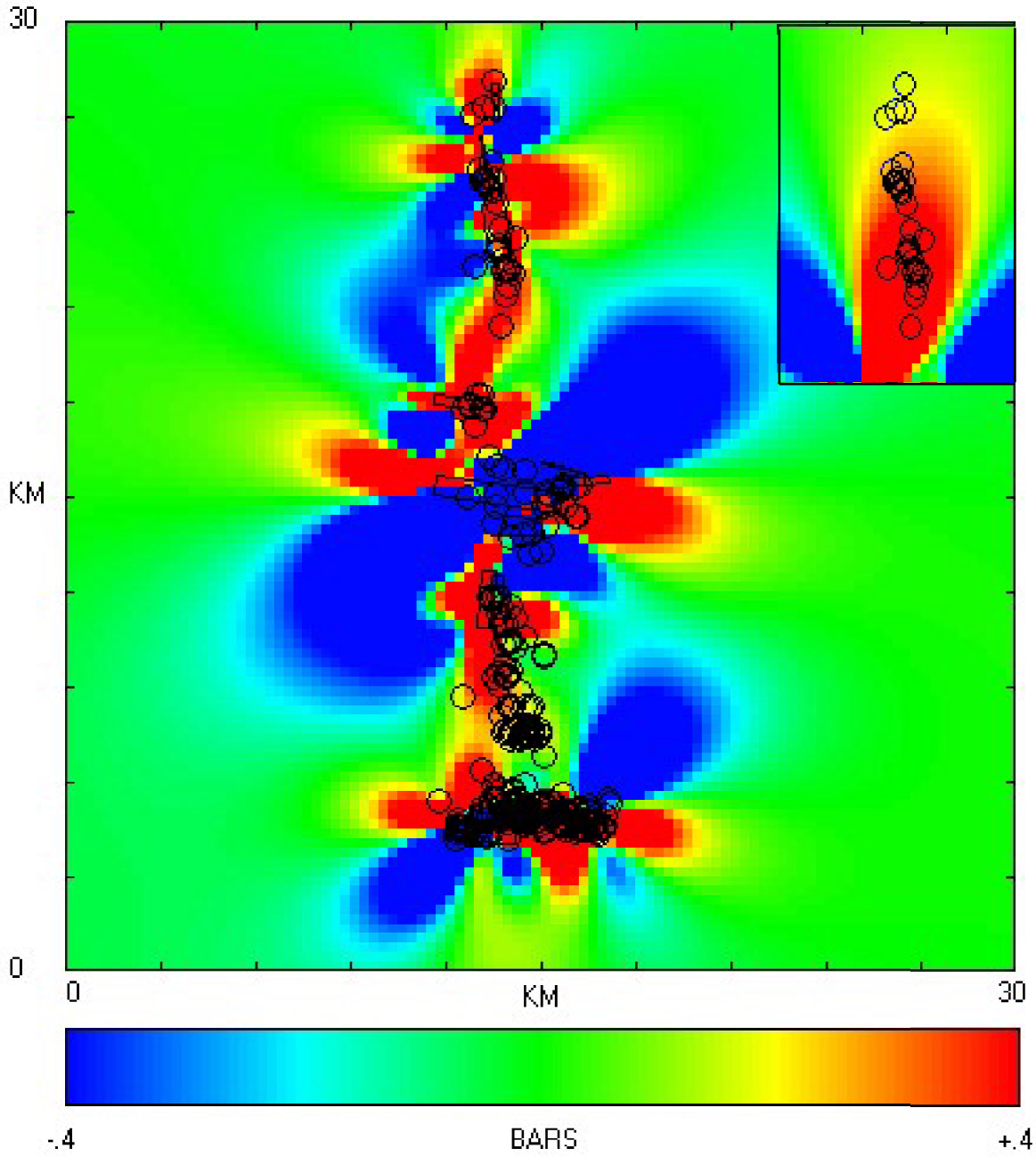

Fig. 4.5 Coulomb failure stress change on optimum oriented failure planes, as a result of the largest 18 events with M >= 4.0 occurred during a time period of about two months since the beginning of the Hida Mt. swarm. The red and blue colors indicate an increase or, respectively, a decrease of the Coulomb stress. The regional stress has a WNW--ESE direction. Double-difference relocated events (M >= 2.5) are superposed on the stress map. The colors indicate a relative stress change between -0.4 and 0.4 Bars, as indicated under the map. The inset shows the distribution of Coulomb Failure Stress change in the north, before the occurrence of earthquakes in this area. Superposed are the events that occurred in the northern cluster. The colors for the inset scale between -0.1 and 0.1 Bars.

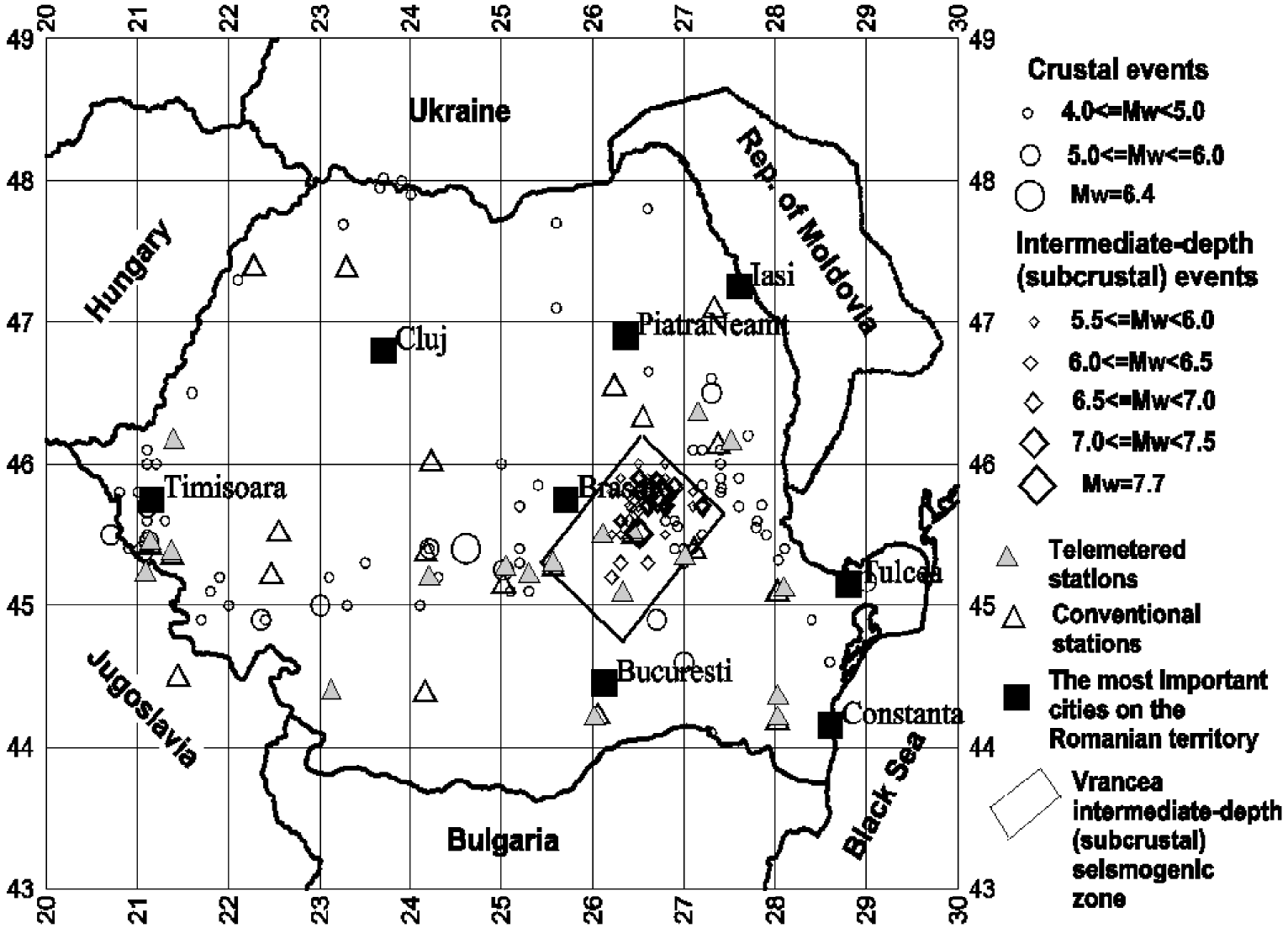

Fig. 5.1 Seismicity (crustal events with M_W >= 4.0 and intermediate-depth events with M_W >= 5.5 from the Romanian Earthquake Catalog, Oncescu et al., 1999) and distribution of seismic stations in Romania.

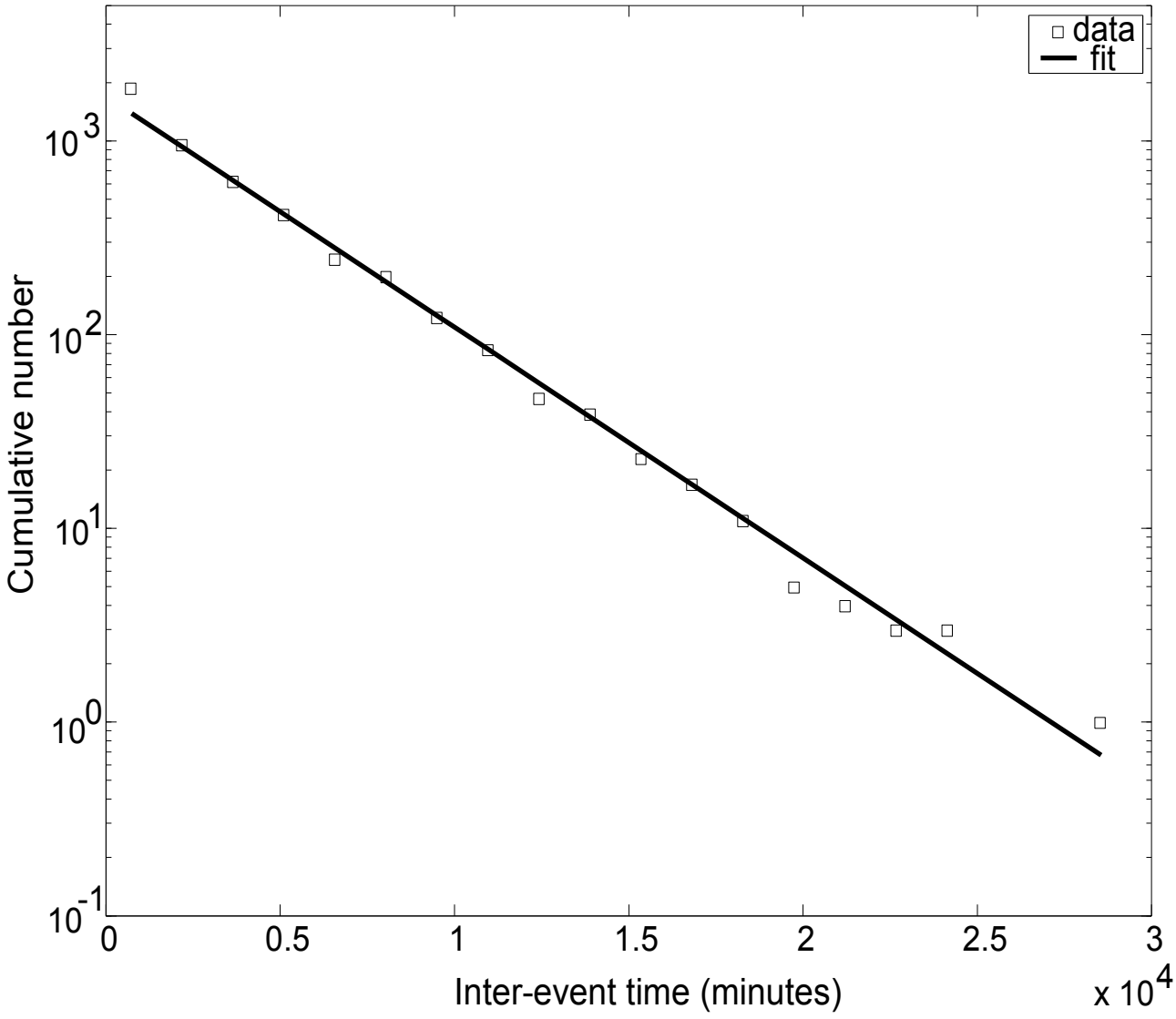

Fig. 5. 2 Inter-event times distribution of the original catalog for M >= 2.6. The exponential distribution fits the data well, with a coefficient of determination close to one.

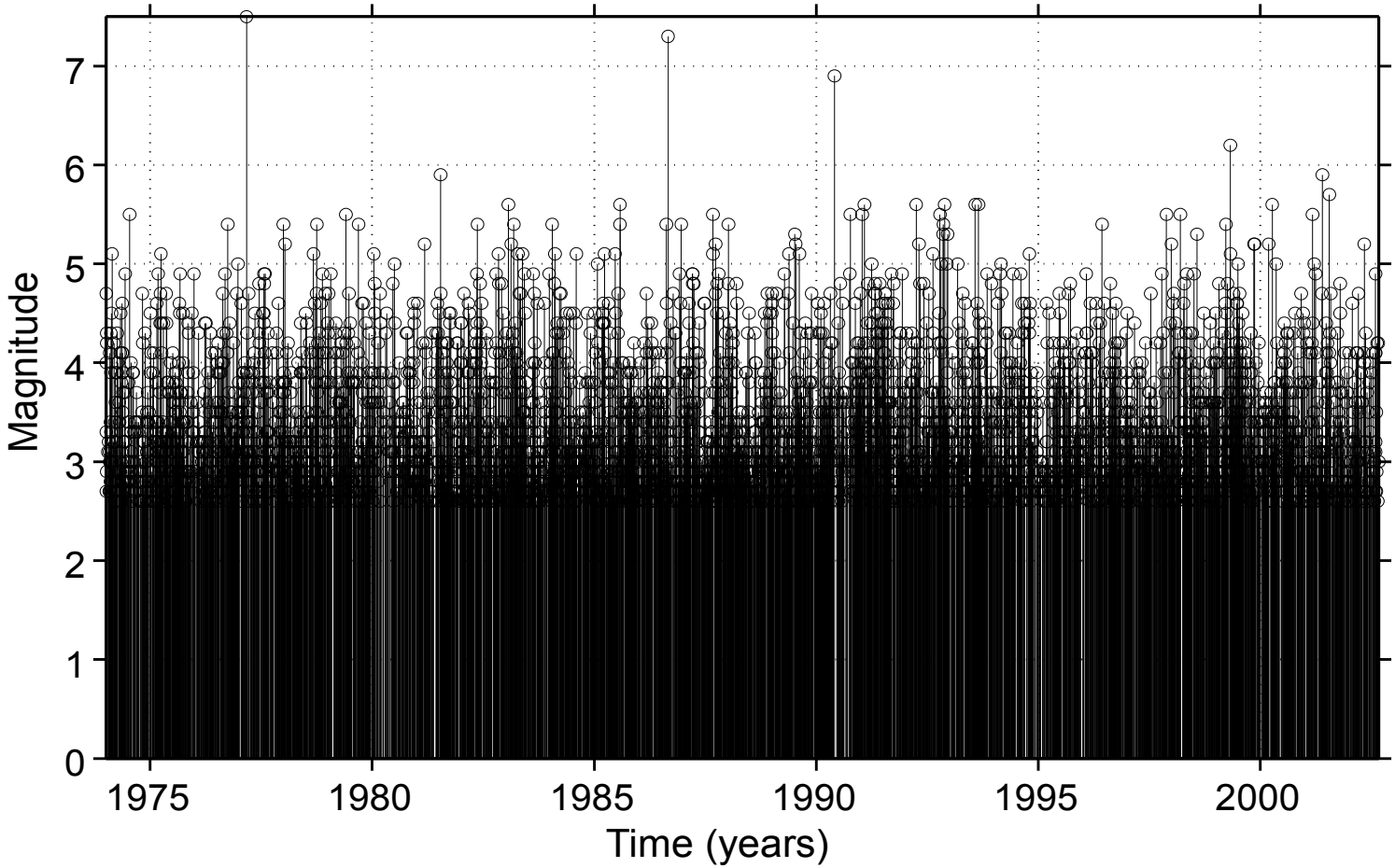

Fig. 5.3 Magnitude of events versus time for the original catalog (M >= 2.6; h >= 60 km). There are major earthquakes in 1977 (Mw = 7.5), 1986 (Mw = 7.3) and 1990 (Mw = 6.9).

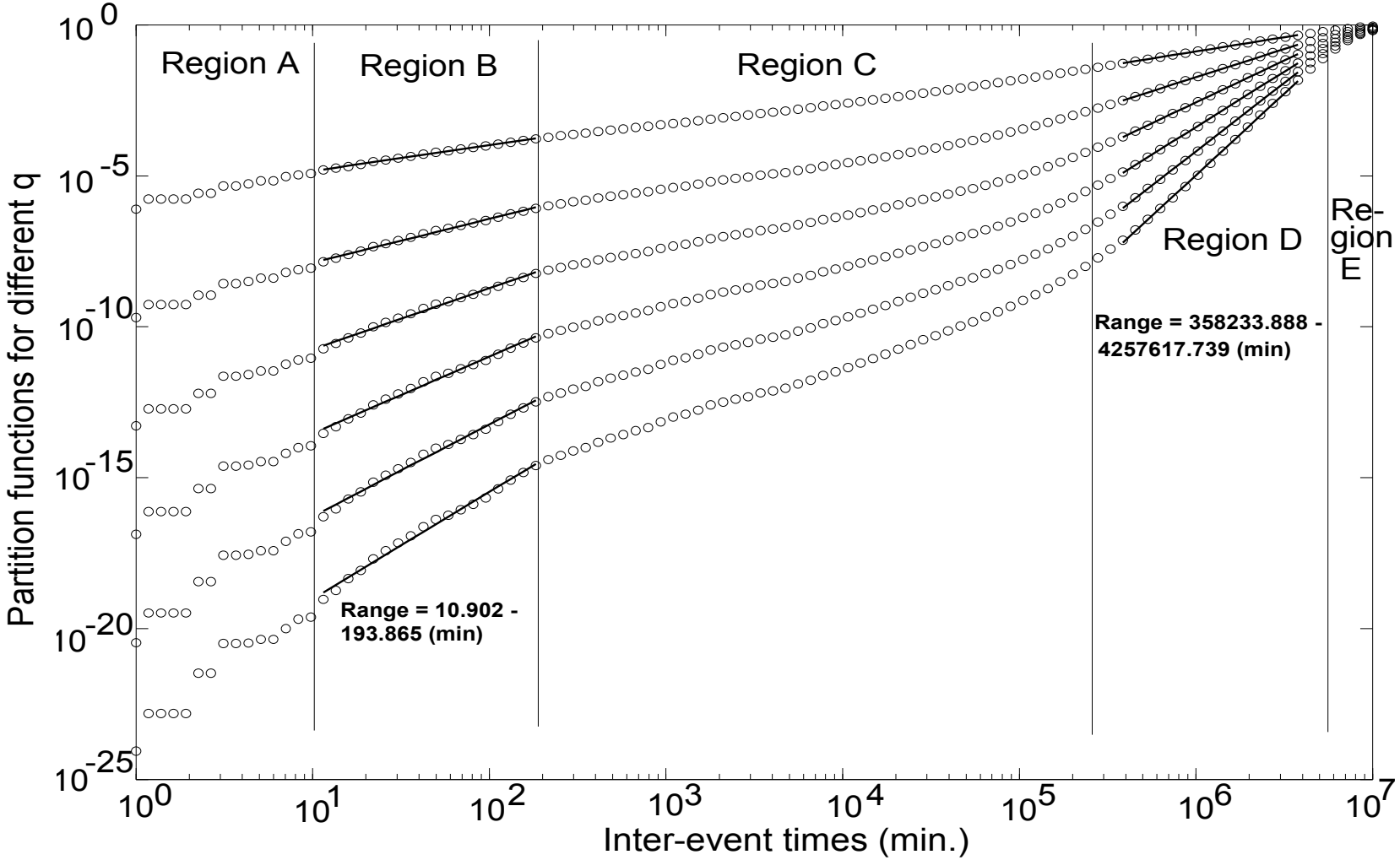

Fig. 5.4 Partition functions (q=2,3,...,7, from top to bottom) for the inter-event times of the Vrancea intermediate-depth earthquakes (undeclustered catalogue). Several regions are delimited, based on their different characteristics. Regions B and D characterize the short-range and long-range interactions, respectively. The partition functions are clearly influenced by “edge effects” in Regions A and E, situated at the ends of the analyzed scaling region. Region C is the transition between regions B and D and has an insufficient number of data for determining a reliable multifractal spectrum. The indicated ranges correspond to the fitted scales in regions B and D.

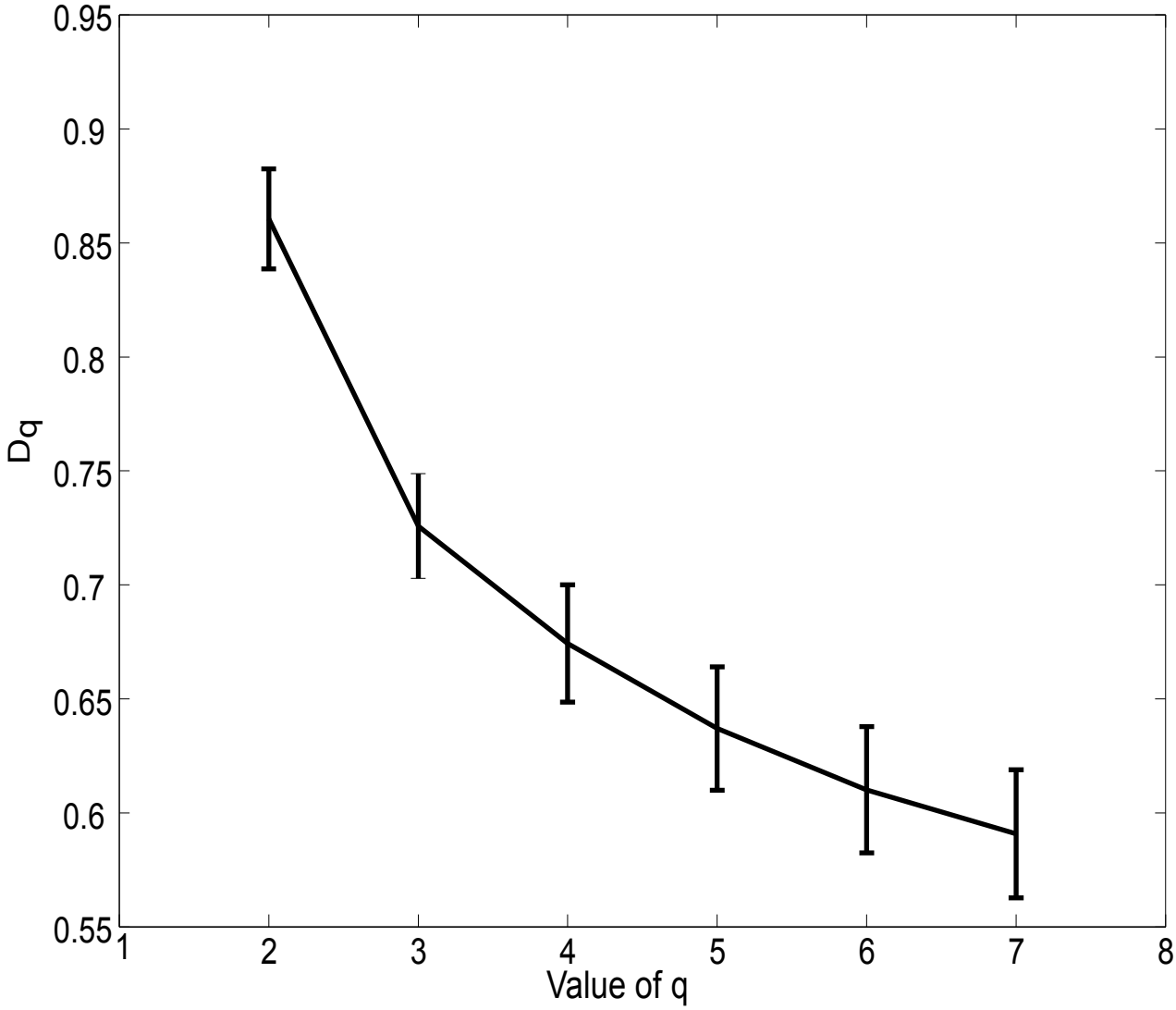

Fig. 5.5 Spectrum of the generalized dimensions for the undeclustered catalogue, corresponding to Region B in Fig. 5.4. There is strong clustering at small scales, undoubtedly associated with the after-shock generation processes. The error bars in this figure, as well as in Figs. 5.6, 5.8 and 5.9, indicate the 95% confidence interval for each dimension estimate, obtained as a result of a linear fit of the corresponding partition function.

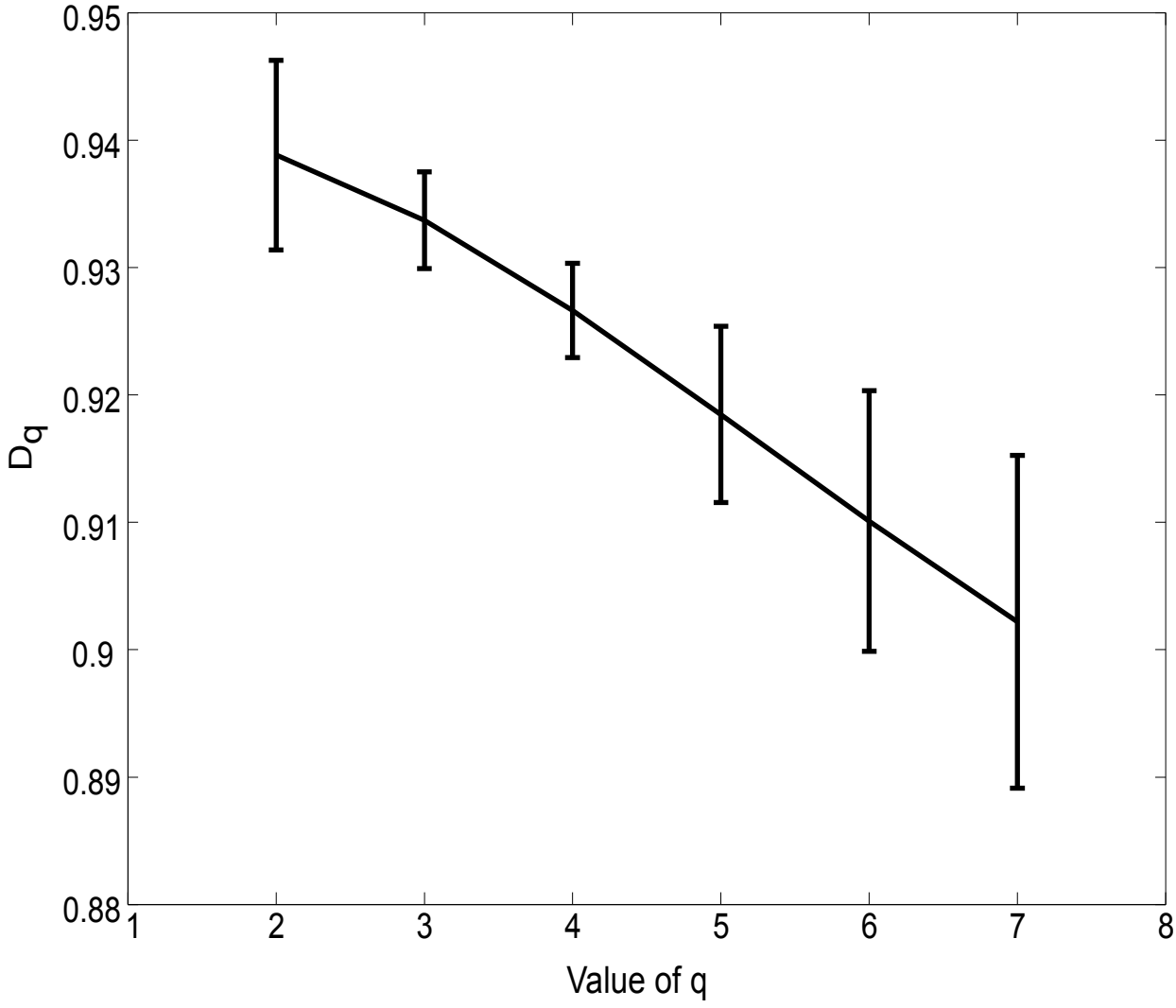

Fig. 5.6 Spectrum of the generalized dimensions for the undeclustered catalogue, corresponding to Region D in Fig. 5.4. This shows randomness or weak clustering at large scales for this area.

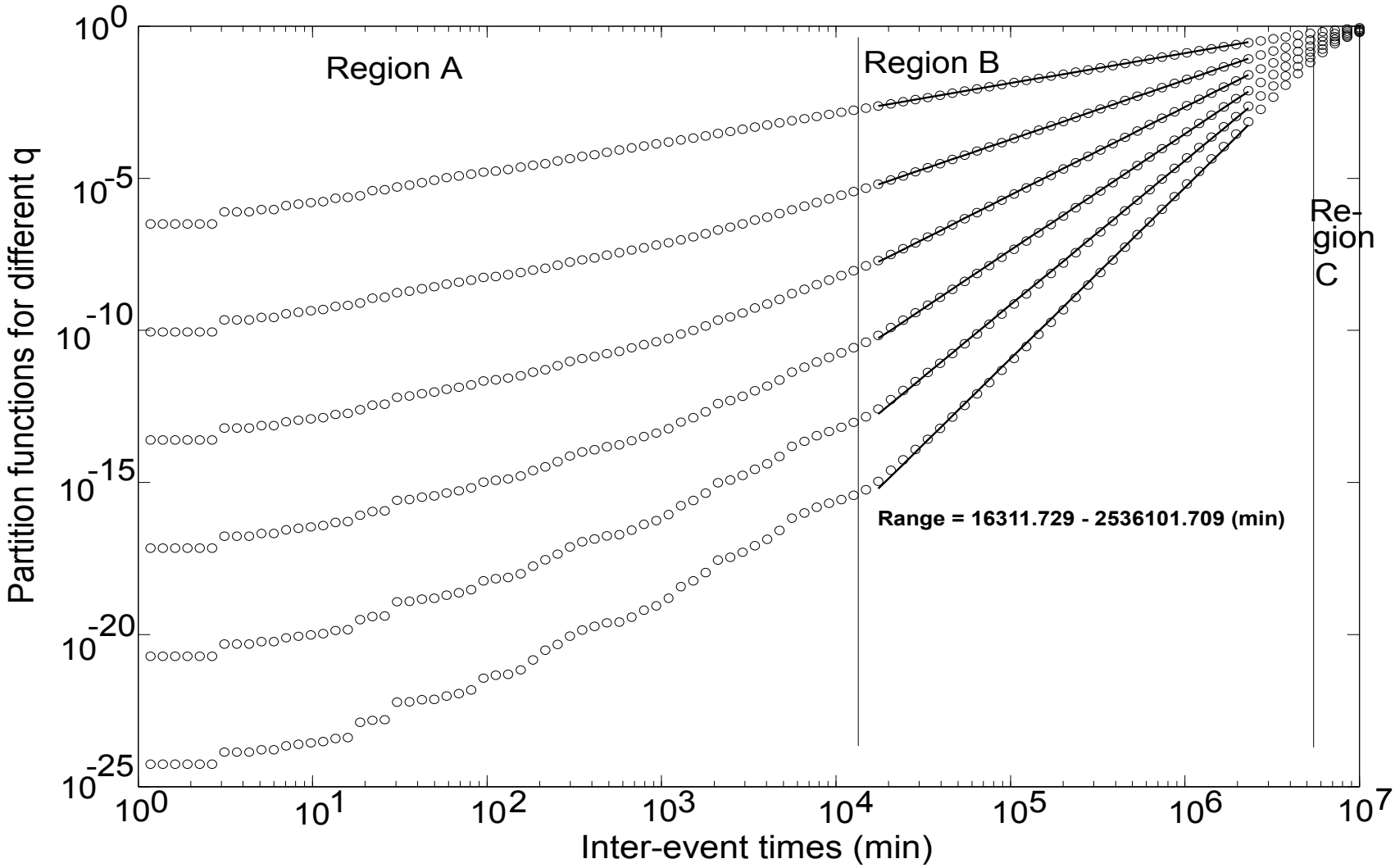

Fig. 5.7 Partition functions (q=2,3,...,7, from top to bottom) for the inter-event times of the Vrancea intermediate-depth earthquakes (declustered catalogue). Regions A and C are characterized by “edge effects” and have an insufficient number of data for determining a multifractal spectrum. The partition functions show a well-defined scaling in Region B.

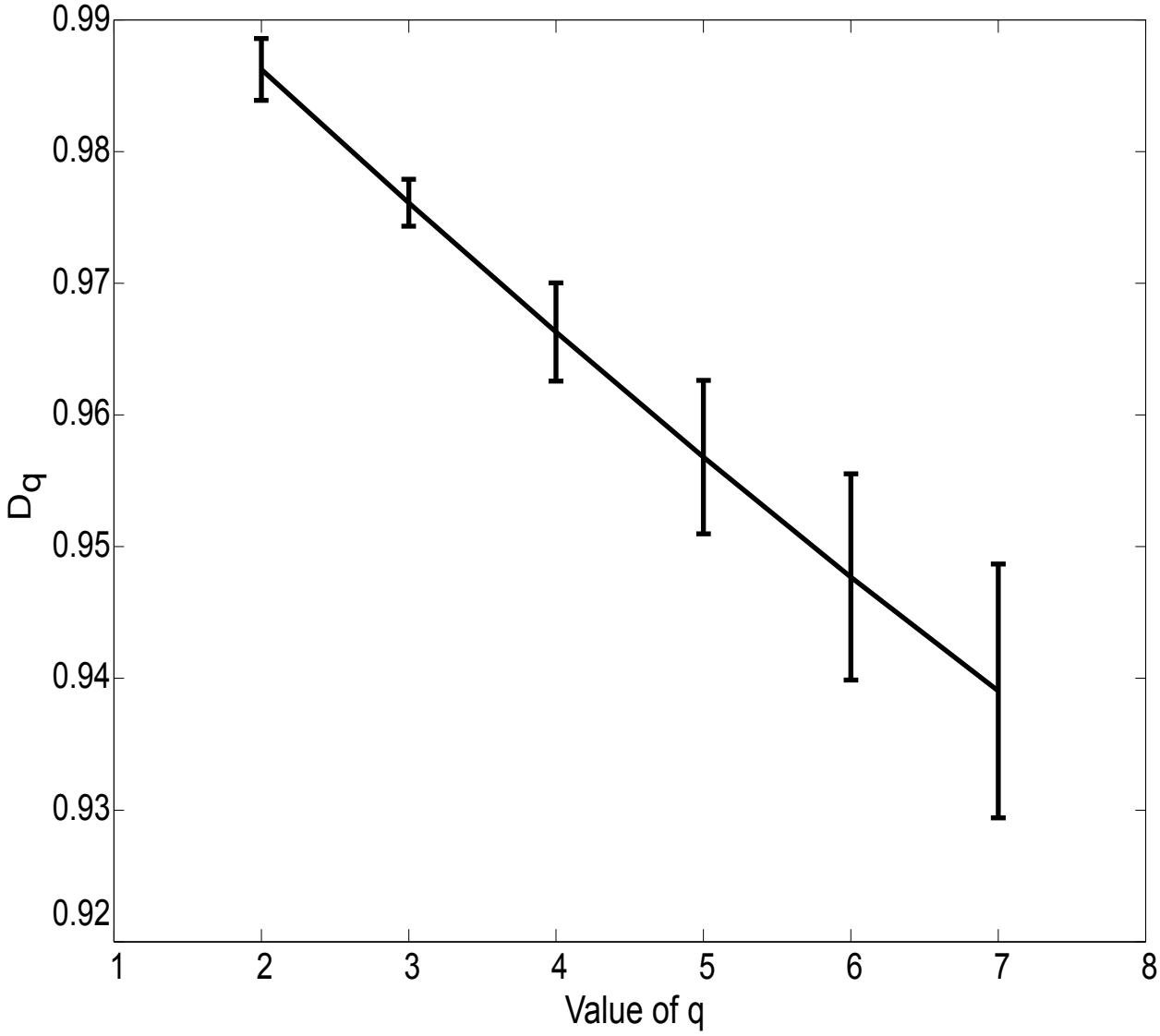

Fig. 5.8 Spectrum of the generalized dimensions for the declustered catalogue, corresponding to Region B in Fig. 5.7. This shows monofractality and very weak clustering (or no clustering) for this area.

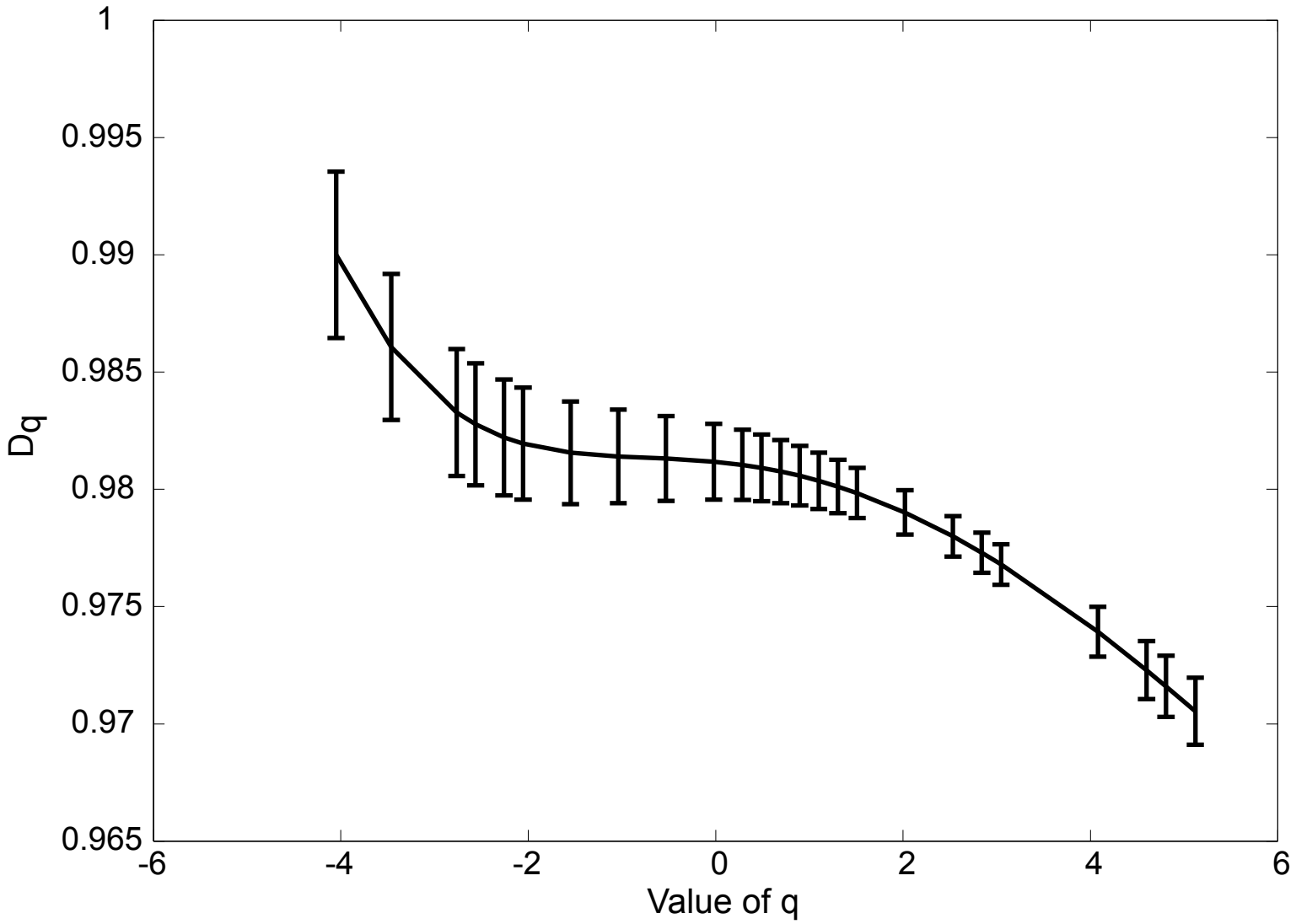

Fig. 5.9 Multifractal spectrum of the declustered catalog (M >= 2.8), by using a fixed-mass approach. The scaling region used for obtaining this spectrum extends from days to several years.

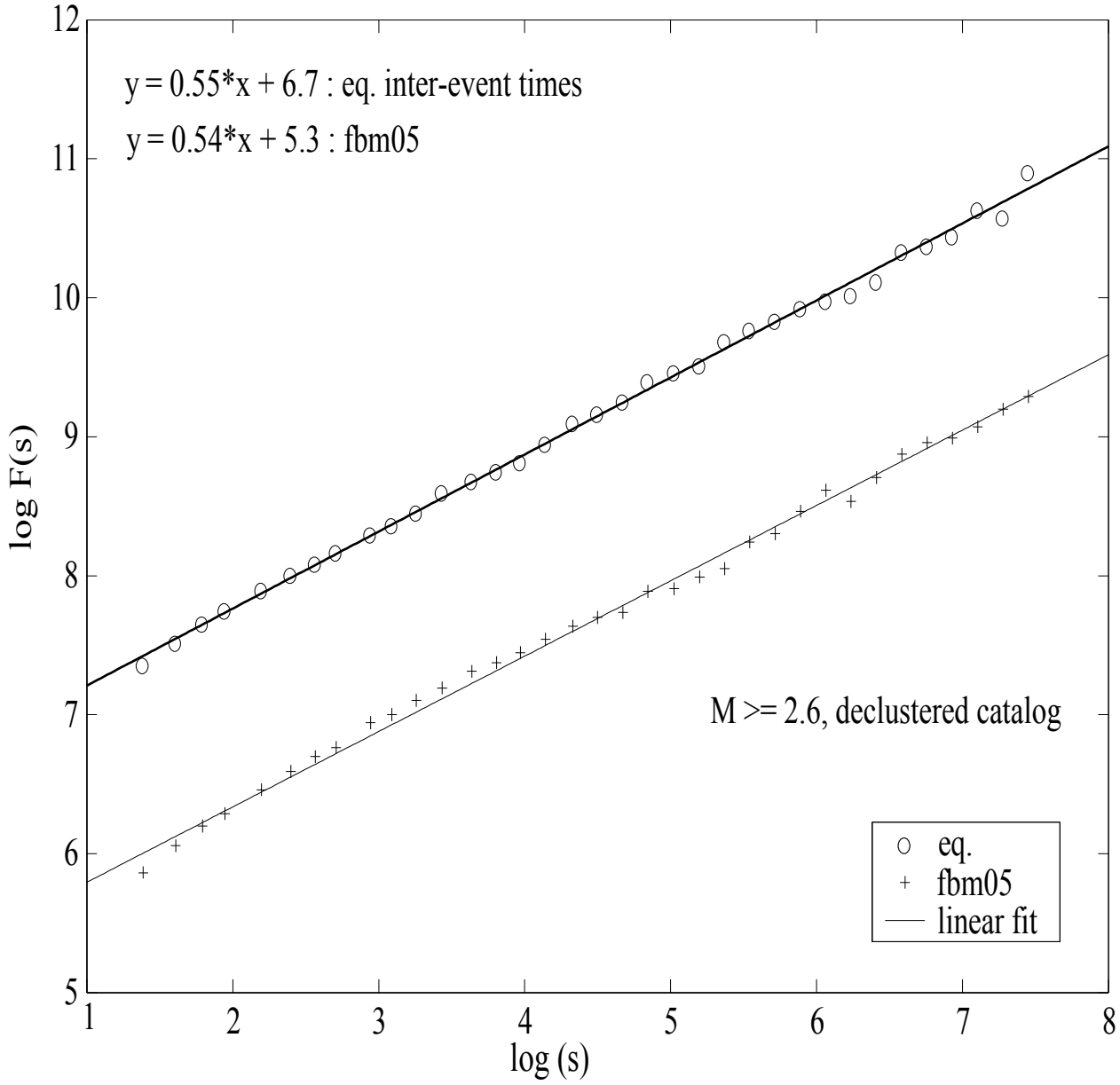

Fig. 5.10 Detrended Fluctuation Analysis (DFA) for the declustered catalog of Vrancea seismicity. Open circles and crosses represent the earthquake data and the Brownian process (fbm05), respectively. The slopes of the two fitted lines (i.e., the scaling exponent *C*) are practically the same, indicating that there are no significant temporal correlations for Vrancea earthquakes. The natural logarithm (base *e*) is used for these analyses.

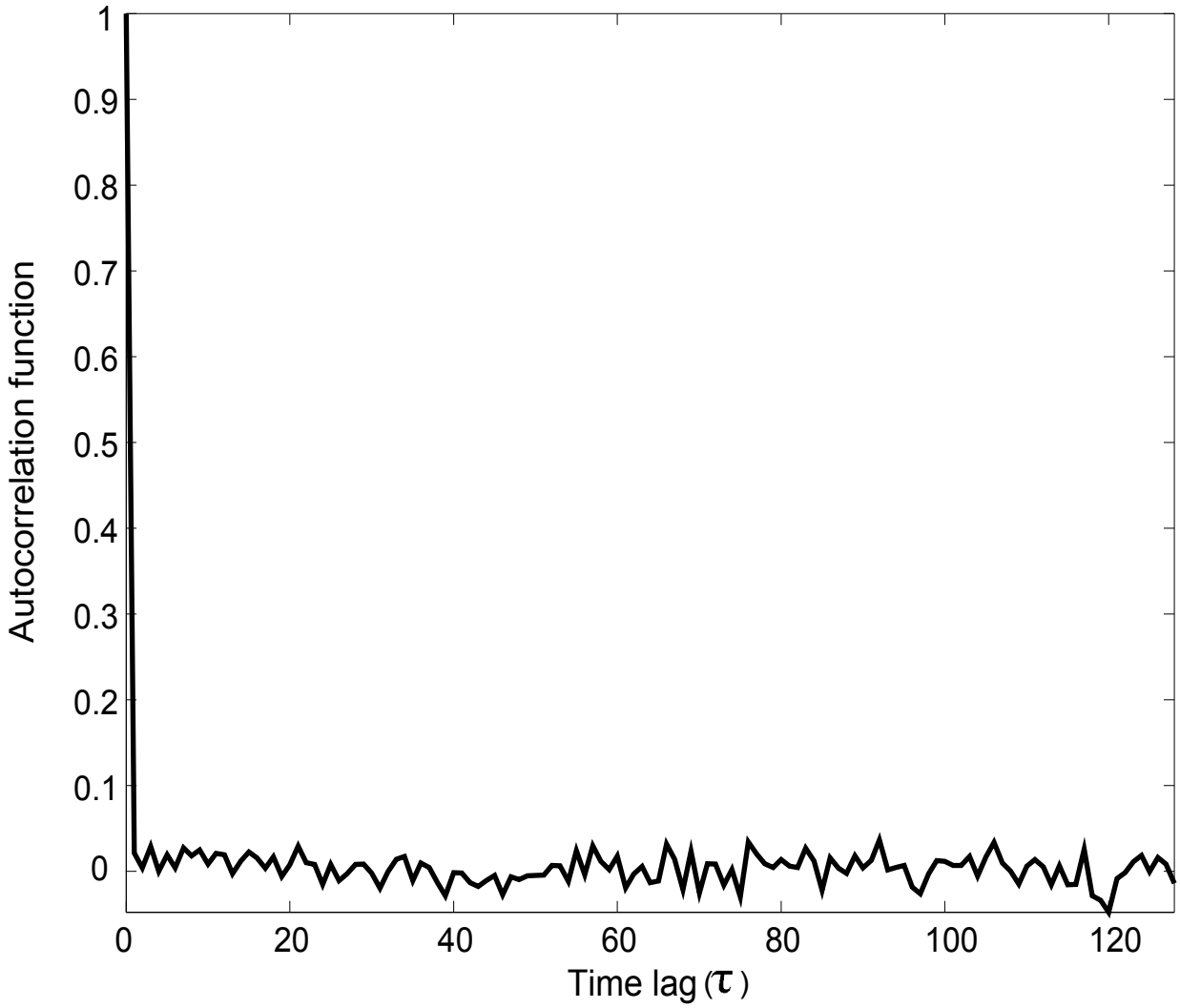

Fig. 5.11 The autocorrelation function versus time lag, τ, for the inter-occurrence times of Vrancea earthquakes (M >= 2.8).

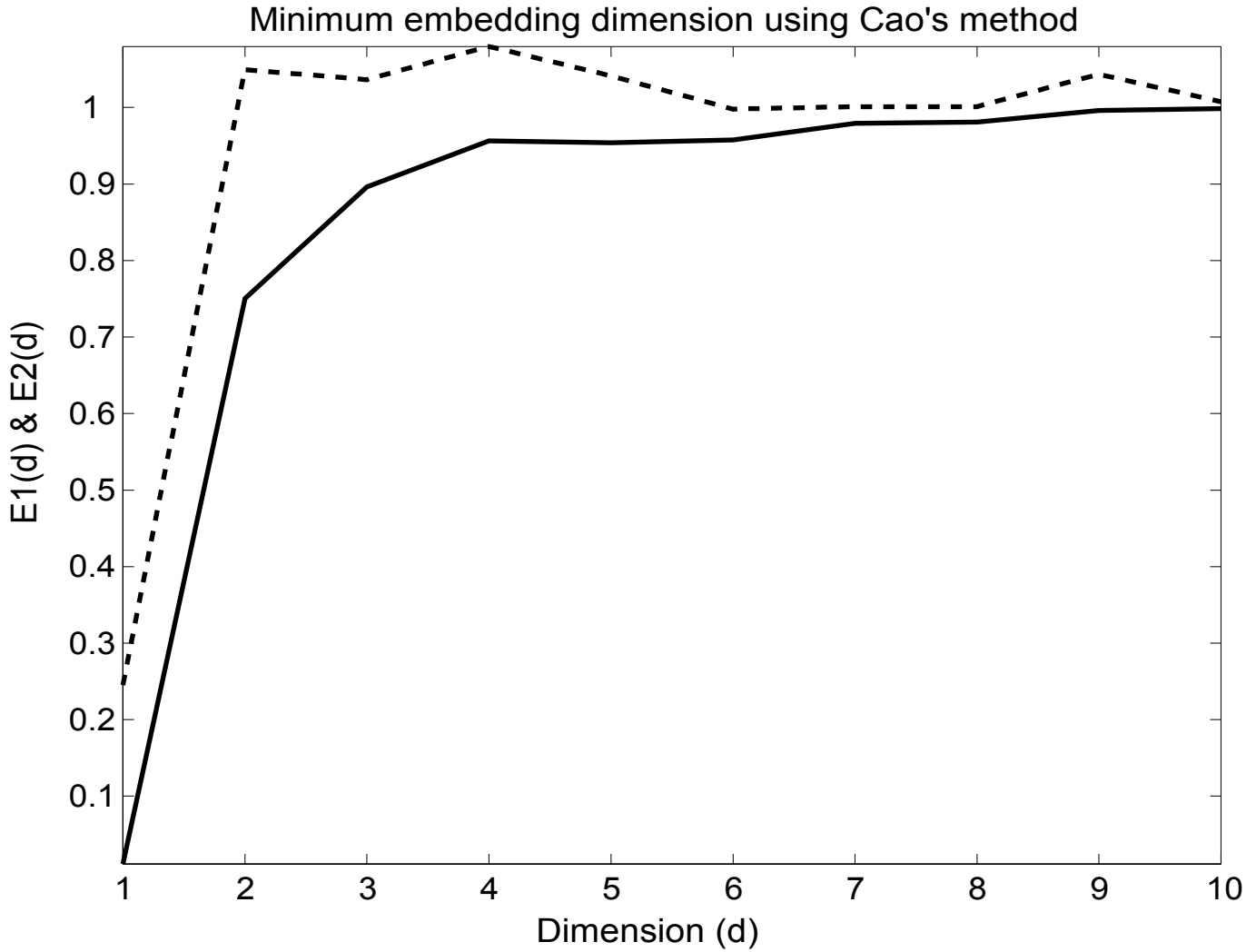

Fig. 5.12 Statistical parameters *E1* and *E2* versus embedding dimension, *d*, for the Lorentz system. From the saturation of *E1* (solid line) and the variation of *E2* (dotted line) one can conclude that the system is low-dimensional, with an embedding dimension of three.

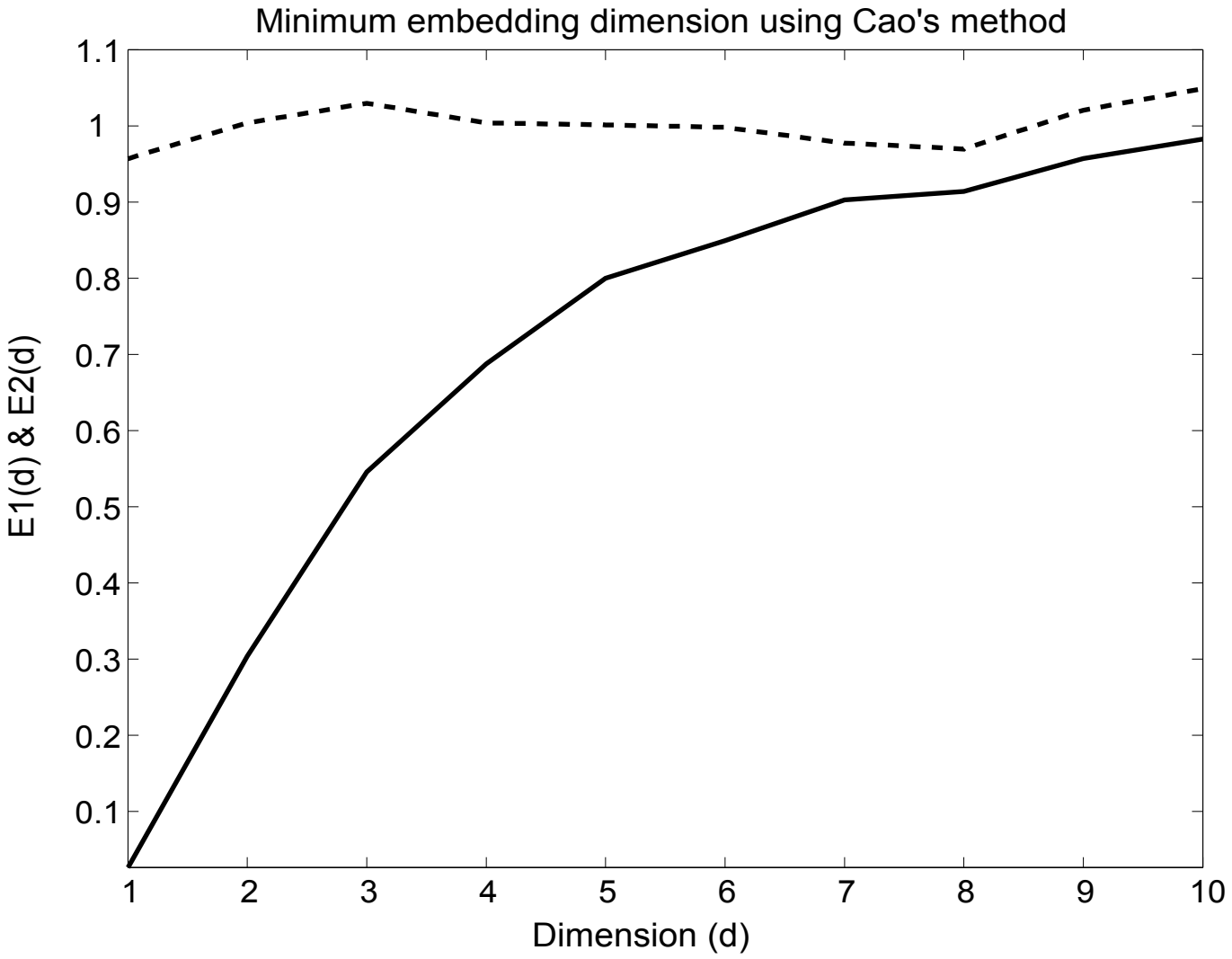

Fig. 5.13. Same as Fig. 5.12, but for the earthquake data. The lack of a saturation of *E1* and the fact that *E2* is always very close to one are strong arguments for the stochastic nature of the Vrancea earthquake system.

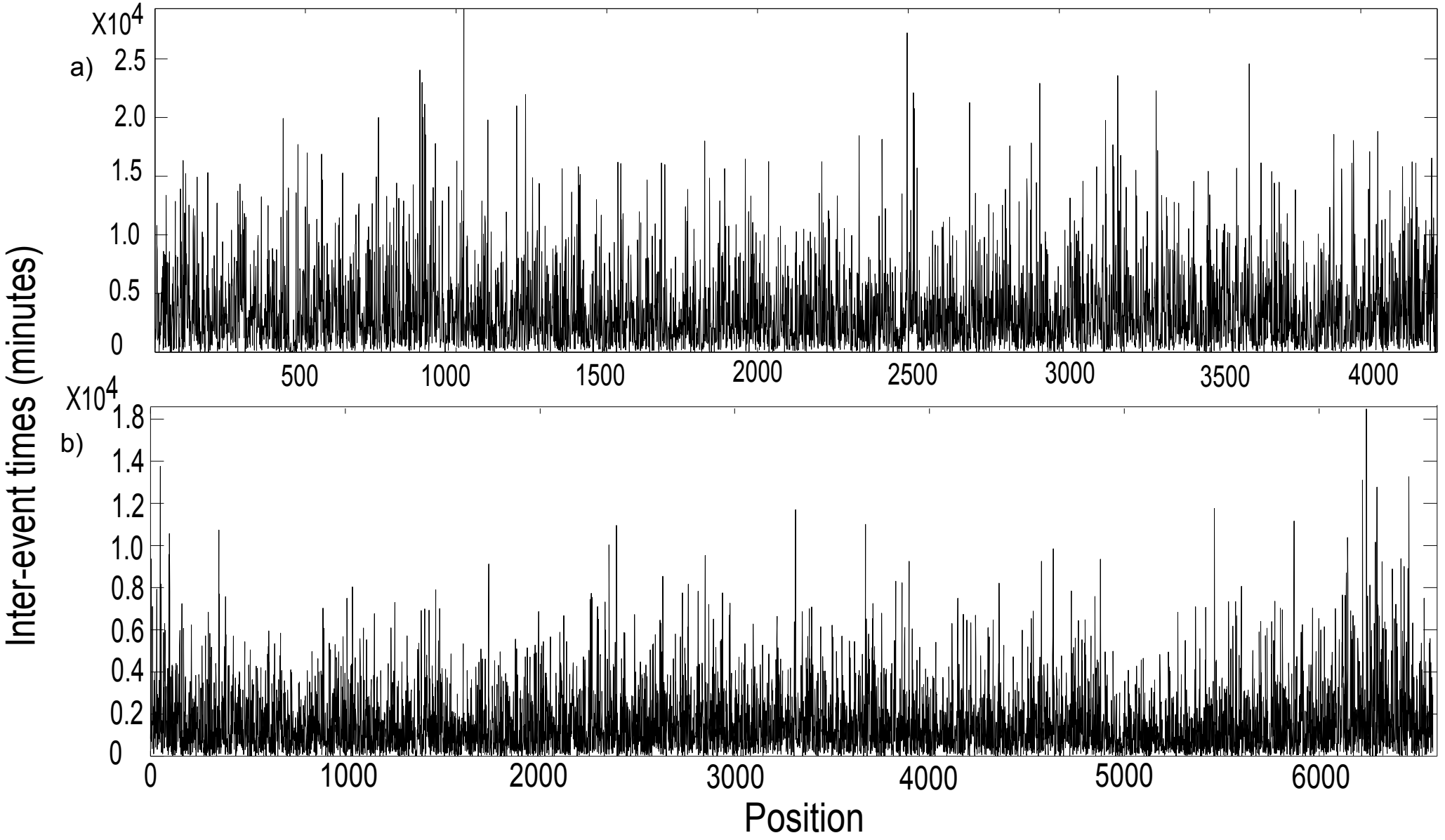

Fig. 6.1 Records of inter-event times, i.e. earthquake intervals, in the case of Vrancea (Romania) earthquakes (a) and the shallow seismicity in the Hyogo region (b).

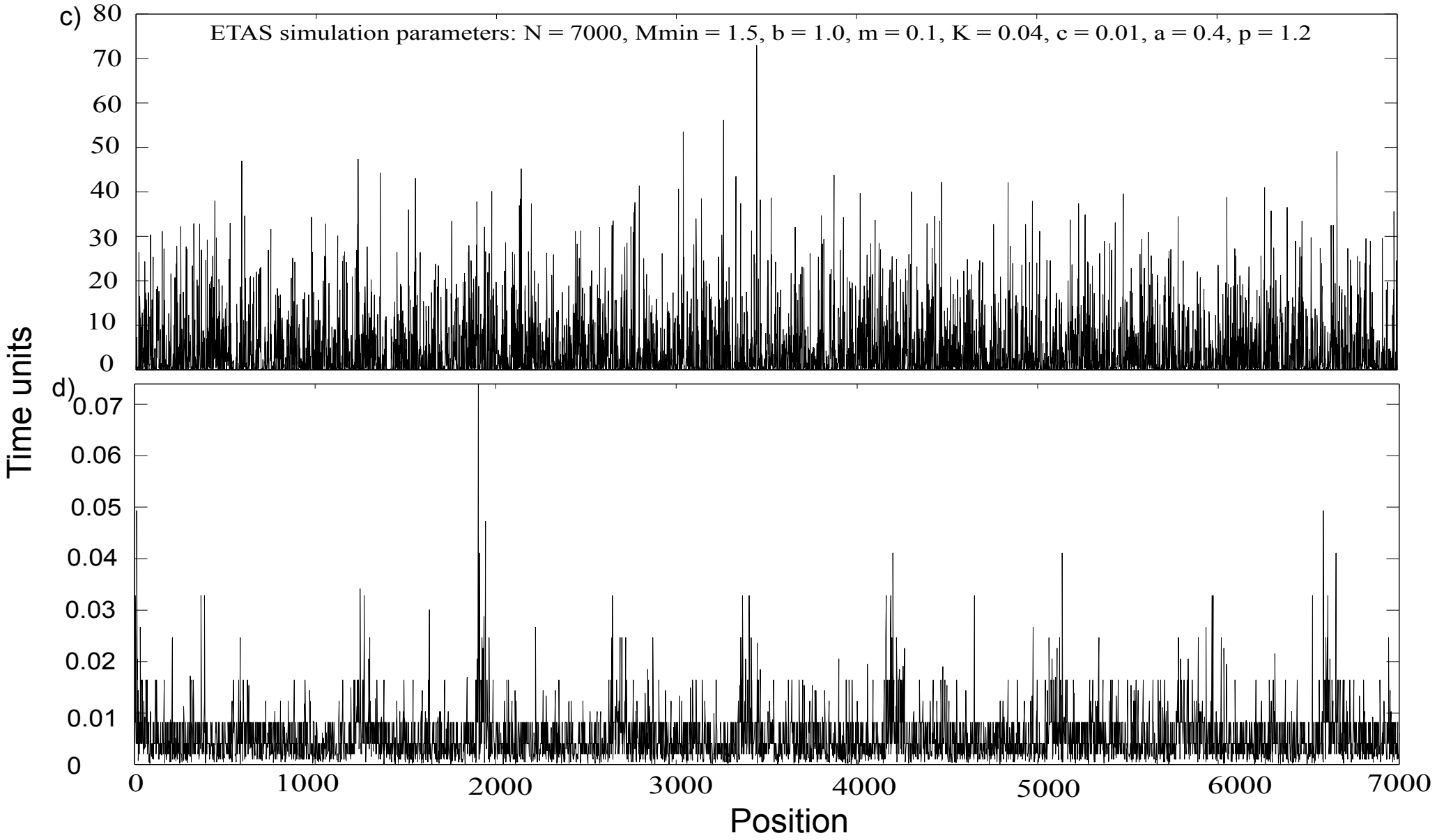

Fig. 6.1. Inter-event time series in the case of ETAS model simulation (c) and EBZ_A simulation (d). For case d) only 7000 earthquake intervals were represented to show clearly the temporal pattern.

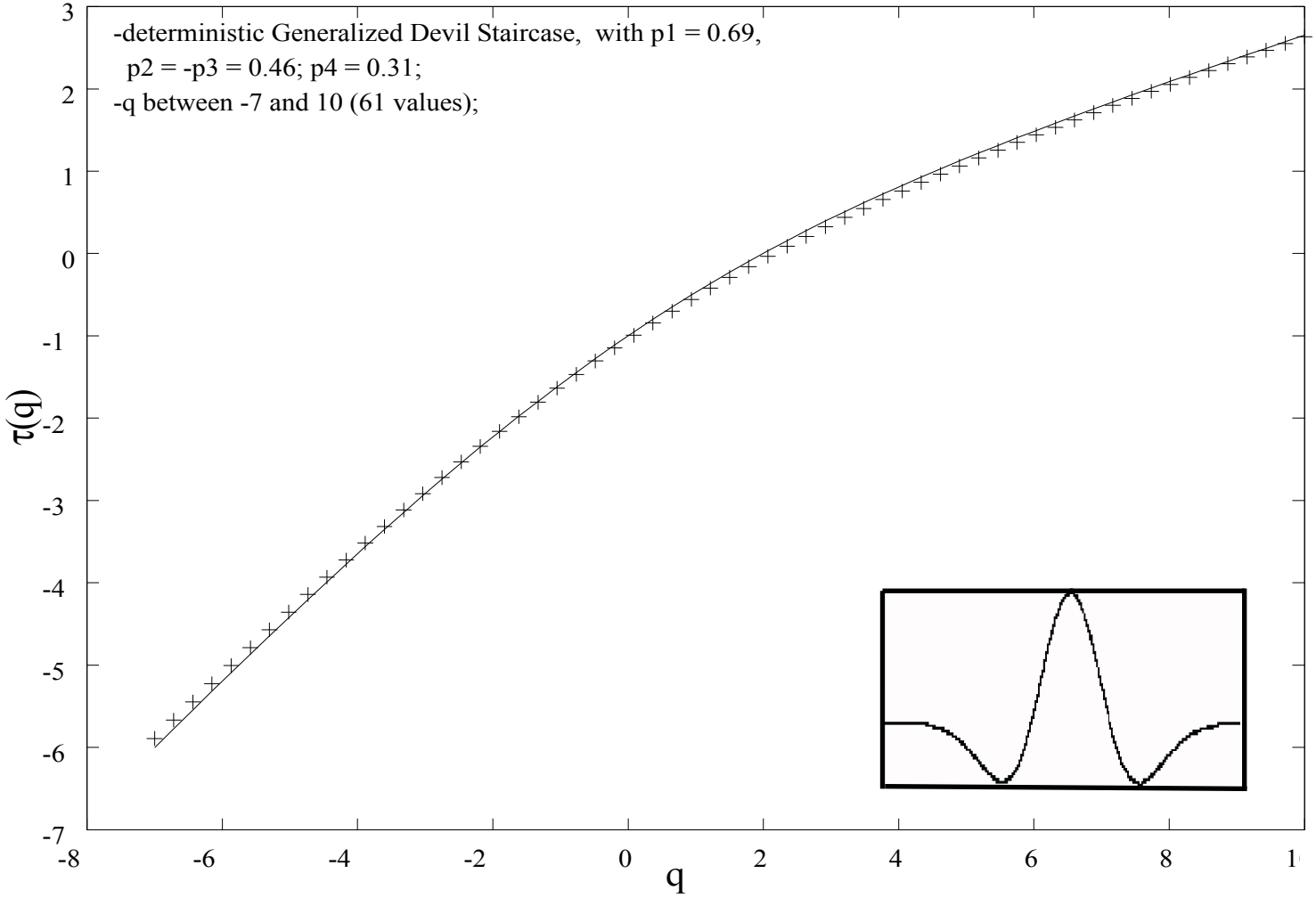

Fig. 6.2 “tau spectrum” for the Generalized Devil Staircase. p1, p2, p3 and p4 are the parameters used to obtain the time series. q takes 61 equally spaced values, between -7 and 10. The scaling range fitted to compute this spectrum extends between 2^2 and 2^9. The theoretical spectrum (continuous line) and the computed one (small crosses) are in very good agreement. The inset shows the analyzing mother-wavelet (the second derivative of the Gaussian) used to compute the CWT in this study.

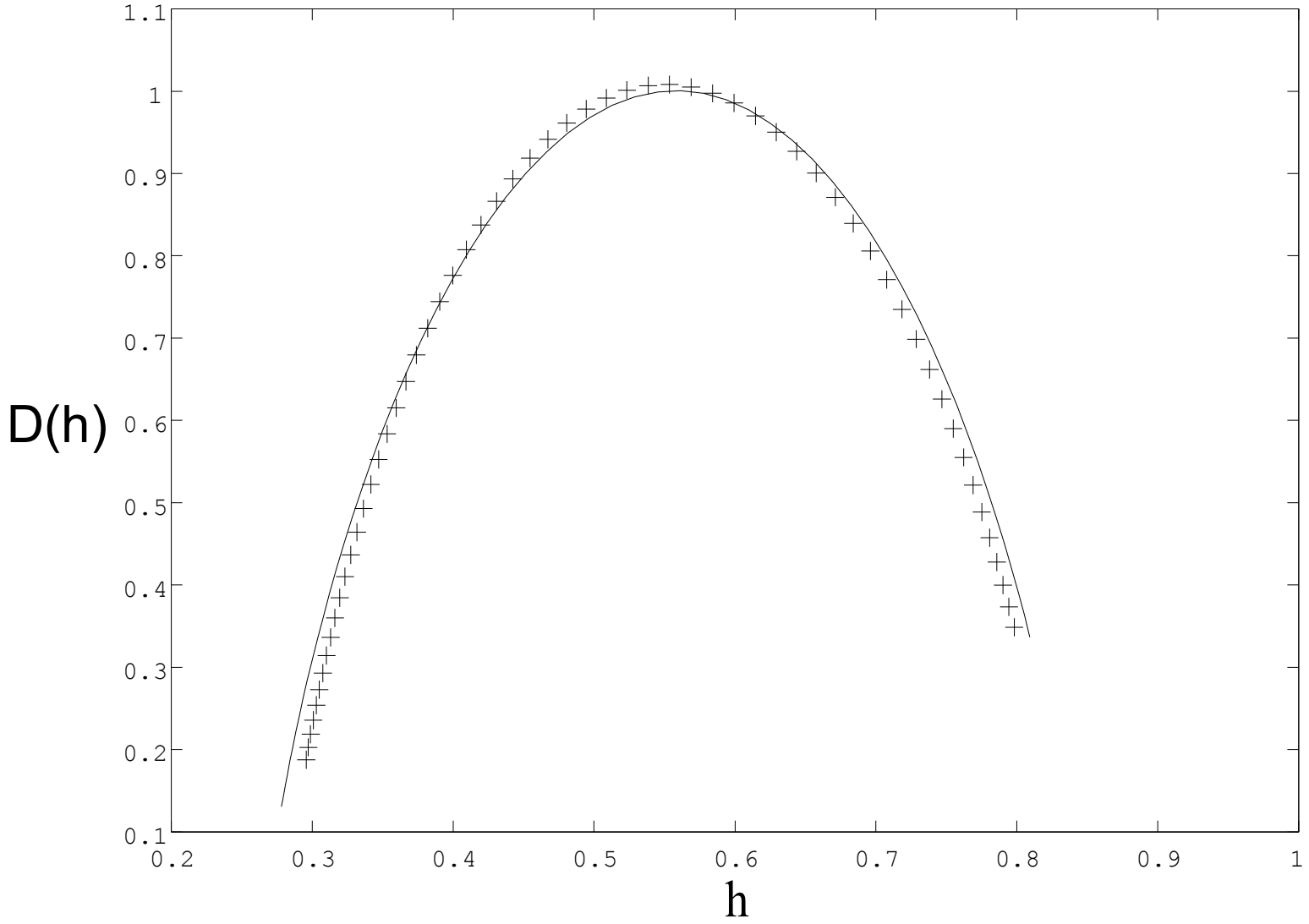

Fig. 6.3 Theoretical (continuous line) and obtained (crosses) D(h) multifractal spectrum in the case of the Multinomial Cantor Measure. One can notice the clear multifractal signature of the simulated time series, as well as the good agreement between the theoretical and computed spectrum.

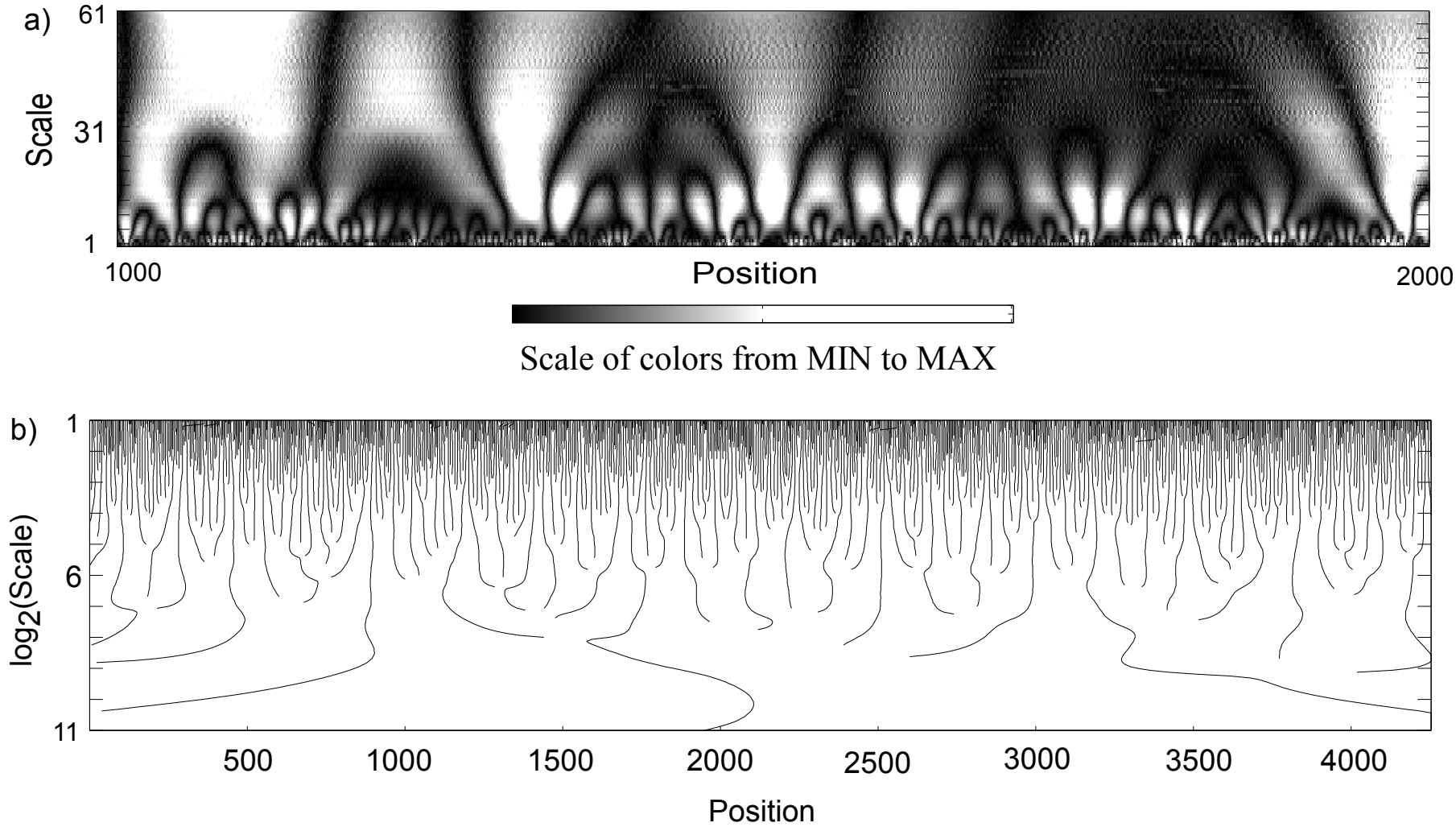

Fig. 6. 4 a) CWT coefficients plot in the case of the Vrancea (Romania) time series, zoomed view. Scale and position are on the vertical and horizontal axis, respectively. The coefficients, taking values between MIN and MAX, are plotted by using 64 levels of gray. The plot was obtained by using the “Wavelet toolbox” of “Matlab” software. b) WTMM skeleton plot. The vertical axis is logarithmic, with small scales at the top.

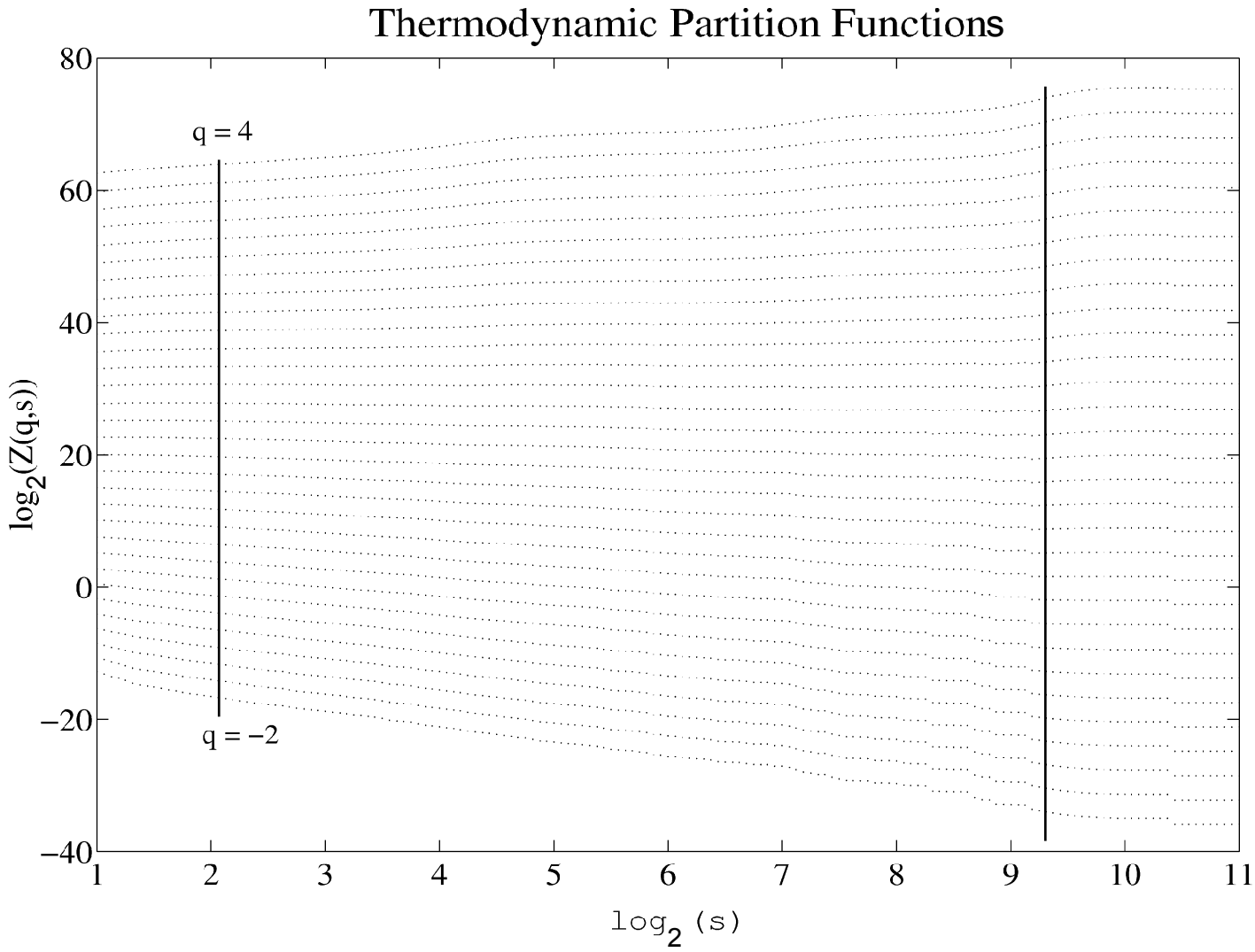

Fig. 6.5 Double-logarithmic plot of the partition functions, for q between 4 to -2 (up to down, constant increment), in the case of Vrancea time series. The vertical lines indicate the limits of the scaling region. Outside this area there are “border effects” due to the limited length of the time series. The scale *s* corresponds to the series of inter-event times, which are expressed in minutes (same for Fig. 6.7, 6.8 and 6.11).

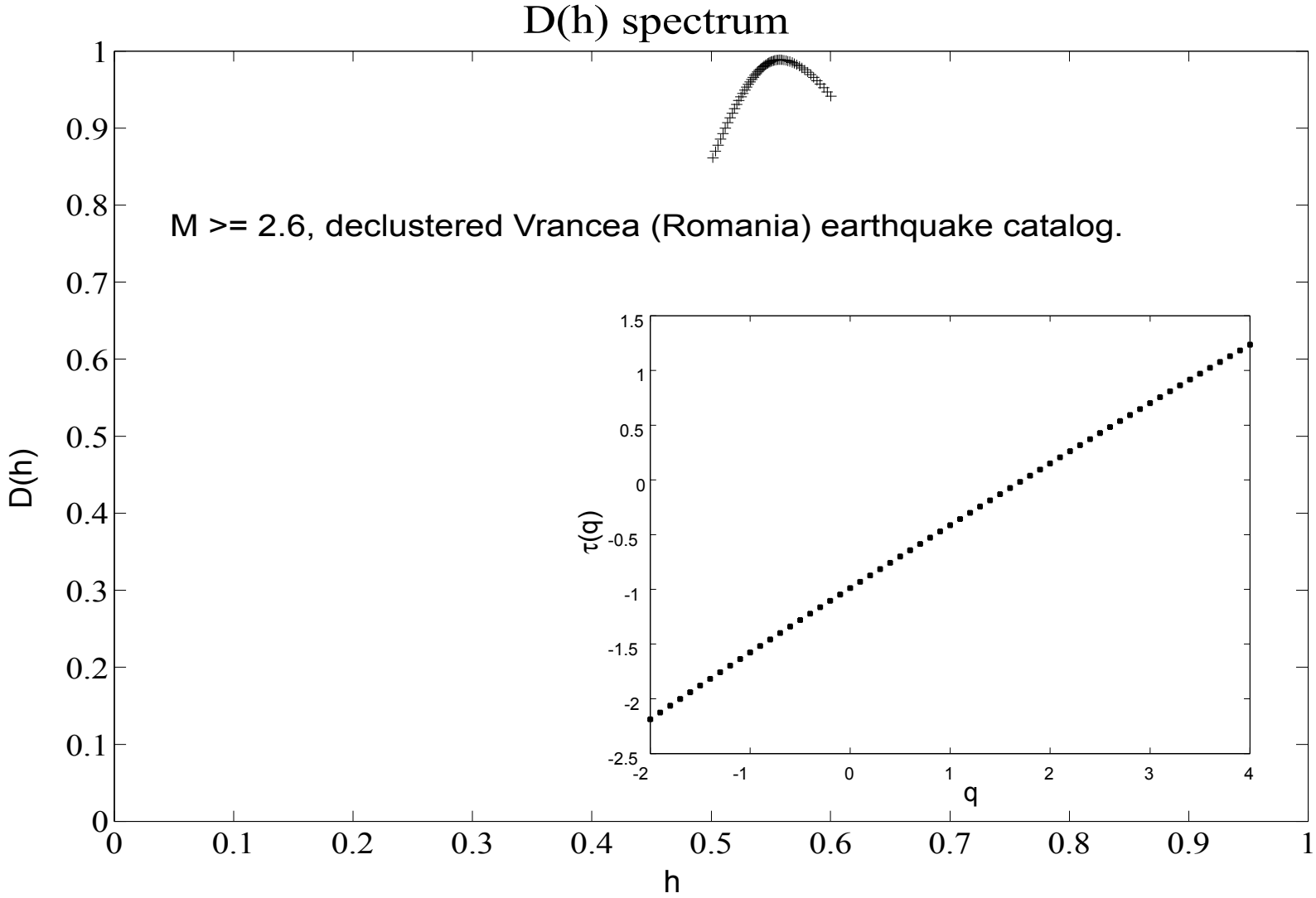

Fig. 6.6 D(h) spectrum of the integrated inter-event times, in the case of Vrancea (Romania) integrated earthquake intervals. The spectrum is quasi-monofractal, centered on 0.56. This value, slightly larger than 0.5, is an indication of quasi-randomness. The inset shows the $\tau(q)$ spectrum, which is very close to a straight line (indication of monofractality).

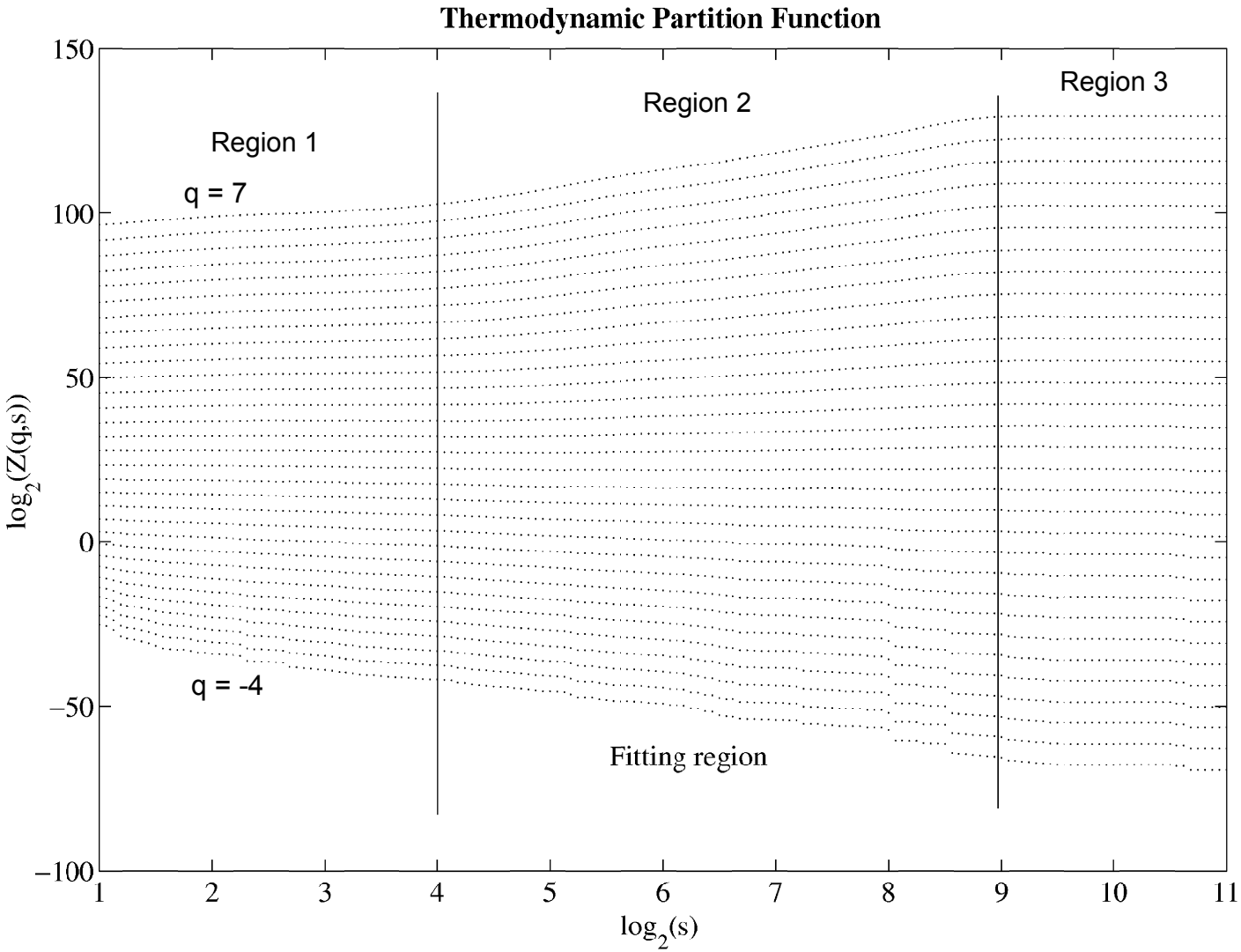

Fig. 6.7 Partition functions for q between 7 to -4 (from up to down, constant increment), for the case of “Kobe time series”. One can notice a different scaling in Region 1 and Region 2. There is no more reliable scaling in Region 3, due to the limited length of the data set.

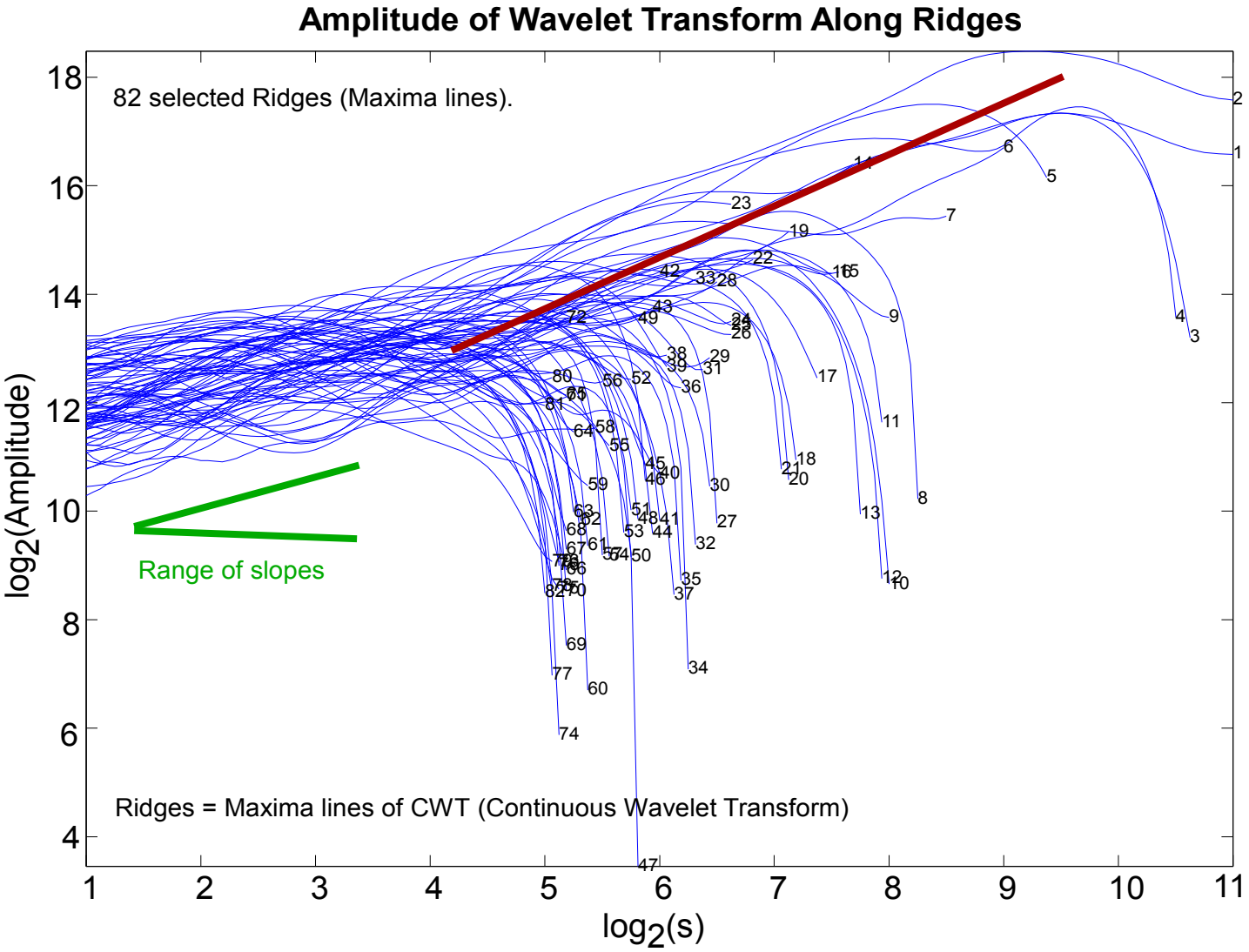

Fig. 6.8 Logarithmic plot of the Amplitude of CWT along ridges (maxima lines of the Continuous Wavelet Transform). At large scales there is only one well-defined, predominant slope of the lines, while at smaller scales there is a range of slopes. Because of the large number of WTMM lines, only a limited set of representative ones were considered in this plot.

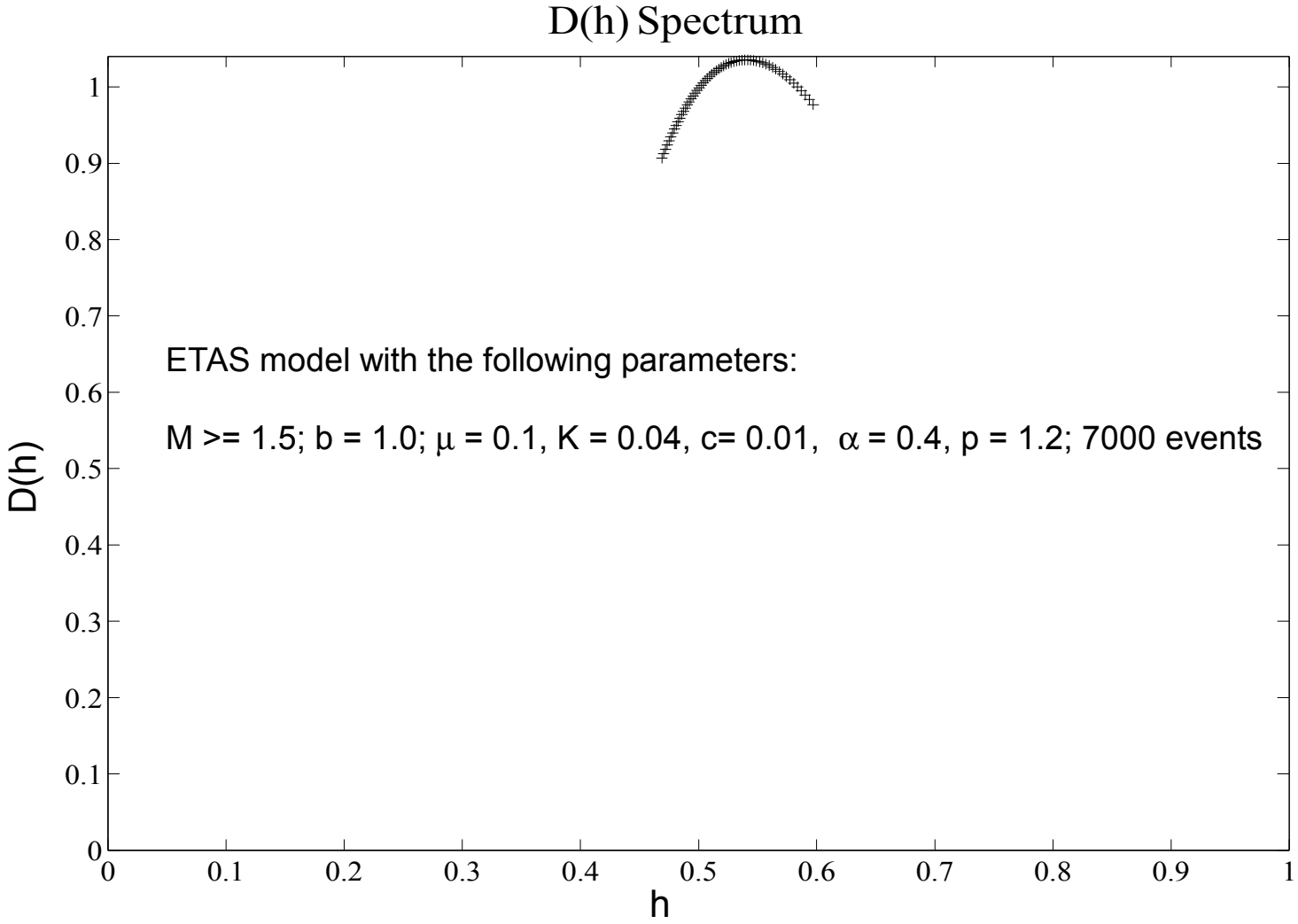

Fig. 6.9 D(h) spectrum, in the case of ETAS model simulation. A scaling range between 2^2 and 2^9 was used to compute the spectrum.

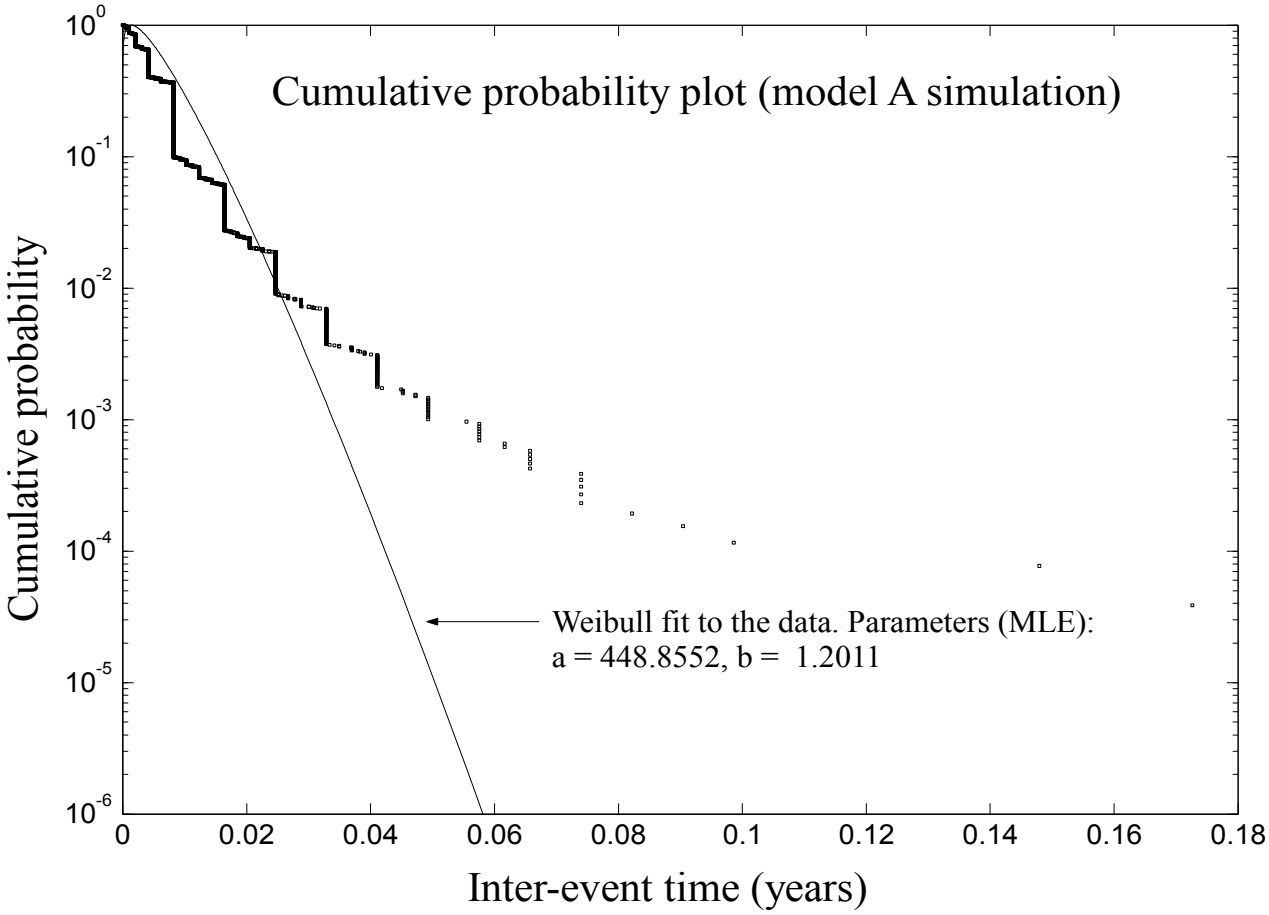

Fig. 6.10 Cumulative probability plot of inter-event times for "model A' simulation. A Weibull probability distribution is fitted to the data.
The graph indicates the non-Poissonian character of the time series and the existence of quasi-periodicities (see text).

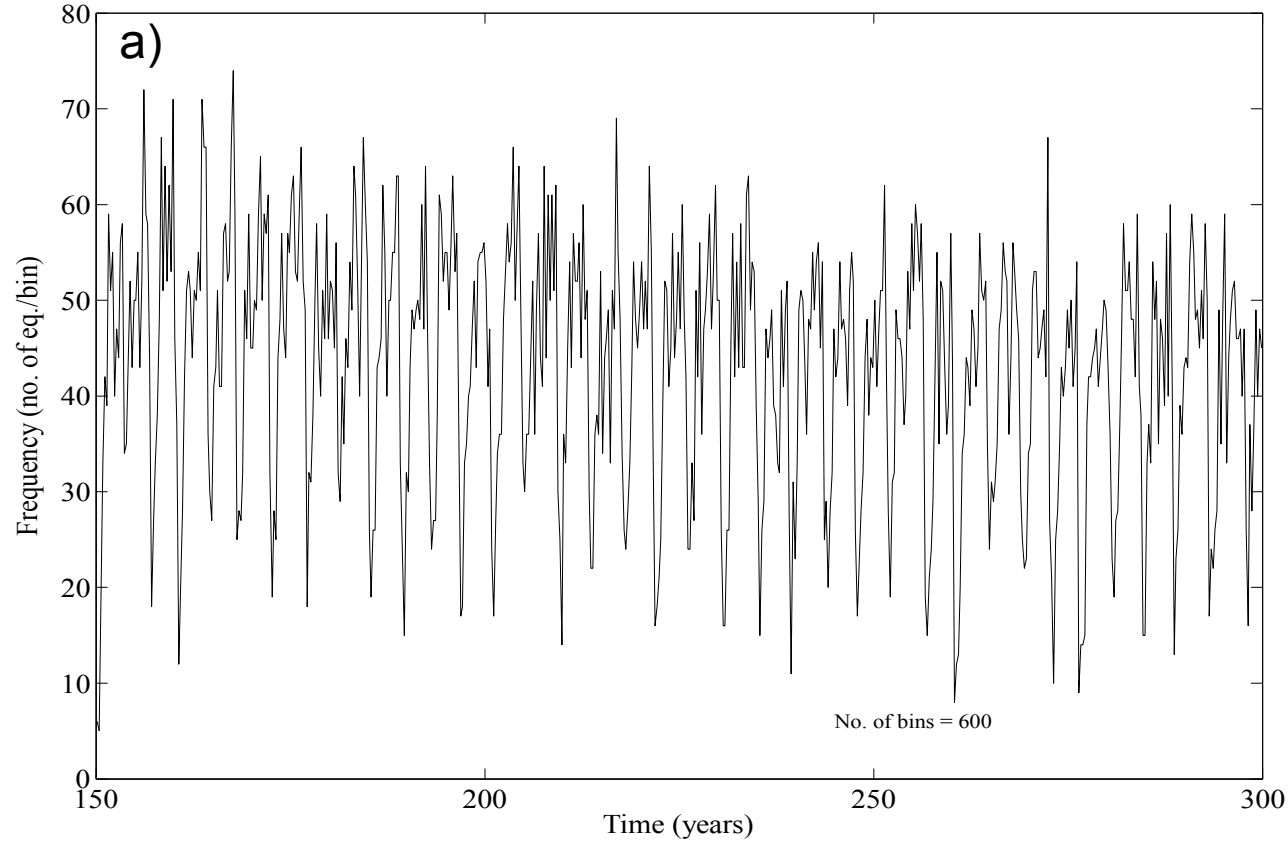

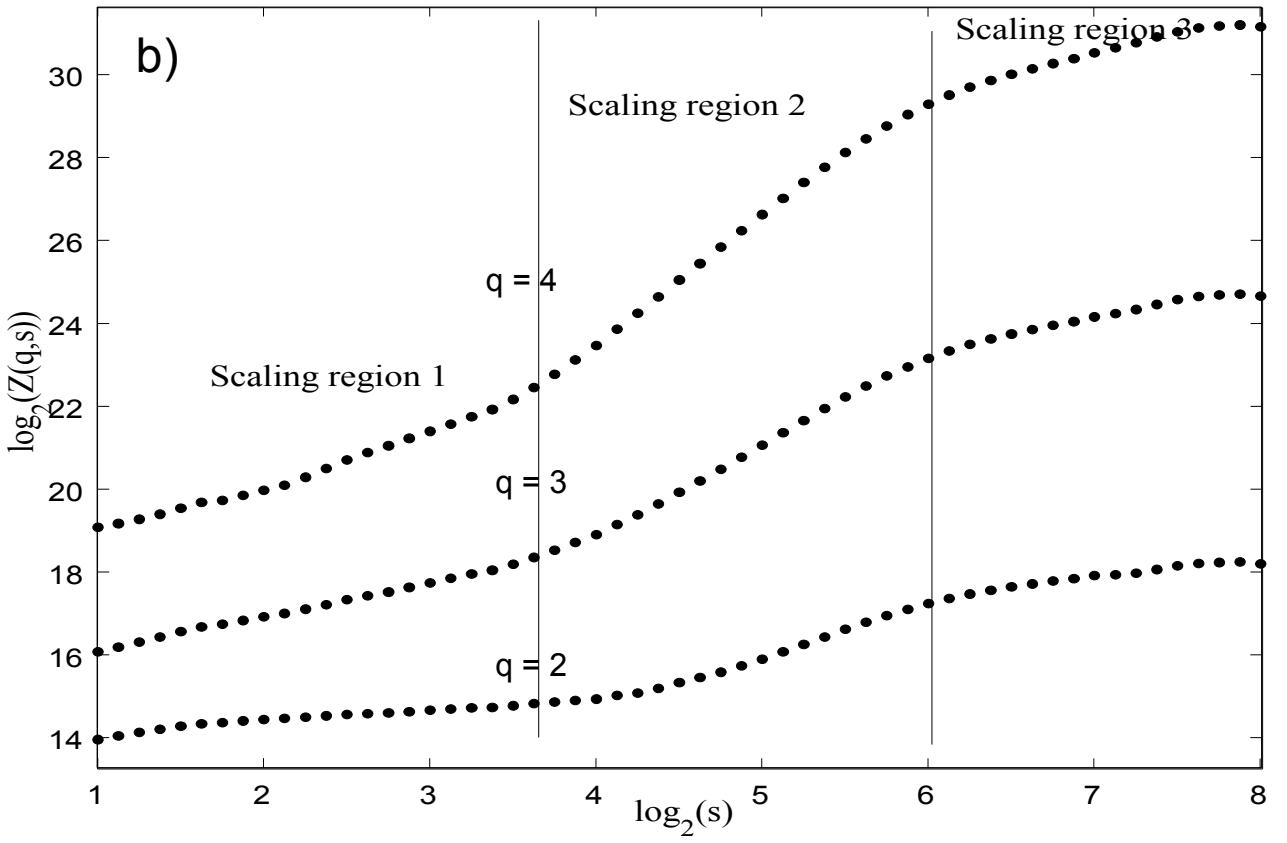

Fig. 6.11 a) Frequency of earthquakes versus time plot, in the case of EBZ_A simulation. Oscillatory behavior is observed.
b) Partition functions, Z, for q = 2, 3, 4, in the case of EBZ_A simulation. Several distinct scaling domains are observed. The vertical lines are the approximate borders of these regions.